Synthesis and Characterization of Zr and Ca modified $BaTiO_3$ Ferroelectric Ceramics

A Thesis Submitted in Partial Fulfillment of the
Requirements for the Degree of

Doctor of Philosophy
in
Ceramic Engineering

By

Ganesh Kumar Sahoo
(Roll No: 509CR101)

Under the Supervision of

Dr. Ranabrata Mazumder
&
Dr. Swadesh K. Pratihar

Department of Ceramic Engineering
National Institute of Technology
Rourkela–769008, Odisha, India
April- 2015

Dedicated to my Parents

DECLARATION

Date:

I hereby declare that the work presented in the thesis entitled **"Synthesis and Characterization of Zr and Ca modified $BaTiO_3$ Ferroelectric Ceramics"** submitted for Ph. D. Degree to the National Institute of Technology, Rourkela has been carried out by me at Department of Ceramic Engineering, National Institute of Technology, Rourkela under the supervision of Dr. Ranabrata Mazumder and Dr. Swadesh K. Pratihar. The work is original and has not been submitted in part or full by me for any degree or diploma to this or any other University/Institute.

Ganesh Kumar Sahoo

Department of Ceramic Engineering
National Institute of Technology
Rourkela-769008
Odisha, India

DEPARTMENT OF CERAMIC ENGINEERING
NATIONAL INSTITUTE OF TECHNOLOGY,
ROURKELA-769008

CERTIFICATE

This is to certify that the thesis entitled **"Synthesis and Characterization of Zr and Ca modified $BaTiO_3$ Ferroelectric Ceramics"** submitted by **Ganesh Kumar Sahoo**, for the degree of **Doctor of Philosophy in Ceramic Engineering** to the National Institute of Technology, Rourkela, is a record of bonafide research work carried out by him under our supervision and guidance. His thesis, in my opinion, is worthy of consideration for the award of degree of Doctor of Philosophy in Ceramic Engineering in accordance with the regulations of the institute.

The results embodied in this thesis have not been submitted to any other university or institute for the award of a Degree.

Co Supervisor
Dr. Swadesh k. Pratihar

Department of Ceramic Engineering
National Institute of Technology
Rourkela

Supervisor
Dr. Ranabrata Mazumder

Department of Ceramic Engineering
National Institute of Technology
Rourkela

ACKNOWLEDGMENTS

First, I would like to express my deepest appreciation to my supervisor Prof. Ranabrata Mazumder for his unlimited guidance, insight and suggestions throughout the research. I thank him from the bottom of my heart for introducing me to the area of electroceramics. I thank him for his great patience, constructive criticism and myriad useful suggestions apart from invaluable guidance to me. I would also like to thank my co-supervisor Prof. S.K Pratihar for his help and support on this project.

I am again grateful to Prof. S.K Pratihar, Head and Department of Ceramic Engineering for his encouragement and help to carry out the thesis work.

I would also take this opportunity to express my gratitude and sincere thanks to Prof. S. Bhattacharyya, Prof. J. Bera, Prof. B.B. Nayak, Prof. S.K. Pal and Mr. A. Chowdhury, Prof. D. Sarkar, Prof. R. Sarkar, Prof. Sunipa Bhattacharyya, Prof. S. Dasgupta, Prof. S.K. Behera, Prof. A.Paul and Prof. P Saha for their invaluable advice, constant help, encouragement, inspiration and blessings.

I would also like to thank the other members of` my DSC committee, Prof. S Panigrahi Department of Physics for his valuable advice. I also sincerely thank to Prof. Pawan Kumar, Department of Physics for allowing me to use the P-E loop tracer during my research work.

I am also thankful to Mr. Rajesh Pattanayak, Department of Metallurgical and Material Engineering for his kind help in SEM analysis and DSC analysis.

I wish my sincere thanks to Satyanarayan Tripathy, Sanjay Swain, Subrat Kumar Mohanty, Smruti rekha Dash, Geetanjali Parida, Akilesh Kumar Singh, Sunil Patra, Prativa Adhikari, Abhisek Chaudhary, Abhinaya, Jayorao Gorinta and Nadiya Bihari Nayak, for their cooperation.

I would take this opportunity to thank all the Research scholar in our lab, Technical, Non-technical staff of ceramic engineering.

I would also express my sincere thanks to laboratory Members of Department of Ceramic Engineering, N.I.T. Rourkela.

Finally, I owe my deepest gratefulness to my sisters, Geeta, Smita and my loving family, your patience, understanding, and unconditional love has given me the strength to make this accomplishment possible.

GANESH KUMAR SAHOO

ABSTRACT

During the last two decades, much effort has been given to developing new lead-free piezoelectric materials to replace the lead-based materials, such as PZT. The $BaTiO_3$ ceramics have been investigated since 1950s, but most of the work focused on the capacitor, thermistor, and transducer applications. However, the $BaTiO_3$ in its pure form exhibits the small permittivity, the poor piezoelectric properties, and low Curie temperature which have been the main obstacle to their wider commercial application. The recent discovery of the high dielectric and piezoelectric properties of Zr, Ca modified $BaTiO_3$ (BZT-BCT) has stimulated a renewed interest in searching for environmentally friendly Lead-free ferroelectrics. However, there are certain critical issues relating to the practical use of BZT-BCT. It requires high phase formation temperature (1300^{o}C) and sintering temperature (>1400^{o}C) and has low Curie temperature (90^{o}C). High sintering temperature may restrict the fabrication of multilayer devices. Very little work has been performed systematically to study the dielectric and piezoelectric properties of xBZT-(1-x)BCT at close compositional modifications around MPB. Keeping the above factors in mind, the primary objectives of the present work are to prepare Zr and Ca modified $BaTiO_3$ at low temperature by exploring various powder preparation techniques and to optimize Zr and Ca content in $BaTiO_3$ to get high dielectric and piezoelectric property. The other objectives are to lower the sintering temperature (<1200^{o}C) of Zr and Ca modified $BaTiO_3$ with additives and to study its dielectric property. In addition, it is also explored whether the MPB composition could be used to form a solid solution with BNT with an aim to improve the dielectric, piezoelectric properties and Curie temperature of parent or BNT.

First, $Ba(Zr_xTi_{1-x})O_3$ [BZT] (x=0.1, 0.15 and 0.2) ceramics have been successfully prepared by a solution based auto-combustion method by synchronizing two fundamental processing parameters such as solution pH, Metal: Citric acid: EDTA ratio. It is found that the all BZT powder possess single phase perovskite structure without secondary phase obtained at 800°C, which is much lower than the solid state method, and can be sintered to more than 98% of the theoretical density at 1350^{o}C. The room temperature dielectric constant increases with the increase in Zr content and loss factor is less than 2.5%. The piezoelectric property depend upon the poling field, and optimum poling field for all ceramics is 1.5kV/mm at room temperature. The highest piezoelectric coefficient (d_{33} = 142 pC/N) is obtained for BZT10 ceramics at an electric field of 1.5kV/mm. The results indicate that BZT10 ceramics is promising candidates for the lead-free piezoelectric applications. The knowledge base of preparation of BZT was utilized to prepare $(Ba_{0.85}Ca_{0.15})(Ti_{1-x}Zr_x)O_3$(BCTZ, x=0.05,0.1, 0.15) by solution based auto-combustion method. Single-phase, and sub-micron $(Ba_{0.85}Ca_{0.15})(Ti_{1-}$

$_{x}Zr_{x})O_3$ powders can be prepared at 700°C, that is much lower compared to the conventional method. Maximum dielectric and piezoelectric property was obtained for $(Ba_{0.85}Ca_{0.15})(Zr_{0.1}Ti_{0.9})O_3$ composition. The same composition can be represented by a pseudobinary solid solution of $0.5Ba(Zr_{0.2}Ti_{0.8})O_3$-$0.5(Ba_{0.7}Ca_{0.3})TiO_3$[BZT- 0.5BCT]. The improvement of the properties can be explained by the formation of the morphotropic phase boundary (MPB). The properties achieved in this process are inferior to the best reported values. Then different solid state synthesis method was used (namely, planetary milling and ball milling) to prepare BZT- 0.5BCT with an aim to improve the dielectric and piezoelectric properties further. It has been observed that planetary milling technique is best to achieve good dielectric and piezoelectric property in BZT-0.5BCT ceramics. By this method, 98% dense ceramic could be prepared at 1350°C. BZT-0.5BCT ceramic prepared by planetary milling shows high relative permittivity (3535) with low dielectric loss (0.014) with high piezoelectric coefficient (d_{33} = 350 pC/N) compared to other two method (combustion synthesis and solid state synthesis via ball milling). It has also been studied that how close compositional modifications (x=1%) around MPB in xBZT-(1-x)BCT (x= 0.47-0.53) alters the structural and ferroelectric property. It is observed that the occurrence of multiple phases at narrow regions around orthorhombic and tetragonal phases, which might be unstable and served as structural bridge in MPB regions and played a significant role in getting high dielectric and piezoelectric property near the MPB at room temperature.

An attempt has also been made to sinter BZT- 0.5BCT at low temperature (<1200°C) and study its dielectric property. It has been found that BZT-0.5BCT could be densified to 98% relative density using $LiBiO_2$ as the sintering aid at a temperature as low as 1100°C. $LiBiO_2$ addition significantly modifies dielectric property and improves dielectric breakdown strength and energy density.

An attempt has been made to study whether BZT-0.5BCT could be used to form a solid solution with NBT with an aim to improve the dielectric, piezoelectric properties and shift Curie temperature to higher temperature of BZT-BCT or BNT. The attempt to increase the T_C of BZT-BCT by incorporating NBT in BZT-BCT failed due to incompatibility between the two phases and poor densification. However, the incorporation of BZT-0.5BCT in NBT is successful. Upto 5 mol% incorporation of BZT- 0.5BCT in NBT improves the dielectric and piezoelectric property of the later.

Key Words: Lead-free Ferroelectric; Solution combustion Method; $BaTiO_3$; Perovskite; X-ray diffraction; Dielectric properties; Ferroelectric properties; Piezoelectric properties; $(Ba_{0.85}Ca_{0.15})(Ti_{0.9}Zr_{0.1})O_3$[BZT-0.5BCT]; $Bi_{0.5}Na_{0.5})TiO_3$[BNT];Low Temperature Sintering.

LIST OF FIGURES

LIST OF TABLES

Nomenclature

N : Avogadro’s number

K : Boltzmann constant

Tc : Curie temperature

λ : X-ray wavelength

θ : Bragg’s angle

JCPDS : Joint committee on powder diffraction standards

XRD : X-ray diffraction

a, b, c : Lattice parameter

(h k l) : Miller indices

t : tolerance factor

ρ : Density

I : Intensity

°C : Degree in Celsius

PVA : Polyvinyl alcohol

IPA : Isopropyl alcohol

C : Capacitance

ε : Relative Permittivity

$\tan\delta$: Dissipation factor

A : Area

d : thickness

d_{33} : Piezoelectric coefficient

Tm : Maximum permittivity temperature

Pr : Remnant polarization

Ec : Coercive field

ΔT_m : Degree of Deviation from the Curie-Weiss law

Tcw : Curie-Weiss temperature

γ : Diffuseness constant

DSC : Differential Scanning Calorimetry

TG : Thermo-Gravimetric Analysis

F : Frequency

I : Current

V : Voltage

s : Second

MAUD : Materials Analysis Using Diffraction

SEM : Scanning Electron Microscope
FESEM : Field emission Scanning Electron Microscope
MPB : Morphotrophic phase boundary
BT : Barium titanate
BZT : Barium zirconate titanate
BCT : Barium calcium titanate
BCTZ : Barium calcium zirconate titanate
BZT10 : $Ba(Zr_{0.1}Ti_{0.9})O_3$
BZT15 : $Ba(Zr_{0.15}Ti_{0.85})O_3$
BZT20 : $Ba(Zr_{0.2}Ti_{0.8})O_3$
BZT-0.5BCT/BCTZ10 : $(Ba_{0.85}Ca_{0.15})(Ti_{0.9}\,Zr_{0.1})O_3$
BCTZ15 : $(Ba_{0.85}Ca_{0.15})(Ti_{0.85}\,Zr_{0.15})O_3$
BCTZ5 : $(Ba_{0.85}Ca_{0.15})(Ti_{0.95}\,Zr_{0.05})O_3$
BNT : $(Bi_{0.5}Na_{0.5})TiO_3$
MS : Microwave Sintering
CS : Conventional Sintering
T_d : Depolarization Temperature
PPT : Polymorphic phase transition

CONTENTS

Chapter 1

Introduction

1. Introduction

Oxide materials with perovskite structure having general formula ABO_3 form the back bone of the ferroelectric industry. For a long time, ferroelectric ceramics have been found to be useful for various practical applications, such as high dielectric constant capacitors, piezoelectric sonar and ultrasonic transducers, radio and communication filters, pyroelectric devices, medical diagnostic transducers, positive temperature coefficient (PTC) sensors, ultrasonic motors and electro-optic light valves.

1.1 Ferroelectrics and related materials

To understand the definition of ferroelectricity, it is necessary to mention piezoelectricity and pyroelectricity because they have interesting relationship in terms of crystal structures. Crystals are classified into 32 point groups based on their symmetry. These 32 point groups are subdivisions of 7 basic crystal systems that in ascending order of symmetry include; triclinic, monoclinic, orthorhombic, tetragonal, rhombohedral (trigonal), hexagonal and cubic. These point groups are divided into two classes which include a center of symmetry and without center of symmetry. There are 21 non-centrosymmetric point groups, 20 (except point group 432) of which exhibit piezoelectricity. Fig. 1.1 shows that there are 10 crystal classes out of a possible 20 that are designated as pyroelectric. This group of materials possess the unusual characteristic of being permanently polarized within a given temperature range. Unlike the more general piezoelectric classes that produce a polarization under stress, the pyroelectrics develop this polarization spontaneously and form permanent dipoles in the structure. This polarization also changes with temperature hence, the term pyroelectricity. A subgroup of the spontaneously polarized pyroelectrics is a very special category of materials known as ferroelectrics. Similar to pyroelectrics, materials in this group possess spontaneous polarization; however, unlike pyroelectrics, the direction of the spontaneous polarization is orientable by an electric field of some magnitude less than the dielectric breakdown of the material itself. As all pyroelectric materials are polar, and ferroelectrics are a sub-group of these pyroelectric materials; all ferroelectrics are pyroelectrics and piezoelectrics both. These crystals show large dielectric constant and high electro-mechanical coupling factor. Polycrystalline ceramics of these materials also show the ferroelectric effect after poling. Ferroelectric materials have four subcategories: the perovskite (ABO_3) group, the pyrochlore group ($A_2B_2O_7$), the tungsten-bronze group (AB_2O_6), the bismuth layer structure group ($A_4B_3O_{12}$), among which the perovskite group is the most important and thus the most widely studied. The ABO_3 type ferroelectric ceramics are further divided into $BaTiO_3$, $Pb(Zr_xTi_{1-x})O_3$, $(Bi_{0.5}Na_{0.5})TiO_3$ and $(K_xNa_{1-x})NbO_3$ family of compositions [1,2].

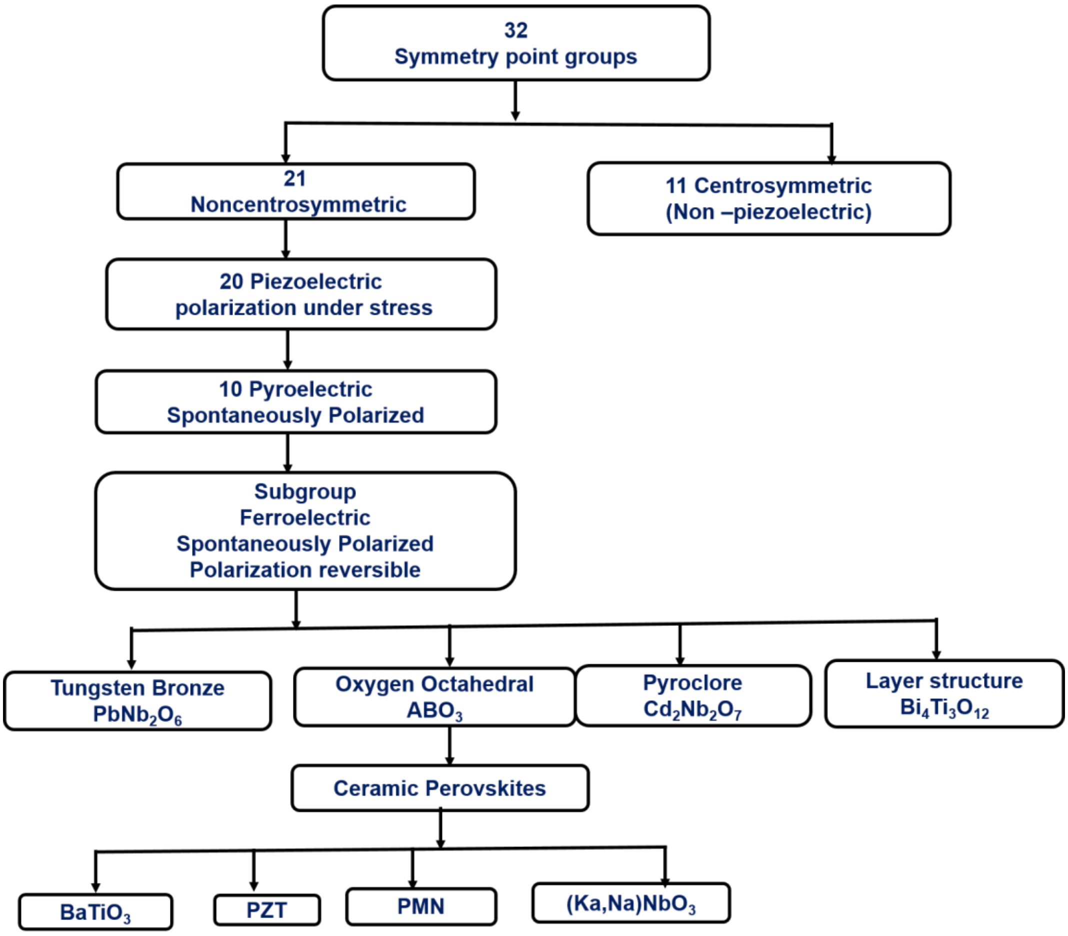

Figure 1.1 Interrelationship of piezoelectric and subgroups on the basis of symmetry [1].

Below the Curie temperature, ferroelectric crystals generally develop a random domain structure, leading to a net zero polarization of each crystal. Within each ferroelectric domain the polarization is in the same direction with a domain wall separating regions with different polarization directions. This structure is necessary to minimize free energy due to the development of anisotropic strains and depolarization fields below T_C. Domain walls are characterized by the angle between the polarization directions on either side of the wall. Thus a 180^o domain wall demarks a boundary between antiparallel domains, while a 90^o wall would be formed at the boundary between domains pointed “up” and “left”, for example. The allowed angles for domain walls depend on the orientation of the spontaneous polarization allowed by symmetry. Thus in rhombohedrally distorted perovskites, there are no 90^o domain walls like a tetragonal perovskite, but instead 71^o and 109^o walls. A more complete picture of the way the polarization changes as a domain wall is crossed is given by Cao and Cross [3].

1.2 Curie temperature (T_C)

Ferroelectric crystals exhibit electric dipole moments even in the absence of an external electric field below a certain temperature and a paraelectric behavior above this temperature. This temperature of structural phase transition from a high-temperature non ferroelectric paraelectric phase to a low-temperature ferroelectric phase is called the Curie temperature (Tc). This polarization can be reoriented or reversed fully or in part by applying an electric field. The spontaneous polarization in a ferroelectric material is usually not uniformly aligned throughout the whole material along the same direction. The regions in the material with uniformly oriented spontaneous polarization are called ferroelectric domains and the region separating two domains is called a domain wall. Ferroelectric domains form to minimize the electrostatic energy of depolarizing fields and the elastic energy associated with mechanical constraints to which the ferroelectric material is subjected as it is cooled through paraelectric - ferroelectric or ferroelectric - ferroelectric phase transition. Types of domain walls that can occur in a ferroelectric crystal depend on the symmetry of both non-ferroelectric and ferroelectric phases of the crystal. The domain walls are usually labeled by the angle between the spontaneous polarization vectors in the domains that these walls separate. For example, 90°-walls are those which separate regions with mutually perpendicular polarization (although the angle between polarization directions on each side of a 90° domain wall is slightly smaller than 90◦) [4, 5].

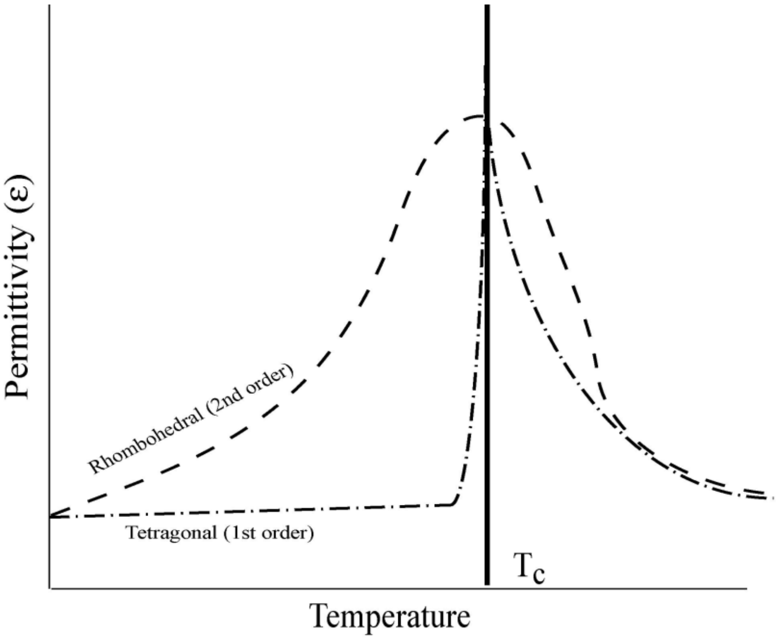

Figure 1.2 Idealized permittivity of ferroelectric material as a function of temperature.

In ferroelectrics dominated by a displacive phase transition, such as perovskite materials, the temperature dependence of the permittivity varies for 1st and 2nd order phase transitions. Fig. 1.2 illustrates the temperature dependence of the permittivity for displacive ferroelectric materials exhibiting first or second order phase transitions. Second order phase transitions, which are common for rhombohedral compositions, are generally characterized by a broad peak in permittivity. Ferroelectrics undergoing first order phase transitions, typical of tetragonal perovskite materials, however show a fairly flat permittivity with increasing temperature right up to the T_c.

The reciprocal permittivity 1/ε is known to be linear with respect to the temperature in a wide range in the paraelectric phase (so-called Curie-Weiss law), stated as

$$\varepsilon = \frac{C}{T - T_0} \qquad (1.1)$$

where C is the Curie-Weiss constant and T_0 the Curie-Weiss temperature. T_0 is slightly lower than the exact transition temperature Tc. For displacive transitions (e.g., $BaTiO_3$, $PbTiO_3$, $KNbO_3$), the Curie Constant is very high (~ 10^4 – 10^5K) and the paraelectric phase is microscopically nonpolar. For order-disorder transition (e.g., TGS, KH_2PO_4), the Curie constant is of the order of T_0 and the paraelectric phase is nonpolar on macroscopic or thermally averaged sense. The reorientable component of the spontaneous polarization of ferroelectric materials falls to zero at the Curie temperature.

1.3. Hysteresis loop

Hysteresis loop, as a simple and effective tool, is the most accepted method to understand ferroelectric materials [6]. In principle, every ferroelectric material has its own unique hysteresis loop, as a fingerprint. Through the hysteresis loops, the ferroelectricity could be identified directly. Fig.1.3 is a typical ferroelectric hysteresis loop, through which the characteristic parameters, such as spontaneous polarization (Ps), remnant polarization (Pr) and coercive field (Ec) can be determined. Owing to the requirement of the energy minima, the grains in polycrystalline materials are always splitting into many domains. The directions of the domains are randomly distributed in such a way to lead to zero net macroscopic polarization. When the external field exceeds the Ec, the polycrystalline ferroelectric ceramic may be brought into a polar state. As shown in Fig.1.3, a macroscopic polarization is induced gradually by increasing the electric field strength. The drastic variation in the polarization in the vicinity of Ec is mainly attributed to the polarization reversal (domain switching), while at high field end, the polarization is saturated and the material behaves as a linear dielectric.

When the electric field strength starts to decrease, some domains would back-switch, but at zero field the net polarization is nonzero, leading to the remnant polarization Pr. To obtain a zero polarization, an electric field with opposite direction is needed. Such field strength is called the coercive field (or coercivity). With increasing the opposite field strength, a similar rearrangement of the polarization is observed in the negative field part. For ferroelectric materials, the spontaneous polarization Ps may be estimated by intercepting the polarization axis with the extrapolated linear segment, as shown in Fig. 1.3. Since ferroelectrics usually possess ferroelastic domains (with the exception of $LiNbO_3$,which only has 180° ferroelectric domains), spontaneous strain is also induced with the external electric field simultaneously.Therefore, if the strain is monitored as well as the polarization, a strain–electric field curve, like “butterfly,” can be observed.

For ideal ferroelectric system, the observed hysteresis loops should be symmetric. The positive and negative E_c and P_r are equal. In reality, the shape of the ferroelectric hysteresis loops may be affected by many factors, such as thickness of the samples, material composition, thermal treatment, presence of the charged defects, mechanical stresses, measurement conditions and so on. Their effects on material properties could be well reflected through the loops. For the same material system, ferroelectric hysteresis loops of single crystalline and polycrystalline ceramic samples show a large difference. This is mainly attributed to the clamping effect of domains with respect to grain boundaries. It can be seen in Fig.1.4, the shape of the P–E loop for $BaTiO_3$ (BT) crystal is rather square, whereas for BT ceramics the loop is slanted at a certain degree. By applying the same electric field, saturated polarization can be induced in BT crystal instead of ceramic, suggesting that the polarization switching in crystal is much easier than that in ceramic, owing to the absence of grain boundary. In addition, due to the crystal symmetry, domains in tetragonal BT single crystal could be switched completely with respect to the external field applied along [001] direction. In contrast, because of the random distribution of the grains, maximum 83% polarization can be switched in ceramics without considering the clamping effect by adjacent grains. This partially explained the lower spontaneous polarization observed in BT ceramic. Thus, BT single crystal was found to possess a lower E_c with a higher P_r, when compared to those of BT ceramics. Fig.1.4 shows ferroelectric hysteresis loops for BT crystal, coarse grain and fine grain ceramics, exhibiting a transition from square loop to slim loop with decreasing the grain size. Here, crystal sample can be considered as a very large grain without grain boundary. Therefore, the clamping effect due to the neighboring grains is absent in crystals.

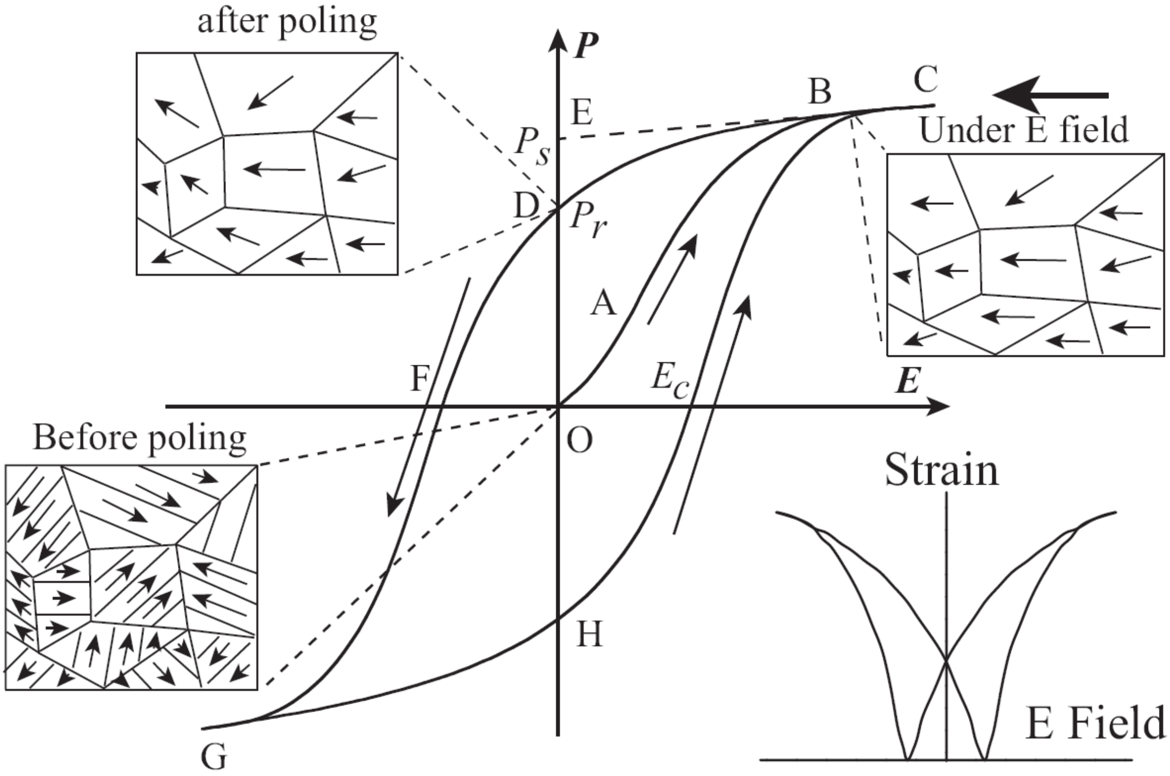

Figure 1.3 A typical hysteresis loop in ferroelectrics and corresponding domain reversal (polarization rotation) and strain–electric field curve [7].

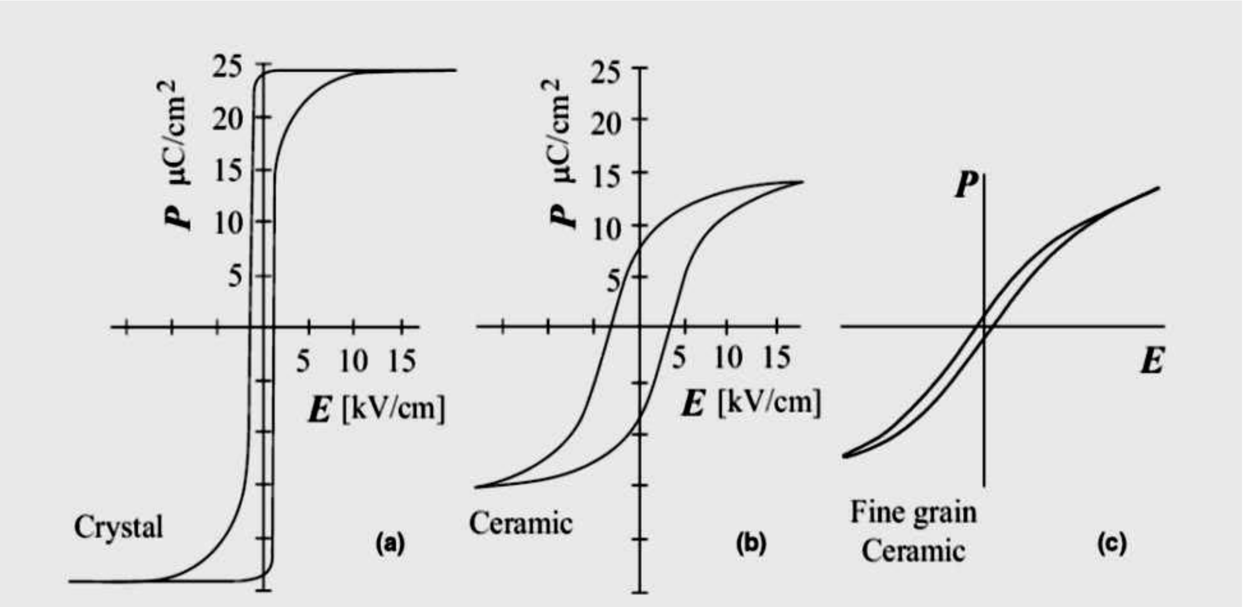

Figure 1.4 Room-temperature P–E hysteresis loops for BT single crystal and ceramics with different grain size. (a) BT single crystal, (b) BT ceramics with coarse grain, (c) BT ceramics with fine grain [8].

1. 4 Different Origins of Ferroelectricity

Recently, Mostovoy et al. [9] classified ferroelectrics into two different classes, viz., 1) proper ferroelectrics and 2) improper ferroelectrics, and the detailed classification is given in Table 1.1. Perovskites consist of corner-sharing O_6 octahedra with a transition metal ion at the centre. Almost all the ferroelectric perovskites contain non-magnetic transition metal ions with an empty *d*-shell (d^0 configuration), for example Ti^{4+}, Nb^{5+} and W^{6+}. These positively charged ions like to form 'molecules' with one (or several) of the neighbouring negative oxygen ions. In all of these systems ferroelectricity originates from a shift of the transition metal ion from the centre of the O_6 octahedron. In this way a stronger covalent bond with one (or three) instead of six weaker bonds with neighbouring oxygen atoms is formed [10]. This collective shift of cations and anions inside a periodic crystal induces a bulk electric polarization. The mechanism of the covalent bonding (electronic pairing) in such molecules is the virtual hopping of electrons from the filled oxygen shell to the empty *d* shell of a transition metal ion.

Table 1.1: Classification of ferroelectrics [9]

	(Mechanism of inversion symmetry breaking)	Materials
Proper	Covalent bonding between $3d^0$ transition metal (Ti) and oxygen	$BaTiO_3$, PZT
	Polarization of $6s^2$ lone pair of Bi or Pb	$BiMnO_3$, $BiFeO_3$, $Pb(Fe_{2/3}W_{1/3})O_3$
Improper	Structural transition 'Geometric ferroelectrics'	K_2SeO_4, Cs_2CdI_4 hexagonal $RMnO_3$
	Charge ordering 'Electronic ferroelectrics'	$LuFe_2O_4$
	Magnetic ordering 'Magnetic ferroelectrics'	Orthorhombic $RMnO_3$, RMn_2O_5, $CoCr_2O_4$

If, on the other hand, polarization is only part of a more complex lattice distortion or if it appears as an accidental by-product of some other ordering, the ferroelectricity is called 'improper' [11]. For example, the hexagonal manganites $RMnO_3$ (R = Ho–Lu, Y) show a lattice transition which enlarges their unit cell. An electric dipole moment, appearing below this transition, is induced by a nonlinear coupling to nonpolar lattice distortions, such as the buckling R–O planes and tilts of manganese–oxygen bipyramids (geometric ferroelectricity) [12].

1.5 Relaxor ferroelectric and diffused phase transition

The properties of most compositions based on $BaTiO_3$ do not vary greatly with frequency above about 500 Hz until the gigahertz range is reached. However, certain ferroelectrics, known as ‘relaxor’, show a pronounced change in permittivity with frequency at temperatures near the Curie point. The term ferroelectric with a ‘diffuse phase transition’ (DPT) appeared in the literature for the first time in 1954 in Smolenskii’s papers [13]. Ferroelectric DPT is often observed in solid solutions or in compounds in which a site is occupied by two or more cations. It is the case for example of a lot of perovskite, pyrochlore and quadratic tungsten bronze compounds, e.g., $Pb(Mg_{1/3}Nb_{2/3})O_3$, $Pb(Fe_{2/3}W_{1/3})O_3$, $Bi_2\ (Mg_{2/3}Nb_{4/3})O_7$ and $(Ba,Sr)(Nb.Ta)_2O_6$. Materials with DPT are characterized by the following:

1. An unusual relaxation of dielectric polarization in the phase transition region characterized by the shape of the curve of the temperature variation of the permittivity and loss factor and their dependence with the frequency of the measuring electric field. Fig.1.5 illustrates the typical relaxor behavior of PMN [$Pb(Mg_{1/3}Nb_{2/3})O_3$] ceramics.
2. A hysteresis loop degenerating slowly as the temperature increases, indicating that the spontaneous polarization does not disappear suddenly at the Curie temperature Tc (or precisely, Tm, temperature of dielectric constant maximum) as it is for a classical ferroelectric such as $BaTiO_3$, but decays more gradually to zero at a temperature far above the value of Tc.
3. An absence of apparent symmetry change as the temperature is lowered down the DPT without any applied external field.

To explain this behavior, Smolenskii’s and his co-workers [14] proposed the existence of composition fluctuations. Because of the dependence of Tm with the composition, different microregions of the crystal have different transition temperatures. Therefore, the global phase transition of the crystal consists in a great number of phase transitions of the microregions and is consequently observed in a wide temperature range. This induces an intimate mixture of ferroelectric (polar) and paraelectric (non-polar) regions, in a wide temperature range. The size of the polar nanodomains has been evaluated to be around 100 nm [15] or even less [16].

Incidentally, relaxors like $Pb(Mg_{1/3}Nb_{2/3})O_3$ or $Pb(Sc_{1/2}Ta_{1/2})O_3$ show [17-19] non-ergodic behaviour at a low temperature as a result of freezing and phase transition into a long range ferroelectric state induced by a dc electric field around the freezing temperature (T_F). The relaxor state arises from the existence of lattice disorder and there is an evidence of the presence of polar nanodomains in a soft mode host lattice at temperatures much higher than Tm. It is believed that random fields generated due to local charge imbalance [20] results in the relaxor behavior either by breaking up [21, 22] a ferroelectric state to nanodomains or by generating a glass state [23, 24] similar to dipolar glasses with randomly interacting polar nanoregions. By considering the fluctuating nanodomains of relaxors as fluctuating giant dipoles, the relaxor effect may be understood [25] as a manifestation of more generalized low frequency dispersion (LFD) phenomenon extended to the radio frequency range.

It may be noted that the relaxation behavior similar to relaxors has been observed in $BaTiO_3$ doped [26, 27] with Zr, Y, Hf, Ce, etc. In case of $BaTiO_3$ ceramics, the dielectric properties of $BaTiO_3$ transform according to the following scenario: first, the temperatures of the transition between different ferroelectric phases increase and come close to each other. Simultaneously, Tc goes down: second, at a certain concentration of substituting elements, all these transitions merge, a so-called pinched transition occurs [28]. The system then directly transforms from the cubic paraelectric to the rhombohedral ferroelectric state. The corresponding peak of ε′(T) is usually much broader than that in $BaTiO_3$, however, without the frequency shift of Tm, a typical of relaxors. Such behavior is occasionally denoted as a diffuse phase transition (DPT) to distinguish it from the relaxor one. Another hallmark of the DPT is a deviation of the dependence of the real part of the dielectric permittivity ε′(T) from the Curie–Weiss law at T > Tm. This deviation usually starts at temperatures significantly larger (up to hundreds of degrees) than Tm. The DPT is considered to be due to local composition fluctuations, resulting in microregions with different local Curie points distributed in a Gaussian fashion around a mean Curie temperature [29].

In order to describe the diffuse phase transition, the modified Curie Weiss law was introduced. The modified Curie–Weiss law is defined by following relation [30]

$$\frac{1}{\varepsilon}-\frac{1}{\varepsilon_m}=\frac{(T-T_m)^{\gamma}}{C'} \qquad (1.2)$$

where γ and C' are constants, ε_m and T_m are the dielectric constant maximum for the corresponding temperature. The parameter γ gives information on the character of the phase transition: for $\gamma = 1$, a normal Curie–Weiss law is followed, whereas $\gamma= 2$ describe a complete diffuse phase transition.

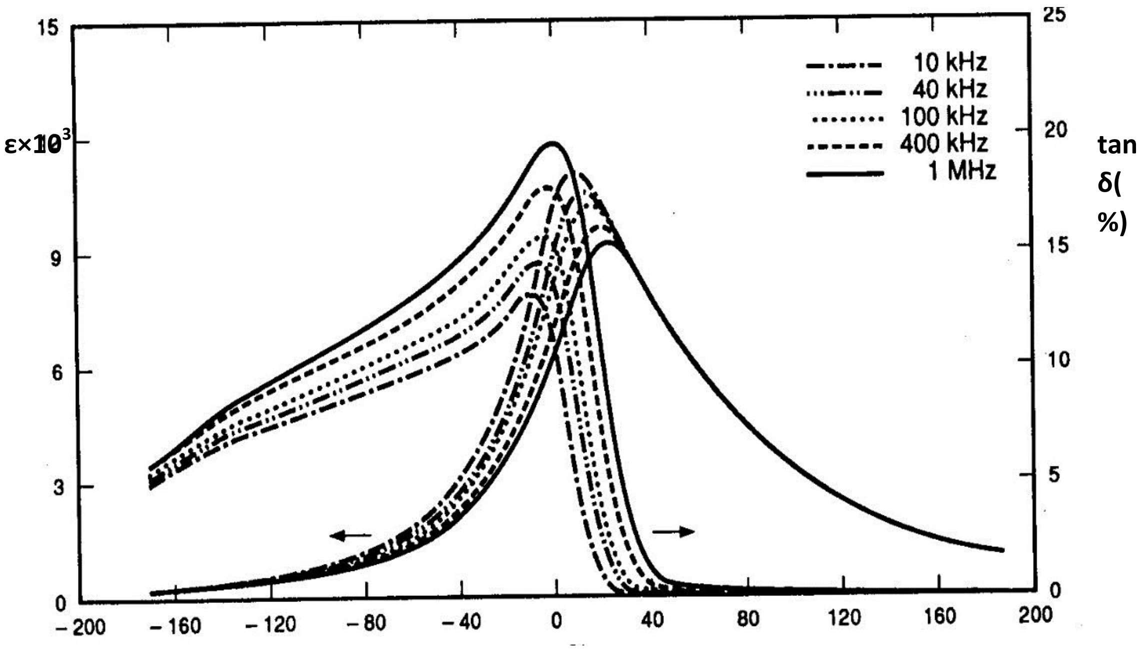

Figure 1.5.Variation of the permittivity and the loss factor with temperature and frequency for PMN [17].

1.6. Piezoelectricity

Piezoelectricity is the ability of some materials to convert mechanical energy to electric energy (direct piezoelectric effect) or electric energy to mechanical energy (converse piezoelectric effect). The piezoelectric effect was first discovered in 1880 by the brothers Pierre and Jacques Curie. The piezoelectric effect occurs in most classes of non-centrosymmetric crystals, in which electric dipole moments can be induced as a result of applied stress.

The mathematical expression for direct piezoelectric coefficient is written by

$$P_i = d_{ijk}\sigma_{jk} \qquad (1.3)$$

where P is the polarization, d_{ijk} is the piezoelectric charge coefficient and a 3rd rank tensor; σ is an applied stress and a 2nd rank tensor, and the subscripts i, j, k run from 1 to 3 using the Einstein convention.

The mathematical expression for converse piezoelectric coefficient is written by

$$x_{ij} = d_{ijk}E_{jk} \qquad (1.4)$$

where *x* is the strain developed, and E is an applied electric field. The piezoelectric coefficient, d, is numerically identical for both direct and converse piezoelectric effects for free boundary conditions.

It should be noted that the notation for the 3rd rank tensor d_{ijk} is often shortened to $d_{ij'}$, where j' = 1, 2, 3, 4, 5, 6 corresponds to jk = 11, 22, 33, 23 or 32, 13 or 31, 12 or 21, respectively (Example d_{333}= d_{33}, d_{311}= d_{31}) [2, 31].

The constant d_{ij} and g_{ij} are related through the equation

$$g_{ij} = \frac{d_{ij}}{\varepsilon_0 \varepsilon_{ij}} \qquad (1.5)$$

where ε_0 and g_{ij} are the permittivity of the free space and piezoelectric voltage co-efficient .

The three imporant operation modes of a piezoelectric crystal(or poled ceramics) are illustrated in Fig.1.6.

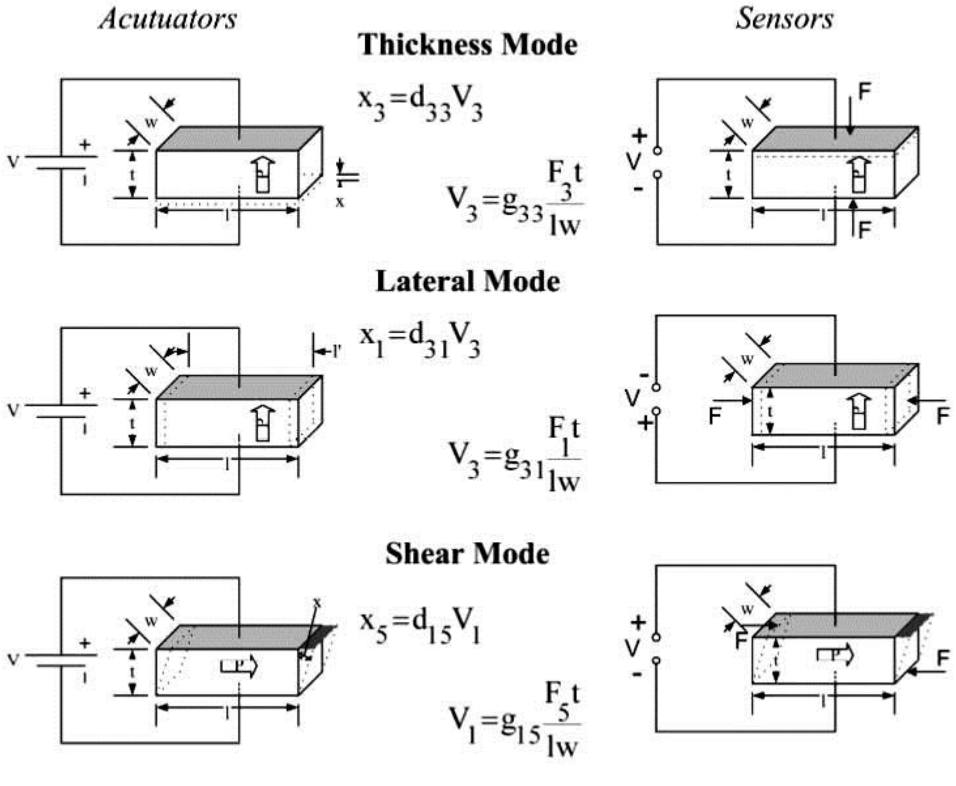

Figure 1.6. Operational modes of piezoelectric actuators, sensors, and accompanying formulae where V=voltage, x=strain, F=force, P = poling direction and t, w, l are relevant dimensions as illustrated in the figure.

In electrostriction, the induced strain is proportional to the square of the electric field. In contrast, the strain is linearly proportional to the field for the converse piezoelectric effect. Another distinction is that electrostriction is observed in all dielectric materials, whereas piezoelectricity is allowed only in non-centrosymmetric materials [2].

The electrostriction can be written as

$$x_{ij} = M_{ijkl} E_k E_l \tag{1.6}$$

Where the 4th rank tensor M_{ijkl} gives the electrostrictive coefficients in terms of electric field. As explained above, strain is proportional to E^2.

Electrostriction can also be described in terms of polarization x_{ij} as,

$$x_{ij} = Q_{ijkl} P_k P_l \tag{1.7}$$

Where the 4th rank tensor Q_{ijkl} gives the electrostrictive coefficients in terms of polarization. Simplifying the above equation for linear dielectric

$$M_{ijkl} = Q_{ijkl} \varepsilon_0{}^2 \varepsilon_r{}^2 \tag{1.8}$$

This equation is a more consistent way to describe the electrostrictive effect in dielectrically nonlinear materials.

The temperature dependence of the piezoelectric coefficients can be written in term of electrostriction (Q) and remnant polarization (P_r)

$$d = 2Q\varepsilon_0 \varepsilon_r P_r \tag{1.9}$$

This implies that materials with high P_r and ε_r should have high piezoelectric coefficients.

The piezoelectric response in ferroelectric materials can be further broken down into intrinsic and extrinsic contributions. Intrinsic contributions are those due only to strain in the crystal lattice. In general, these are reversible contributions and occur without loss [32]. Extrinsic contributions generally vary as a function of time, frequency and field and are non-linear and lossy, and may contribute substantially to the bulk piezoelectric response in ferroelectric materials. Extrinsic effects are generally attributed to the motion of domain walls separating regions with different local polarization directions and phase boundary shifts [33]. Understanding the contribution of both intrinsic and extrinsic components of piezoelectric response is vital to controlling and optimizing the properties of piezoelectric materials.

Another important parameter of a piezoelectric specimen is electromechanical coupling coefficient k which is defined as follows

$$k^2 = \frac{\text{Electrical energy converted in to mecanical energy}}{\text{Input electrical energy}} \tag{1.10}$$

or
$$k^2 = \frac{\text{Mecanical energy converted in to electectri cal energy}}{\text{Input mecanical energy}} \quad (1.11)$$

If an AC voltage of varying frequency is applied to a piezoelectric ceramic (piezoelectric transducer) of a certain shape, it can be seen that there is a specific frequency at which the ceramic produces a very strong vibration. This frequency is called the resonant frequency, f_r and depends on the ceramic's specific elastic vibration (resonance) frequency, which is a function of the size and shape of the material. Piezoelectric ceramics have various vibration modes (resonant modes) which depend on the shape of the ceramics, orientation of polarization, and the direction of the electric field (e.g., radial modes, thickness mode, shear mode etc.). Radial mode for a thin disk is described as a vibration mode along the radial direction, where the polarization is oriented along the thickness of the disk. In the thickness mode, vibration is oriented along the direction of polarization. In the shear mode, electrical field is orthogonal to the direction of polarization, causing a shear vibration along the surface.

1.7 Lead zirconate titanate (PZT)

PZT is a solid solution of $PbZrO_3$ and $PbTiO_3$ and the compositions around $Pb(Zr_{0.52}Ti_{0.48})O_3$ are of technical importance. PZT and modified PZT are materials of choice for transducer applications [2, 34]. The PZT phase diagram is shown in Fig.1.7 [35] where it can be seen that the morphotropic phase boundary (MPB) is a significant feature. An MPB denotes an abrupt structural change with composition at constant temperature in a solid solution range. It has a coercive field of about 1 kV/mm and a remnant polarization of about 35µC/cm^2. Unipolar electric field excursions typically from zero electric field to 2–3 kV/mm, corresponding to a potential of about 200V at a typical layer thickness of 80 mm, provide a strain of 0.1%–0.2%. A large- signal piezoelectric coefficient as large as 779 pm/V has been reported for doped PZT [36].

The more recent discovery of very high piezoelectric response in relaxor-ferroelectric single crystals, $Pb(Mg_{1/3}Nb_{2/3})O_3$–$PbTiO_3$ and $Pb(Zn_{1/3}Nb_{2/3})O_3$–$PbTiO_3$, which exhibit coupling coefficients as high as 94% and piezoelectric coefficients of 2500 pC/N (or five times higher than commercial PZT) have triggered a parallel search for high-performance lead-free single crystals[37,38].

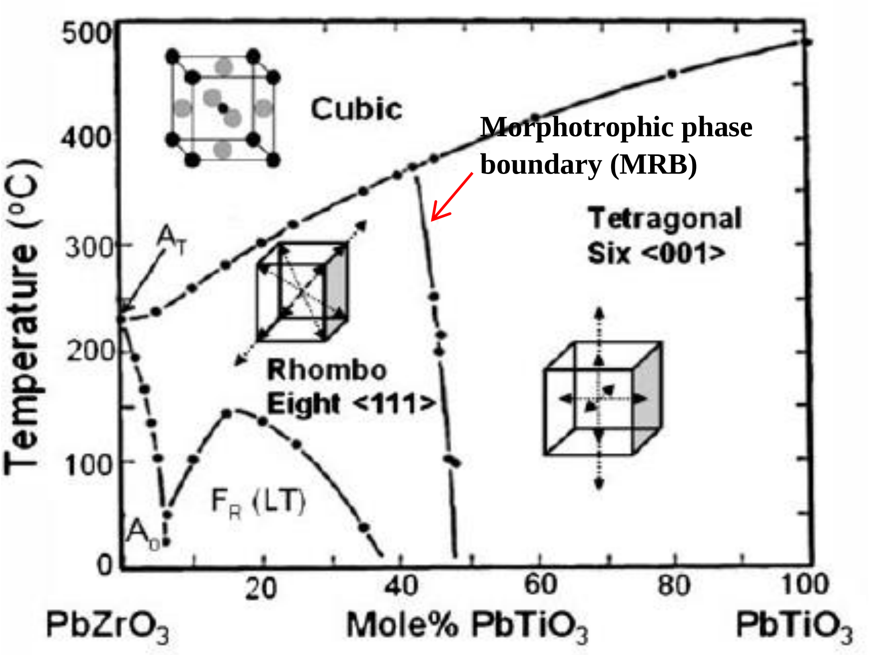

Figure 1.7 Phase diagram of $PbZrO_3$ -$PbTiO_3$ ceramic [35].

1.8. Lead free ferroelectric ceramics

The major drawback of PZT concerns its lead content. The amount of lead in the usual lead-containing ceramics is more than 60 wt%, and once the lead comes into the human body, it accumulates in various organs, leading potentially to fatal effects to fetus, infertility, cancer and so forth. Note that not only the lead in lead-based compounds such as PZT but also the lead oxide as a starting material are known to dissolve when they are exposed to an aqueous environment[39]. However, high volatilization of lead oxide and its toxicity can contaminate the environment and harm to human health, and then causes a serious problem of environment pollution. In 2006, the European Union has already adopted the well-known directives Waste Electrical and Electronic Equipment (WEEE) and Restriction of the use of certain hazardous substances in electrical and electronic equipment (RoHS) with the purpose of protecting human health as well as environment by exclusion or substitution of hazardous substances used in electrical and electronic devices. Similar regulations are also planned or established in North America, Japan, Korea and China. A lot of literature sources about lead-free ferroelectric ceramics are available now-a-days however the deeper research is needed in order to substitute lead-based materials [40, 41]. Therefore, tremendous efforts have been devoted in last decade for the development of competitive lead free counterparts, such as $BaTiO_3$, $(Bi_{1/2}Na_{1/2})TiO_3$(BNT)-based perovskite, (K, Na)NbO_3 (KNN) based perovskites, bismuth layer-structured ferroelectrics (BLSF) and so on [42-45]. Fig. 1.8 provides statistics for refereed publications on lead-free piezoceramics from 1950 up to 2008.

Till date the properties of developed lead free piezoelectrics are not comparable to that of PZT based compositions. $BaTiO_3$ is a model ferroelectric mostly utilized for capacitor and thermistor applications [35, 46, 47]. The breakthrough made by Liu and Ren et al. in $BaTiO_3$-based ceramics with co-dopants of Zr and Ca has offered a significant impact on the development of lead-free piezoceramics [48]. The pure $BaTiO_3$ ceramics are normally associated with a poor piezoelectric coefficient d_{33} as low as 191 pCN^{-1} [2], the value reported by Liu and Ren et al. [48] reached more than 500 pC/N, comparable to that of soft PZT ceramics. The proposed origin of high piezoelectricity was formation of MPB between $Ba(Zr_{0.2}Ti_{0.8})O_3$-$0.5(Ba_{0.7}Ca_{0.3})TiO_3$[BZT- 0.5BCT]. The piezoelectric properties of lead free and lead based family are shown in Fig 1.9.

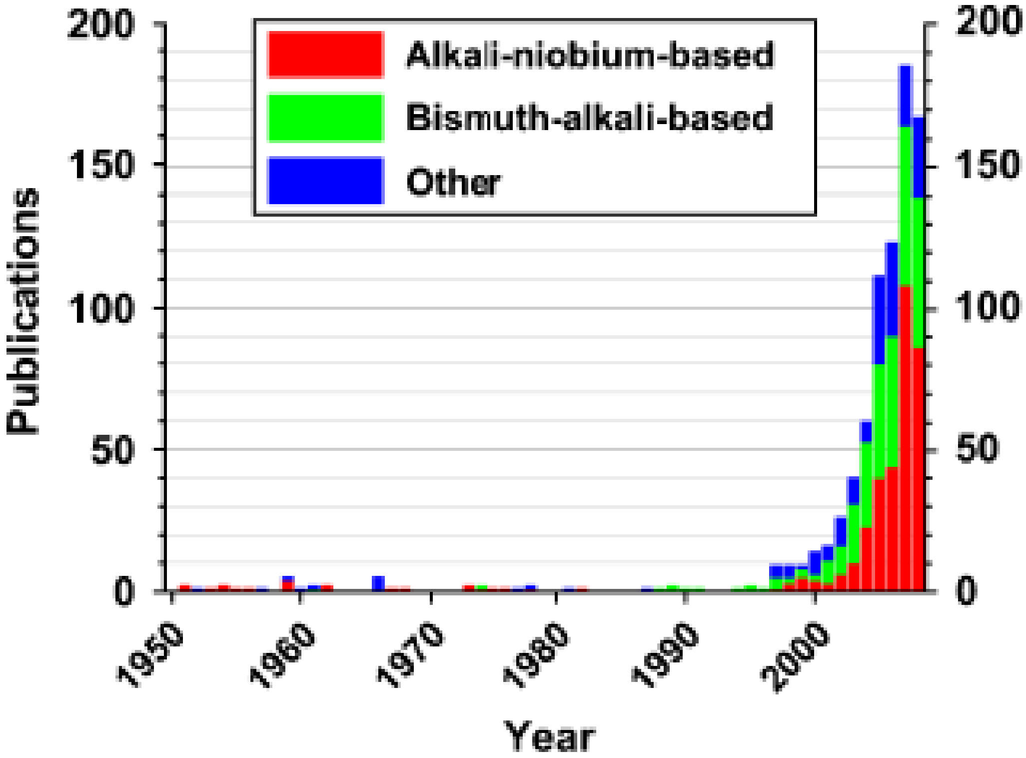

Figure1.8. Publications on lead-free piezoceramics in refereed journals for the time range from1950 to November 2008[39].

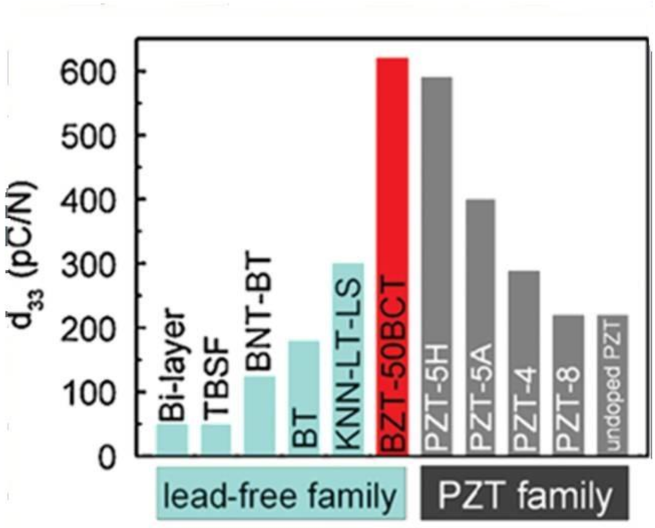

Figure 1.9 Comparison of piezoelectric coefficient for lead free piezoelectrics and PZT family [48].

1.8.1 $BaTiO_3$ Ceramics

Barium titanate is the first ferroelectric ceramic material which was described by Wul and Goldman in 1946 [49]. It is isostructural with the mineral perovskite ($CaTiO_3$) and so is referred to as 'a perovskite'. The generalized perovskite structure ABO_3, is visualized as based on a cubic close-packed assembly of composition AO_3 with the A-ion cordinated with 12 oxygen ions and the B-ion in the octahedral interstices are shown in Fig. 1.10. In the ABO_3 structure, the large cation (A) is at the corners while the small cation (B) is at the body center and oxygen is located at the center of the faces.

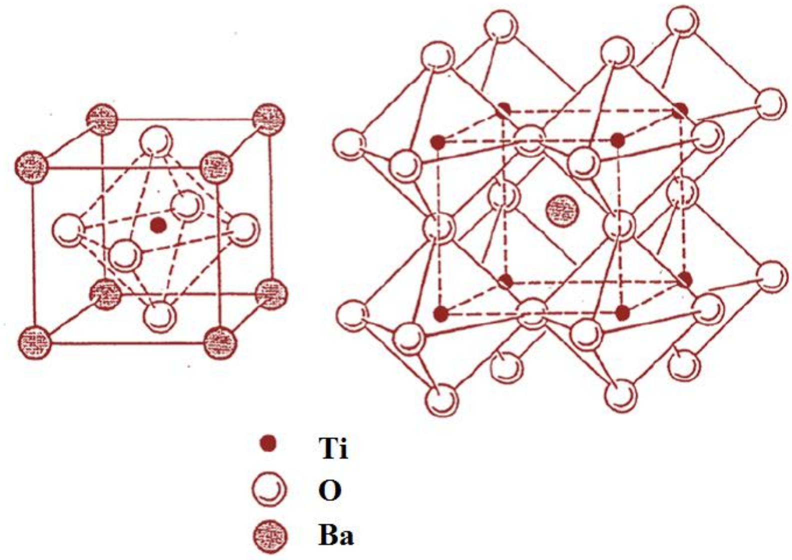

Figure 1.10 Schematic view of the perovskite ABO_3 unit cell for cubic $BaTiO_3$ ceramic with the space group (Pm3m) and lattice constant ~4Å [50].

According to Goldschmidt (1926), the geometrical requirement for the formation of the perovskite structure is that the ionic radii r_A, r_B and r_O of the A, B and the O ions must satisfy the following relationship:

$$t = \frac{r_A + r_O}{\sqrt{2}(r_B + r_O)} \qquad (1.12)$$

where t is called the tolerance factor. An ideal cubic perovskite structure where t=1.0 and r_A, r_B and r_O indicate the ionic radius of large cation, small cation and anion respectively. In general ferroelectric ABO_3, the most stable structure is tetragonal for $t \geq 1$, cubic for $t \approx 1$ and rhombohedral or orthorhombic symmetries for $t < 1$[51, 52].

For $BaTiO_3$, above its Curie point (approximately 130°C) the unit cell is cubic. Below the Curie point the structure is slightly distorted to the tetragonal form with a dipole moment along c direction. Other transformations occur at temperatures close to 0°C and -90°C: below 5°C the unit cell is orthorhombic with the polar axis parallel to a face diagonal and below -90°C it is rhombohedral with the polar axis along a body diagonal. The various phases of $BaTiO_3$ is shown in fig 1.11

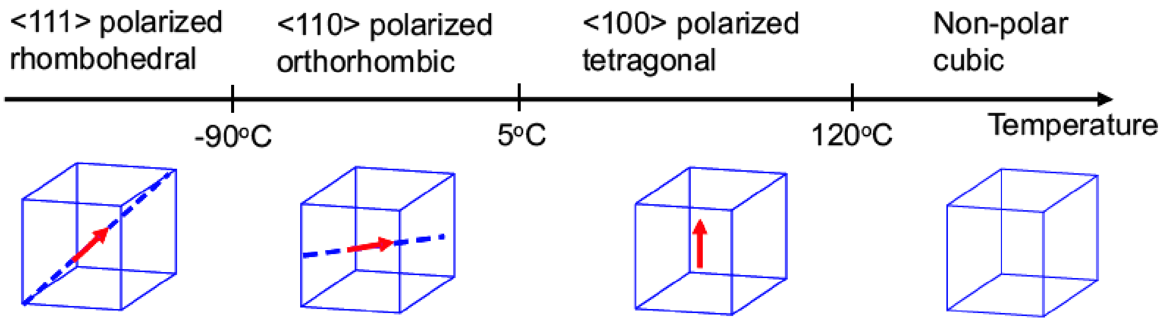

Figure 1.11 various phases of $BaTiO_3$ [2].

$BaTiO_3$ is tetragonal (4mm) which is ferroelectric. The tetragonal unit cell results from the distortion of the original cubic cell. Ferroelectricity arises due to the off-centre displacement of the oxygen (at face centers) and titanium (at body centers) in opposite directions along <100>. As a result, one of the cube edges is elongated to become polar c axis of the tetragonal phase. Since there are six equivalent<100> directions in the cubic phase, the polar axis can be parallel to any one of these directions. This leads to the formation of 90 degree and 180 degree domain walls in the tetragonal phase. In the temperature range of 50°C to –90°C, the structure of $BaTiO_3$ is orthorhombic which is a ferroelectric phase having the polar axis along one of <110> direction of the original cubic unit cell. There are 12 equivalent

<110> directions. The displacement of titanium and oxygen ions along one of the <110> cubic direction leads to an elongation of the face diagonals of the original cubic unit cell, producing shear of the original cube. Below -90°C, a new ferroelectric phase of $BaTiO_3$ appears with a rhombohedral structure (3m). The polar axis for this phase lies along one of the 8 equivalent original cubic <111> directions. The rhombohedral distortions can be visualized as the stretching of the original cubic cell along one of the body diagonals. Variation of dielectric constant, spontaneous polarization and lattice parameter in different phases of $BaTiO_3$ is shown in the Fig.1.12. The tetragonal phase of $BaTiO_3$ has been the object of most investigations as this phase is stable at and above room temperature. Due to the presence of 90° and 180° domains, macroscopic spontaneous polarization is not observed even for a single crystal of tetragonal phase, in the absence of the DC electric field. Application of a DC field may result in merging of these domains to give monodomain crystal with measurable spontaneous polarization. The orientation of all the domains along applied external DC field is not possible for $BaTiO_3$ ceramic. This results in low value of saturation and remnant polarization for ceramic samples in comparison to single crystals.

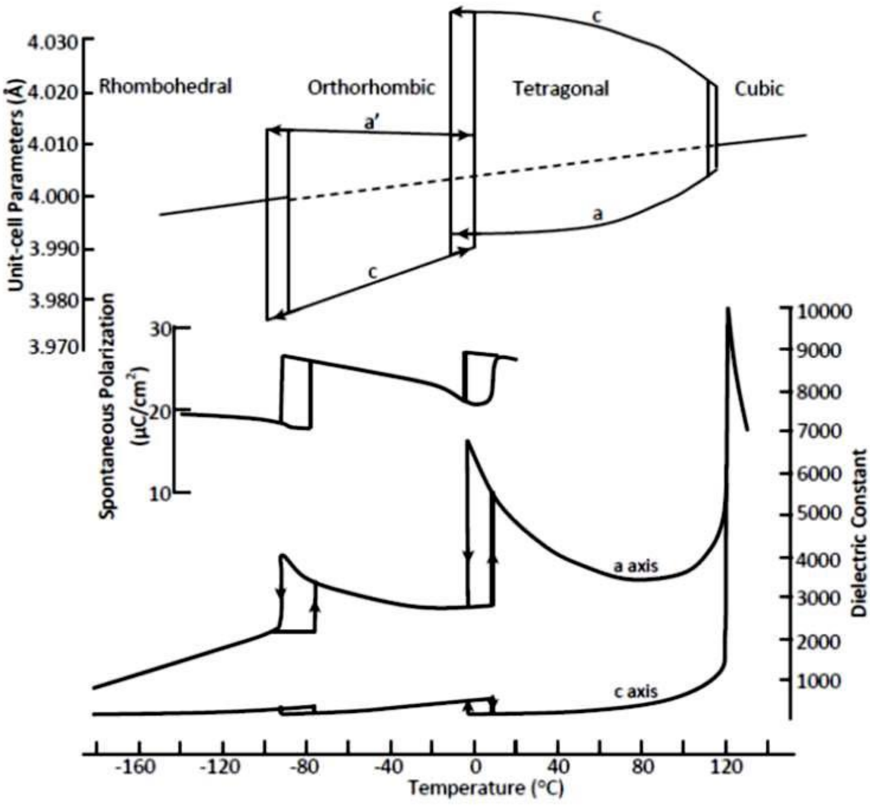

Figure 1.12 various lattice parameters, spontaneous polarization and dielectric constant in different phases of $BaTiO_3$ [53-55].

1.8.2 $KNbO_3$ based ceramic material

In 1951, Matthias and Remeika [56] discovered ferroelectricity in $KNbO_3$ reporting both its Curie temperature (T_C =435°C) and a second transition temperature at around 225°C. Further investigations revealed a sequence of phase transformations similar to those observed in $BaTiO_3$ [57].

$$\text{Rhombohedral} \xrightarrow{-10°C} \text{orthorhombic} \xrightarrow{220°C} \text{tetragonal} \xrightarrow{420°C} \text{cubic}$$

Pure $KNbO_3$ ceramics are difficult to fabricate [2], however, single crystals have been produced and interesting nonlinear electro-optic properties and piezoelectric coefficients along certain crystallographic directions have been reported. High coupling coefficients (k_T =0.69) and excellent temperature stability up to 160°C make $KNbO_3$ single crystals attractive for ultrasonic and acoustic wave transducer applications, however, other uses of $KNbO_3$'s piezoelectric properties are limited [58-60].

Sodium potassium niobate [$(Na, K)NbO_3$] is the solid solution of ferroelectric potassium niobate ($KNbO_3$ or KN) and antiferroelectric sodium niobate ($NaNbO_3$ or NN) [61]. Both have orthorhombic structure at room temperature. KNN exhibits an MPB at around 50/50 composition separating two orthorhombic phases and as for PZT, an increase in the properties for composition near to this MPB. The hot pressed KNN ceramics (99% of the theoretical density) have been reported to possess a high Curie temperature (T_C ~ 420°C), piezoelectric longitudinal response d_{33} =160 pC/N and a high planar coupling coefficient k_p ~45% [62, 63]. Spark plasma sintering has also resulted in high-density (98%) KNN ceramics and with enhanced piezoelectric coefficients (d_{33} = 148pC/N) [64]. However, KNN ceramics prepared by ordinary sintering shows relatively lower electrical properties d_{33}~80 pC/N, k_p ~36% due to difficulty in the processing of dense ceramics. There are two reasons of this problem: first, the phase stability of pure NKN ceramics is limited to 1140°C according to the phase diagram for $KNbO_3$-$NaNbO_3$ [61]. Therefore, a high sintering temperature is not possible. In addition, Na_2O and K_2O easily evaporate at high temperature, which slightly forms an extra phase. The extra phase easily deliquesces when exposed to humidity. Potassium excess might provide some densification helping liquid phase but some of the formed extra phases are highly hygroscopic in nature.

To improve the sinterability and properties of KNN ceramics, various solid solutions such as KNN–$BaTiO_3$, KNN–$LiNbO_3$, KNN–$SrTiO_3$, KNN–$LiTaO_3$, and KNN–$Li(Nb,Ta,Sb)O_3$, KNN–$LiSbO_3$, NKN-$CaTiO_3$, NKN-$BiFeO_3$,NKN-($Na_{.5}Bi_{.5}TiO_3$) etc. based composition at the MPB were used [65-69]. Saito et al. [70] investigated MPB system between $(K_{0.5}Na_{0.5})NbO_3$, $LiTaO_3$ and $LiSbO_3$, and on the basis of Cohen's calculation for the titanate-perovskite system [10] exploited the hybridization of covalency onto ionic bonding for further improvement in piezoelectricity. They reported $(K_{0.44}Na_{0.52}Li_{0.04})(Nb_{0.84}Ta_{0.10}Sb_{0.06})O_3$[LF4] ceramics with an electric field-induced strain comparable to that of a typical actuator-grade PZT. They achieved this through the combination of the invention of the MPB and the development of a processing route leading to highly (001) textured polycrystals (LF4T). The ceramic exhibited d_{33} of above 300pC/N, and the texturing of the material led to a peak d_{33} of 416 pC/N and Curie temperature was nearly 253°C. The observed enhancement of the piezoelectric coefficient was at first attributed to an MPB between orthorhombic and tetragonal phases. However, the authors themselves and more recent studies observed temperature dependence of the electromechanical properties near the room temperature and the existence of the orthorhombic–tetragonal polymorphic phase transition (PPT) near room temperature in both the LF4 and LF4T compositions [71].

Morphotropic phase boundary (MPB) vs a Polymorphic phase transition (PPT)

MPB-based piezoceramics typically exhibit relatively flat temperature dependence of the poled piezoelectric properties and broad usage temperatures approaching $\sim 1/2T_C$. Conversely, PPT-based piezoceramics generally exhibit large temperature dependence of the piezoelectric coefficient and rapid degradation of poled piezoelectric coefficient (due to partial depoling) subsequent to temperature excursions close to the PPT temperature. Recently, the depolarization temperature (T_d) has been proposed to describe the temperature at which a poled ferroelectric material completely or partially depolarizes, as determined from pyroelectric measurements. This temperature typically coincides with the ferroelectric Curie temperature [72]. However, in materials exhibiting one or more polymorphic phase transitions below the ferroelectric Curie temperature but above room temperature, T_d refers to the temperature of the lowest of these phase transitions [73]. For composition close to a vertical MPB this means that temperature variations always keep the material close to the MPB, i.e. close to the instability condition; see Fig. 1.13 (a). If the MPB is temperature dependent, then properties will be enhanced close to the temperature of the phase transition and the MPB. As temperature changes, the material are brought away from both MPB and PPT instabilities and properties decrease (Fig. 1.13 (b)).

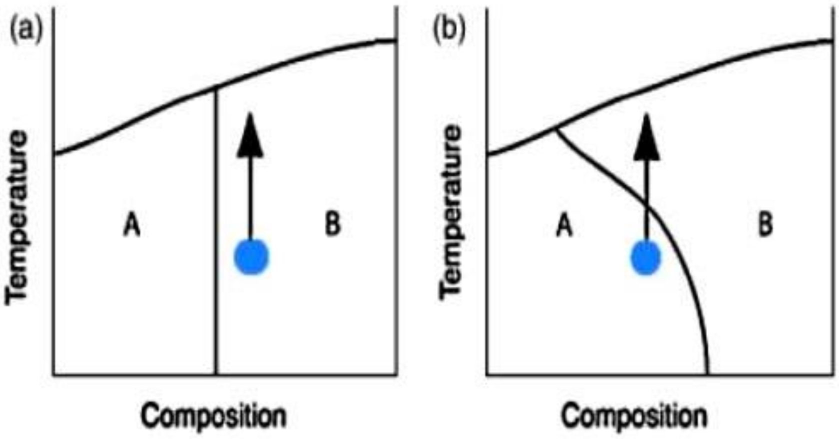

Figure 1.13 (a) A vertical MPB showing temperature independent properties while (b) a curved MPB showing temperature dependent properties [39].

1.8.3 Bismuth Sodium Titanate based Materials

Bismuth sodium titanate, $(Bi_{0.5}Na_{0.5})TiO_3$ (BNT), first reported by Smolenskii et al in 1960, is another important lead-free piezoelectric material [74]. $(Bi_{0.5}Na_{0.5})TiO_3$ is a perovskite with rhombohedral symmetry at ambient temperature, shows strong ferroelectric properties with a large remnant polarization, Pr =38 C/cm^2, and a high Curie temperature, Tc= 320^{o}C. However, BNT-based ceramics undergo another phase transition below Tc that is known as depolarization temperature (T_d), which often occurs below 200°C.When the depolarization takes place at this phase transition, the piezoelectric properties of these ceramics are reduced significantly. The depolarization T_d is an important parameter for BNT based ceramics from the viewpoint of practical application. Preparation of dense $(Bi_{0.5}Na_{0.5})TiO_3$ ceramics is difficult as it require high sintering temperatures above 1200°C, which results in significant loss of bismuth. High leakage currents and high coercive field (Ec=73kV/cm) negatively impact the poling process and polarization saturation is difficult to achieve in conventionally fabricated $(Bi_{0.5}Na_{0.5})TiO_3$ samples. However, dense ceramics have been obtained using excess Bi or hot pressing methods, yielding samples with saturated polarization loops. Large piezoelectric constants are expected for the BNT-based solid solutions with an MPB. The BNT-based composition modified with $BaTiO_3$ and bismuth potassium titanate, $(Bi_{1/2}K_{1/2})TiO_3$, $NaNbO_3$, $BiFeO_3$,etc showed improve properties and easier treatment in poling process [75,76].

Subsequently, the binary system $(Bi_{0.5}Na_{0.5})TiO_3$–$BaTiO_3$ (BNT–BT) was investigated by Takenaka et al.[75]. Fig 1.14 shows the phase diagram of BNT-BT purpose by Takenaka.

There is an MPB between rhombohedral and tetragonal phases at 6–7mol% $BaTiO_3$, with highly enhanced dielectric and piezoelectric properties [75]. The piezoelectric constant d_{33} was found to be 125 pC/N, $\varepsilon_{33}^T/\varepsilon_0=580$, $k_{33}=55.0\%$ and $\tan\delta=1.3\%$. However, Tc dropped significantly at the MPB to values as low as 288°C, and more importantly, T_d became very low at the MPB due to the formation of an antiferroelectric phase.

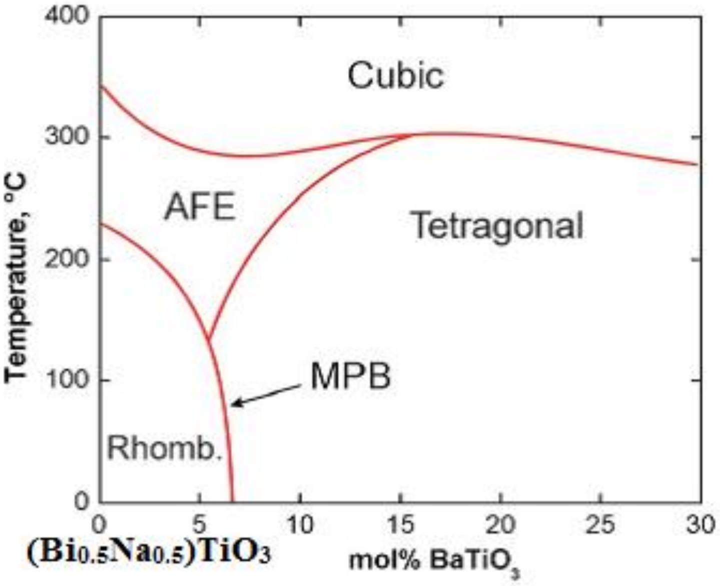

Figure1.14. Phase diagram for the $(Bi_{0.5}Na_{0.5})TiO_3$–$BaTiO_3$ solid solution [75].

1.8.4 Bismuth layer-structure ferroelectrics

The bismuth layer-structured ferroelectrics (BLSFs) with general formula ($Bi_2A_{n-1}B_nO_{3n+3}$) consist of n- perovskite layers $(A_{n-1}B_nO_{3n+1})^{2+}$ sandwiched between bismuth oxygen sheets $(Bi_2O_2)^{2+}$. A is a mono-, di- or tri-valent ion or a mixture of them. B is a combination of cations well suited to form an octahedron, and n can be 1, 2, 3, 4 or the mixture of the adjacent them. There are total five types, which are Bi_3TiNO_9-based, $Bi_4Ti_3O_{12}$-based, $MBi_2N_2O_9$-based, $MBi_4Ti_4O_{15}$-based, and the intergrowth bismuth layer-structured ferroelectrics (iBLSF), where M is Sr^{2+}, Ca^{2+}, Ba^{2+}, $(Bi_{0.5}Na_{0.5})^{2+}$,$(Bi_{0:5}K_{0:5})^{2+}$ and N is Nb^{5+}, Ta^{5+} . Fig.1.15. shows crystal structure of BLSF ceramic with n=2. A typical representation of BLSF type is $Bi_4Ti_3O_{12}$ (BIT), where A=Bi^{3+}, B=Ti^{4+} and n=3.

BLSFs are characterized by their low dielectric constant, low dielectric dissipation factor, high Curie temperature and large anisotropy in the electromechanical coupling factor. Therefore, the BLSF ceramics are considered as superior candidates for high temperature piezoelectric, sensors, filters, resonators and/or pyroelectric sensors applications.

BIT is monoclinic in the ferroelectric phase but is generally represented using an orthorhombic setting with the c-direction perpendicular to the layers and the major component of the spontaneous polarization in the a-direction of the perovskite plane. Cummins and Cross reported anisotropic spontaneous polarizations in BIT single crystals (50 µC/cm^2 along the *a*-axis and 4μC/cm^2 along the *c*-axis) [77]. On the other hand, fully reliable piezoelectric properties of BIT ceramics have not been reported because of some problems such as low resistivity and large coercive field [77]. To solve these problems, Nb^{5+} and V^{5+} ions were doped into BIT ceramics to obtain higher resistivities [78, 79]. The highest d_{33} of 20 pC/N was achieved with a composition corresponding to $Bi_4Ti_{2.86}Nb_{0.14}O_{12}$ with a T_c of 655°C.

A few bismuth oxide layered perovskite materials, such as $SrBi_2Nb_2O_6$ (SBN), $SrBi_2Ta_2O_9$ (SBT), $SrBi_2(Nb,Ta)_2O_9$ (SBTN) and $SrBi_4Ti_4O_{15}$ have increased attention in the research community, because they are fatigue-free and lead-free and possess ferroelectric properties independent of film thickness for FeRAM application. However, layered perovskite ferroelectrics have two drawbacks: a relatively low remnant polarization and a high processing temperature. Recently, efforts have been made to enhance the properties of layered perovskite ferroelectrics by the addition or substitution of alternative ions [80].

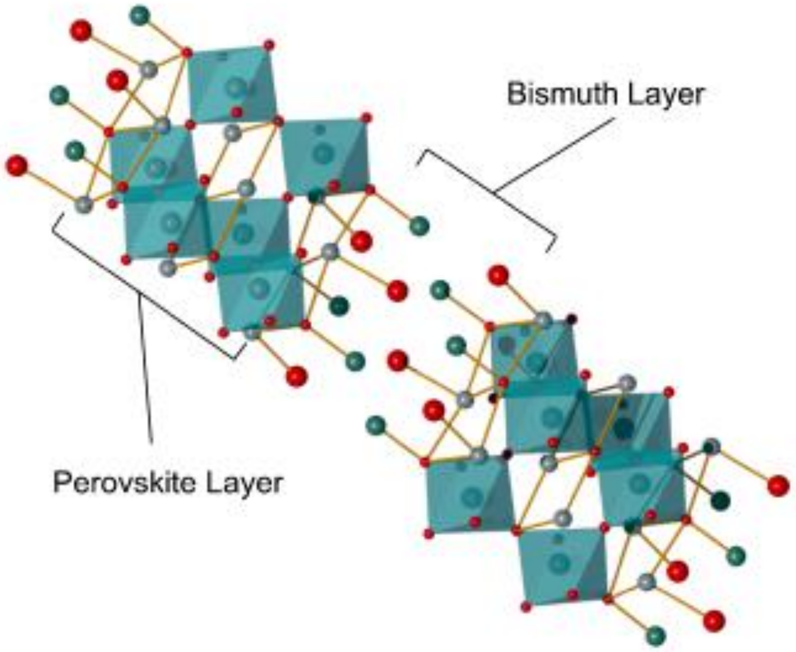

Figure1.15 Schematic representations of the crystal structure of BLSF ceramics.

Room temperature properties of several important dielectric and piezoelectric material are shown in Table 1.2.

Table 1.2: Dielectric and Piezoelectric properties of different lead free ferroelectric ceramics

Material	**ε_r**	**loss**	**d_{33}(pC/N)**	**k_p**	**k_{33}**	**$T_{O\text{-}T}$**	**Tc(°C)**	**Ref**
$BaTiO_3$	1700	0.01	190	0.36	0.5		115	[2]
$BaTiO_3$	1400		140	0.36	0.5		130	[81]
BZT-CuO	1546	0.011	300	0.493	65.1			[82]
BZT(0.03725)	1322	0.006	260	0.421	53.8			[82]
BZT-BCT(0.5)	3060		620	0.53	65		93	[48]
BZT-BCT	4800		328	0.376				[83]
KNN	290	0.04	80	0.36				[62]
KNN(SPS)	559	0.036	148			220	395	[64]
KNN(HP)	420		160					[6]
KNN-Li (6%)	534	0.4	235	0.44		75	465	[84]
KNN-LS-LT(LF4T)	1570		416	0.61		25	253	[70]
KNN-LT-LS	1473	0.02	263			50	353	[85]
NBT	500	0.018	64			~200	310	[74]
NBT-BT(6%)	826	0.025	155	0.36		288	105	[75]
NBT-KBT-BT	820	0.03	145	0.162	0.519	302	224	[86]
$CaBi_2NbTiO_9$	97	0.015	5			936		[87]
$Bi_4Ti_3O_{12}$	176	0.01	4			672		[88]
$Bi_4Ti_3O_{12}$-Nb_2O_5	224	0.002	18			630		[88]
$Na_{0.5}Bi_{4:5}Ti_4O_{15}$	153	0.003	18			668		[89]

T- Texture HP- Hot press, SPS-spark plasma sintering, BT-$BaTiO_3$,BZT-$Ba(Zr,Ti)O_3$, BZT-BCT-$Ba(Zr_{0.2}Ti_{0.8})O_3$-$(Ba_{0.7}Ca_{0.3})TiO_3$, $(K_{0.44}Na_{0.5}2Li_{0.04})(Nb_{0.84}Ta_{0.10}Sb_{0.06})O_3$[LF4], KNN-$(K_{0.5}Na_{0.5})NbO_3$, KBT-$(K_{0.5}Bi_{0.5})TiO_3$

As stated above, tremendous efforts have been devoted in last decade to the development of competitive lead free counterparts, such as $BaTiO_3$, $(Bi_{1/2}Na_{1/2})TiO_3$(BNT), (K, Na)NbO_3 (KNN), and their derivatives. Till date, the properties of developed lead-free piezoelectrics are not comparable to that of PZT based compositions. KNN based system suffers from alkali evaporation during sintering, poor sinterability, moisture sensitivity of the raw materials. BNT based system suffers from high leakage current. $BaTiO_3$ is a model ferroelectric mostly utilized for the capacitor, thermistor applications. The breakthrough made by Liu and Ren et al. in $BaTiO_3$-based ceramics with co-dopants of Zr, and Ca has offered a significant impact on the development of lead-free piezoceramics [48]. The pure $BaTiO_3$ ceramics are associated with a poor piezoelectric coefficient (d_{33}) as low as 191 pCN^{-1} [2]. The value reported by Liu and Ren et al. [48] reached more than 500 pCN^{-1}, comparable to that of soft PZT ceramics. The proposed origin of high piezoelectricity was the formation of MPB between $Ba(Zr_{0.2}Ti_{0.8})O_3$-$0.5(Ba_{0.7}Ca_{0.3})TiO_3$[BZT- 0.5BCT].

The present thesis attempts to study the dielectric and piezoelectric properties of $BaTiO_3$- based system by addressing different drawbacks of these materials. So, a thorough literature review is required, focused on different modification of $BaTiO_3$, preparation method and sintering technique which affects the crystal structure, microstructure, dielectric and piezoelectric properties.

Chapter 2

Literature Review, Objective

Literature Review

2.1 Zr modified $BaTiO_3$ ceramics

$BaTiO_3$ based ceramics have received a great deal of attention from the scientific community in searching for environment friendly lead free ferroelectric materials. $BaTiO_3$ in its pure form has relatively low T_c of 120°C which limits its use as high-power transducers and low electromechanical coupling factor in comparison to PZT which limits its operational output. Big disadvantage of pure barium titanate is, in fact, the high-temperature coefficient of capacitance near the Curie temperature which is a consequence of the transition from the tetragonal to the cubic phase that restricts the temperature range of application. The addition of heteroatoms can serve to form solid solutions to shift the transition temperature. Barium titanate, however, is limited to use as a piezoelectric material, due to multiple ferroelectric-ferroelectric phase transitions and the resulting significant temperature dependence of piezoelectric properties. Chemical substitutions at the Ba^{2+} and Ti^{4+} sites are made to tailor the properties to meet a variety of device and performance requirements. $BaZr_xTi_{1-x}O_3$ (BZT, $x \leq 0.1$) has become a good piezoelectric material, due to its larger piezoelectric coefficients, electromechanical coupling coefficients and more stable structure [28, 90].

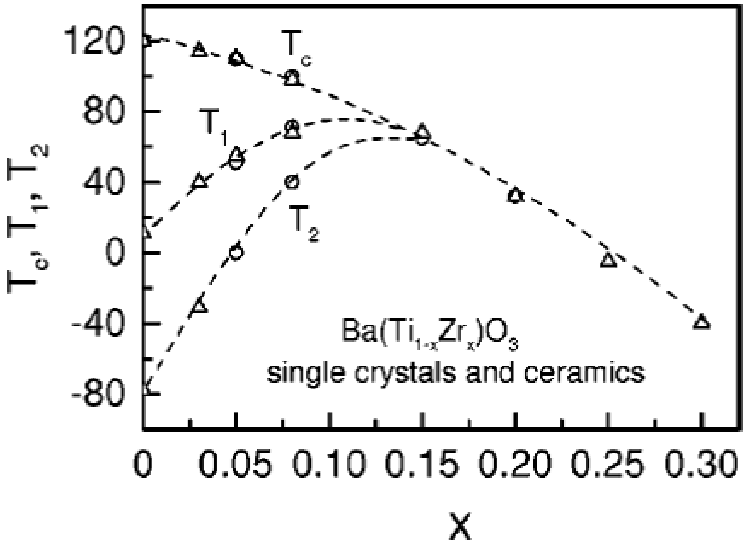

Figure 2.1 Phase diagram of $Ba(Ti_{1-x}Zr_x)O_3$ ceramics with Zr content ($0 \leq x \leq 0.3$)[(For various compositions, data were taken at 1 kHz. (Symbols are experimental data: up-triangles: data for ceramics; open circles: single crystal data; Dash curves: guide to the eyes [91].

The nature of the ferroelectric phase transition at the Curie temperature (T_C) of BZT ceramics is known to change strongly with the Zr content. At higher Zr contents ($x>0.08$), BZT ceramics show a broad dielectric constant vs temperature (ε~T) curve near T_C, which is caused by inhomogeneous distribution of Zr ions in Ti sites and mechanical stress in the grain. It can be considered as a result of pinch off of the three phase transitions of pure $BaTiO_3$ at the high Zr concentration (x~0.15). With the increase in Zr content, the phase-transition temperatures approach each other until a Zr content of (x~0.20) where only one phase transition exists. When the Zr^{4+} concentration becomes 0.25, it exhibits a typical relaxor-like behavior both in bulk and thin film. The phase diagram of $Ba(Ti_{1-x}Zr_x)O_3$ ceramics within composition range $0<x<0.3$ is shown in fig 2.1[91]. Verbitskaya et al. [92] have reported several modifications on rhombohedral(R), tetragonal (T) and cubic(C) in the composition range of $0.10 \leq x \leq 0.15$, in the phase diagram of BZT ceramics. Above this Zr content, the ferroelectric–paraelectric phase transition involves a structural change from R to C symmetry [92-96].

$Ba(Ti_{1-x}Zr_x)O_3$ with low Zr concentration showed very high strain behavior. By using the templated grain growth (TGG) method, Rherig et al.(1999) showed that some $Ba(Ti_{1-x}Zr_x)O3$ (x= 0.045 and 0.085) crystals grown in millimeter size exhibit strain as high as ~0.5% at 50 kV/cm and piezoelectric strain coefficient (d_{33}) of 355 pC/N at room temperature[95]. Later Yu et al. [90] observed almost hysteresis free very high strain (~0.25%) and high piezoelectric strain coefficient d_{33} (~236 pC/N) in the $Ba(Ti_{1-x}Zr_x)O_3$ (x= 0.05) ceramics by conventional solid state technique. Recently, Dong et al. reported high piezoelectric coefficient of ~420pC/N in the $Ba(Ti_{1-x}Zr_x)O_3$ (x= 0.06), prepared by solid state method with sintering temperature of 1400°C for 100h [97].

2.1.1 Solid state method

The Zr modified $BaTiO_3$ powders conventionally synthesized by solid-state reaction between carbonates and oxides, which require calcination of the mixture at high temperature. The high calcination temperature required by solid-state reaction process leads to many disadvantages of these powders, such as large particle size, wide size distribution and the high degree of particle agglomeration. It also possesses impurity contents due to their inherent problems such as high reaction temperature and heterogeneous solid phase reaction, which results in poor electrical properties of the sintered ceramics.

The Zr modified $BaTiO_3$ [BZT] was prepared by solid-state reaction using a calcination temperature (1100-1300°C) [98, 99] and time (2h- 12h). The sintering temperature (1400-1550°C) and soaking time (2h - 100h) [97, 100] were also optimised to get large grain ceramic.

The maximum density of the ceramics was found to be 90-95%, average particle size around 2-3µm and grain size around 10-70µm (1400°C for 100h). Mahesh et al. [101] synthesized BZT composition with x=0.15, using solid-state reaction method by adopting high-energy ball milling technique. The particle size was reduced to 0.2µm, and 94% of the theoretical density was obtained at 1350°C for 5h.

2.1.2 Wet chemical method

Chemical synthesis of Zr modified $BaTiO_3$ has grown up through different techniques such as sol-gel, co-precipitation, hydrothermal, polymeric precursor method and autocombustion method. The advantage of the chemical methods is the quasi–atomic dispersion of constituent components in a liquid precursor, which facilitates the synthesis of the crystallized powder with submicron particles and high purity at low temperatures.

2.1.2.1 Sol-gel method

Tang et al. **[**102**]** synthesized $Ba(Zr_{0.2}Ti_{0.8})O_3$ powder by the sol-gel method using zirconium-n-propoxide, titanium n-butoxide as precursors of zirconia and titania, respectively and 2-methoxyethanol as the solvent. The phase pure powder was obtained at 1100°C/5h in the air and three different grain sizes (2µm, 15µm and 60 µm) were obtained at sintering temperature of 1350-1550°C/5h. They observed that coarse-grained sample undergoes a structural phase transition from ferroelectric (tetragonal, T) to paraelectric (cubic, C) phase, but medium- and fine-grained samples showed diffuse phase transition characteristics (one phase transition). Phase transition temperature and maximum dielectric constant increased with the increase in grain size and loss factor was decreased with the increase in grain size. They also found that the density could reach up to 98% of the theoretical density of these ceramics sintered at 1550°C/5h. The single phase cubic perovskite structure was obtained at room temperature [103].

Binhayeeniyi et al. [104] synthesized $Ba(Zr_xTi_{1-x})O_3$ (x=0-0.2) ceramic via sol-gel method using titanium (IV) isopropoxide and zirconium (IV) propoxide and calcined the resulting gel at 1100°C/2h. The calcined powder has an average particle size of around 0.29µm, and the density of these ceramics was found to be 84% at 1250°C. They suggested that the crystalline phases of $Ba(Zr_{0.05}Ti_{0.95})O_3$ is orthorhombic while the $Ba(Zr_{0.10}Ti_{0.90})O_3$ and $Ba(Zr_{0.15}Ti_{0.85})O_3$ are rhombohedral and $Ba(Zr_{0.2}Ti_{0.80})O_3$ is cubic. Average grain size was decreased with an increase in Zr content. They observed high piezoelectric coefficient (d_{33}~126pC/N) and good electromechanical coupling for $Ba(Zr_{0.05}Ti_{0.95})O_3$ ceramic. Additionally, Li_2O(1.5wt%) as a sintering aid was used in $Ba(Zr_{0.05}Ti_{0.95})O_3$ ceramic to decrease the sintering temperature from 1250°C to 900°C. Diffusion of Li^+ ions not only significantly affected the phase transition temperature but also largely reduced the grain size which led to a wider dielectric curve with the lower dielectric constant. Thanachayanont et al. [105] also studied the crystal structure of $Ba(Zr_xTi_{1-x})O_3$ (x=0-0.2) powders using Rietveld refinement x-ray diffraction and convergent beam electron diffraction (CBED). The phase transition from tetragonal to cubic was determined from tetragonality (c/a) (x=0.15).

Chen et al. [106] synthesized $Ba(Zr_{0.20}Ti_{0.80})O_3$ powder via sol–gel method at a low temperature using tetrabutyl titanate, zirconium (IV) nitrate tetrahydrate, and acetylacetone as precursors. The single phase perovskite type cubic structure was obtained at 900°C/4h with average particle size of 20 nm. They used three polyalcohol surfactants: butanol (BTOL), polyethylene glycol (PEG) and polyvinyl alcohol (PVA) to reduce the agglomeration of these powders. It was found that PEG has a better effect on reducing agglomeration of BZT powders than that of the BTOL and PVA.

2.1.2.2 Combustion Method

Combustion method (glycine-nitrate, urea based, and other modifications) has been proposed as one of the most promising methods to prepare perovskite oxide. This method constitutes a highly exothermic self-combustion reaction between the fuel (usually glycine, urea and citric acid) and the oxidant (metal nitrates), that produces enough heat to obtain the ceramic powders. Compared to the solid state method, this synthesis route has much faster reaction times and lower calcination temperatures leading to powders with significant compositional homogeneity and nanometric particle sizes.

Chakrabarti et al. [107] have prepared homogeneous $Ba(Zr_xTi_{1-x})O_3$ (x=0.05-0.2) powder via citrate –nitrate gel combustion at low temperature (800°C) with citrate to nitrate ratio (C/N)=0.6. $TiCl_4$ was used as a starting material to prepare $TiO(NO_3)_2$ solution. The average particle diameter of the synthesized powder was 1.36 µm for C/N=0.6. These powders could be sintered to 92-93% density at 1300°C with average grain size of 3µm. With an increase in Zr concentration, the Curie temperature decreased and the permittivity peaks broadened. Lower relative permittivity value 1000-2000 was obtained for Zr modified ceramics at room temperature.

Julphunthong et al. have developed a novel combustion technique to prepare BZT10 powder using urea (CH_4N_2O) as fuel [108]. The single perovskite phase was obtained at 1000°C/ 5h and the powders exhibited an irregular shape with a porous agglomerated form. The average particle size increased in the range of 133 to 369nm, with increase in calcination temperature or dwell time. The highest theoretical density of 97% was obtained at 1400°C/2h with average grain size 21.1µm.They suggested that BZT(x=0.1) has a mixture of cubic and tetragonal phase and that the cubic phase content increased with the increase in firing temperatures and dwell time. The T_c occurred at around 76°C and the highest maximum dielectric constant of 16500 and lowest dielectric loss of 0.015 was observed. Julphunthong et al. have also studied the different composition of $Ba(Zr_xTi_{1-x})O_3$ (x=0.025-0.15) ceramics[109]. The maximum theoretical density of 97% was obtained for BZT(x=0.125) ceramics at 1375°C/2h. The crystal structure was transformed from orthorhombic to rhombohedral or tetragonal or cubic phase depending on the zirconium content. The lowest and the highest dielectric constants were 9930 and 19,600 for BZT(x=0.075) and BZT (0.125), respectively.

Bernardi et al. prepared $BaTi_{1-x}Zr_xO_3$ (x=0, 0.2, 0.8 and 1) nanometric powders by the polymeric precursor method using $Zr(OC_3H_7)_4$ and $Ti(OC_3H_7)_4$ as the precursors of zirconia and titania respectively. The citric acid to metal ratio was kept as 3.5:1 and pH were adjusted to 3-4 with ethylendiamine, depending on the composition [110]. The phase pure powder was obtained at 900°C with average particle size around 150nm.

Deluca et al. [111] obtained single phase and dense $BaTi_{1-x}Zr_xO_3$ (x=0.1, 0.15, 0.2) ceramics by a modified pechini method. The molar ratio of $BaCO_3$: $Ti(iOC_3H_7)_4$: $Zr(OC_3H_7)_4$:Citric acid: ethylene glycol was kept at 1:(1-x):x:7.5:21. The phase pure powder formed at 850°C/2h and 87-91.2% of theoretical density was observed at 1300°C/8h with average grain size of 1.2 µm for BZT10 and 23.5µm for BZT20 ceramics. The intergranular (on small grain) and transgranular (on coarse grain) fracture was observed in BZT15 ceramics. The crystal structure changed from rhombohedral to cubic form as the Zr content was increased from x=0.10 to x=0.2 and the Curie temperature decreased (~82°C for BZT10, ~50°C for BZT15 and ~25°C for BZT20). Lower Zr content x=0.10 showed the diffuse ferroelectric-paraelectric phase transition due to the lower grain size which include additional microstresses.

2.1.2.3 Hydrothermal method

Vivekanandan et al.[112] have prepared fine powders of $Ba(Ti,Zr)O_3$ by hydrothermal method starting from a reactive gel of hydrated titanium and zirconium oxides, precipitated from the respective oxychlorides by using ammonia. The product, after suspension in a barium hydroxide solution, was autoclaved for 2-6 h at temperatures between 85 and 130°C. The synthesized powder was cubic and converted to tetragonal phase after heat treatment at 1200°C, accompanied by the loss of residual hydroxyl ions. The hydrothermally prepared $Ba(Ti,Zr)O_3$ with >12 mole % Zr remain unchanged after the heat treatment as observed from the x-ray diffraction pattern. Particle size of $BaTiO_3$ varied from 0.2 to 0.5 µm whereas that of

$BaZrO_3$ was larger (1-3 µm). The sintering temperature was increased from 1300 to 1400°C with increase in Zr/Ti ratio.

Lee et al.[113] synthesized BZT20 powders by the hydrothermal reaction using amorphous $BaZr_xTi_{1-x}$-peroxohydroxide. First, $BaZr_xTi_{1-x}$-peroxo-hydroxide precursors were prepared by co-precipitation of $BaCl_2$, $ZrOCl_2$, $TiOCl_2$ and H_2O_2 aqueous solutions by adding ammonia solution with additional $Ba(OH)_2$ as a mineralizer. Phase pure BZT powders with a cubic perovskite structure were observed under mild hydrothermal conditions (100–130°C, ≤1.5MPa) and the powders consisted of nano-sized crystallites with BET surface area $30m^2/g$. The density of $BaZr_{0.2}Ti_{0.8}O_3$ was found to be 93% of theoretical density at a sintering temperature of 1150°C/1h. The higher Zr content led to a higher dielectric constant at room temperature and a more diffuse ferroelectric-to-paraelectric transition, which resulted in a reduced temperature dependence of the dielectric constant for the BZT20 ceramics.

2.1.2.4 Co-precipitation Method

Reddy et al. [114] have synthesized $BaZr_xTi1_{-x}O_3$ (x=0.10-0.30) powders by aqueous co-precipitation method using $TiCl_4$ and $ZrOCl_2$ as starting materials. NaOH solution (15M) was used as precipitating agent upto a pH of more than 12. The particles have a mixture of different shapes (spherical, elliptical, acicular and cube) with an average particle size of 30 nm and crystallite size of 13nm. The maximum density of 96% was observed at sintering temperature of 1600°C/4h, with average grain size of 3µm.The highest dielectric constant of 11000 was obtained for BZT10. Zr content has almost no influence on the grain size of the sintered BZT ceramics.

Qi et al. [115] have synthesized BZT nanoparticles (25-30nm) under very mild conditions (at low temperature and under atmospheric pressure). Tetrabutyl titanate and zirconium isopropoxide were used as a precursor of zirconia and titania, respectively. Barium carbonate phase was found as impurity in the final product.

2.2 Ca modified $BaTiO_3$ ceramics

Calcium is most commonly doped in the $BaTiO_3$ ceramics. It has been reported that Ca^{2+} can occupy both Ba^{2+} and Ti^{4+} sites [116-118]. Phase relations in the $BaTiO_3$–$CaTiO_3$ system were studied by Devries and Roy [119]. According to their phase diagram, $CaTiO_3$ up to ~18mol% forms a homogeneous solid solution with $BaTiO_3$ at 1400°C. According to Kuper et al. [120], BCT single crystal shows Curie temperature at 98°C and does not show any structural transition down to −120°C. By partial replacement of Ba^{2+} with Ca^{2+}, the temperature dependent dielectric constant was broadened improving the electromechanical behavior. It also inhibited the formation of the unwanted hexagonal phase of $BaTiO_3$.Berlincourt and Kulesar [121] found that the Ca substitution in $BaTiO_3$ ceramic caused only negligible changes in the Curie temperature but strongly lower the tetragonal–orthorhombic transition temperature, which improved the temperature stability of piezoelectric/electostrictive properties. McQuarrie and Behnke reported that Ca-doped $BaTiO_3$ showed a slight decrease in the Curie temperature [122]. Mitsui et al and Jaffe et al. [123,2], from the dielectric and X-ray diffraction (XRD) studies, deformed that the Curie point of $Ba_{1-x}Ca_xTiO_{3,}$(BCT) increases from 130°C for pure $BaTiO_3$ to 136.1°C for x=0.08 and then decreases slightly for continuous increase in Ca concentration up to 25%. Wakino et al. [124] have investigated Ca-doped $BaTiO_3$ multilayer ceramic capacitors for use with base metal electrodes, which can be sintered in a reducing atmosphere. According to Zhuang et al. [116], addition of even a small quantity of Ca ions at Ti-sites leads to a diffused phase transition and significantly lowers the phase transition temperatures.

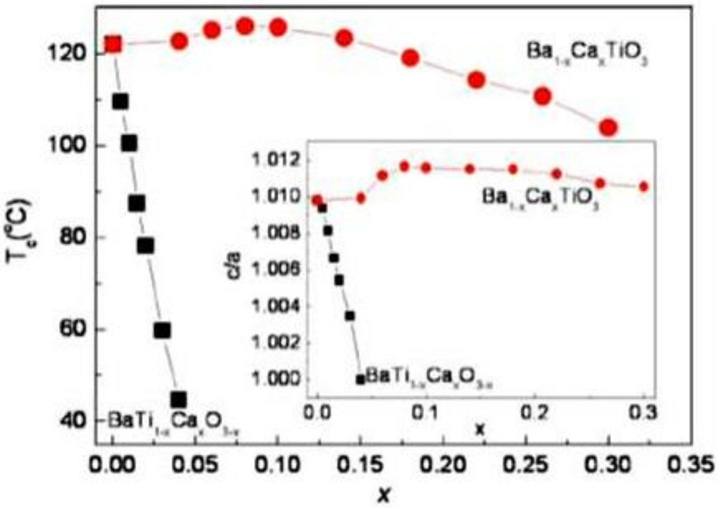

Figure 2.2 Phase transition temperature vs Ca content for $Ba_{1-x}Ca_xTiO_3$ (BCT), and $BaTi_{1-x}Ca_xO_{3-x}$(BTC) Inset shows c/a vs Ca content for BCT and BTC [126].

Tiwari et al. and Zhuang et al. [125, 126] also reported that calcium doping increases the phase transition temperatures of BCT ceramics and substitution Ba^{2+} by Ca^{2+} leads to diffused transition curve. Ca-substitution at Ba-site leads to diffuseness whereas Ca replacement at Ti-site leads to sharpening of phase transition curve. Zhang et al. reported the phase transition temperature of Ca^{2+} doped $BaTiO_3$ ceramics. Phase transition temperature of A and B site Ca^{+2} doped $BaTiO_3$ ceramics are shown in Fig 2.2 [126]. A low level of Ca^{2+} doping on B site (≤4at %) in $BaTiO_3$ have a dramatic and detrimental effect on Tc and grain conductivity. Ca^{2+} doping on A-site in $BaTiO_3$ showed the desired enhancement of Tc.

2.3 Ca and Zr modified $BaTiO_3$ ceramics

The (Ca, Zr) co-doped $BaTiO_3$ ceramics was earlier used in capacitor composition [127, 128,129]. The (Ca, Zr) co-doping plays a critical role in maintaining the electrical properties of $BaTiO_3$ ceramics. There are no. of reports available on the dielectric properties and tunabilities of $(Ba_{1-x}Ca_x)(Zr_yTi_{1-y})O_3$ ceramics, and only a few studies have focused on the high piezoelectric properties of $(Ba_{1-x}Ca_x)(Zr_yTi_{1-y})O_3$ materials [130]. Recently, Liu and Ren [48] have reported that Pb-free $Ba(Zr_{0.2}Ti_{0.8})O_3$-$(Ba_{0.7}Ca_{0.3})TiO_3$ (BZT-BCT) solid solution exhibits an MPB starting between rhombohedral and tetragonal phase ending at a tricritical point with a cubic paraelectric phase. The high piezoelectric coefficient d_{33} ~300-600pC/N was reported in ceramic samples near this tricritical point, which is comparable to high-end PZT ceramics. This finding led to a surge of worldwide investigation on BT- based ceramics possessing an excellent potential for replacement of lead containing PZT material. The phase diagram of pseudo-binary $Ba(Zr_{0.2}Ti_{0.8})O_3$-$x(Ba_{0.7}Ca_{0.3})TiO_3$ ceramics is shown in Fig 2.3. There are three typical compositions in BZT–xBCT solid solutions, which are x=0.14, 0.32, and 0.50, respectively, corresponding to the cubic phase at room temperature, cubic–rhombohedral–tetragonal (C–R–T) triple point near 57 °C, and tetragonal phase at room temperature, with a very high piezoelectric coefficient [131]. The piezoelectricity is enhanced at MPB composition due to small polarization anisotropy. This low polarization anisotropy leads to a small energy barrier between two ferroelectric phases, and facilitates the rotation between the coexisting rhombohedral (P_S[111]) and tetragonal (P_S[100]) phases. The enhanced piezoelectric performance has been attributed to the vanishing polarization anisotropy and the polarization rotation in the presence of a tricritical point. On the other hand, polymorphic phase transition (PPT) plays an important role to improve the dielectric and piezoelectric properties. However, the crystal structure for MPB composition of BZT-xBCT piezoceramic is still under debate. Previous crystallographic studies suggest that the two binary phases in the phase diagram, tetragonal and rhombohedral phases, coexist in the high-property MPB composition. On the contrary, an intermediate orthorhombic phase (Amm2) has been reported in a narrow composition/temperature regime in the BZT-xBCT system, and the phase diagram has been modified as shown in Fig 2.4. The authors used high-resolution synchrotron X-ray diffraction techniques to prove the presence of intermediate orthorhombic phase. [132].

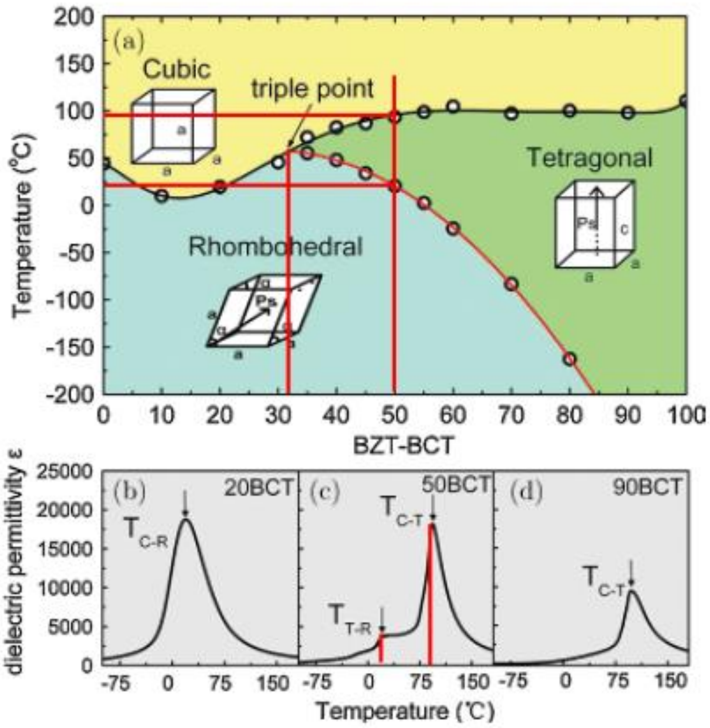

Figure 2.3(a) The phase diagram of pseudo-binary ferroelectric $Ba(Zr_{0.2}Ti_{0.8})O_3$-$(Ba_{0.7}Ca_{0.3})TiO_3$ [BZT-xBCT] ceramics (b)-(d) Dielectric permittivity curves for 20BCT, 50BCT and 90BCT, respectively [48].

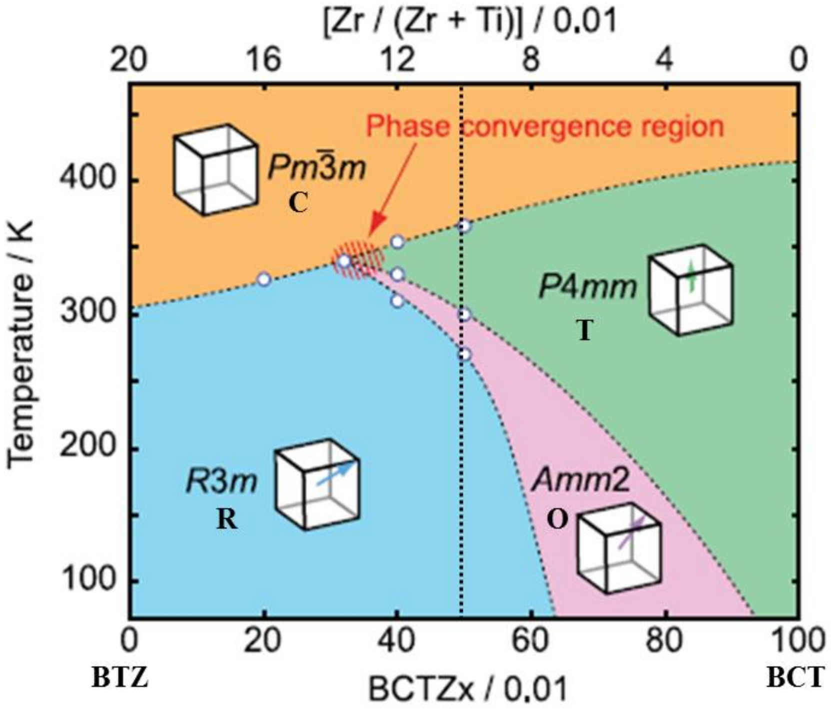

Figure 2.4 Modified phase diagram of pseudo-binary ferroelectric $Ba(Zr_{0.2}Ti_{0.8})O_3$-$(Ba_{0.7}Ca_{0.3})TiO_3$ ceramic [132].

Liu et al. [48] reported a large piezoelectric effect (d_{33}~560–620 pC/N) in the pseudobinary ferroelectric system (1-x)$Ba(Zr_{0.2}Ti_{0.8})O_3$-x$(Ba_{0.7}Ca_{0.3})TiO_3$, especially for x=0.5, which is located near the MPB in the phase diagram. Additionally, Xue et al. [133] determined a full set of elastic, dielectric and piezoelectric constants for the BZT-0.5BCT ceramic by using a resonance method and measured the temperature dependence of some electrical properties. They observed that resonant method gives piezoelectric properties d_{33}~546 pC/N, and high electromechanical coupling factor k_{33}~65%. Piezoelectric coefficient d_{31} can maintain an appreciable level of 93pC/N even at -50°C. Li et al. [83] had reported a low d_{33} of 328pC/ N and high dielectric constant of 4800 in $(Ba_{0.84}Ca_{0.16})(Ti_{0.9}Zr_{0.1})O_3$ ceramics with a coexistence of rhombohedral and orthorhombic phases. They also reported a d_{33} of 365 pC/N in $(Ba_{0.92}Ca_{0.08})(Ti_{0.95}Zr_{0.05})O_3$ ceramics with an MPB between orthorhombic and tetragonal phases, at an optimal sintering temperature. They also further reported a d_{33} of 387pC/N in $(Ba_{0.99}Ca_{0.01})(Ti_{0.98}Zr_{0.02})O_3$ ceramics with relatively high Curie temperature T_c =115°C. They also modified simultaneously Ca and Zr in $(Ba_{1-x}Ca_x)(Ti_{1-y}Zr_y)O_3$ [$(Ba_{0.92}Ca_{0.08})(Ti_{0.95}Zr_{0.05})O_3$, $(Ba_{0.93}Ca_{0.07})(Ti_{0.95}Zr_{0.05})O_3$, $(Ba_{0.99}Ca_{0.01})(Ti_{0.98}Zr_{0.02})O_3$ and found piezoelectric coefficient in between 325-387pC/N using optimal sintering temperature[134-136]. Zhang et al. [137] obtained a d_{33} of 338 pC/N in $(Ba_{0.95}Ca_{0.05})(Ti_{0.96}Zr_{0.04})O_3$ ceramics with a coexistence of orthorhombic and pseudocubic phases. Benabdallah et al. [138] have found transverse piezoelectric coefficients (d_{31}) as high as 200 pC/N and 120 pC/N for BZT-0.5BCT and $0.68Ba(Zr_{0.2}Ti_{0.8})O_3$-$0.32(Ba_{0.7}Ca_{0.3})TiO_3$ [BCTZ32], respectively, at room temperature which is comparable to soft and hard PZT. They obtained density of 90% for pure BZT-0.5BCT ceramic (without TiO_2 excess) and density improved up to 96% for 1mol% TiO_2 addition in BZT-0.5BCT ceramic. Wang et al.[139] obtained high piezoelectric properties of d_{33} ~ 650 and dielectric constant of 4500 for BZT-0.5BCT ceramics using optimum calcination (1300°C) and sintering temperature (1540°C).The ceramic forms at MPB between rhombohedral and tetragonal phase at room temperature having phase transition temperature (Tc)=85°C. Su et al. [140] investigated the dependence of poling field on d_{33} and aging of electrical properties of BZT-0.5BCT ceramics. They obtained d_{33} of 630 pC/N and planar electromechanical coupling factor of 56% for BZT-0.5BCT at a poling field and temperature of $2.5E_c$ and 40°C, respectively. They also reported that these materials exhibit extremely high aging rate, 30% and 25% loss of d_{33} and k_p, respectively, after 10^4 min of poling). It may be due to a rather low depolarization temperature (below 80–90°C) of BZT-BCT. Wu et al. [131] studied the effect of dwell time on piezoelectric properties of BZT-0.5BCT ceramics. The highest d_{33} ~ 492 pC/N and k_p ~ 51.5%

was obtained for optimum sintering condition of temp/5h.the reason for getting better properties were structural distortion together with a dense microstructure and larger grain size. The T_C value increased with the increase in the dwell time (<6h). Gao et al.[141] studied the microstructure evolution around its MPB composition by transmission electron microscopy(TEM). Hao et al. [142] studied the correlation between microstructure and electrical properties of BZT-0.5BCT ceramic. They have used three different sintering methods (spark plasma sintering, two-step sintering, and normal sintering) of BZT-0.5BCT ceramic to obtain grain size in the range of 0.4 to 32μm. The optimum piezoelectric properties (d_{33} >472 pC/ N, k_p> 0.48) were obtained for grain size more than 10 μm. Tan et al. [143,144] studied the phase transition behavior and electrical properties of BZT-0.5BCT ceramics. The maximum piezoelectric, electromechanical coupling coefficient and dielectric constant (d_{33}=572, k_p=0.57, ε_r=4821) were observed near MPB region. Yao et al. [145] reported the high pyroelectric coefficient of $4.80\times10^{-4}Cm^{-2}K^{-1}$ and $5.84\times10\text{-}4Cm^{-2}K^{-1}$ at 300K for BZT-50BCT ceramics measured by Bayer-Roundy method. Damjonovic et al. [146] reported temperature-induced anomalies in the dielectric, piezoelectric, elastic coefficients and Raman spectroscopy of BZT-.5BCT ceramics. Lue and Ren et al. [48] predicted giant piezoelectric coefficient (d_{33}) ~ 1500–2000pC/N for the single crystal form of BZT–0.5BCT composites at the MPB.

2.3.1 Effect on Curie temperature (T_c)

In most of the literatures, the overall high piezoelectric properties at a relatively low Curie temperature, in between 65-103°C, was achieved for BZT-0.5BCT ceramics. However, the low Curie temperature of these materials restricted their use in practical applications. Bao et al.[147] have reported a modified (1-x)BZT-xBCT system with higher Tc without altering their colossal electromechanical response. The modified system $Ba(Zr_{0.15}Ti_{0.85})O_3$–$x(Ba_{0.8}Ca_{0.2})TiO_3$ showed a higher T_C of 114°C and d_{33} of 450pC/N at x = 53. The Curie temperature was increased by increasing both R and T terminals suitable doping. Li et al. [134,135] have reported the modified $BaTiO_3$ ceramics with relatively high Curie temperature (~ 110°C for $(Ba_{1-x}Ca_x)(Ti_{0.95}Zr_{0.05})O_3$ and 115°C for $(Ba_{1-x}Ca_x)(Ti_{0.98}Zr_{0.02})O_3$)).

2.3.2 Different preparation techniques

(Ca and Zr) modified $BaTiO_3$ were synthesized through different techniques by various researchers. The selected methods for synthesizing these ceramics depend on cost as well as applications. The quality of the powders is not only influenced by the synthesis route but also by the starting materials used. The synthesis method of ferroelectric powders has played a significant role in determining the microstructural, electrical and optical properties of ferroelectric ceramics. The unique dielectric properties and piezoelectric properties of Ca and Zr modified $BaTiO_3$ mainly depends on the purity, particle size, agglomerate size and crystal structure [50, 148].

The conventional solid state reaction method is generally used to prepare BZT- BCT ceramics. It requires a relatively higher calcination temperature (1200-1350°C) for powder preparation and sintering temperature more than 1400^oC-1550°C. The highest piezoelectric properties were obtained at an optimum calcination temperature (1300°C) and sintering temperature (1540°C) for BZT-0.5BCT ceramics. Only a few literatures are available on BZT-BCT ceramics derived from powders synthesized by wet chemical methods.

Tan et al. [149] also reported the synthesis of $(1-x)BaTi_{0.8}Zr_{0.2}O_3-xBa_{0.7}Ca_{0.3}TiO_3$ (x=0.2-0.4) powder by sol-gel method at temperatures of 900°C for 2 h .These pellets were sintered at 1250℃ for 3h with heating rate of 10°C/min. The piezoelectric coefficient (d_{33}) ~ 391pm/V and highest dielectric constant (~ 9000) at x=0.3 composition was observed, which is near the C-R-T triple point in the phase diagram.

Yang et al. [150] have prepared $(Ba_{0.88}Ca_{0.12})(Zr_{0.12}Ti_{0.88})O_3$ ceramics via sol-gel method using tetrabutyl orthotitarate and zirconium oxynitrate as the precursors. The phase pure powder was obtained at 800^oC for 2h and the crystallite size was ~37nm. These ceramics were sintered at 1280°C/2h. The Curie temperature, dielectric constant and piezoelectric coefficient d_{33} (calculated from the slope of the piezoelectric displacement curve) were 95°C, 2588 at room temperature and 215pm/V, respectively.

Wang et al. synthesized $0.5Ba(Zr_{0.2}Ti_{0.8})O_3-0.5(Ba_{0.7}Ca_{0.3})TiO_3$ (BZT-0.5BCT) nanocrystallites via a citrate precursor method at a low temperature of 700°C [151]. The flow chart of the citrate sol–gel processing is shown in Fig 2.5. They obtained phase pure perovskite with particle size in the range of 30nm to 60 nm by using appropriate calcination temperatures. But they have not studied sintering and electrical properties of the synthesized powders.

Praven et al. [152] have synthesized BZT – 0.5BCT by the sol–gel method using barium acetate, zirconium oxychloride, calcium nitrate tetrahydrate and titanium isopropoxide as raw materials. The as-synthesized powders were calcined at 1000°C, and the particle size was found to be 35–50 nm. The XRD patterns of the calcined powders contain few unreacted phases which were removed after sintering. They showed a complete formation of single-phase perovskite for BZT–0.5BCT ceramics and the density was found to be ~ 93 % of the theoretical density, obtained at 1550°C. The grain size of BZT-0.5BCT ceramic was found to be 10–20μm. They observed the phase transition temperature at 72°C with highest value of dielectric constant 11,768. High piezoelectric coefficient of d_{33} ~ 490 pC/N was obtained by this method. Praven et al. also observed remnant polarization (P_r) of 11.55 µC/cm^2 and d_{33} of 530 pC/N relative permittivity of 20,020 at the Curie temperature (95°C).

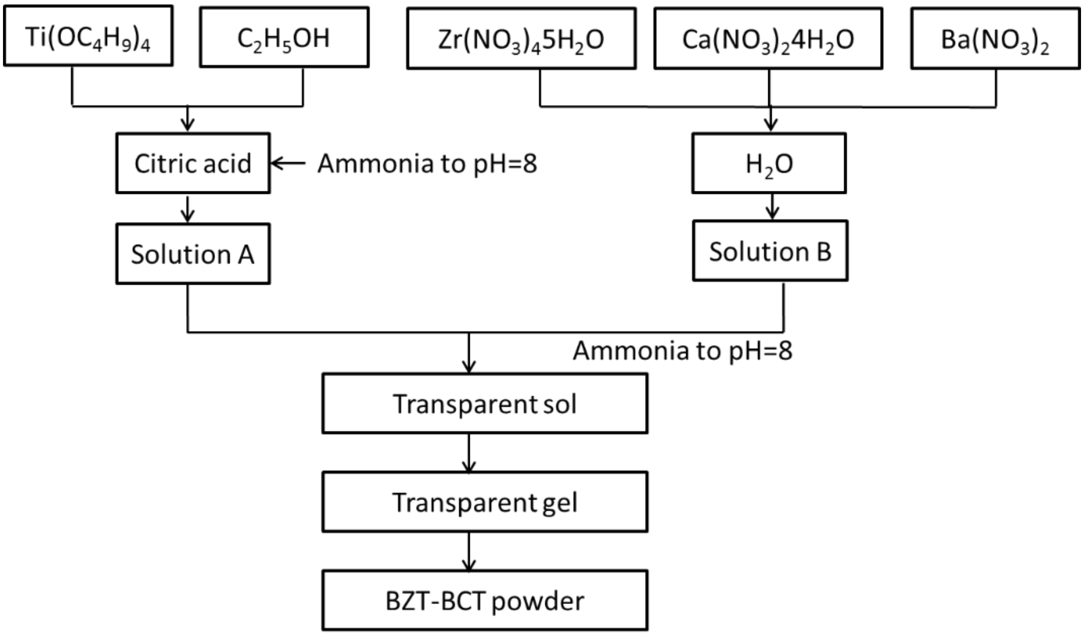

Figure 2.5 Flow chart of the citrate sol–gel processing for BZT- 0.5BCT powders [151].

Puli et al. [153] prepared high dielectric constant and low loss of $[(BaZr_{0.2}Ti_{0.8})O_3]1-x-[(Ba_{0.7}Ca_{0.3})TiO_3]$ (x = 0.10, 0.15, 0.20) (BZT–BCT)ceramics by sol-gel method. The phase pure powder was obtained at 800°C for 2 h. The pellets were sintered at 1280°C for 2h in carbolite furnace and the densities were in the range of 5.32 to 5.49 gm/cc for different composition. They observed the average grains size of 0.5 µm to 2µm for different composition. The average grain size decreases with the increase in calcium content. Dielectric constant and Curie temperature (Tc) values decreased with the increase in Ca content. They found the d_{33} of the various are independent of Ca content and the values lie in the range of 174pC/N to 177pC/N. These materials have practical applications in the development of Y5V capacitors.

Montero et al.[154] prepared $Ba_{0.9}Ca_{0.1}Ti_{0.9}Zr_{0.1}O_3$ powder by polymeric precursor combustion method at 700°C/1h. Dense ceramics was obtained from these reactive precursors using sintering temperatures below 1300°C. They found that ceramics sintered at 1275°C/5h exhibited the best piezoelectric properties d_{33} = 390 pC/N, d_{31} = ~143 pC/N, k_p = 50% , dielectric constant 2253 and tanδ = 0.06 (100 kHz), at room temperature. The T_C was found to be 112°C.

2.3.3 Effect of doping

Recently, some researchers have investigated the effects of small amount of dopants such as Pr, Ce, Cu, La, Zn, Y, etc into BZT-0.5BCT ceramics, which can reduce the sintering temperature from 1550 to 1350°C and improve the electrical properties. Wu et al. [155] studied that the ZnO (0.06mol %) modified BZT-0.5BCT ceramics exhibit good piezoelectric properties (d_{33}~ 521 pC/N, k_p ~ 47.8%) and dielectric constant of 4500. However, the addition of ZnO significantly reduced the Curie temperature (T_c) of BZT-0.5BCT ceramics and increased the grain size, because ZnO is responsible for enhancing the grain growth. Cui et al. [156] reported the low-temperature sintering for CuO modified BZT-0.5BCT ceramics. They observed that the addition of CuO (0.04wt %) into BZT-0.5BCT ceramics significantly reduce the sintering temperature from 1540 to 1350°C with d_{33}~510 pC/N, k_p~45% dielectric constant of 3762 and Curie temperature of 95°C. They also studied the effect of Ce_2O_3 [157] and Y_2O_3 [158] on the piezoelectric and dielectric properties of BZT-0.5BCT ceramics. It has been found that Ce_2O_3 (0.04 wt.%) modified BZT-0.5BCT ceramics exhibits high d_{33} of 600 pC/N, k_p of 51%, dielectric constant of 4843 at a lower sintering temperature of 1350°C. Similarly Y_2O_3 (0.06wt %) modified BZT-0.5BCT ceramics exhibit the piezoelectric constant d_{33} ~ 561pC/N. Hana et al. also [159] Studied the effect of Pr_2O_3 (0.06wt%) doping in BZT-0.5BCT and found the dielectric constant of 4638, piezoelectric constant of 460 pC/N at sintering temperature of 1400°C. Moreover, the crystal structure was not changed for Pr_2O_3 modified BZT-0.5BCT ceramics. Lin et al.[160] reported the effects of La-doping on the microstructure, dielectric and piezoelectric properties of BZT-0.5BCT ceramics. It has been found that La doped BZT-0.5BCT exhibits grain growth and decreased the ferroelectric to paraelectric phase transition temperature (T_C). They observed that the $(Ba_{0.85}Ca_{0.15})_{1-x}La_{2/3x}\ Ti_{0.9}Zr_{0.1}O_3$+1 mol%$MnO_2$ ceramic with x= 0 exhibits the optimum piezoelectric properties d_{33} = 272 pC/N and k_p = 30.3 %, respectively sintered at 1320°C. They additionally found that La doping degrades the ferroelectricity and piezoelectricity of the BZT-0.5BCT ceramics.

2.4. Effect of other isovalent substitution in $BaTiO_3$ ceramics

The dielectric properties of $BaTiO_3$ can be modified by doping with various isovalent cations on both A (Ba) and B(Ti) sites. For example substitution by Pb^{2+}, $Sr^{2+}$and Ca^{2+} can be made for part of the Ba^{2+} ions, maintaining the ferroelectric characteristics. Similarly, the Ti^{4+} ion can be partially replaced with Sn^{4+}, Hf^{4+} and Zr^{4+}[161]. The Curie temperature of $BaTiO_3$ ceramics can be shifted by the doping of Pb^{2+} ion to replace the Ba^{2+} ion to high temperature [2, 162].However, lead based system has some drawback as already discussed in Chapter 1.

The strontium (Sr) is widely used to modify the electrical properties of $BaTiO_3$, and it forms solid solutions in whole composition range ($Ba_{1-x}Sr_xTiO_3$ or BST). It has been reported that the Curie temperature of BST ($Ba_{1-x}Sr_xTiO_3$) decreases linearly with increasing concentration of Sr. The Sr^{2+} modified $BaTiO_3$ ceramics exhibits high dielectric constant, low leakage current, and low dielectric dispersion against frequency makes BST one of the promising candidates for capacitor applications but not suitable for piezoelectric applications[163-168].

Partial replacement of titanium by tin or hafnium leads to a reduction in Tc and an increase in the permittivity maximum with dopant content [169]. The chemical property of hafnium (Hf) is very much similar to that of zirconium (Zr) but the atomic weight of Hf (178.5 g/mol) is much larger than that of Zr (91.2 g/mol). Tian et al. reported 5 mol% Hf in Ti site can stabilize orthorhombic and rhombohedral phases and shows high piezoelectric properties of d_{33} ~305 pC/N and k_{33}~57%. [170]. However, Hafnium is rarely available and costly than that of Zr.

The partial replacement of Ti^{4+} by Sn^{4+} produces the $Ba(Ti_{1-x}Sn_x)O_3$, solid solution that shows diffuse phase-transition behavior and Curie temperature (Tc) decreases with the Sn^{4+} incorporation [14,171]. $BaSn_{0.2}Ti_{0.8}O_3$ shows a quasi-relaxor ferroelectric behavior that is an intermediate between a normal ferroelectric and a relaxor ferroelectric. $BaSn_{0.3}Ti_{0.7}O_3$ shows typical relaxor ferroelectric behavior. [172]. The paraelectric–ferroelectric phase transition temperature of $BaSn_{0.1}Ti_{0.9}O_3$ and $BaSn_{0.15}Ti_{0.85}O_3$ are 40°C and 5°C, respectively [173,174].

2.5. Microwave sintering

Microwave sintering has emerged as new sintering technique in recent years and has shown major advantages against conventional sintering **[**175]; some of these advantages include, time and energy saving, rapid heating (>400^oC/min), considerably reduced sintering time and temperature, fine microstructure, and so on. The microwave sintering technique has proved to densify materials without triggering grain growth, and its mass transport mechanism can accelerate the diffusion of the species in the materials more efficiently than the surface transport mechanism of conventional sintering **[**176,177].

Microwave energy is a type of electromagnetic energy with frequency ranging from 300MHz to 300GHz. Microwave heating is a technique in which material absorb the electromagnetic energy and transform into heat. In conventional heating, heat transfer takes place by conduction, convection and radiation. The material's surface is heated first followed by the movement of heat inside the body. Whereas in microwave sintering, heat is generated inside the body first and then the entire volume gets heated [178]. The comparison of heating mechanism in conventional and microwave sintering is shown in fig 2.6. In other words, microwave heating has no thermal lag, which makes it possible to reach high temperatures very rapidly. The rapid sintering in the microwave also limits the grain growth and leads to fine microstructure, consequently improving the mechanical, dielectric, and magnetoelectric properties of the material.

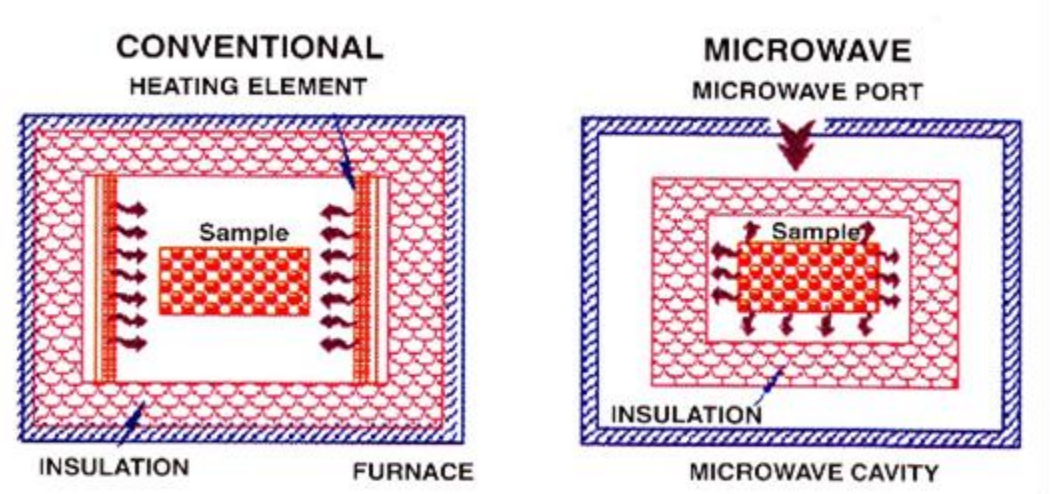

Figure 2.6 Comparison of heating mechanism in conventional and microwave sintering.

Mahajan et al. [179] studied the structural, piezoelectric, and ferroelectric properties of conventional (CS) and microwave sintered (MS) $BaZr_xTi_{1-x}O_3$ (x=0.10) ceramics. For CS, the total heating-cooling cycle time was about 22 h at the sintering temperature of 1400°Cfor 6h. Whereas for microwave (1.1 kW, 2.45 GHz) sintering the total heating-cooling cycle time was about 4 h at the sintering temperature of 1400°Cfor 2h. They found the average grain size of 13 and 5µm for samples sintered by conventional and microwave techniques, respectively. For room temperature piezoelectric application, the MS ceramics (d_{33}~122pC/N) appear to be better and stable in their properties as compared to CS ceramics (d_{33}~108pC/N). There are no reports available on the microwave sintering of Zr and Ca modified $BaTiO_3$.

2.6. Summary of literature review and scope of the work

- Barium titanate ($BaTiO_3$)-based ceramics is considered to be one of the promising lead-free ferroelectric ceramics of interest in the context of capacitor and piezoelectric transducer. However, the $BaTiO_3$ in its pure form has exhibits low permittivity. The poor piezoelectric properties and low Curie temperature has been the main obstacle to their wider commercial application.
- Chemical substitutions at the Ba^{2+} and Ti^{4+} sites are made to tailor the properties to meet a variety of device and performance requirements.
- The electrical properties of $Ba(Zr_xTi_{1-x})O_3$ solid solutions have been studied extensively; however most of the work focuses on the nature of phase transition, the temperature dependence of the dielectric constant or the ferroelectric relaxor behavior of the systems with composition x usually higher than 0.15. Recently, the compositions $x<0.15$ found immense importance for possible application as lead-free piezoelectric.
- The conventional preparation of BZT ceramics consist of solid state reaction between oxides and carbonates, requires higher phase formation temperature (1100-1300°C) and higher sintering temperature (>1400°C).
- There are many reports available on the synthesis of BZT through different chemical routes, which have the major advantage of homogeneous molecular level mixing of different raw materials and control of particle size, low temperature phase formation. However, chemical process uses costly metal alkoxides precurrors. For example, titanium isopropoxide, titanium tetrabutoxide, $TiCl_4$ are used.
- On the other hand, literature available for the preparation of BZT, either confined to only powder preparation or upto dielectric property measurement. Very few reports are available on the studies of dielectric and piezoelectric properties of $Ba(Zr_xTi_{1-x})O_3 (x<0.2)$ prepared using solution method.
- The newly discovered BZT- 0.5BCT have attracted great attention due to the excellent dielectric and piezoelectric properties.
- In contradiction to Liu et al. many researchers reported the piezoelectric constant of BZT-0.5BCT composition around 200-350pC/N.
- Little work has been performed to systematically study the dielectric and piezoelectric properties of xBZT-(1-x) BCT at close compositional modifications around MPB.

- It is well known that microstructure and their properties may differ greatly in ceramics with the same composition fabricated with different processes, even if the same technique but different processing parameters. It will be interesting to study how the microstructure and electrical properties of BZT-BCT ceramics depends on different preparation method and processing condition. There are very few literatures available on wet chemical synthesis of BZT-BCT and that is also using alkoxide precursors.
- Microwave sintering is a useful technique for making dense ferroelectric ceramics at low temperature
- There are very few reports available on low temperature sintering of BZT-BCT using additives, but sintering temperature could not be lowered below 1300^{o}C. Normally, in ferroelectric ceramics, formation of solid solution with other perovskite greatly modifies the electrical properties.
- It will be also interesting to study how the dielectric and piezoelectric properties and microstructure of BZT-BCT ceramics varies on forming solid solution with high T_C lead free perovskite.

2.7. OBJECTIVES

Keeping the above factors in mind, primary objectives of the present research work are

i) To develop $BaTiO_3$ based composition by substituting for A and/or B site of $BaTiO_3$ by Ca and Zr with an aim to get high dielectric and piezoelectric property.

ii) To use solution combustion synthesis method avoiding alkoxide precursor to get phase pure and highly reactive powders at low temperature so that it could be sintered to lower temperature.

iii) To use solid state method (namely, planetary milling, ball milling) to prepare best composition and to compare the electrical properties with solution combustion synthesized sample with an aim to improve the dielectric and piezoelectric properties further.

iv) To investigate the presence of any morphotropic phase boundary (MPB) in Ca and Zr modified $BaTiO_3$ by studying crystal structure, phase composition and electrical properties at close compositional modifications.

v) An attempt was made to sinter the MPB composition at low temperature ($<1200^oC$) by using $LiBiO_2$ as additives and to study the dielectric property of the resultant composite.

vi) Another objective is to explore whether the MPB composition could be used to form a solid solution with BNT with an aim to improve the dielectric, piezoelectric properties and Curie temperature of parent or BNT.

2.8 Organization of the Thesis

The thesis has been divided into five chapters:

Chapter–I presents a brief introduction to basics of ferroelectric and piezoelectric properties and important lead-based and lead-free ferroelectric materials.

Chapter–II deals with the detailed literature review of structural, dielectric and piezoelectric properties of Ca-modified $BaTiO_3$, Zr modified $BaTiO_3$, Zr, Ca-co-doped $BaTiO_3$ and BZT-BCT. Syntheses of modified $BaTiO_3$ by the different method and its sintering have also been reviewed in details. This literature review provides background information for understanding the aims and objectives of this investigation, and also reviews recent reports by other investigators with which these results can be compared.

Chapter–III deals with the detail experimental process related to this research work.

Chapter–IV describes the results and discussion, which has been divided into 6 sections, where, **Section 1** describes the Preparation of $Ba(Zr_xTi_{1-x})O_3$ (where x=0.1, 0.15, 0.2) powder through solution combustion method, sintering behavior, microstructure, dielectric and piezoelectric properties **Section 2** presents preparation of $(Ba_{0.85}Ca_{0.15})(Zr_xTi_{1-x})O_3$ (where x=0.05, 0.1, 0.15) powder through solution combustion method and structural, dielectric and piezoelectric characterization of sintered sample **Section 3** describes the solid state synthesis (via planetary milling and ball milling) of $(Ba_{0.85}Ca_{0.15})(Zr_{0.1}Ti_{0.9})O_3$ [BZT- 0.5BCT]* **(**best composition of section 2**)** ceramic and compare the properties with solution combustion synthesis with an aim to improve the dielectric and piezoelectric properties further. Microwave sintering was used to enhance the grain size of the sintered ceramics and properties are also compared with conventional sintered sample **Section 4** narrates the study of the structural, dielectric and piezoelectric properties of xBZT-(1-x)BCT ceramics with close compositional modification around Morphotropic Phase Boundary region [x=0.47-0.53]., **Section 5** deals with the low temperature sintering of BZT-0.5BCT Ceramics using $LiBiO_2$ as a sintering aid and their dielectric properties, **Section 6** describes the study of the structural, dielectric and piezoelectric properties of $(1-x)[(Bi_{0.5}Na_{0.5})TiO_3]$- $x[Ba(Zr_{0.2}Ti_{0.8})O_3-(Ba_{0.7}Ca_{0.3})TiO_3]$ ceramics.

Chapter–V contains the concluding remarks and the scope of future work.

$^*(Ba_{0.85}Ca_{0.15})(Zr_{0.1}Ti_{0.9})O_3$ can be represented by a pseudobinary solid solution $Ba(Zr_{0.2}Ti_{0.8})O_3-0.5(Ba_{0.7}Ca_{0.3})TiO_3$[BZT- 0.5BCT]

A complete list of references has been provided at the end of the thesis. Finally, a concise list of publications in peer reviewed international journals related to present research work has been presented in the end.

Chapter 3

Experimental Work

3.1 Introduction

In this chapter, the methods and experimental procedures used throughout this thesis are presented and have been divided into two categories: on one hand the different techniques for powder synthesis and characterising of powders, comprising the powders characterisation with electron microscopy, X-ray diffraction, Raman spectroscopy and particle size distribution and on the other hand the techniques for the determination of the dielectric, ferroelectric and piezoelectric properties of the ceramics. $Ba(Zr_xTi_{1-x})O_3$ [BZT (x=0.1, 0.15, 0.2)] and $(Ba_{0.85}Ca_{0.15})(Zr_xTi_{1-x})O_3$[BCTZ,(x=0.05, 0.1, 0.15)] were prepared by solution combustion method using analytical grade reagents. Here, the Ti-nitrate solution was prepared from TiO_2. $(Ba_{0.85}Ca_{0.15})(Zr_{0.1}Ti_{0.9})O_3$ [BZT-0.5BCT] powder was also prepared by solid state method via planetary milling and ball milling. In the later stage, $LiBiO_2$ was added for low-temperature sintering of BZT-0.5BCT. In the end, BZT-0.5BCT-BNT solid solution was prepared by planetary milling method.

3.2 Powder synthesis

3.2.1 Solution Combustion Method

$Ba(Zr_xTi_{1-x})O_3$ and $(Ba_{0.85}Ca_{0.15})(Zr_xTi_{1-x})O_3$ were prepared by solution combustion method. Reagent grade titanium dioxide [TiO_2 (99.0%)], zirconium oxychloride octahydrate [$ZrOCl_2.8H_2O$ (99.0%)], barium nitrate [$Ba(NO_3)_2$ (98.0%)], citric acid [$C_6H_8O_7$ (99.5%)], Ethylene diamine tetraacetic acid [EDTA ($C_{10}H_{16}N_2O_8$) (99.0%)] and calcium nitrate tetrahydrate [$Ca(NO_3)_2.4H_2O$ (99%)] were used as starting materials. Ti-nitrate solution has been prepared by using commercially available TiO_2. To prepare a Ti^{4+} nitrate solution, the titania (TiO_2) powder was dissolved in concentrated H_2SO_4 in the presence of $(NH_4)_2SO_4$ by constant stirring at 100°C until a clear solution of titanium sulphate was formed. The ratio of TiO_2: NH_4OH : H_2SO_4 was 10gm :80gm : 200ml. The solution was cooled to room temperature and then diluted with an addition of distilled water (1:3) in an ice bath. Ammonium hydroxide (NH_4OH), in excess, was added to the titanium sulphate solution up to pH ~10 for complete precipitation of titanium hydroxide, in an ice bath. Then the precipitate was washed with distilled water and then dissolved in nitric acid (1:1) to form a clear solution. The strength of the solution was measured by gravimetry as per the procedure cited in [180]. The Ti- nitrate solution is unstable under normal conditions and hence the resulting solution was stored inside a refrigerator. The following reactions for the preparation of Ti-nitrate solution may be written.

$$TiO_2 + H_2SO_4 = TiO(SO_4) + H_2O$$

$$TiO(SO_4) + 2NH_4OH = TiO(OH)_2 \downarrow + (NH_4)_2SO_4$$

$$TiO(OH)_2 + 2HNO_3 = TiO(NO_3)_2 + 2H_2O$$

The flow chart for the preparation of Ti- nitrate solution is shown in Fig 3.1. Similarly, Zr- nitrate solution was prepared by using zirconium oxychloride octahydrate. The zirconium oxychloride was dissolved in distilled water with constant stirring and ammonium hydroxide was added to adjust the pH between 10 and 11, for complete precipitation of zirconium hydroxide. The precipitate was washed with distilled water and then dissolved in nitric acid (1:1) to form a clear solution of Zr^{4+} ions. The strength of the solution was measured by gravimetry.

For the preparation of BZT powders, calculated amounts of zirconium nitrate solution (0.2M), titanium nitrate solution (0.2M), $Ba(NO_3)_2$, $C_6H_8O_7$ and EDTA were taken in a beaker. Ti:Zr was kept at 0.90:0.1(BZT10), 0.85:0.15(BZT15), and 0.80:0.2(BZT20).The molar ratio of metal, citric acid and EDTA was optimized at 1:1.5:0.1 and pH was also optimized at 9, to get a uniform and complete combustion. Here citric acid has a dual role, being the metal ion's complexant as well as the fuel. EDTA acts as a complexant for metal ions [181]. The solution was concentrated by heating and continuously stirring on a hot plate at 100°C. The flow chart for the preparation of BZT power is shown in Fig 3.2. After the formation of viscous gel, the stirrer was removed from the beaker and gel was further heated. The gel began to foam and swell, and finally burnt on its own (autoignition) due to the strong exothermic reaction between the citrate and nitrate species. The as-burnt ash was ground and calcined at 800°C in air atmosphere to get BZT powder.

Similarly, for the preparation of BCTZ powders, calculated amounts of zirconium nitrate solution (0.2M), titanium nitrate solution (0.2M), $Ba(NO_3)_2$, $Ca(NO_3)_2.4H_2O$, C_6H_8O7 and EDTA were taken in a beaker. Ti:Zr was kept at 0.95:0.05(BCTZ5), 0.90:0.10(BCTZ10) and 0.85:0.15(BCTZ15). The molar ratio of metal, citric acid, and EDTA were kept at 1:1.5:0.1 and pH~9, which was optimized to a get uniform and complete combustion. Finally, the as burnt ash was ground and was calcined at 700°C to get BCTZ powder. The flow chart for the preparation of BCTZ powder is shown in Fig.3.3.

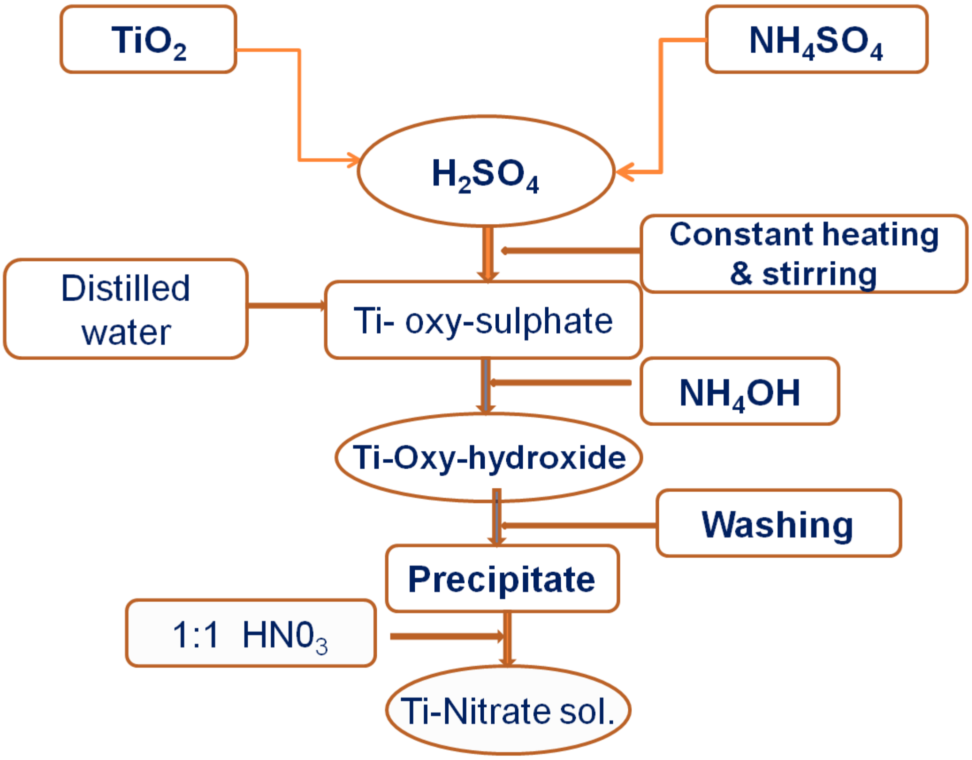

Figure 3.1 Flow chart for the preparation of Ti- nitrate solution

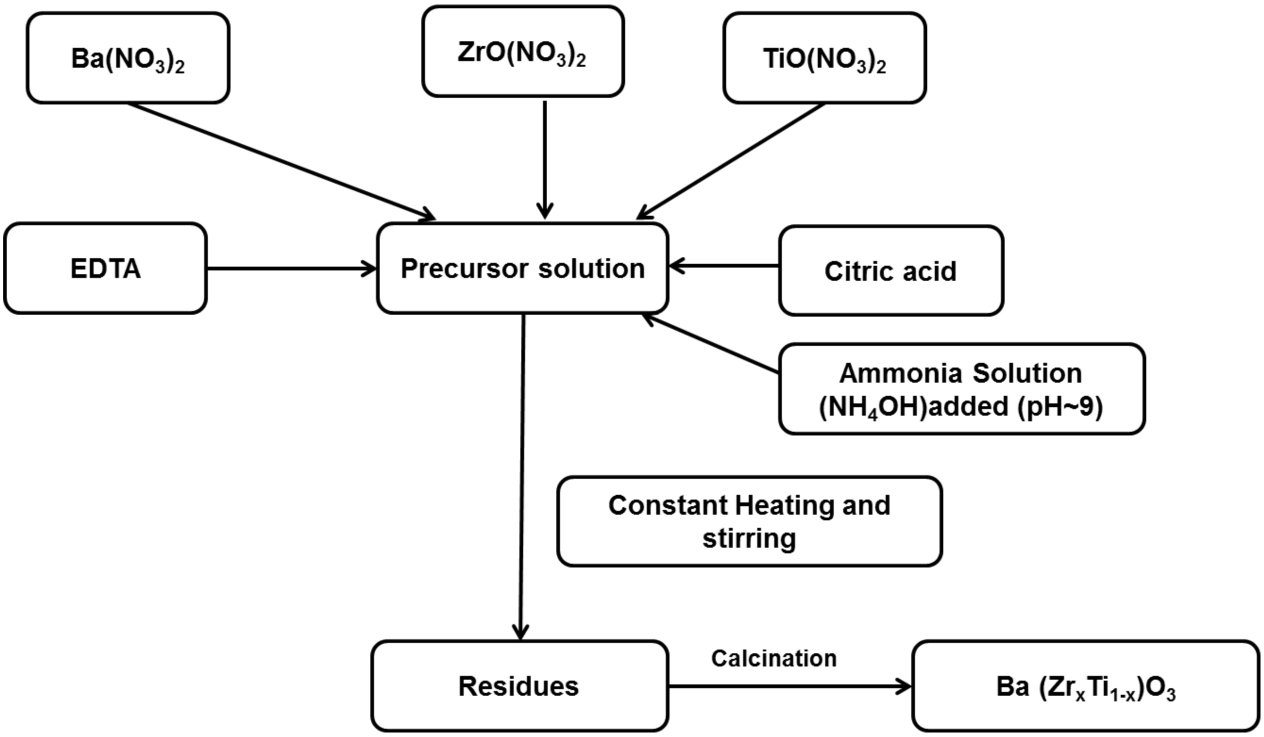

Figure 3.2. Flow chart for the preparation of BZT ceramics using solution combustion method.

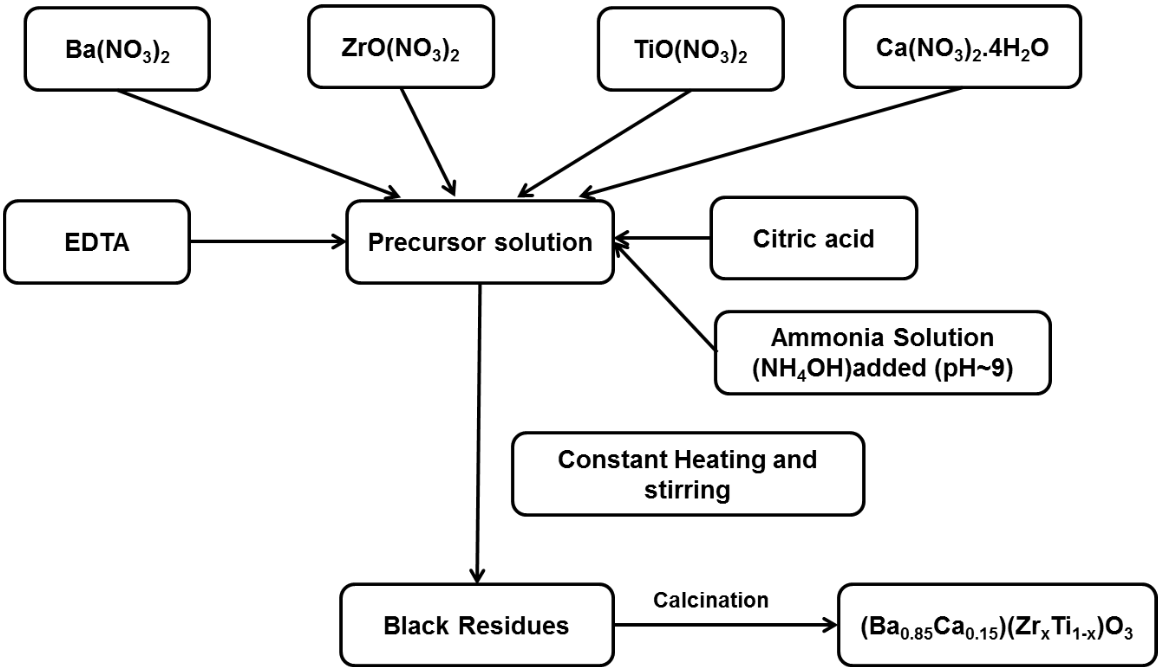

Figure 3.3. Flow chart for synthesis of BCTZ ceramics using solution combustion method.

3.2.2 Planetary milling and ball milling

Planetary milling:

The planetary ball mill owes its name to the planet-like movement of its vials. These are arranged on a rotating support disk and a special drive mechanism causes them to rotate around their axes. The centrifugal force produced by the vials rotating around their axes and that produced by the rotating support disk both act on the vial contents consisting of the material to be ground and the grinding balls. The superimposition of the centrifugal forces produces grinding ball movements with high pulverization energy. The centrifugal forces acting on the grinding jar wall initially carry the grinding balls in the direction in which the grinding jar is rotating. Differences occur between the speed of the grinding jar wall and the balls; this results in strong frictional forces acting on the sample. The schematic configuration of the planetary mill is shown in Fig. 3.4. As the rotational movement increases, Coriolis forces act on the balls to displace them from the grinding jar walls. The balls fly through the grinding jar interior and impact against the sample on the opposite grinding jar wall. This releases considerable dynamic impact energy. The combination of the frictional forces and impact forces causes the high degree of size reduction of planetary ball mills [182, 183].

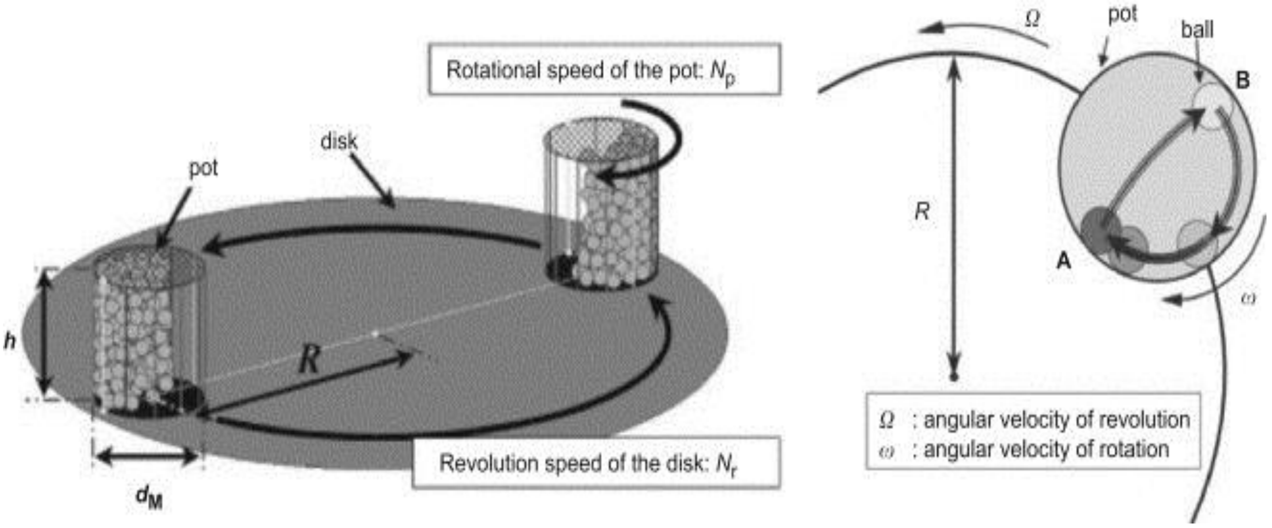

Figure 3.4 Schematic diagram of the planetary ball mill and the movement of a ball in the pot [183].

The $(Ba_{0.85}Ca_{0.15})(Zr_{0.1}Ti_{0.9})O_3$ [BZT- 0.5BCT] powder was prepared by solid state mixing method via planetary milling and ball milling. Reagent grade of barium carbonate [$BaCO_3$ (99%)], calcium carbonate [$CaCO_3$ (99%)], zirconium dioxide [ZrO_2 (99.9%)] and TiO_2 (99.0%) were used as the starting materials. Stoichiometric amount of powders were mixed by planetary mill (Fritizsch Pulveriser 5) for 10h (RPM 300) with zirconia ball. In case of powder mixing by ball milling (zirconia ball in nylon jar) using isopropyl alcohol as the media, the mixing time was 12h. The mixture was dried at 80°C overnight in an oven. The mixture was placed in an alumina crucible, which was subsequently inserted into a furnace and heated in the temperature range of 800-1400°C, at 3°C/min in the air. Fig. 3.5 shows the flow chart for the preparation of BZT-0.5BCT ceramics. xBZT-(1-x)BCT powder was also prepared by planetary milling method. Similarly, (1-x)BNT-(BZT-0.5BCT) (x=0,03,0.05,0.07) ceramics were prepared by planetary mill method as shown in fig 3.6.

$LiBiO_2$ [LBO] added BZT-0.5BCT ceramics were prepared by the conventional solid-state reaction method. Firstly, BZT-0.5BCT powders are prepared by planetary milling method. In the later stage, calculated amount of Li_2CO_3 and Bi_2O_3 was added to the calcined BZT-0.5BCT powder so that during sintering it can produce $LiBiO_2$ (LBO) in situ. The oxides are added in such a way that finally 3, 5, 7 wt% $LiBiO_2$ (designated as 3LBO, 5LBO, 7LBO respectively) were formed. This mixture was ball milled for 12h in ethanol media and the resulting slurry was dried and fired at different temperature.

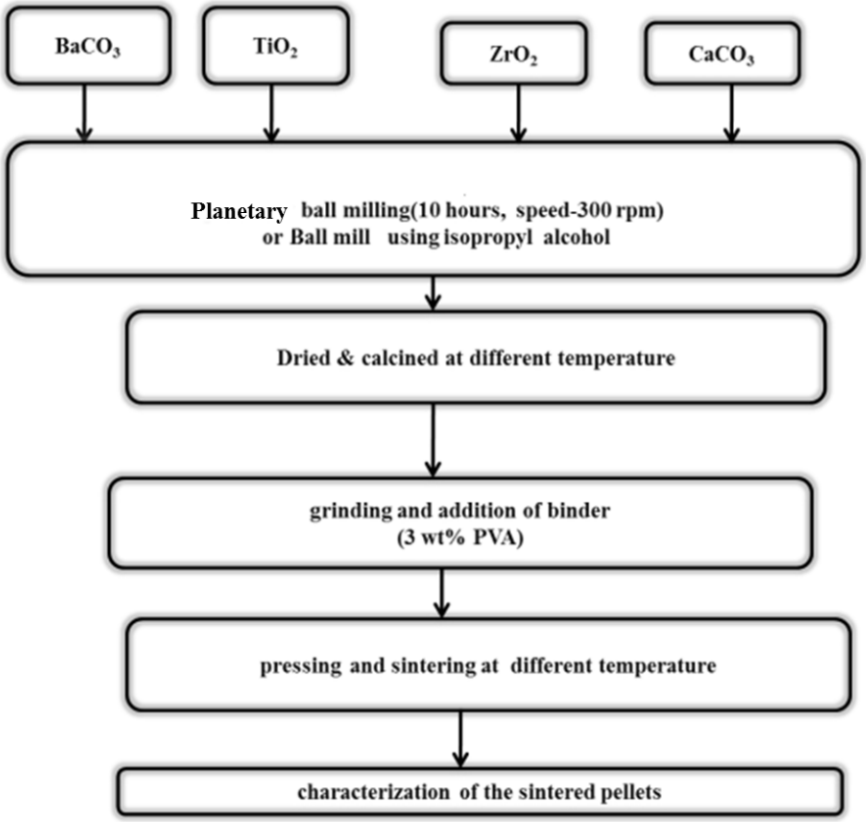

Figure 3.5 Flow chart of BZT-0.5BCT ceramics prepared by planetary milling and ball milling method.

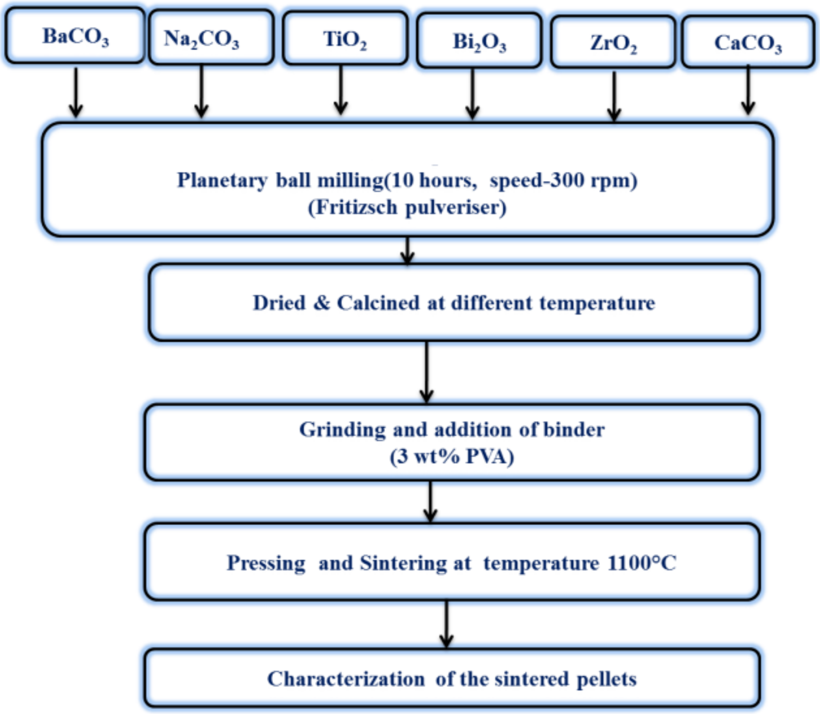

Figure 3.6 Flow chart for preparation of (1-x)BNT-(BZT-0.5BCT) ceramics prepared by planetary milling method.

3.3 General Characterization

3.3.1 Thermal Analysis

3.3.1.1 Differential Scanning Caloriemetry (DSC) and Thermo-gravimetric (TG)

The dried gel was characterized by DSC and TG [NETZSCH STA (Model No 409C)] in the nitrogen atmosphere, with a heating rate of 10^oC/min, using α-Al_2O_3 as a reference material. DSC/TG provided the information about the decomposition and crystallization behaviour of gel.

3.3.1.2 Densification Study

Densification kinetics of the samples was investigated by dilatometer [NETZSCH model DIL 402C]. The specimen was kept in a specimen holder at the center of the furnace of a dilatometer. The linear dimensional change i.e. shrinkage or expansion of the specimen is transmitted through the push rod (pressed against the sample inside the furnace) to the measuring head. Samples were made in the form of bars, having diameter 5mm and length 15 mm, for dilatometer experiment. The heating rate was maintained at 10°C/min. The measurement was carried out from room temperature to 1350°C in air atmosphere.

3.3.2. Structure and Phase analysis

3.3.2.1 X-ray diffraction of calcined and sintered specimen

X-Ray Diffraction (XRD) has proven to be a powerful and versatile tool for analysis of many aspects of fabricated barium titanate based material. This non-destructive method measures constructively interfered monochromatic x-rays diffracted at specific angles by crystal planes internal to the sample [184]. The phase evolution of the calcined powder, as well as that of the sintered samples was studied by X-ray diffraction technique (Philips PAN analytical, Netherland) using Cu Kα radiation. The instrument was run at power settings of 35 kV and 25 mA. The samples were scanned in 2θ ranges from 15 to 80° with the step size of 0.02° and a count time of 4s per step.

Phases present in the sample has been identified with the search match facility available with Philips X'pert high score plus software.

The crystallite size of the calcined powders was determined from X-ray line broadening using the Scherrer's equation as follows:

$$t = \frac{0.9\lambda}{\beta \cos\theta} \qquad (3.1)$$

where, t = crystallite size, λ = wavelength of the radiation, θ = Bragg's angle and β = full width at half maximum (FWHM) peak. Line broadening due to instrument was subtracted from the peak width before calculating the crystallite size using the following formula:

$$\beta^2 = \beta^2{}_{meas} - \beta^2{}_{equi} \qquad (3.2)$$

where, β_{meas} = measured full width at half maximum from peak, β_{equi}= instrumental broadening [Standard Silicon sample was used, whose β value was 0.09821 at 2θ = 29° with (hkl) value (111)].

The lattice parameters were estimated by Rietveld refinement method in MAUDWEB (software 2.23 version) software. This software is especially designed to refine simultaneously both the structural and microstructural parameters through a least-square fitting procedure. The peak shape was assumed to be the pseudo-Voigt function with asymmetry. The background factor of each pattern was fitted to a polynomial of degree 5 [185-187].

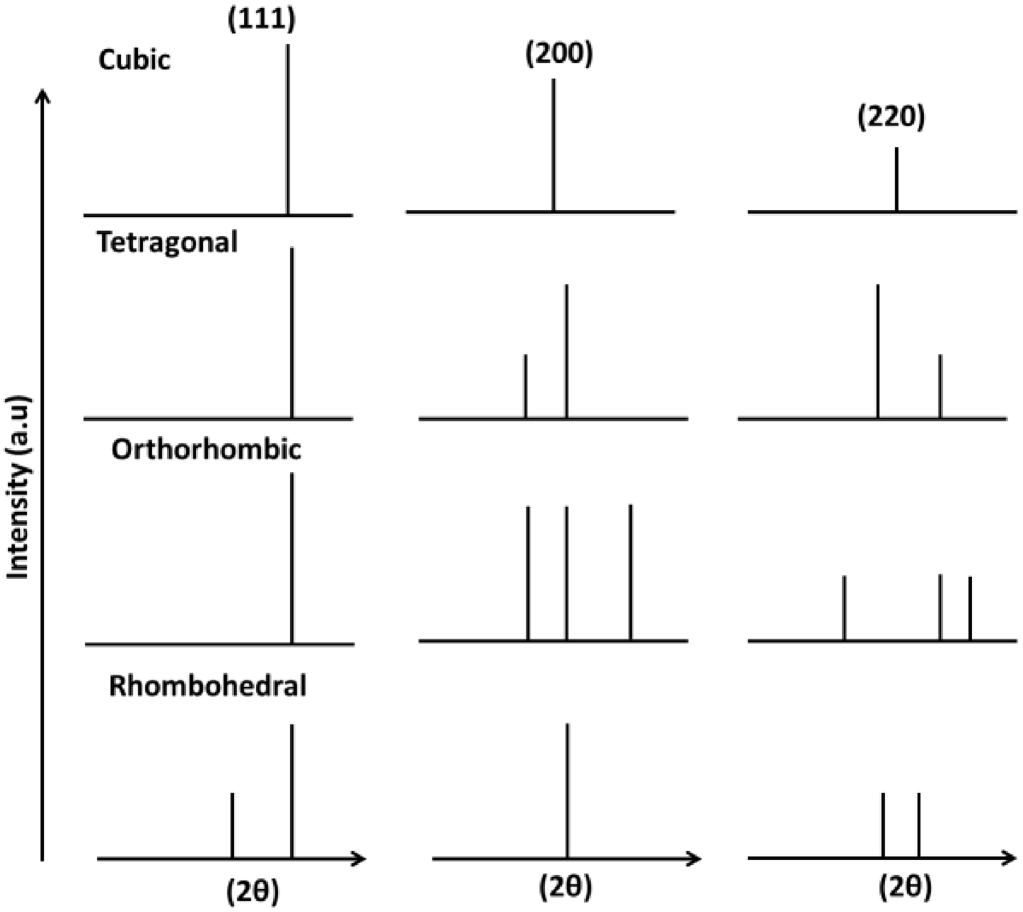

Figure 3.7 Characteristic X-ray diffraction patterns for various symmetries showing the corresponding splitting with respect to the cubic (111), (200) and (220) reflections[188].

X-ray diffraction patterns can be used to monitor chemical reactions and structural properties such as phase purity and change of symmetry (phase transition). If a crystal structure changes from cubic to tetragonal, the interaxial angles remain same (α, β, γ, =90°) where the lengths of the unit cell are different (a = b ≠ c). It will affect the d-spacing of the lattice that results in the splitting or merging of peaks as shown in Fig. 3.7. This characteristic X-ray diffraction pattern can be used to identify the symmetry and phase components of the materials [188].

3.3.3 Microstructure

3.3.3.1 Scanning Electron Microscopy (SEM) and Field Emission Scanning Electron Microscopy (FESEM)

Powder morphology, grain shape and size were observed by SEM (JEOL JSM 6480LV) and FESEM (Nova Nano SEM 450) equipped with an energy dispersive X-ray spectrometer (EDX). The samples were coated with carbon and gold for SEM and FESEM, respectively, using a sputter coater.

3.3.3.2 Transmission Electron Microscopy (TEM)

Morphology of powder was studied using high resolution TEM (HRTEM) (TechnoG230STwin).The powders were dispersed in ethanol/acetone with the help of an ultrasonic bath. The specimens were obtained by drying droplets onto 300 mesh Cu grids, coated with a lacey carbon film. TEM images were taken at an accelerating voltage of 200 kV. TEM and SAED (Selected Area Electron Diffraction) provided the information about the particle size, morphology crystallinity of BCTZ powder.

3.3.4 Surface area

The surface area of ceramic powders is an important parameter to predict sintering characteristics. This can be measured by BET (Brunauer, Emmet, and Teller) method. Specific surface area of calcined powders was determined using Quantachrome Autosorb (Model No: Nova 1200 BET). About 0.2 gm of sample was taken in the sample cell and degassed at 300°C in vacuum up to a maximum of 3 mbar. The sample holder mouth was closed by a stopper. The sample was cooled, and the cell was placed in liquid nitrogen bath. The equipment measured the amount of gas adsorbed on the surface of the sample, and the specific surface area was calculated. The average particle diameter (D_{BET}) can be calculated from BET surface area as per the following equation.

$$D_{BET} = \frac{6000}{BET_{sa} \times \rho} \tag{3.3}$$

Where ρ is the density and BET_{sa} is BET surface area.

3.3.5 Particle Size Analysis

A laser diffraction method with a multiple scattering technique has been used to determine the particle size distribution of the powder. The relation between particle size and the scattering angle is such that large particles scatter light at low angles while small particles scatter light at high angles. In order to find out the particles size distribution, the $BaTiO_3$ based powders were dispersed in water by ultrasonic processor [Vibronics, model:VPLP1].Then the experiment was carried out in computer controlled particle size analyzer [ZETA Sizers Nanoseries (Malvern Instruments Nano ZS)] to find out the particles size distribution.

3.3.6 Atomic absorption spectroscopy (AAS)

Atomic absorption spectroscopy (AAS) is a spectroanalytical procedure for the quantitative determination of chemical elements employing the absorption of optical radiation (light) by free atoms in the gaseous state.

About 0.3 g of powdered sample was weighed into a Teflon beaker. 10 mL HCl conc. was added and warmed up in a sand bath for about 10 min. Subsequently a few drops of H_2SO_4 were added .After a few minutes the decomposition was completed giving a clear solution which was placed in a 100 mL Teflon -volumetric flask and diluted with deionized water. All calibration and “blank-matrix” standards were prepared from stock solutions of 1 g/L from Inductively Coupled Plasma (ICP) standard solutions and with acids of trace select grade. An Atomic Absorption Spectrophotometer (Perkin-Elmer, Analyst 200, USA) was used for the investigations. We used AAS (Atomic Absorption Spectroscopy) for determining the presence of certain impurities (Na, K, Fe, Si, and Al) which are detrimental to ferroelectric properties.

3.3.7. Raman Spectra analysis

The room temperature spectroscopic measurement was performed in the frequency range of 150 cm^{-1} to 1000 cm^{-1} using an FT-Raman Spectrometer (BRUKER RFS 27). It relies on inelastic scattering or Raman scattering of monochromatic light, usually from a laser in the visible, near-infrared or near ultraviolet range. Phonons or other excitations in the material are absorbed or emitted by the laser light, resulting in the energy of the laser photons being shifted up or down. The shift in energy gives information about the phonon modes in the system. Raman scattering have been used to study the phase transition, phase formation and B-site ordering/disordering of normal ferroelectric and relaxors.

3.3.8 Preparation of Bulk Sample

For the preparation of the bulk sample, calcined powders were mixed with 3 wt. % PVA (Poly Vinyl Alcohol) solution with the help of mortar and pestle and dried. The dried powders were pressed into cylindrical pellets (12 mm diameter, 1-2mm thickness) at 350MPa in a hydraulic press (Carver Inc., USA) with a holding time of 120 seconds. The pressed green compacts were sintered in air with a heating rate of 3°C/min in the temperature range of 1100 -1400^{0}C for 4h, with binder burnout at 650°C for 1h in a conventional furnace.

Table 3.1 Calcination and Sintering temperature for different compositions.

Composition and preparation Method	Calcination temperature	Sintering Temperature
$Ba(Zr_xTi_{1-x})O_3$ (x=0.1,0.15,0.2) (combustion method)	800°C	1350°C
$(Ba_{0.85}Ca_{0.15})(Zr_xTi_{1-x})O_3$ (x=0.1,0.15,0.2) (combustion method)	700°C	1250-1325°C
$(Ba_{0.85}Ca_{0.15})(Zr_{0.1}Ti_{0.9})O_3$ (Planetary Milling)	1200°C	1250-1400°C
xBZT-(1-x)BCT (x=0.47-0.53) (Planetary milling)	1200°C	1350°C
$(Ba_{0.85}Ca_{0.15})(Zr_{0.1}Ti_{0.9})O_3$ (Planetary Milling) [Microwave sintering(20°/min]	1200°C	1350°C/10min
$(Ba_{0.85}Ca_{0.15})(Zr_{0.1}Ti_{0.9})O_3$ (Ball Milling)	1300°C	1350-1400°C
$(Ba_{0.85}Ca_{0.15})(Zr_{0.1}Ti_{0.9})O_3$-$xLiBiO_2$ (x=0,0.03,0.05,0.07) (Planetary Milling)	-	1000-1100°C
$(1-x)Na_{0.5}Bi_{0.5}TiO_3$-$x(Ba_{0.85}Ca_{0.15})(Zr_{0.1}Ti_{0.9})O_3$ (x=0,0.03,0.05,0.07) (Planetary Milling)	700°C	1100°C

3.3.9 Density measurements

The bulk density of the samples was measured by Archimedes principle. The formula for the calculation of bulk density is as follows.

$$Bulk\ density = \frac{W_d}{W_s - W_{su}} \times Density_{liquid}$$

$$\mathrm{Re}lative\ \ density = \frac{bulk\ density}{Theoretica\,l\ density} \times 100$$

Where W_d , W_s and W_{su} are the dry weight, soaked weight and suspended weight of the sample, respectively. The liquid used for calculation was kerosene of density 0.81 g/cc.

3.3.10 Dielectric measurements

For electrical measurements, both the surfaces of the pellets were painted uniformly with silver conductive paste (Alfa Aesar) and cured at 500°C for half an hour. Thus, a pellet with two parallel electrodes acts as a single layer capacitor.

The dielectric constant or relative permittivity (ε_r) is defined as the ratio of the permittivity of the material to the permittivity of free space. The dissipation factor is defined as the tangent of the loss angle (tan δ). It is a measure of the amount of electrical energy which is lost through conduction when a voltage is applied across the piezoelectric element. The dielectric constant (ε_r) and dielectric loss factor (tan δ) was measured using Solatron SI 1260 Impedance /Gain-phase analyzer and HIOKI 3532-50 LCR Hitester. Measurements are carried out in the frequency range of 100Hz to 1MHz. Dielectric behavior has also been studied as a function of temperature with the temperature ranging from room temperature to 550°C depending on the composition. The samples were placed in between two platinum sheets each of which is connected to a platinum wire. The whole arrangement was covered with an alumina tube. A small force was applied using a spring to ensure good contact with the sample electrodes. The dielectric measurement was carried out in a Carbolite furnace at a heating rate of 2°C/min.

The relative permittivity (ε_r) is calculated from the measured values of capacitance and physical dimension of the specimen. The relations are expressed as:

$$C = \frac{\varepsilon_0 \varepsilon_r A}{t} \qquad (3.4)$$

where ε_r the relative permittivity of the piezoelectric material, ε_0 is the relative permittivity of free space (8.854×10^{-12} F/m), t is the distance between electrodes (m), A is the area of the electrodes (m^2).

In an alternating electric field the dielectric permittivity or relative permittivity is a complex quantity and can be written as

$$\varepsilon_r * = \varepsilon' + \varepsilon'' \qquad (3.5)$$

where ε' is the real part of the dielectric permittivity and ε'' is the imaginary part of permittivity and related to the energy loss in the system.

When the dielectric is subjected to the ac voltage, the electrical energy is absorbed by the material and is dissipated in the form of heat. The dissipation is called dielectric loss. In this case, current leads the voltage by (90-δ), where δ is called the loss angle, and tanδ is the electrical loss, as shown in Fig 3.8.

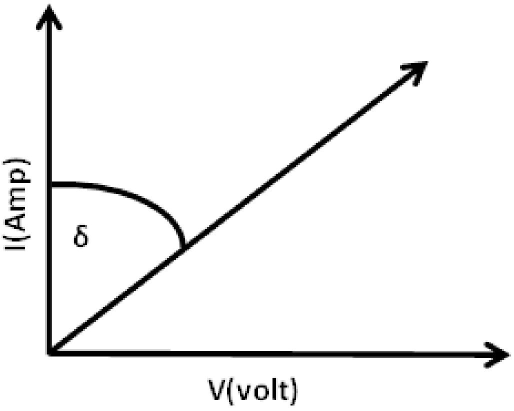

Figure 3.8 Phase diagram between current and voltage.

The loss tangent can be expressed [189,190] as

$$\tan\delta = \frac{\varepsilon''}{\varepsilon'} \qquad (3.6)$$

Curie temperature (Tc): It is the temperature above which the spontaneous polarization (Ps) of the ferroelectric materials vanishes and it goes to paraelectric state.

Dielectric breakdown strength of the samples was measured at room temperature in a silicone oil bath by applying a DC electric field (Neo-Tele-Tronix).

3.3.11 Impedance Spectroscopy

The electrical behavior of the compound has been studied over a range of temperature and frequency (typically 1–10^6 Hz) using the complex impedance spectroscopy (CIS) technique [179,191,192]. This technique enables us to separate the real and imaginary components of the electrical parameters and hence provides a true picture of the material properties. Each representation can be used to highlight a particular aspect of the response of a sample. The electrical properties often presented in terms of immittance functions [impedance (Z), admittance (Y), permittivity (ε), and electrical modulus (M)]. The frequency dependent dielectric properties of materials can normally be described in terms of the complex dielectric constant (ε*), complex impedance (Z*), electric modulus (M*), and dielectric loss (tanδ).

The impedance measurement on a material gives us data having both resistive (real part) and reactive (imaginary part) components. It can be displayed conventionally in a complex plane plot (Nyquist or Cole–Cole diagram) in terms of following representations:

$$\mathrm{M}^* = \mathrm{j}\omega \mathrm{C}_0 \mathrm{Z}^* \qquad (3.7)$$

$$\varepsilon^* = (\mathrm{M}^*)^{-1} \qquad (3.8)$$

$$Y^* = (\mathrm{Z}^*)^{-1} \qquad (3.9)$$

$$\mathrm{Y}^* = \mathrm{j}\omega \mathrm{C}_0 \varepsilon^* \qquad (3.10)$$

Where ω= 2πf is the angular measurement frequency and C_0 the vacuum capacitance of the space within the measuring cell. For many heterogeneous dielectrics, the most useful information can be obtained from combined spectra of the imaginary component of the electric modulus, M″(f), and the imaginary component of the impedance, Z″(f). Based on a single, parallel Resistor (R) and Capacitor (C) element to represent an electroactive region, these two functions can be described by the following equations:

$$\mathrm{M}'' = \frac{\mathrm{C}_0}{C}\left[\frac{\omega \mathrm{RC}}{1+(\omega RC)^2}\right] \qquad (3.11)$$

$$\mathrm{Z}'' = R\left[\frac{\omega \mathrm{RC}}{1+(\omega RC)^2}\right] \qquad (3.12)$$

From Eqs. (3.11) and (3.12), the position of the maxima in M″(f) and Z″(f) spectra is given by

$$\omega_{\max} = 2\pi f_{\max} = (RC)^{-1} \qquad (3.13)$$

Where $f_{\max}$ is the position of the maxima and RC is the time constant.

The height of the maxima in M″(f) /(M″max) and Z″(f)/(Z″max) spectra can be calculated by substituting Eq. (3.13) into Eqs. (3.11) and (3.12), given as

$$M''_{\max} = \frac{C_0}{2C} = \frac{1}{2\varepsilon_r} \qquad (3.14)$$

$$Z''_{\max} = \frac{R}{2} \qquad (3.15)$$

By correcting for sample geometry, the M″ peak is also commonly presented as a relative value:

$$\frac{M''_{\max}}{\varepsilon_0} = \frac{1}{2\varepsilon_0\varepsilon_r} = \frac{1}{2C_{corr}} \qquad (3.16)$$

Where C_{corr} is capacitance corrected after sample geometry (pellet thickness/area). In this work, all M″ data are presented as a relative value corrected after sample geometry. Hence, the maxima in M″(f) spectra are dominated by components with the smallest C value and usually pertain to intragrain (bulk) responses, whereas the maxima in Z″(f) spectra are dominated by those with the largest R value and are often associated with resistive intergrain (grain boundary) responses in electroceramics. If the maxima in M″(f) and Z″(f) spectra occur at the same frequency (f_{max}), that is, they share the same time constant, it suggests that they pertain to the same electroactive region. On the contrary, a localized dielectric relaxation associated with a resistive grain boundary would result in separate positions for the maxima in the Z″(f) and M″(f) spectra [193]

3.3.12 P-E Loop Measurement

The Polarization hysteresis measurement was carried out by an automatic P-E loop tracer (Marine India, Electronics). For these measurements, the thickness of the pellets was reduced to ~1mm. The pellets were electroded with silver paste and cured at 500°C for 30min. All the measurements were carried out at room temperature to near Curie temperature (120°C) of the material.

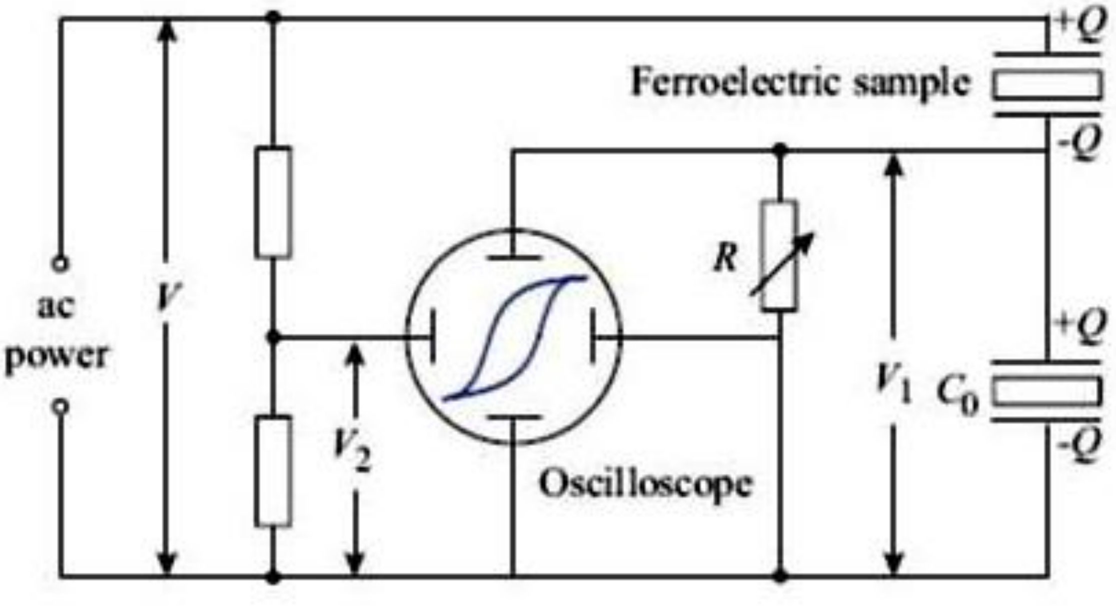

Figure 3.9 Schematic circuit of the Sawyer–Tower Bridge for measuring the P–E characteristics of ferroelectrics [190].

The polarization hysteresis measurements based on standard Sawyer- Tower circuit is shown in Fig. 3.9. In order to avoid dielectric breakdown in air, silicon oil with a high dielectric strength is used to cover the sample. An approximate value of the electric field strength in the sample is obtained with the input voltage and the sample thickness.

3.3.13 Piezoelectric coefficient (d_{33}) measurement

In ferroelectric ceramics, adjoining dipoles form regions of local alignment called domains. The alignment gives a net dipole moment to the domain, and thus a net polarization. The direction of polarization of neighboring domains is random. So, the ceramic element has no overall polarization.

Poling is a process during which a high electric field is applied to the ferroelectric samples to force the domains to reorient the direction of the applied electric field. The poling is possible in the ferroelectric ceramics, and poling steps are shown in fig 3.10.

For the piezoelectric measurements, the pellet samples were first poled in silicon oil under an applied different field at room temperature for 20min. The NBT-[BZT-0.5BCT] ceramics were poled at a temperature of~120°C in a silicon oil bath under a dc field ~3kV/mm for 20min.The d_{33} coefficients of the poled samples were measured after 24h with a d_{33} meter (YE2730A d_{33} Meter, APC International Ltd.). A force of 0.25N is applied to the sample, and the corresponding d_{33} coefficient is measured.

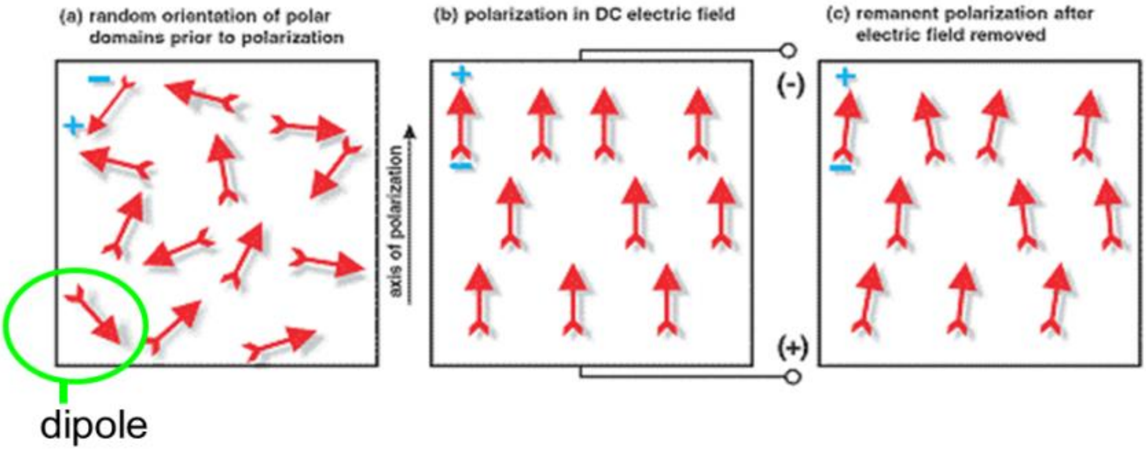

Figure 3.10 Poling of ferroelectric material

Electromechanical coupling factor (k) is used to measure the conversion efficiency between the electrical and mechanical energy in the piezoelectric material. It can be determined by measuring the impedance of the electrically poled samples in a frequency range 10kHz to 5 MHz using a Solatron S1 1260 Impedance /Gain-phase analyzer or HIOKI 3532-50 LCR Hitester.

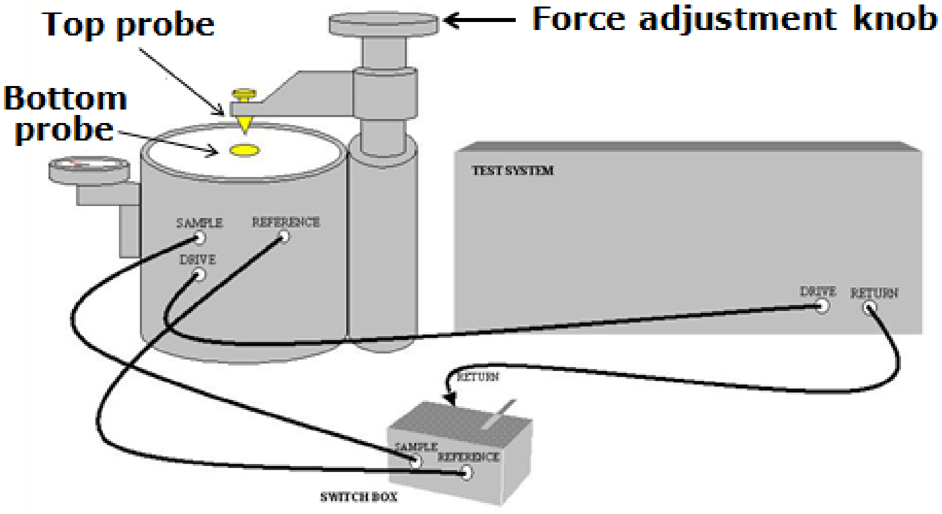

Fig. 3.11 Schematic of piezoelectric constant (d_{33}) measurement

The electromechanical coefficient [190] is calculated using the formula mentioned below:

$$K_{eff} = \sqrt{\frac{{f_a}^2 - {f_s}^2}{{f_a}^2}} \tag{3.17}$$

Where f_s resonant frequency and f_a is the antiresonant frequency.

Chapter 4

Results and Discussion

Chapter-4.1

Synthesis and Characterization of Zr modified $BaTiO_3$ by solution Combustion method

4.1.1 Introduction

Barium zirconate titanate [$Ba(Zr_xTi_{1-x})O_3$, (BZT)] ceramics are based on the solid solution of $BaTiO_3$ and $BaZrO_3$.The BZT ceramics are attractive candidates for microwave technology, multilayer ceramic capacitor (MLCC), dynamic random access memory (DRAM) and piezoelectric transducers due to their high dielectric constant, low dielectric loss, large tunability (discussed in chapter 2). The electrical properties of $Ba(Zr_xTi_{1-x})O_3$ solid solutions have been studied extensively; however most of the work focuses on the nature of phase transition, the temperature dependence of the dielectric constant or the ferroelectric relaxor behavior of the systems with composition x usually higher than 0.15[28, 194]. Recently, the compositions $x<0.15$ found immense importance for possible application as lead-free piezoelectric [90, 97]. The conventional preparation of BZT ceramics is a solid state reaction between oxides and carbonates requires at higher phase formation temperature (1200-1350°C) and higher sintering temperature (>1400^{o}C) [100, 195]. Several reports are available for the preparation of BZT powders by conventional solid-state method and many reports of its synthesis through different chemical routes [103,107, 111,113,114,196], which have the major advantage of homogeneous molecular level mixing of different raw materials and control of particle size, low temperature phase formation. However, chemical process uses costly metal alkoxides raw materials. For example, titanium isopropoxide, titanium tetrabutoxide, titanium chloride are used. On the other hand, literature available on the preparation of BZT is either confined to only powder preparation or upto dielectric property measurement. Very few reports are available on the studies of dielectric and piezoelectric properties of $Ba(Zr_xTi_{1-x})O_3(x<0.2)$ ceramics prepared by solution method.

This chapter presents the synthesis of $Ba(Zr_xTi_{1-x})O_3$ [where x= 0.1, 0.15,0.2 denoted by BZT10, BZT15, BZT20, respectively] through a citrate-nitrate autocombustion method avoiding alkoxide based precursor. The thermal decomposition behaviour and phase formation during heat treatment of precursor powders were investigated. The synthesized BZT was characterized with respect to structural analysis, densification behavior, dielectric, diffuse phase transition behavior, ferroelectric hysteresis, piezoelectric constant (d_{33}) and impedance spectrocscopy.

4.1.2 Results and discussion

4.1.2.1 Effect of EDTA and pH

Figure 4.1.1 shows the room temperature X-ray diffraction patterns of the BZT10 powders calcined at 800°C/ 4h and synthesized at different pH and EDTA ratio. Initially, BZT was prepared by keeping metal to citric acid (M:C) ratio at 1:1.5 at pH seven without any EDTA addition. Calcined powder contains carbonates impurities.Here citric acid has a dual role, as a complexant for metal ions and fuel for the combustion reaction [181]. Then EDTA was introduced and studied for two ratios metal: citric acid: EDTA (M: C: E) ratio of 1:1.5:0.1 and 1:1.5:0.15 at pH 7. Impurity content in the calcined powder significantly reduced with the introduction of EDTA but at 0.15, it further increases. However, the powder prepared without using EDTA at pH~7, no. of secondary phases were found to appear along with perovskite phase. EDTA contains both of carboxylate and aliphatic amine groups to participate in the complexation of metal ions and have stronger chelating ability than that for citric acid, which contains only carboxylate groups [197].

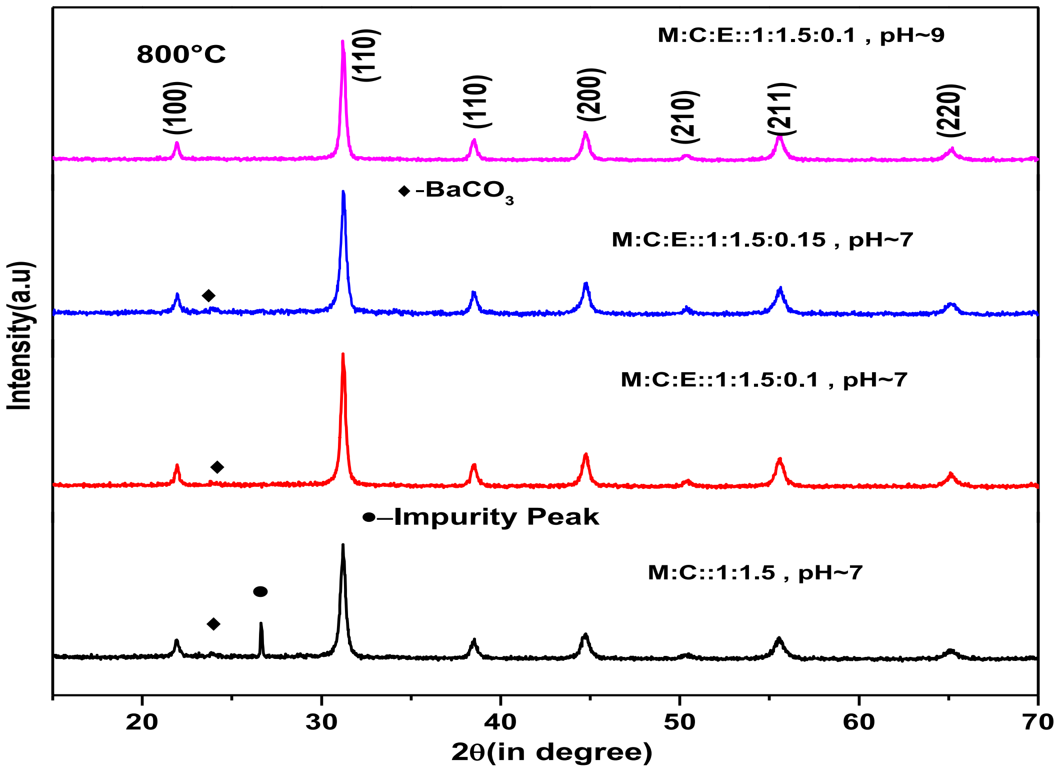

Figure 4.1.1 X-ray diffraction patterns of BZT10 powder with different pH and EDTA content calcined at 800°C.

It was observed that at M: C: E: :1:1.5:0.1, with the increase in pH from 7 to 9 produces pure perovskite phase at 800^{o}C. It is to be mentioned that the increase of the pH facilitates ionization of more EDTA, and more carboxylic groups can be available to chelate the metallic ions in the solution at higher pH conditions. When the pH value is around 9, the environment facilitates to form stable metal EDTA complexes [198]. It was also observed that at lower pH values (pH <7), white precipitates appeared, which might be nitrates and hydrous metal oxides. Formation of precipitates indicating the incomplete complexation of the metal ions took place in an acid medium. To facilitate the formation of stable Ba–Zr–Ti precursor solution, ammonia additions were used in this work as an easily removed pH modifier to obtain higher pH values. The best composition for the formation of pure BZT powder was M: C: E:: 1:1.5:0.1 and pH~9.

AAS (Atomic Absorption Spectroscopy) was used for determining the presence of certain impurities (Na, K, Fe, Si, and Al) which are detrimental to ferroelectric properties. It is found that Na, K, Fe, Si, and Al present as 5, 6, 2, 23, 4 ppm, respectively in the final ceramics.

4.1.2.2 Thermal Analysis and Phase Evolution

The typical thermal decomposition behaviour of the precursor gel of BZT10 is shown in fig 4.1.2. It shows one endothermic peak at 138°C as well as two exothermic peaks at 244°C and 273°C. The endothermic peak at 138°C corresponds to dehydration of adsorbed water, which leads to a weight loss of 11%. The exothermic peak at 244°C and 273°C corresponds to the decomposition of the metal complex, pyrolysis of organic groups and phase formation, resulting in weight loss of 74%.The weight loss beyond 273°C was negligible. It shows highly exothermic and single stage decomposition. Instantaneous rise in temperature and sharpness of the weight change of TG plot indicates a self-propagating type autocombustion reaction.

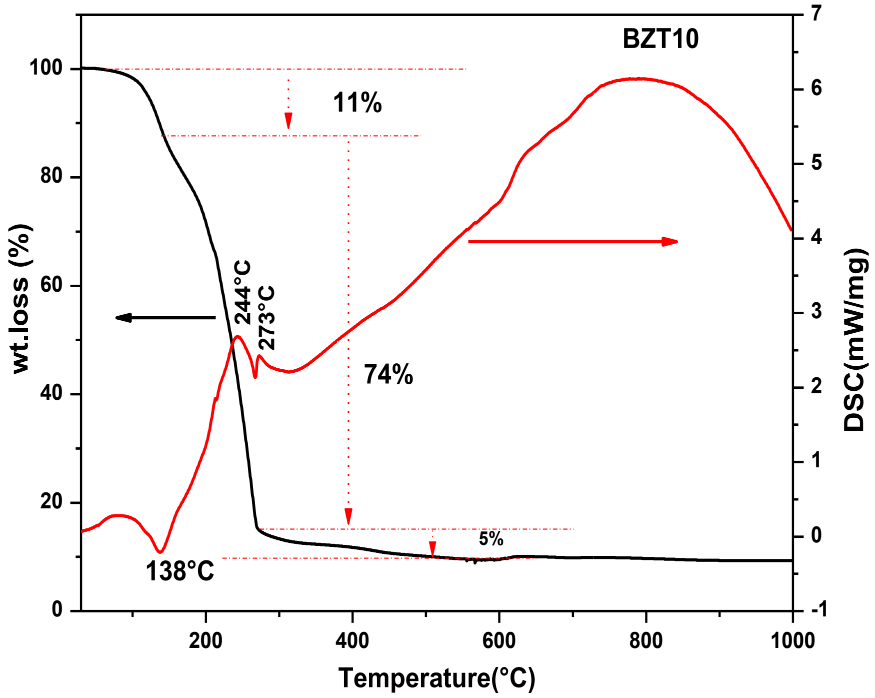

Figure 4.1.2 DSC-TG curve for BZT10 gel with the optimum ratio.

It is to be mentioned that the addition of ammonia to enhance the pH produces ammonium nitrate by reaction of the ammonia with the NO_3^- groups from the barium, titanium and zirconium nitrate as water is removed. This compound significantly accelerates the decomposition of the gel precursors on heating, producing strongly exothermic reactions that facilitates the formation of perovskite phase at as burnt state with small amount of oxide and carbonates impurities (shown in Fig. 4.1.4).Finally, the broad exothermic peak at higher temperature corresponds to the crystallization,reaction of left over $BaCO_3$, TiO_2, and ZrO_2 to form perovskite and oxidation of the residual carbonaceous mass [106,107,199,200].The mechanisms of chelation of citric acid and EDTA with metal ions are shown in fig 4.1.3.

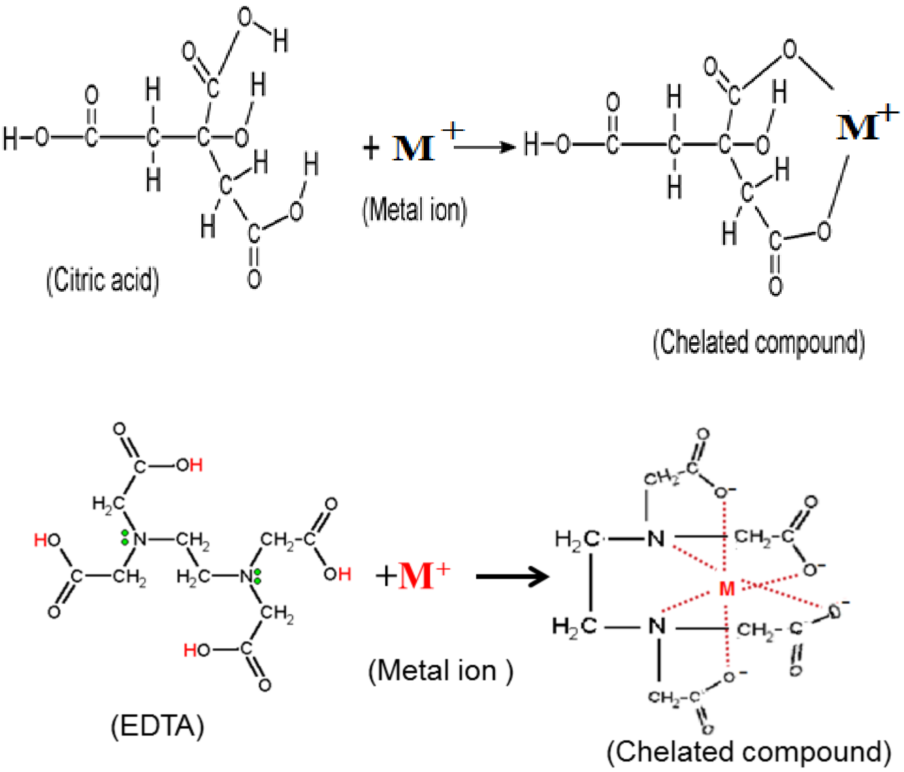

Figure 4.1.3 Chelation of citric acid and EDTA with metal ions.

The possible reaction in the autocombustion method can be described by the following equation:

$$Ba(NO_3)_2 + 0.1\,ZrO(NO_3)_2 + 0.9TiO(NO_3)_2 + C_6H_8O_7 + C_{10}H_{16}N_2O_8 \xrightarrow{9.5O_2} BaZr_{0.1}Ti_{0.9}O_3 + 16CO_2 + 12H_2O + 3N_2$$

The X-ray diffraction pattern for the BZT10 powder calcined at different temperature is presented in Figure.4.1.4. It can be observed that the as burnt (without calcination) powder consisted of pure perovskite phase with a small amount of impurity phase. It proves that pure perovskite phase formed around 275^{o}C. Such a low-temperature phase formation may be attributed to effective complex formation with the metal ion, near to one-step decomposition of complex and ignition at low temperature [181, 107]. It is observed that powder calcined at 500°C and 700°C, the perovskite structure was detected together with an intermediate phase, attributed to the $BaCO_3$. The height of the diffraction peaks belonging to $BaCO_3$ decreases with the increasing of calcination temperature. The complete phase purity is obtained at 800°C which is much lower than the powder prepared by the conventional method [94] and sol-gel method [104,105]. Chen et al **[**106**]** prepared BZT20 powders by sol-gel method at 900°C. Chakrabarti et al.[107] synthesized BZT powder at 800°C by autocombustion method using $TiCl_4$ as starting material. Julphunthong et al. [108] prepared BZT10 powder at 1000°C for 5h by autocombustion method using urea as a fuel.

Fig.4.1.5 shows the X-ray diffraction patterns for the BZT powders calcined at 800°C. All the compositions possess a pure perovskite structure without any secondary phase. This is a clear indication that Zr^{4+}forms solid solutions in $BaTiO_3$ lattice with isovalent substitution of Ti^{4+} (ionic radius 0.605Å) by Zr^{4+} (ionic radius 0.72Å) to form homogeneous solid solutions whose symmetry gradually changes with Zr addition [94, 201]. Moreover, it is clear that the position of diffraction peaks of the BZT ceramics has shifted to lower angle with increase in Zr content. Due to the fact that the ionic radius of Zr^{4+}(0.72Å) is larger than that of Ti^{4+}(0.605Å), thus the substitution of Ti^{4+} ion by Zr^{4+} ion could increase the lattice parameter of the ceramics.

The tetragonality (c/a ratio) decreases with increasing Zr^{4+} ion content which indicates that change of zirconium content highly influences on the crystal structure of BZT ceramics[202].X-ray diffraction pattern of BZT ceramics sintered at 1350°C/4h are shown in figure 4.1.6 (a). It also confirms that the single phase perovskite structure with no impurity is present in the sintered samples. It is reported in the literature that [91,100] BZT may have tetragonal, orthorhombic, rhombohedral or cubic structure at room temperature depending upon the Zr content. The BZT10 sample showing both tetragonal phase and orthorhombic phase which can be matched with JCPDS file no. 89-1428 and 81-2200 respectively. Moreover, when zirconium content is higher than 10%, the diffraction peak changed from non-symmetry to near symmetry resembled the pseudo cubic phase. The splitting of (002) and (200) diffraction peaks of BZT ceramics confirms the tetragonal phase as shown in figure 4.1.6(b) [203].

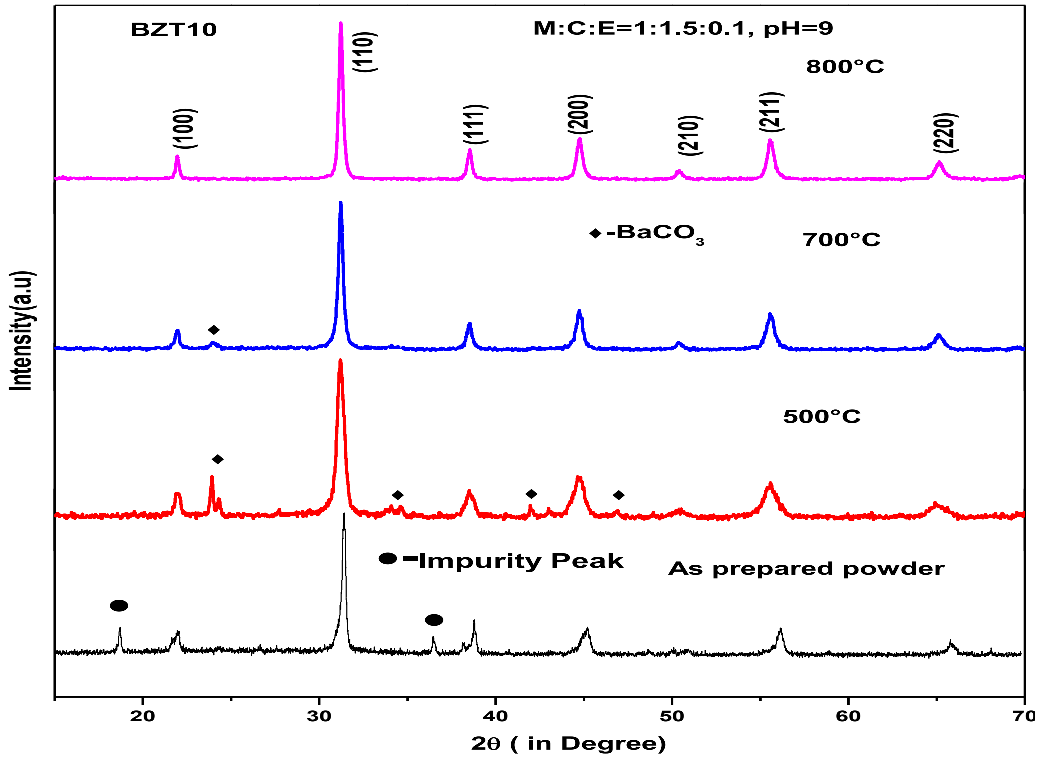

Figure 4.1.4 X-ray diffraction pattern for BZT10 powder calcined at different temperature.

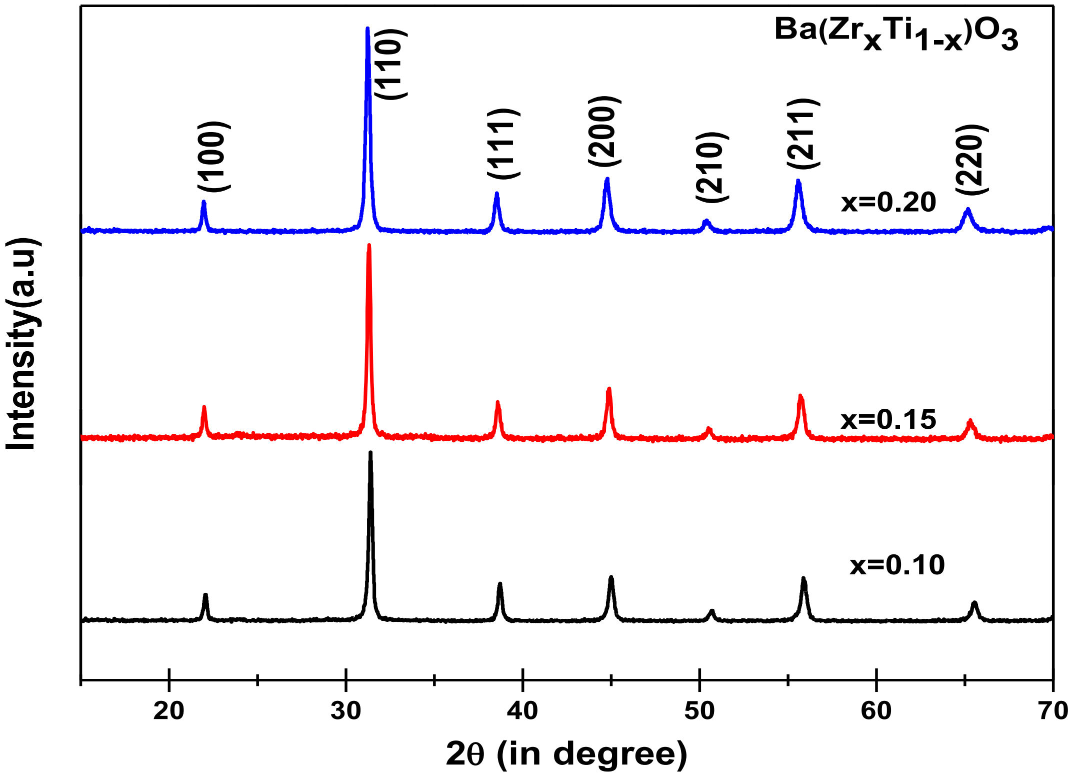

Figure 4.1.5 X-ray diffraction patterns for $Ba(Zr_xTi_{1-x})O_3$ (x= 0.10, 0.15, 0.20) powder calcined at 800°C.

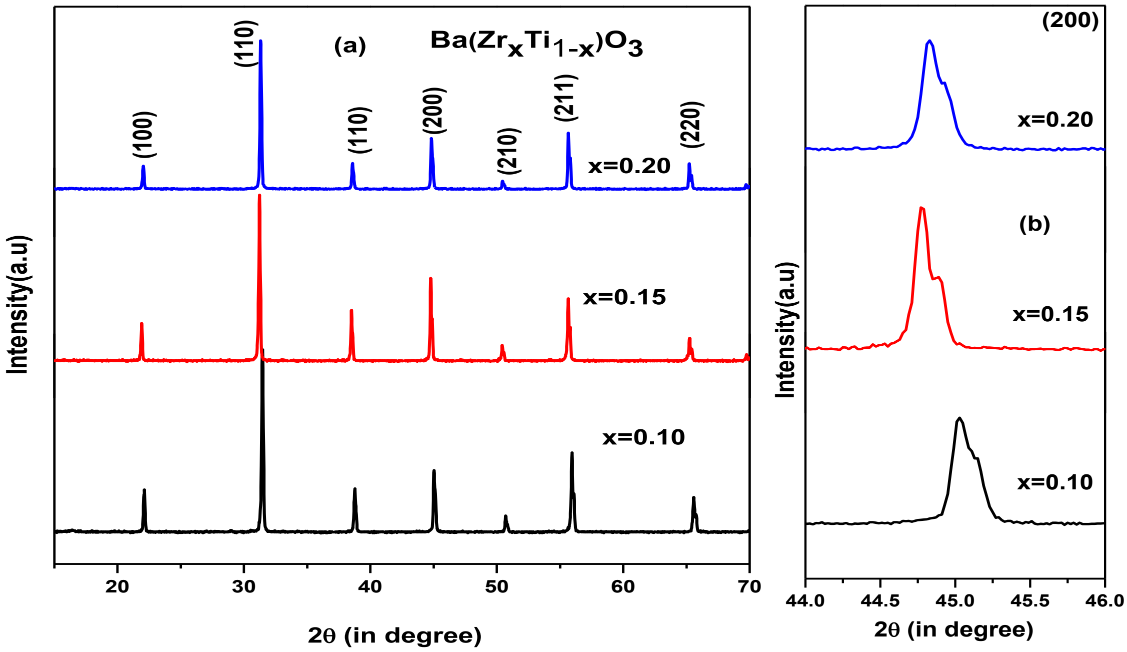

Figure 4.1.6 (a) X-ray diffraction patterns of BZT (x=0.1, 0.15, 0.2) ceramics sintered at 1350°C (b) magnification in the range 44°-46°.

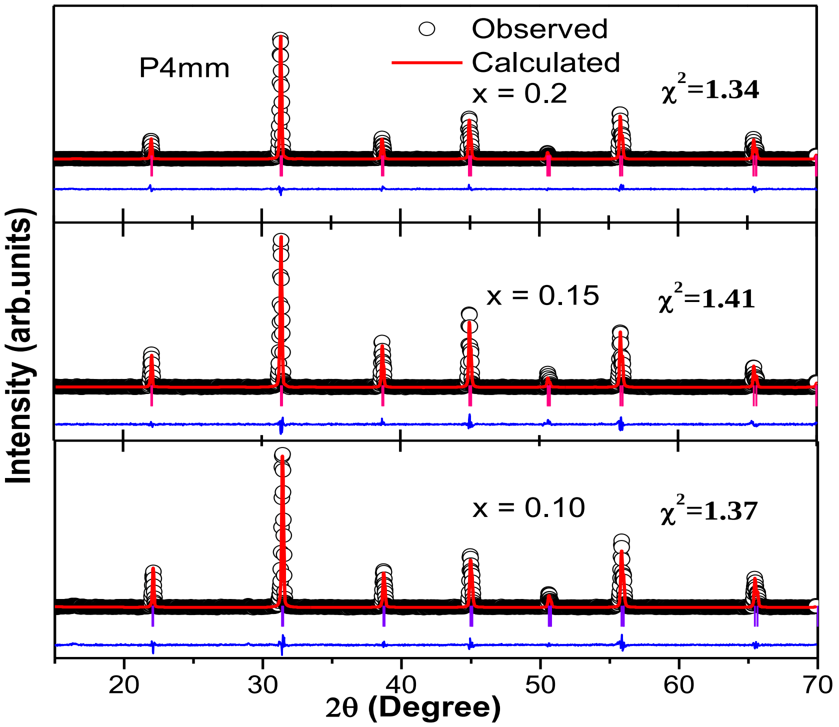

Figure 4.1.7 Rietveld refinement of X-ray diffraction pattern for sintered BZT (x=0.1, 0.15, 0.2) ceramics. The observed data points are given as round (o) and the calculated data are shown as solid line. The trace on the bottom is the plot of difference between calculated and observed intensities.

Starting parameters for Rietveld refinement were taken from as stated by Swanson et al. [204] with tetragonal symmetry, space group P4mm (No. 99) and initial cell parameters of a =b= 3.9998 Å, and c = 4.038 Å. Starting atomic coordinates and atomic displacements were also taken from the same reference. The refinement consisted of the parameters set including the modeling of background scale factor, lattice parameters, detector zero, point and profile parameters. Some constraints were imposed during the refinement to limit the no of refined parameters. Each constraint was systematically verified.

Fig.4.1.7. shows the Rietveld refinement output curve for various BZT ceramics. Table 4.4.1 shows the refined lattice parameters, and Sigma. The observed patterns have good agreement with the calculated patterns with $\chi2$ (goodness of fit) are 1.37, 1.41 and 1.34 for BZT10, BZT15 and BZT20, respectively. These lattice parameters obtained were similar to those obtained by other researchers [205]. The lattice parameters are shown in Table 4.1.1. Furthermore, Deluca et al.[111] reported co-existence of orthorhombic, tetragonal and rhombohedral phases at room temperature in BZT ceramics depending upon Zr content. The identification of the phase contents by XRD however, is not very precise because of the proximity of the diffraction angle of these phases [206]. However, Raman spectroscopy may provide some additional information in order to detect the presence of some tetragonal and/or orthorhombic modifications at RT in our BZT samples.

Table 4.1.1 Space group, Refined lattice parameters ‘*a*’, and ‘*c*’, Unit cell volume and Sigma ($\chi2$) of various BZT ceramics.

Composition	**Space group**	**a(Å)**	**c(Å)**	**Cell volume (Å^3)**	**Sigma**
BZT10	P4mm	4.0225(3)	4.0243(20)	65.11	1.37
BZT15		4.0428(18)	4.0466(22)	66.13	1.41
BZT20		4.0405(7)	4.0437(9)	66.01	1.34

Fig. 4.1.8 illustrates the Raman spectra of BZT samples which contain five normal modes (A1, A2, A3, A4, E1 modes, where the number is only named for convenience) at 188, 299, 519, 716 and 254 cm^{-1}, respectively, which is a signature of coexistence of both tetragonal and orthorhombic phase, generally encountered in BaTiO$_3$ at room temperature [207-209]. As Zhang et al. suggested that the peak at 187.2cm^{-1} signifies orthorhombic phase and peaks at 267.8, 522.1, 715.6, 308.6 cm^{-1} are the common characteristic of tetragonal and orthorhombic symmetry. Dobal et al.[96] reported that it is very difficult to distinguish the rhombohedral and orthorhombic phase by Raman spectroscopy. It can be conclude that both tetragonal and orthorhombic phase coexist at

room temperature in BZT10 and BZT15. In addition, the presence of temperature independent peak at 796cm^{-1}, appears to be associated with the presence of compositional disorder [111]. The room temperature Raman mode shows identical behavior of BZT10 and BZT15 composition. The vibration of Ti atoms in the oxygen cage results in an A(TO_1) mode at 180 cm^{-1}. Dobal et al.**[96]** reported that the A(TO_1) mode could be shifted to about 129 cm^{-1} for substantial replacement of Ti by Zr. The A1 mode frequency of our BZT samples decreases from 188 for BZT10 to 182cm^{-1} for BZT20 could therefore, be assigned to a normal mode involving Zr atoms.

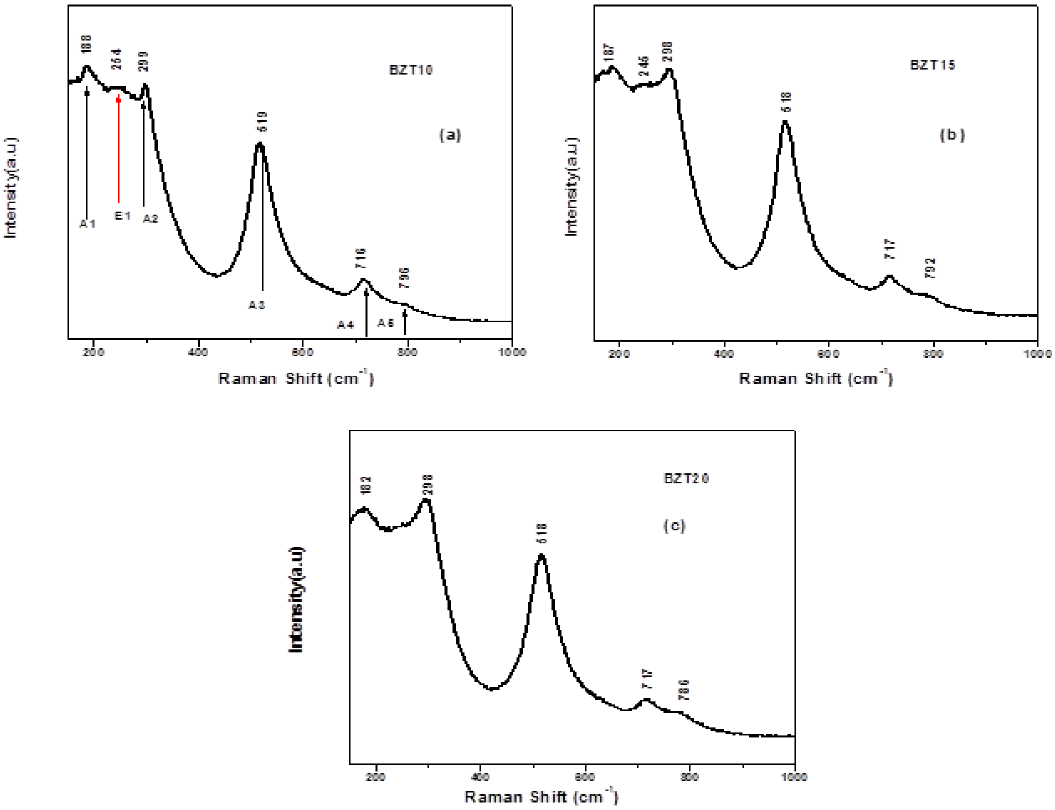

Figure 4.1.8 Raman spectra of BZT ceramics at room temperature (a) BZT10, (b) BZT15(c) BZT20.

4.1.2.3 Particle Size

Fig 4.1.9 shows the FESEM micrograph BZT10 powders calcined at 800°C prepared by the solution based autocombustion method. The synthesized powder has agglomeration of the calcined powder, the size of agglomerates is in the range of 200–400 nm. It can be seen that the presence of agglomerated spherical particles of which the average particle size is about 50nm.This result is consistent with the calculated crystallite size obtained from the XRD analysis (~35nm). The particle-size distribution histograms shows that all the particles have a narrow size distribution ranges; the average particle sizes (D_{Fesem}) evaluated from FESEM data are 50 to 60nm, using the

ImageJ software [210]. Similar particle sizes were observed for all the composition. The value of specific surface area of BZT (x= 0.1, 0.15, 0.2) powders, were found to 3.19 m^2/g, 3.59 m^2/g and 2.93 m^2/g respectively. The equivalent particle size (D_{BET} =6/ρ*S_{BET}, where ρ is the theoretical density of the powder) calculated from the value of specific surface area were 312 nm, 278nm and 340nm respectively. Basically, particle size measured by BET surface area provides only agglomerate size of the powder. The agglomerate size is in good agreement with FESEM analysis. Julphunthong et al.[108] have found the average particle size in the range of 139-369 nm of BZT10 powder prepared by autocombustion method using urea as fuel.

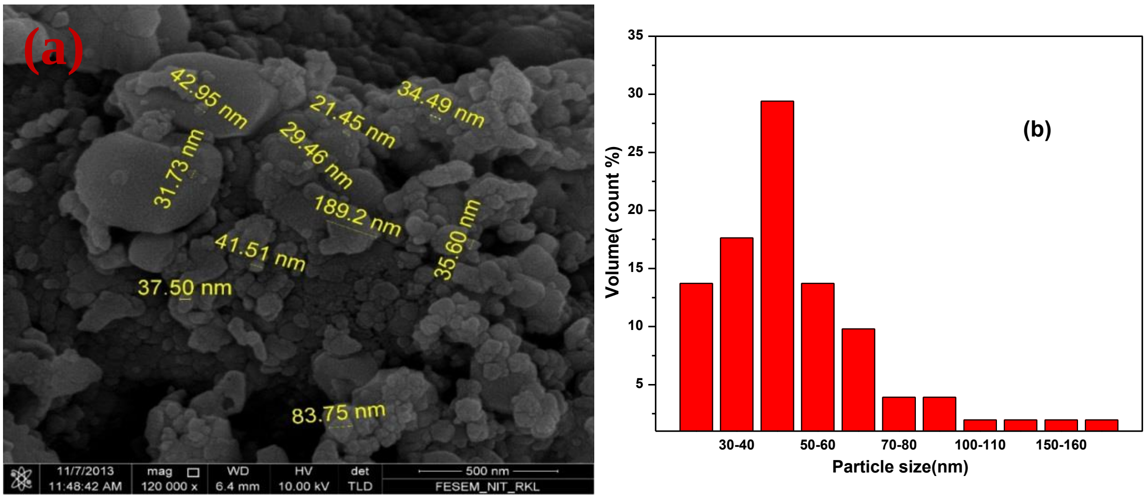

Figure 4.1.9 (a) FESEM micrograph (b) corresponding particle-size distribution of BZT10 powder calcined at 800°C.

4.1.2.4 Densification Behavior

Figure 4.1.10(a) and (b) shows the linear shrinkage and linear shrinkage rate as a function of temperature for different BZT ceramic. The linear shrinkage and linear shrinkage rate both increase with an increase in Zr substitution. The temperature of the maximum of the shrinkage rate ($T_S$max) was decreased with increase in Zr substitution. This behavior reveals that Zr has an influence on the sintering process. The different parameters of dilatometer experiments were summarized in Table 4.1.2.The BZT10 sample starts to sinter at T_0=1150°C, reaches the end of its densification at T_f=1360°C and the maximum shrinkage rate at 1268°C. Moura et al. [100] was observed the highest shrinkage rate at 1338°C for BZT10 sample prepared by solid state method, which is higher compared to our result. The density of the different BZT sample was mentioned in Table 4.1.2. In our case, all the BZT sample could be sintered to more than 97% of relative density at 1350°C/4h. These relative densities are higher compared to those of BZT ceramics prepared by the conventional solid-state reaction method and the wet chemical method sintered at 1300°C or higher temperatures [94, 104, 114]. Deluca et al. [111] prepared similar BZT compositions by modified Pechini method using alkoxide based precursor and achieved only around 90% of relative density. The density and sintering temperature comparison with other literature summarized in Table 4.1.4. In our case smaller particle size could have been the reason for achieving high sintered density at low temperature.

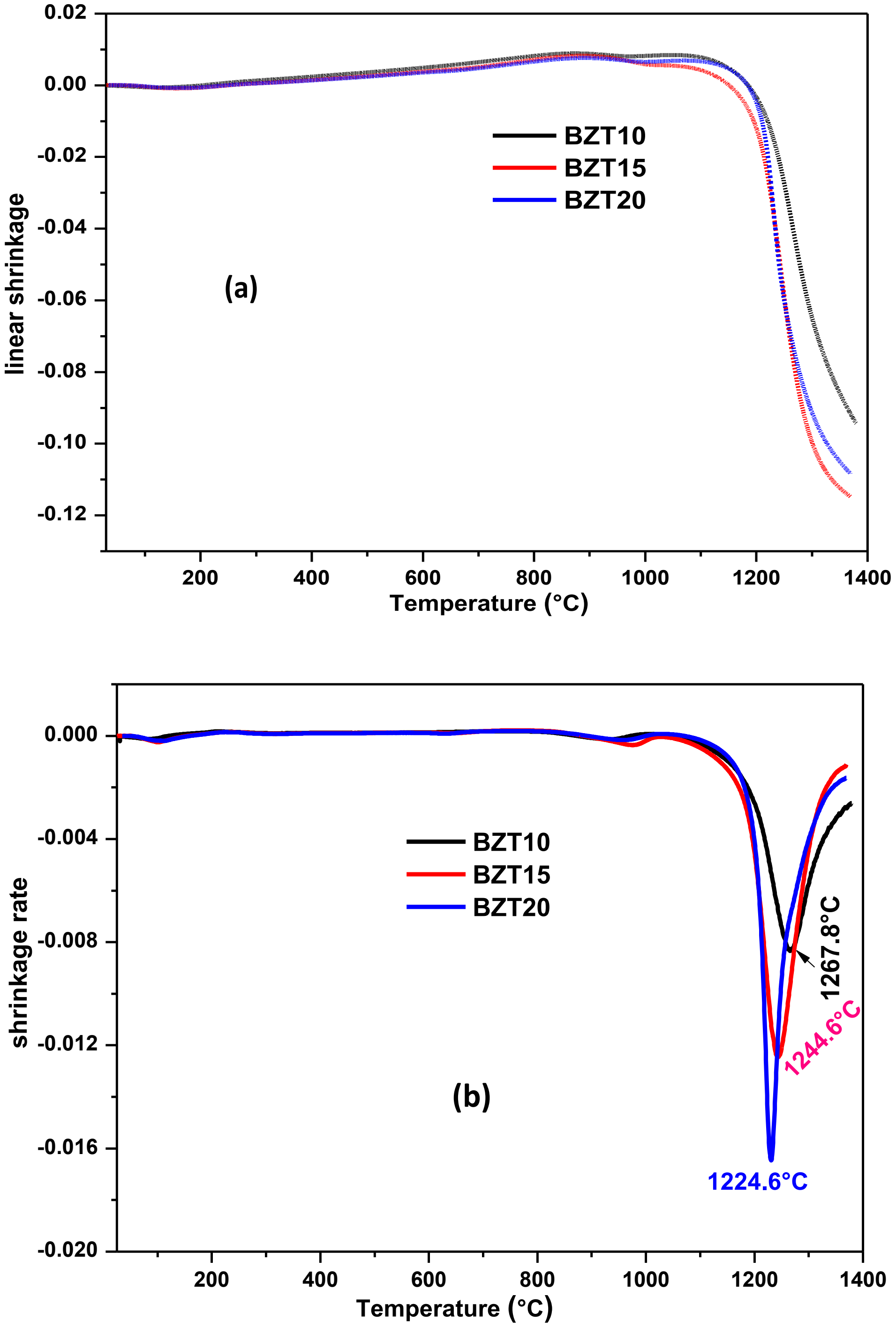

Figure 4.1.10 (a) Linear shrinkage (b) linear shrinkage rate as a function of temperature for BZT powder calcined at 800°C.

Table 4.1.2: Results from dilatometer experiment: onset Temperature (T_0), temperature of the maximum of the shrinkage rate ($T_S$max), temperature at which densification stops (T_f)and width of temperature interval where shrinkage occurs ($\Delta T=T_f-T_0$)

Sample types	BZT10	BZT15	BZT20
Onset temperature(T_0)(°C)	1150	1150	1140
Ts max	1267.8	1244.6	1224
T_f	1360	1360	1360
$\Delta T=T_f-T_0$(°C)	210	210	220
Shrinkage	9.5%	10.8%	11.6%
Relative density(1350°C)	97%	98.5%	98.8%

4.1.2.5 Microstructure

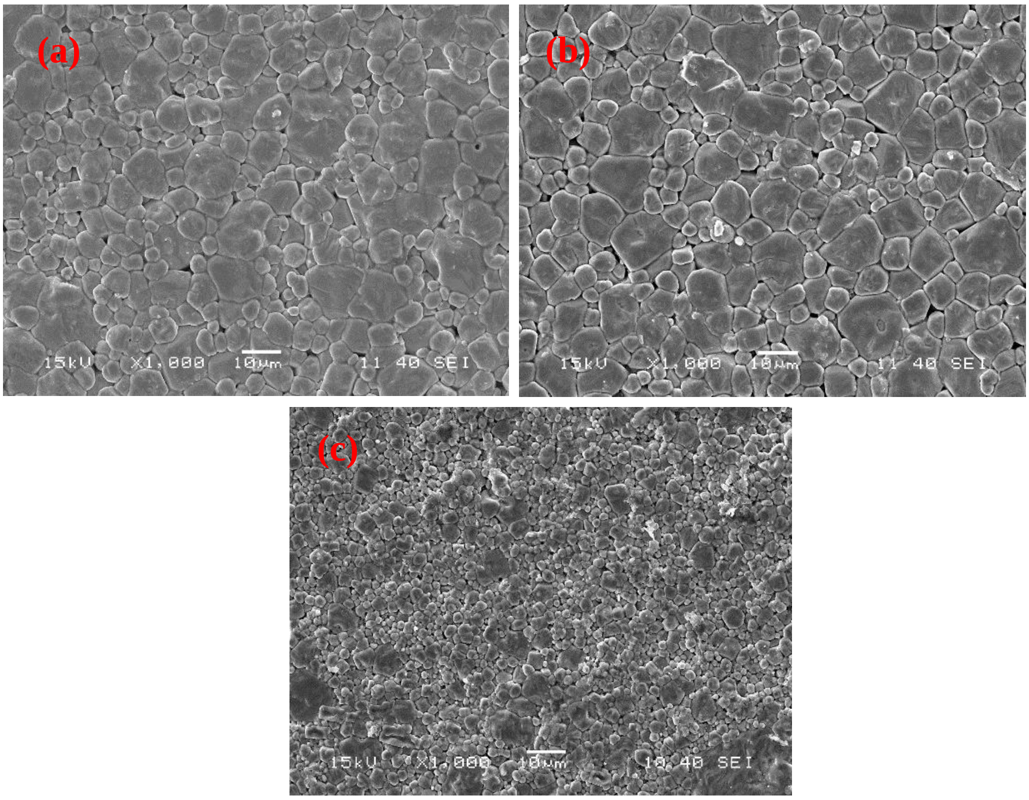

Figure 4.1.11 SEM micrographs of BZT ceramics sintered at 1350°C/4h. (a) BZT10 (b) BZT15 (c) BZT20.

Fig 4.1.11 (a)-(c) shows the SEM micrograph of BZT samples sintered at 1350°C with x=0.10, 0.15, 0.20 Zr content, respectively. It is clearly seen that all the samples exhibit dense microstructure and clear grain boundaries with bimodal grain size distribution, consisting of both polyhedral, faceted grains.The grain size range is 1.6-11.7 μm for BZT10, 2.2-13.0μm for BZT15 and 1.0-5.2μm for BZT20. The grain sizes first increase marginally and then decreases significantly with increasing Zr content. It implies the Zr ions substitution of Ti ions has a strong effect on the grain sizes. The Zr^{4+}doping reduce the grain size of $BaTiO_3$ ceramics by lowering the grain growth rate. The lower grain-growth rate caused by slow diffusion of the larger Zr^{4+} ion which has a larger ionic radius than Ti^{4+} (smaller ions lead to fast diffusion and grain growth)**[**98**]**.

4.1.2.6 Dielectric Properties

Figure 4.1.12 shows the relative permittivity and loss factor as the function of frequency (100Hz to 1MHz) for the Zr modified BZT ceramics measured at room temperature. It can be observed that the room temperature relative permittivity values for BZT (x= 0.1, 0.15, 0.2) samples are 2415, 3505 and 9375 respectively at 1 kHz. The room temperature relative permittivity of BZT ceramics increased with increasing Zr content. The loss factor of all BZT ceramics is less than 2.5% at 1kHz.The relative permittivity of BZT ceramics in all compositions in this study are higher compared to report literature [103,104, 107**,**111,113,114].The higher permittivity can be attributed to the high density and uniform microstructure of the samples. The increment in permittivity with increase in Zr concentration can be explained by the increase in domain wall vibration (called the orientation polarization) and lattice vibration (ionic polarization) of the ceramics. Zr doping generates internal stress which can be released by developing non-180° domains with multiple configurations as the same mechanism in pure $BaTiO_3$ in which 90° domains are developed to relieve transformation stress when the ceramic is transformed from the paraelectric state into the ferroelectric state [97]. Therefore, the increases in number of domain wall give rise to an improved dielectric response with the increase in Zr-content because domain wall vibration is one contribution component to the dielectric constant [211]. The other contribution component is lattice vibration. Zr-substitution modifies the structure at microscale and generates local dipoles which can be polarized by external alternative electric field and contributes to the overall increase in permittivity **[**97**].**

Temperature dependence of relative permittivity for the BZT ceramics measured at the different frequency is shown in Fig. 4.1.12. For BZT10, two peaks are observed at about 50°C and 80°C, correspond to the phase transition of orthorhombic-tetragonal($T_{O\text{-}T}$) and tetragonal-cubic (T_C), respectively. With increasing content of Zr, the Curie point (T_C) shifts to the lower temperature, whereas the other transitions shift to higher temperatures. With further increase of Zr content, at BZT15, the three phase transitions merge in one broad peak. This is the well-known pinching effect of this composition [96]. These results are in good agreement with the reported literatures [90]. For BZT20, the transition temperature (T_C) decreases to 35°C implying that the Zr^{4+} substitution for Ti^{4+} in $BaTiO_3$ influences the transition temperatures [212]. Since Zr^{4+} has larger ionic size as compared to Ti^{4+}, the addition of Zr increases the chemical pressure imposed on the surrounding lattice and, therefore results in lower T_m and lower maximum dielectric constant. The highest permittivity (ε_m = 14,975) at transition temperature is observed for the BZT15 at 1 kHz, which is comparable to the ceramics prepared by other wet chemical routes [111] and higher than the ceramics made by the solid state route [100]. Meanwhile, the dielectric constant of BZT ceramics with a higher Zr content exhibited broad peaks. The broadness indicates the diffuse phase transition from ferroelectric to paraelectric phase.

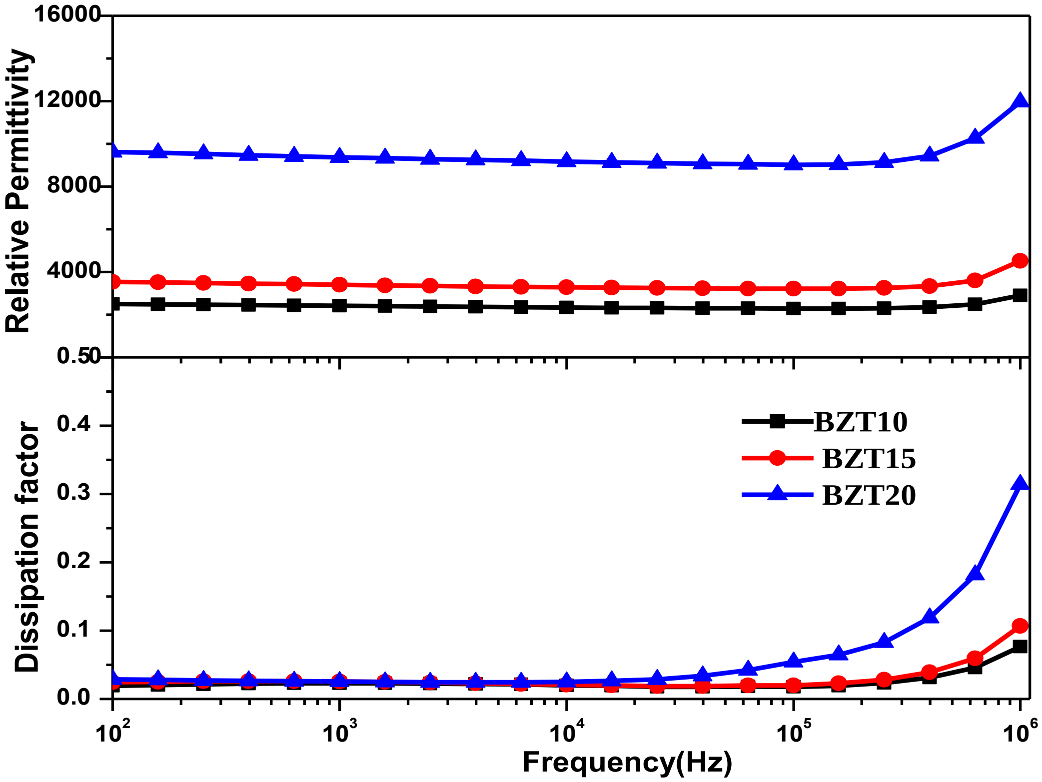

Figure 4.1.12 Relative permittivity and loss factor as the function of frequency for BZT ceramics at room temperature.

Moreover, the diffuse transition behavior is enhanced with increasing Zr content, indicating a composition-induced diffuse transition. In addition, relative permittivity maxima are also noticeably frequency independent [111].

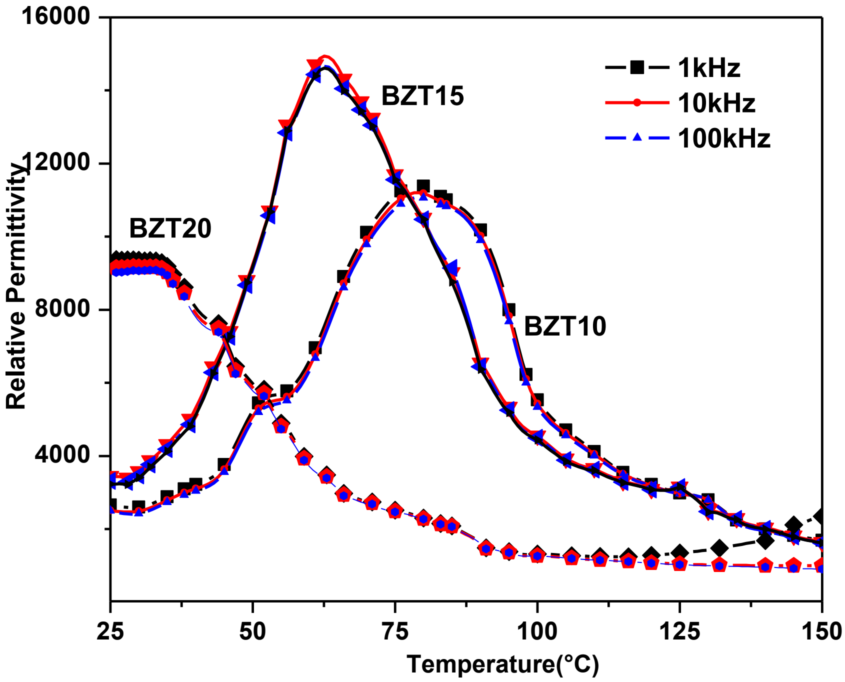

Figure 4.1.13. Relative permittivity as a function of temperature for BZT ceramics

A modified Curie–Weiss law was proposed to describe the diffuseness of the ferroelectric phase transition [30] as

$$\frac{1}{\varepsilon}-\frac{1}{\varepsilon_m}=\frac{(T-T_m)^{\gamma}}{C'}$$

where γ and C are constant, ε_m and T_m represent the dielectric constant maximum and the corresponding temperature. The parameter γ provides the information on the character of the phase transition for $\gamma = 1$, ideal ferroelectric and equation reduces to Curie–Weiss law, whereas $\gamma = 2$ represents an ideal relaxor [202]. The plots of $\log(1/\varepsilon - 1/\varepsilon_m)$ as a function of $\log(T - T_m)$ for BZT ceramics is shown in Figure 4.1.13. A linear relationship was observed for the BZT ceramics. The γ value varies from 1.35 to 1.80 (See Table 4.1.3, which summarizes the dielectric and piezoelectric properties of the sintered ceramics). In BZT solid solution, Zr^{4+} and Ti^{4+} occupy the B-site of ABO_3 perovskite structure: the cation disorder will break the ordered state at the microscopic level by forming ZrO_6 and TiO_6 octahedral clusters. The existence of non-polar ZrO_6 (no displacement of Zr^{4+} with respect to octahedron center) cluster will cause local order-disorder into the $BaTiO_3$ matrix and inhomogeneity in the sample may generate a composition fluctuation in macroscopic level. Both micro- and macro-level disorder will contribute to the diffuse phase transition of the BZT ceramics [90]. In our samples the frequency independent permittivity maxima may be due to, the generated internal stress (result of Zr substitution) is not enough to reveal the relaxor behavior due to insufficient impedance mismatch between the ZrO_6 and TiO_6 clusters [97]. The relaxor phase transition behavior has also been reported in Ba(Zr_xTi_{1-x})O_3 with x> 0.25 [28]. Chen et al. [202] observed γ value of 1.49, 1.68 and 1.92 for solid state route prepared Ba(Zr_xTi_{1-x})O_3 (x=0.1, 0.15, 0.2) ceramic, respectively. Xiong et al. also found the similar result for Nb doped BZT ceramic prepared by solid state method [213]. Julphunthong et al.[108] reported dielectric properties of BZT10 ceramics prepared by solid state combustion method using urea as fuel. In their case γ increased with sintering temperature and value was 1.76 for 1400°C/2h sintered sample with grain size 21.1μm. Tang et al.[102] reported grain size effect on dielectric properties of BZT20 prepared by alkoxide based sol-gel method. It was found that γ = 1.82, 1.78, 1.64 for BZT ceramics with grain sizes of 2, 15 and 60 μm, respectively. In our case, for BZT20, γ is 1.8 whereas average grain size is less than 5 μm.

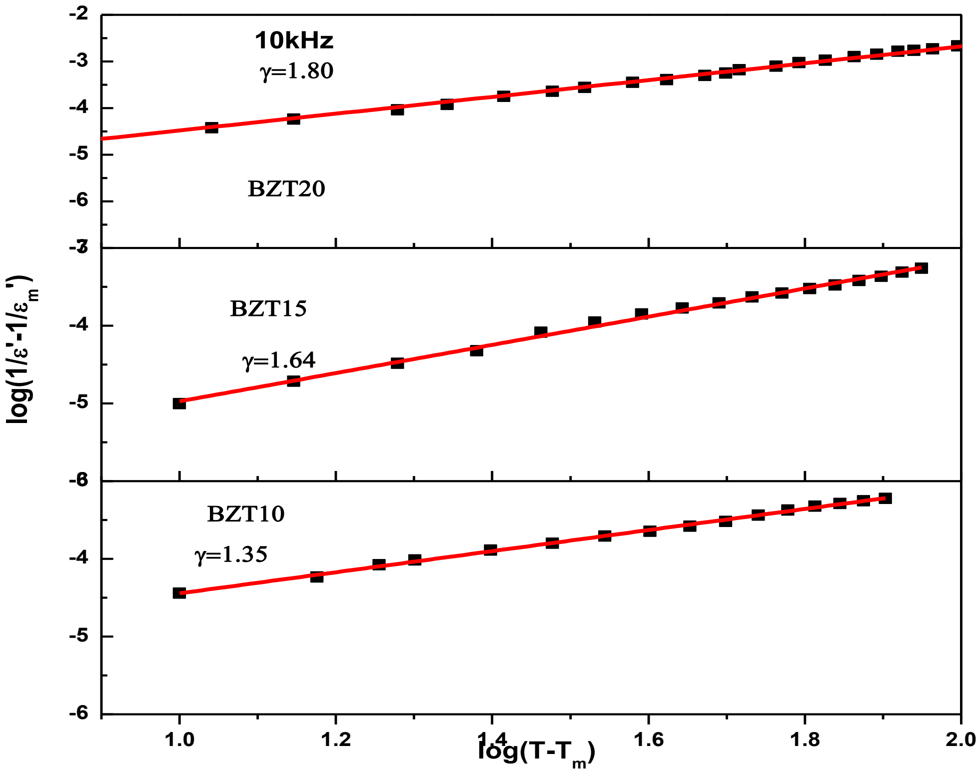

Figure 4.1.14 plot of $\log[(1/\varepsilon' - 1/\varepsilon_m')]$ as a function of log(T−Tm) for the Zr modified BZT ceramics.

4.1.2.7 Ferroelectric and Piezoelectric Properties

Fig 4.1.15 shows the polarization-electric field characterization of the Zr modified BZT ceramics at room temperature. It is found that the remnant polarization (P_r) and coercive fields (E_c) decreases with increasing zirconium content. Well saturated hysteresis loops with regular shape can be observed for BZT10 and BZT15 ceramics but in case of BZT20 ceramic the loop almost closed.

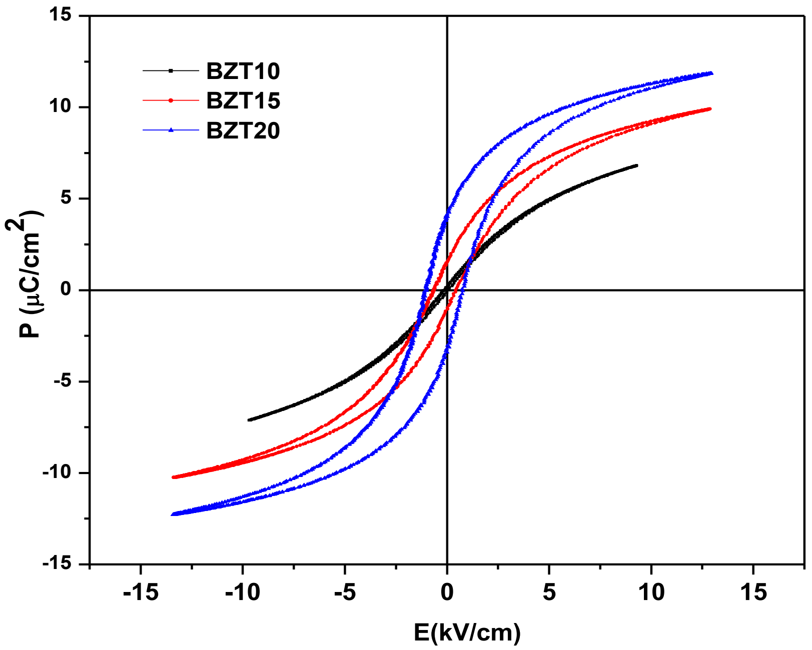

Figure 4.1.15 P–E hysteresis loops (at room temperature) of Ba(Zr_xTi_{1-x})O_3 ceramics with x=0.1, 0.15, 0.2 under varying electric field at 50Hz.

The effect of poling field on the piezoelectric properties of Ba(Zr_xTi_{1-x})O_3 (x=0.1, 0. 15, 0.2) ceramics is summarized in Table 4.1.3. The poling field varies from 0.5 to 3.0 kV/mm, The Piezoelectric constant (d_{33}) increases with increase in poling field from 0.5 to 1.5kV/mm for BZT10 and BZT15 and then decreases, confirming that the poling field is an important factor to affect the piezoelectric properties of BZT ceramics. In general the low poling electric field makes the polarization switching inadequate and excessive poling electric field tends to over-pole a sample which leads to physical flaw or eventually to the dielectric break down of the sample that degrades the piezoelectric properties [140**,** 214]. In our case, the optimum poling field for BZT ceramics is 1.5kV/mm at room temperature. The highest d_{33}(142pC/N) value obtained for BZT10 which is better the ceramics prepared by other wet chemical routes[104] and similar result was obtained by solid state method which was sintered at 1400°C/5h[215]. Yu et al.[90] reported the d_{33} value of 130pC/N for Ba($Zr_{0.08}Ti_{.92}$)O_3 ceramics. The superior piezoelectric properties should be attributed to the dense microstructure and a large grain size. Moreover, the enhancement of piezoelectric properties is attributed to the coexistence of orthorhombic and tetragonal phase (confirmed by Raman spectroscopy) near room temperature which leads to the easier rotation of domain when poled [216]. It is also found that the Piezoelectric coefficient (d_{33}) decreased with increasing zirconium content and becomes nearly zero (d_{33} =20pC/N) for BZT20. This can be explained by the stabilization of more symmetric structure and paraelectric phase at room temperature.

Table 4.1.3 Dielectric permittivity, dissipation factor, γ and piezoelectric properties with different poling field of various BZT ceramics.

Sample types	**BZT10**	**BZT15**	**BZT20**
Grain size	1.6-11.72(5.34μm)	2.2-13μm(5.87μm)	1.08-5.2μm(2.30μm)
ε_r at RT	2415	3505	9375
loss fator at 1kHz	0.022	0.025	0.025
T_m(°C)	80	63	33
Tcw(°C)	125	125	52
ΔTm=Tcw-Tm	45	65	20
γ	1.35	1.64	1.80
d_{33}(0.5kV/mm)	130	35	6
d_{33}(1.5kV/mm)	142	83	20
d_{33}(3kV/mm)	115	78	20

Table 4.1.4 summarizes the processing condition and electro-physical properties of our sample along with the reported data for BZT ceramics for comparison. It is seen from Table 4.1.4 that the dielectric properties and piezoelectric constant of our samples are better than the published results.

Table 4.1.4 Preparation route, calcination temperature, sintering temperature, density, dielectric permittivity and piezoelectric properties of BZT Ceramics.

			Relative density (%)			ε at RT			d_{33}			
Synthesis method	Calcination Temp	Sintering Temp	0.1	0.15	0.2	0.1	0.15	0.2	0.1	0.15	0.2	Ref
Solution combustion	800°C/4h	1350°C/4h	97	98.5	99%	2415	3505	9375	142	83	20	Our work
Solid state	1200°C/2h	1350°C/2h				1900	2000	4100				[202]
Solid state	1200°C/2h	1500°C/4h				~2500	~3500					[110]
combustion	1000°C/5h	1375°C/2h	96	95.5		~2000	~3700		-	-	-	[109]
Co-precipation	-	1600°C/2h	96			~2000	-	-	-	-	-	[114]
Sol-gel	100°C/2h	1250°C/2h	~84	~89	90	1957	3704	5118	83	36	0	[104]
Autocombustion	800°C/4h	1300°C/4h	92-93	92-93	92-93	~800	~1300	~1800	-	-	-	[107]
Combustion	1000°C/5h	1300 - 1500°C/2h	91-97	-	-	~2500-3000			-	-	-	[108]
Pechini	850°C/2	1300°C/8h	91.2	88.3	87.9	~2800	~3500	6500	-	-	-	[111]

4.1.3 Conclusions

$Ba(Zr_xTi_{1-x})O_3$ [BZT] (x=0.1, 0.15 and 0.2) ceramics have been successfully prepared by a solution based auto-combustion method. Their structure, dielectric, ferroelectric and piezoelectric properties have been studied. It was found that the all BZT powder possess single phase perovskite structure obtained at 800°C, which is much lower than the wet chemical method, and can be sintered to more than 98% of the theoretical density at 1350^{o}C. The room temperature dielectric constant increases with the increase in Zr content and loss factor have less than 2.5%. The ferroelectric-paraelectric phase transition, piezoelectric coefficient, Pr, and Ec decreases with the increase in Zr content. The piezoelectric properties depend upon the poling field and optimum poling field for all ceramics are 1.5kV/mm at room temperature. The highest piezoelectric coefficient (d_{33} = 142 pC/N) is obtained for BZT10 ceramics at electric field of 1.5kV. The results indicate that BZT10 ceramics is promising candidates for the lead-free piezoelectric applications.

Chapter-4.2

Synthesis and characterization of Zr and Ca modified $BaTiO_3$ by solution Combustion method

4.2.1 Introduction

In the previous chapter, the synthesis of $Ba(Zr_xTi_{1-x})O_3$ (where x= 0.1, 0.15,0.2) through a citrate-nitrate autocombustion method and dielectric and piezoelectric property of the sintered ceramic has been discussed. $Ba(Zr_{0.1}Ti_{0.9})O_3$ shows best piezoelectric property and good dielectric property.

In BZT ceramics the $T_{O\text{-}T}$ transition shifts to the high temperature and the Tc shift to the low temperature with increasing Zr content. Recently, it is reported that $Ba(Ca_xTi_{1-x})O_3$ ceramics shows a large piezoelectric/electrostrictive strain [217-219]. In the lead-free ceramics, the enhanced piezoelectric properties are accompanied by the occurrence of polymorphic phase transition (PPT) around room temperature [134,220], and they are thus considered to be closely associated with the coexistence of phases. In the $BaTiO_3$- $CaTiO_3$ ceramics, Ca^{2+} replace Ba^{2+} has negligible change of the Tc but strongly lower the $T_{O\text{-}T}$ transition temperature. Recently, high piezoelectric constants d_{33} = 200~600 pC/N, superior to PZT has been obtained in the Zr and Ca co-modified $BaTiO_3$ ceramics [48, 83, 138, 221]. The presence of the morphotropic phase boundary is reported for these compositions. For the preparation of BCTZ ceramics, mostly conventional solid-state reaction method was used. It requires relatively higher calcination temperature (1200°C to 1350°C) for powder preparation and sintering temperature is more than 1400°C [48]. The high temperature calcination and the sintering produce wide grain size distributions, multiple phases, existence of porosity and inhomogeneity. Benabdallah et al.[138] reported that it is difficult to achieve more than 90% of theoretical density in BZT- BCT and 95% of the theoretical density can only be achieved with 1 mol% of TiO_2 excess. Only a few literatures are available on the synthesis of BCTZ powders using the wet-chemical methods [149-152]. No report is available for the synthesis of BCTZ ceramics by solution based autocombustion method without using alkoxides precursor.

In this chapter structural, densification, dielectric and piezoelectric property of the BZT will be studied with 15 mol% Ca substitution in A-site. For this Ca substituted sample, 20 mol% Zr case has been discontinued due to poor piezoelectric property of the BZT20 sample (discussed in chapter 4.1) and 5 mol% Zr substitution in Ti has been introduced. So the compositions will be $(Ba_{0.85}Ca_{0.15})(Ti_{1-x}Zr_x)O_3$(BCTZ, x=0.05,0.1, 0.15). $(Ba_{0.85}Ca_{0.15})(Zr_xTi_{1-x})O_3$ (BCTZ5, BCTZ10, BCTZ15 are designated for x= 0.05, 0.1, 0.15, respectively) powders are prepared by solution based autocombustion method without using alkoxides precursors. The effect of Ca and Zr substitution on phase formations, density, crystal structure, dielectric and piezoelectric properties of the BCTZ ceramics are studied and the properties are also compared with BZT sample (already discussed in chapter 4.1).

4.2.2Results and Discussion

4.2.2.1 Thermal Analysis and Phase Evolution

In the previous section, the best compositions (Metal: Citric acid: ethylene diaminetetraacetic acid 1:1.5:0.1 and pH~9) for solution combustion of BZT has been found out and similar ratios are used to prepare BCTZ powder. The typical thermal decomposition behavior of the precursor BCTZ gel is shown in fig 4.2.1. It shows an endothermic peak at 130^{o}C and two exothermic peaks at 250^{o}C and 279^{o}C.The endothermic peak at 130^{o}C corresponds to the dehydration of adsorbed water, which leads to a weight loss of 23%. The exothermic peaks at 250^{o}C and 279^{o}C correspond to the decomposition of the metal complex, pyrolysis of the organic groups and the phase formation, resulting in the weight loss of 69%. The weight loss beyond 280^{o}C was negligible. The instantaneous rise in temperature and the sharpness of the weight change of TG plot indicate a self-propagating type autocombustion reaction. Finally, the broad exothermic peak at higher temperature corresponds to the crystallization and the oxidation of the residual carbonaceous mass [106,107, 180].

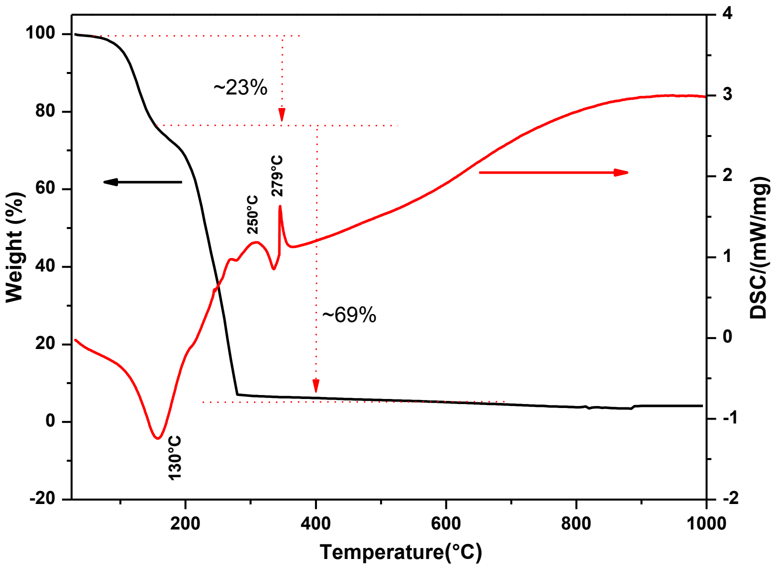

Figure 4.2.1DSC and TG plots of BCTZ10 gel

Fig 4.2.2 shows the X-ray diffraction patterns of BCTZ 10 powders calcined at different temperatures. It can be observed that the as burnt (without calcination) powders consist of the pure perovskite phase with a small amount of impurity phases. It proves that pure perovskite phase was formed around 280°C (maximum temperature generated during the combustion was conformed from DSC/TG). Such a low temperature phase formation may be attributed to the effective complex formation with the metal ions, almost one step decomposition of the metal complex and the auto-ignition at a low temperature [107, 181]. The powder, calcined above 500°C, shows the complete removal of the small impurity phases like $BaCO_3$, $Ba(NO_3)_2$ and TiO_2. The complete phase purity was obtained at 700°C which is much lower than the powder, prepared by the conventional method [48] and sol-gel method [150, 152].

Fig.4.2.3 (a) shows the X-ray diffraction patterns of the BCTZ powder calcined at 700°C. All the compositions possess a pure perovskite structure and without any secondary phase. The phase formation temperature is much lower than the temperature required by conventional method [138] and sol-gel method [152].It suggests that the Ca and Zr have diffused into the lattice site of $BaTiO_3$ to form homogeneous solid solution. Moreover, it is clear that the position of diffraction peaks of the BCTZ has shifted to lower angle with increase in Zr content indicating increase of the lattice parameters of the ceramics. It is due to the distortion of crystal lattice induced by the substitution of Ti^{4+}(0.68Å) by larger Zr^{4+}(0.79 Å).The BCTZ5 ceramics exhibit tetragonal phase and matching with the JCPDS No. 79-2265 having space group P4mm [143].

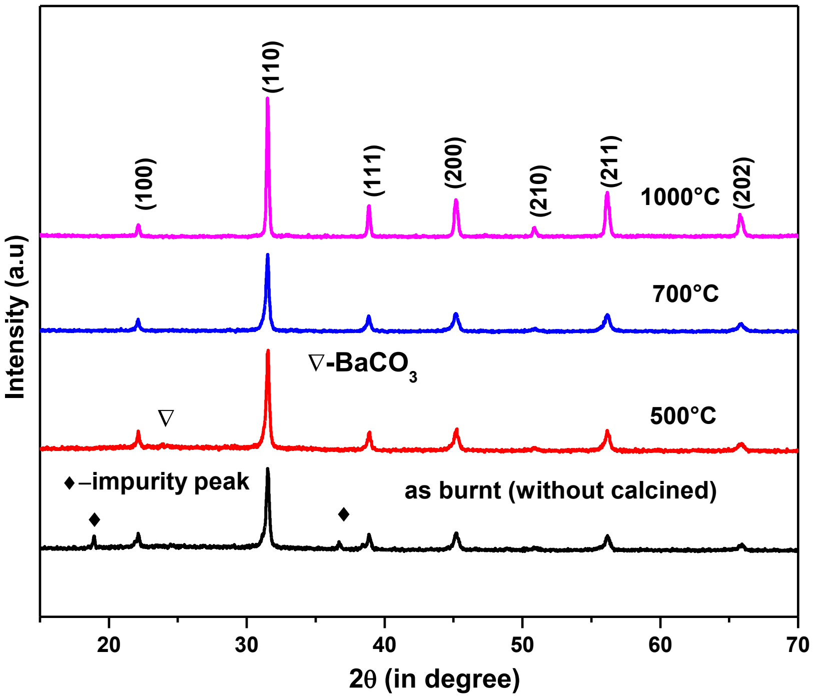

Figure 4.2.2. X-ray diffraction pattern of BCTZ10 powder calcined at different temperatures

Furthermore, it is observed from fig 4.2.3(b) that the (200) peak splits into two diffraction peaks, which can be attributed to the tetragonal (T) feature diffraction peaks of $(002)_T$ and $(200)_T$, suggesting the existence of tetragonal phase in BCTZ5. The peak at (202) also signifying similar nature. In case of BCTZ10, the formation of the triplet around (202) peak signifies the presence of the orthorhombic phase and the doublet at (200) peak corresponds to the tetragonal phase [132, 222].The coexistence of tetragonal and orthorhombic phases at room temperature was also reported by the other researchers **[**83,188,222**]**. There is a transition from tetragonal phase to orthorhombic phase with increasing Zr content at room temperature. Therefore, orthorhombic phase and tetragonal phase are confirmed to coexist in the BCTZ10 ceramic at room temperature [132]. In contrast to our report many reports are available with a coexistence of tetragonal and rhombohedral phase for the similar composition [48, 221]. With further increase in Zr content, for BCTZ15 the splitting of (200) peak near 2θ = 45° was not prominent and the (202) peak near 2θ = 65° become broadened. It suggests that BCTZ15 exhibits a pseudo-cubic structure. The lattice parameters were refined using a least-square fitting method [186] and summarized in Table 4.2.1.

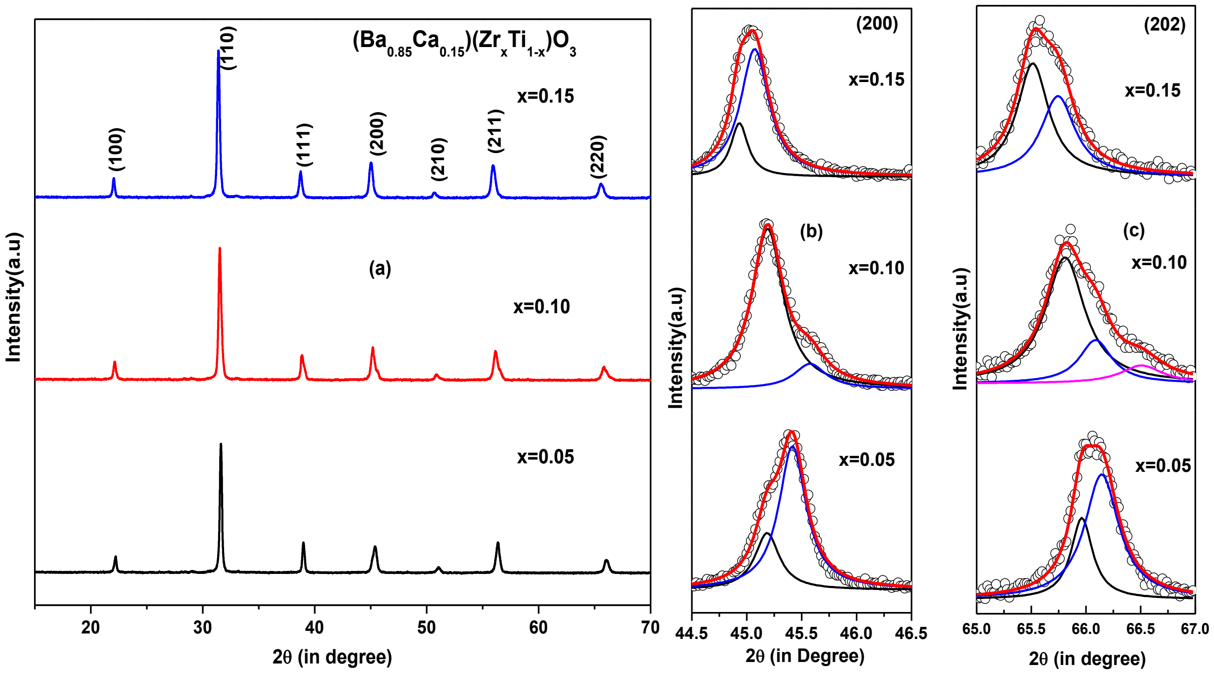

Figure 4.2.3 (a) X-ray diffraction patterns of different BCTZ powder calcined at 700^{o}C. (b)& (c) X-ray diffraction pattern of different BCTZ powder in the range of 44.5 to 47^o and 65 to 67°. The least-square fitting of (200) and (202) peak is presented by considering mixed phase P4mm and Amm2.

Table 4.2.1 Lattice parameters and unit cell volume of different BCTZ ceramics.

Composition	**Space group**	**a, ,b, c[Å]**	**Cell volume [Å^3]**
BCTZ5	P4mm	a=3.9933(5),c=4.0164(8)	64.05
BCTZ10	P4mm	a=4.0087(5),c=4.0178(5)	64.56
	+		
	Amm2	a=3.9982(4), b=5.658(2), c=5.6814(3)	128.47
BCTZ15	P4mm	a=4.0211(7),c=4.0263(7)	65.1

The room temperature Raman spectra in the region of 150–1000 cm^{-1} was characterized for further investigating the phase evolution of BCTZ ceramics, shown in Fig. 4.2.4.The Raman spectra for BCTZ5 ceramics exhibits the tetragonal crystal structure and almost similar results from the literature for tetragonal $BaTiO_3$ [223,224].For BCTZ10 sample, the room temperature tetragonal phase is characterized by the band at 296 cm^{-1} and the asymmetric broader bands at 520 and 720 cm^{-1}. Raman spectrum of the two phases such as the tetragonal and the orthorhombic relates to the feature in the range of 180cm^{-1} to 190 cm^{-1}. The peak at 190 cm^{-1} is originated from orthorhombic symmetry as observed by the other researchers [225-227].The peaks around 522 and 724 cm^{-1} correspond to phonon vibrations of the Ba-O bonds while the peaks in the range 180–300 cm^{-1}correspond to the phonon vibrations of Ti–O bonds. A weak Raman active asymmetric breathing mode (A_{1g}) was seen at 806 cm^{-1} for BCTZ15 while this mode is not prominent for BCTZ5 and BCTZ10. The broad peak around 806 cm^{-1} was also reported in literature for different BCTZ compositions and is due to the presence of several dissimilar atoms at A- and B-sites forming a complex perovskite solid solution [153]. In addition, the Raman mode observed at around 292–298 cm-1 is shifted to the lower frequency region with the increase in Zr content in BCTZ and that can be ascribed to the asymmetric Ti–O phonon vibrations. This shifting is also related to the lowering of the Curie temperature. The x-ray diffraction patterns and Raman spectrum show that the unusual phenomenon appears for the BCTZ10 ceramic, confirming the involvement of a phase transition in such a ceramic system.

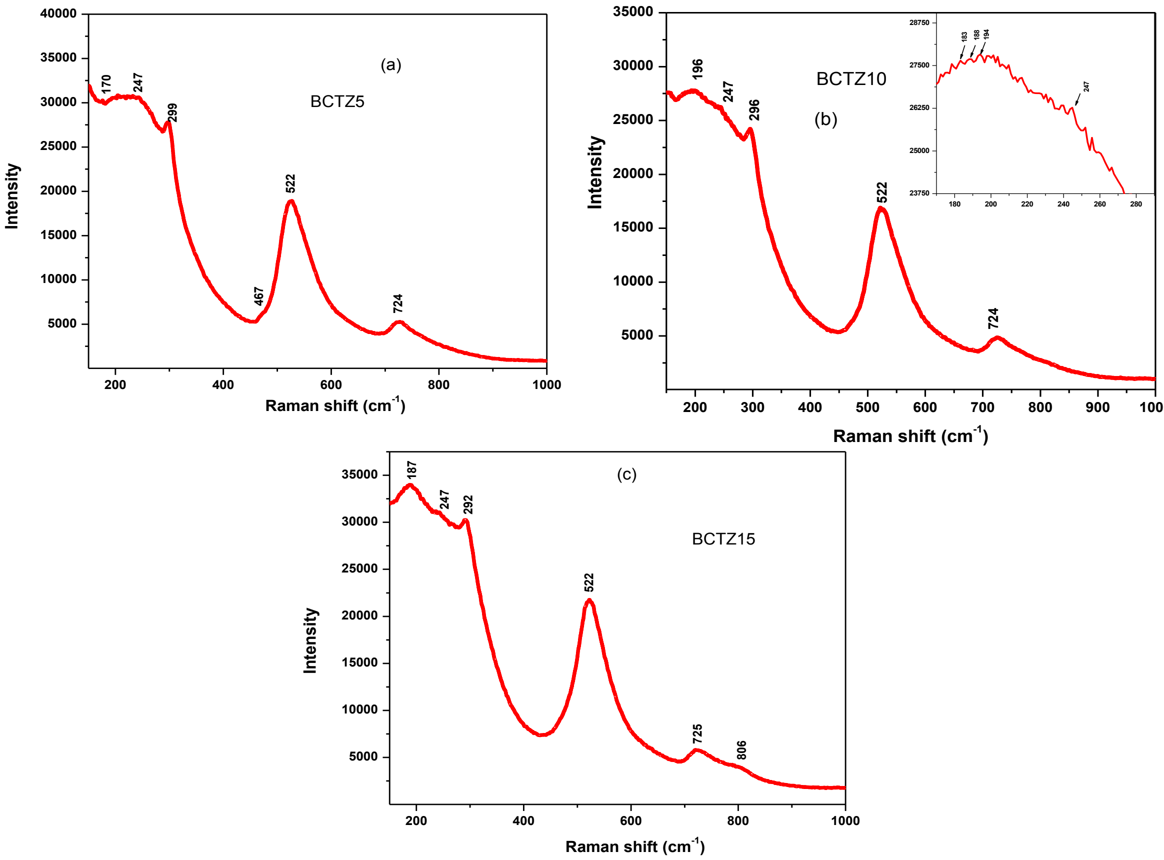

Figure 4.2.4 Raman spectra of BCTZ ceramics at the room temperature (a) BCTZ5 (b) BCTZ10 and (c) BCTZ15

4.2.2.2 Particle Size

Table 4.2.2 summarizes the powder characteristics in terms of crystallite size and agglomerate particle size of different composition. Fig. 4.2.5 shows the particle size distribution of three BCTZ compositions. Primarily particle size distribution measured by DLS technique provides agglomerate size of the powder. Fig 4.2.6 shows the TEM micrograph of calcined BCTZ10 powder. It can be observed that the particles are agglomerated, and agglomerates size is in the range of 250-400nm with an irregular to spherical shape particles. It is also supporting the agglomerate size data received from DLS measurement. It could be observed that many fine particles with particle size 40-70 nm existed in the sample. Selected Area Electron Diffraction pattern (given in the inset) shows polycrystalline nature of the powder.

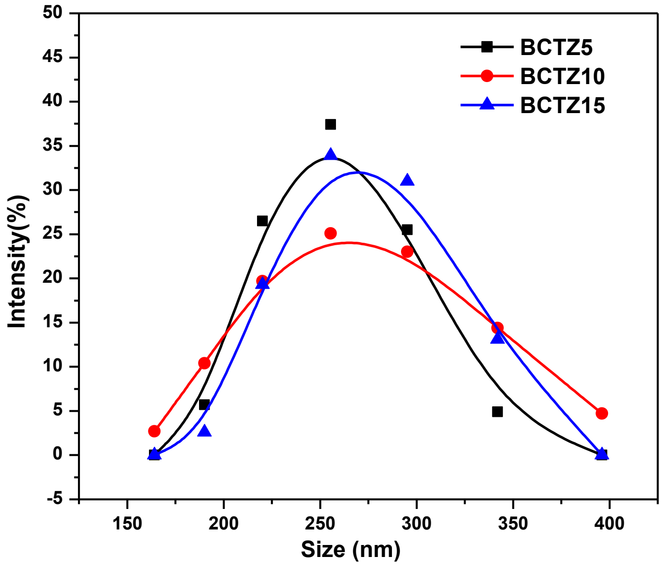

Fig. 4.2.5 Particle size of different BCTZ compositions

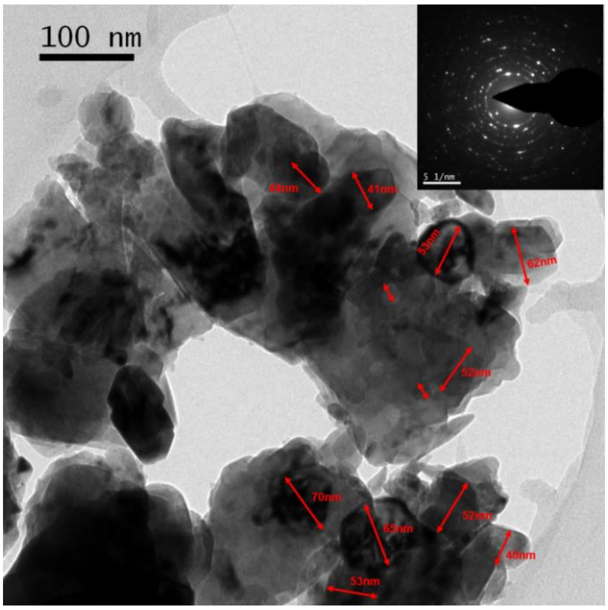

Figure 4.2.6 TEM micrograph of BCTZ 10 powder calcined at 700°C.

Table 4.2.2 Crystallite size and particle size of different BCTZ powders.

Composition	Crystallite size in nm	Particle size distribution
BCTZ5	38.2	190-342
BCTZ10	39.1	160-396
BCTZ15	35.7	190-342

4.2.2.3 Densification behavior

Fig 4.2.7 (a) & (b) displays the linear shrinkage versus temperature for BCTZ and BZT powder. The BCTZ powder has lower shrinkage (9.2% for BCTZ10 and 9.4 for BCTZ15) than that of BZT (9.5% for BZT10 and 10.8% for BZT15) powder. Fig 4.2.7(c) shows the linear shrinkage rate as a function of temperature for BZT10 and BCTZ10. It can be observed that the two peaks are present in BCTZ10 sample, and one peak is present in BZT10 sample in shrinkage rate curve. Two-stage shrinkage in BCTZ may be attributed to the presence of agglomerates which starts densification at different temperatures [182]. Table 4.2.3 shows the relative density and grain size for BZT and BCTZ ceramic. It shows that BZT ceramics has higher relative density than that of BCTZ ceramics. It can be concluded that Ca-substitution on BZT reduces the sinterability of the powder.

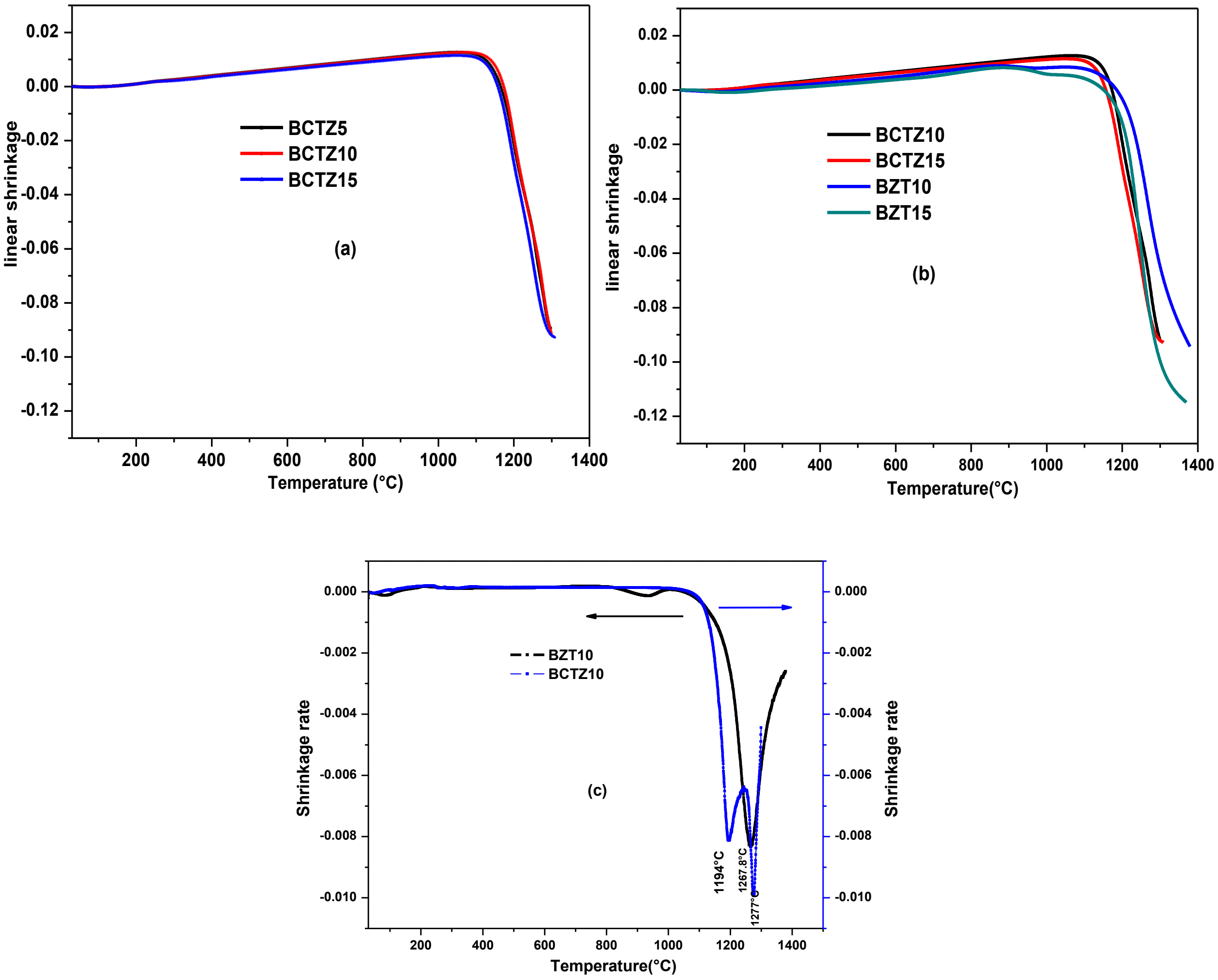

Figure 4.2.7 linear shrinkage as a function of temperature for (a) BCTZ (5, 10, 15) (b) BCTZ (10, 15) and BZT (10, 15) and (c) the shrinkage rate as a function of temperature for BZT10 and BCTZ10 powder.

4.2.2.4 Microstructure

Figure 4.2.8 shows the microstructure for the BCTZ5, BCTZ10, and BCTZ15 ceramics sintered at 1300°C. In the BCTZ ceramics, polyhedral grains are changed to cuboidal shape. The average grain sizes are shown in Table 4.2.3 It can observed that BCTZ10 ceramic has higher grain size (5.6-12.9µm) than that of BZT10 ceramics. The result shows that Ca^{2+} ion substitution in BZT modifies the grain size and morphology. Such evolution in grain size and morphology may be explained by the change of interface atomic structure or grain boundary structure caused by Ca substitution, which significantly affects the microstructure evolution during sintering [228-230].

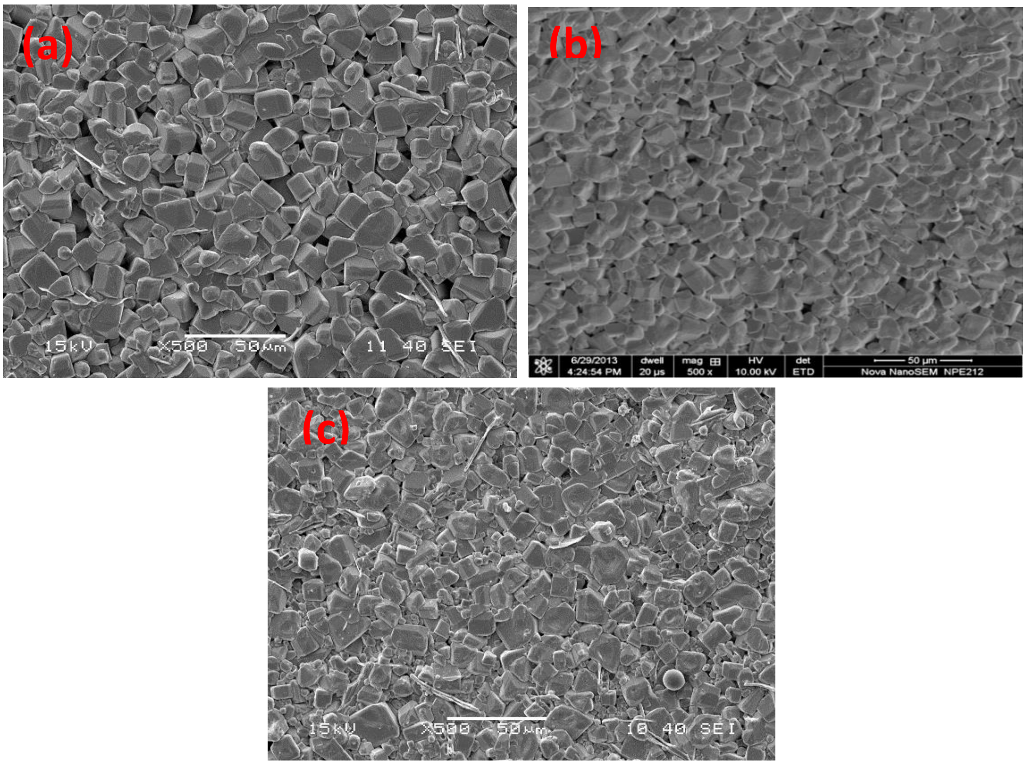

Figure 4.2.8 Microstructure (as fired surface) of various BCTZ ceramics (a) BCTZ5 (b) BCTZ10 (c) BCTZ15.

Table 4.2.3 Relative density and grain size for BZT and BCTZ ceramics

Composition	Relative density(1350°C)	Average grain size (µm)
BZT10	97%	1.6-11.7 (Microstructure shown in chapter 4.1)
BZT15	98.5%	2.2-13.0 (Microstructure shown in chapter 4.1)
BCTZ05	93%(1300°C)	4.2-14.9
BCTZ10	94% (1300°C)	5.1-12.9
BCTZ15	93%(1300°C)	4.9-12.6

4.2.2.5 Dielectric properties

Figure 4.2.9 shows the variation of relative permittivity with temperature as a function of frequency for BZT and BCTZ ceramics. It can be seen that all the BCTZ ceramics exhibit a broad peak at around Curie temperature. The peak maxima (T_m) shift towards the room temperature with increase in Zr content and the peak position is independent of frequency. The T_m of different BCTZ(x= 0.05, 0.1, 0.15) ceramics are 118^{o}C, 102^{o}C and 70^{o}C, respectively. The T_m of BZT (x=0.1, 0.15) ceramics are 80°C and 63°C respectively.

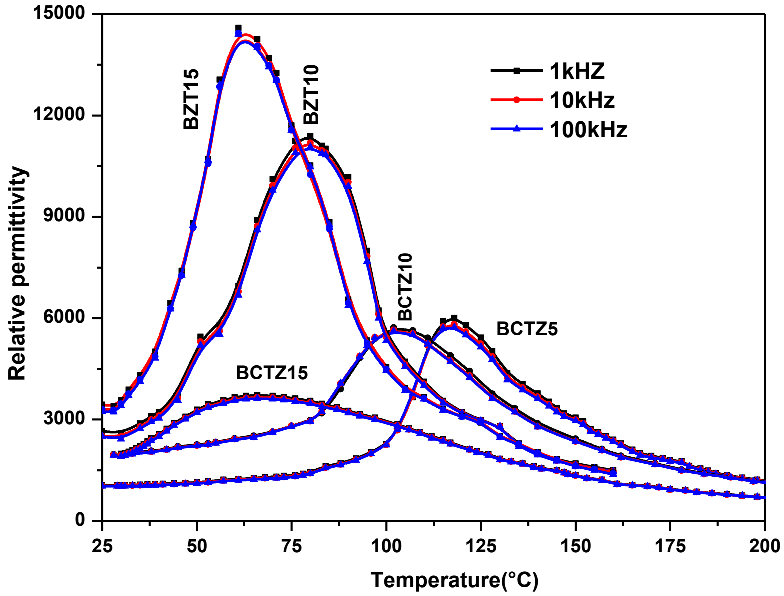

Figure 4.2.9 Temperature dependent relative permittivity for BZT and BCTZ ceramics at various frequencies.

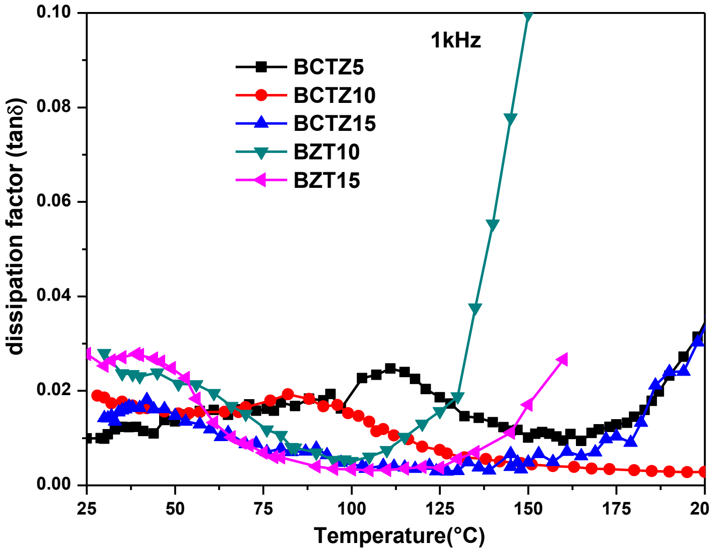

Figure 4.2.10 Temperature dependent dissipation factor (tanδ) for BZT and BCTZ ceramics at 1kHz.

It is explained in earlier section (4.1) that with increase in Zr substitution in $BaTiO_3$ depress the oriented displacement of the B-site ions in the oxygen octahedra [100]. Therefore, the interaction between the B-site ions and O^{2-} would become weaker, resulting in a decrease in phase transition temperature [231]. BCTZ10 has higher phase transition temperature (102°C) than that of BZT10 (80°C). It suggests that Ca substitution (15 mole%) in A-site has enhanced the Curie temperature in BZT ceramics. The polymorphic phase transition temperature (T_{O-T}) is shifted to the lower temperature for 15mol% of Ca substitution (peak at 50^oC visible in BZT10 but it is not prominent in BCTZ10).It also confirms that the $Ca^{2+}$is occupying the A-site in BZT [121, 125,126].In contrast to our report Ca-substitution in A-site in $BaTiO_3$, $Ba_{1-x}Ca_xTiO_3$ (BCT), shows an increase in T_C by $\sim 8\text{-}10^oC$ for composition upto x~0.08. For higher addition of Ca, upto x~0.30, T_C decreases at a rate of 1^oC/at%. It is also reported that Ca-substitution at Ba-site leads to diffuseness whereas Ca replacement at Ti-site leads to sharpening of phase transition curve. The origin of the increase in T_C in our case is not fully understood, and it may be a strain effect associated with A-site cation variance. In our case, Ca-doping in BZT reduces the permittivity. Figure 4.2.10 shows the temperature dependence loss factor (tanδ) for BZT and BCTZ ceramics at 1kHz. It can be observed that all the BCTZ ceramics have lower dissipation factor (< 3%) in the temperature range of room temperature to 200°C, which suggests good temperature stability. Moreover, all these ceramics exhibits a broad peak at around Curie temperature which suggest a diffuse phase transition.

Table 4.2.4 Relative Permittivity, dissipation factor, diffuseness constant (γ) and piezoelectric properties for BZT and BCTZ ceramics.

Composition	ε at RT	tanδ at RT	Tm(°C)	γ	d_{33}at 1.5kv/mm
$Ba(Zr_{0.1}Ti_{0.9})O_3$(BZT10)	2415	0.022	80	1.35	142
$Ba(Zr_{0.15}Ti_{0.85})O_3$(BZT15)	3505	0.025	63	1.64	83
$Ba_{0.85}Ca_{0.15})(Zr_{0.05}Ti_{0.95})O_3$(BCTZ5)	1138	0.012	118	1.41	115
$(Ba_{0.85}Ca_{0.15})(Zr_{0.1}Ti_{0.9})O_3$(BCTZ10)	2244	0.016	102	1.62	215
$Ba_{0.85}Ca_{0.15})(Zr_{0.15}Ti_{0.85})O_3$(BCTZ15)	1984	0.013	70	1.87	90

Curie-Weiss law modified Curie-Weiss law, degree of deviation from the Curie-Weiss law are explained in section 4.1 of chapter 4.1 (page no.81). Fig 4.2.11 shows the inverse relative permittivity as the function of temperature at 1 kHz for the BCTZ ceramics prepared by solution combustion method.

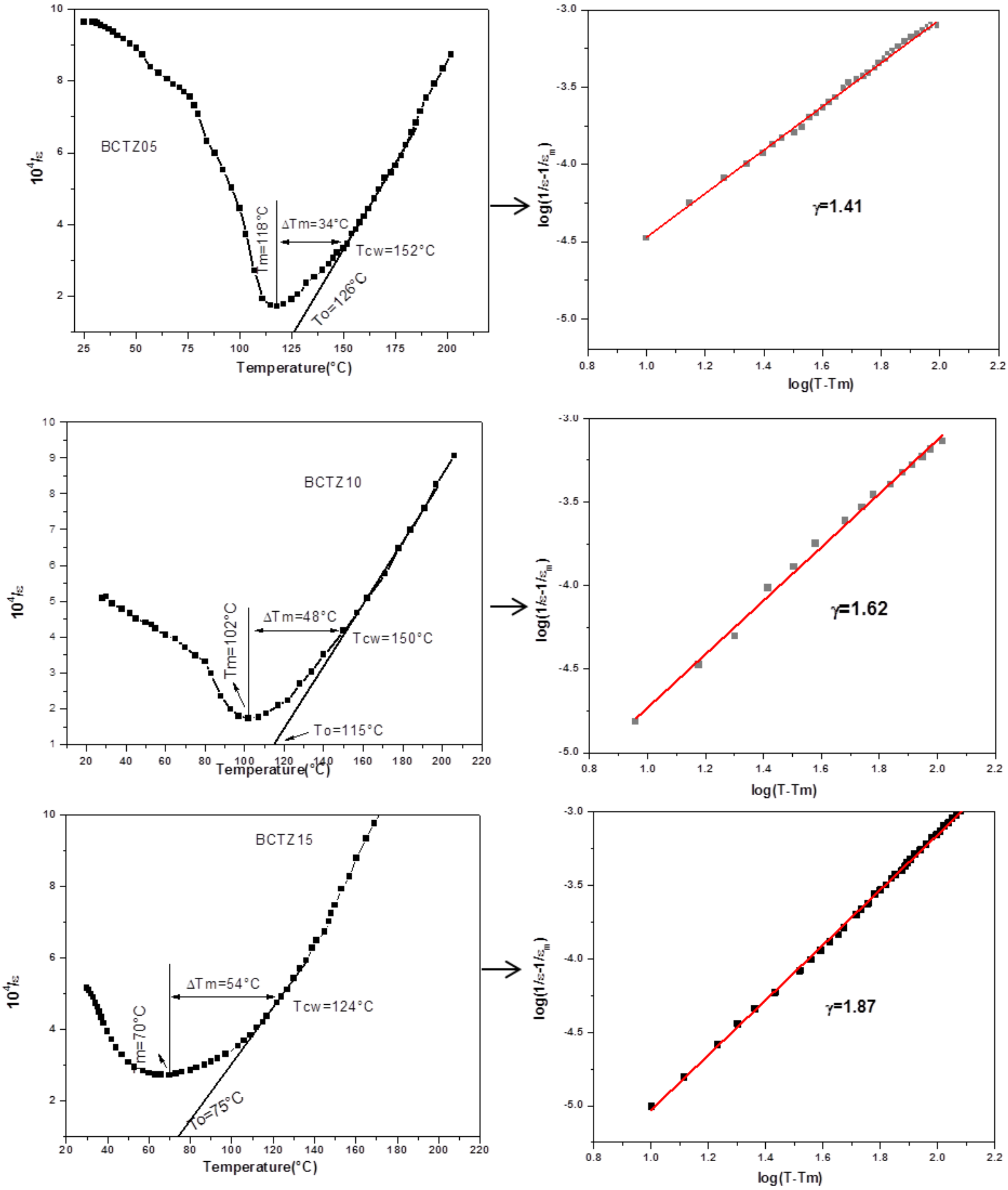

Figure 4.2.11 Curie-Weiss plot for the inverse of the relative permittivity at 1 kHz as a function of temperature for BCTZ ceramics and the corresponding curves of log(1/ε- 1/ε_m) against log(T-T_m).

The values of the degree of deviation from the Curie-Weiss law (ΔT_m)of BCTZ5, BCTZ10, and BCTZ15 are 34, 48 and 54, respectively, which indicates that the diffuse phase transition behavior.

A linear relationship is observed in the plot of log(1/ε−1/ ε_m) Vs log (T−T_m)for all BCTZ samples (Inset of Fig. 4.2.11). The slope of the fitting curves is used to determine the γ value. It is observed that γ = 1.41, 1.62 and 1.87 for BCTZ5, BCTZ10, and BCTZ15, respectively. The diffuseness constant γ is increases with the increase in the Zr contents. BCTZ10 has higher γ value (1.62) than that of BZT10 (1.35). Similar enhancement of γ value is observed in the case of BCTZ15 (1.87) and BZT15 (1.64). It suggests that Ca substitution (15 mole %) in A-site has enhanced the γ value in BZT ceramics. It is interesting to note, though the γ value for BCTZ15 is close to 2, but relative permittivity maxima are noticeably frequency independent. This behavior of BCTZ may be due to cationic disorder and composition fluctuation induced by simultaneous A- and B-site substitutions.

4.2.2.6 Piezoelectric properties

The Piezoelectric coefficient (d_{33}) (summarized in Table 4.2.4) of BCTZ5, BCTZ10 and BCTZ15 samples are 115pC/N, 215pC/N and 90pC/N, respectively. BCTZ10 has higher d_{33} value than that of BZT10 (142pC/N). It suggests that Ca substitution (15 mole %) in A-site has enhanced the d_{33} value in BZT ceramics. The gradual decrease of piezoelectric and dielectric responses with higher Zr content (x=0.15) may be mainly related to the increased diffuse phase transition. From Table 4.2.4, it is clear that the highest piezoelectric and dielectric properties observed for the BCTZ10 among all BCTZ composition. This particular composition has different structural feature (Table 4.2.2 and Fig. 4.2.3(b)) compared to other BCTZ sample. It is to be mentioned that particularly BCTZ10 can be represented by a pseudobinary solid solution of $0.5Ba(Zr_{0.2}Ti_{0.8})O_3$-$0.5(Ba_{0.7}Ca_{0.3})TiO_3$ (BZT-0.5BCT). The enhancement of dielectric and piezoelectric property can be explained by the existence of Morphotropic Phase Boundary (MPB) in this composition. The coexistence of tetragonal and orthorhombic phase facilitates higher number of polarization direction and polarization rotation and polarization extension/contraction. The piezoelectric and dielectric properties obtained for BCTZ10 [$(Ba_{0.85}Ca_{0.15})(Zr_{0.1}Ti_{0.9})O_3$ or BZT-0.5BCT] are higher than that of some Pb-free systems KNN, BNT-BT [72]. Wu et al. reported a d_{33} value around 300 pC/N for similar MPB composition with grain size of 20μm [232]. The MPB composition BCTZ10 has T_m =102°C with room temperature relative permittivity ε~2244 which is much higher than the similar material prepared by sol-gel method [150] and comparable with conventionally prepared sample [138]. Lower value of d_{33} for MPB composition (BCTZ10) may be due to lower density (94%) and grain size (5.1-12.9μm). Further investigation is required whether the piezoelectric property of BCTZ10 [$(Ba_{0.85}Ca_{0.15})(Zr_{0.1}Ti_{0.9})O_3$ or $Ba(Zr_{0.2}Ti_{0.8})O_3$-$0.5(Ba_{0.7}Ca_{0.3})TiO_3$[BZT- 0.5BCT]] can be improved.

4.2.2.7Approach to increase the sintered density and grain size of BCTZ10 (BZT-0.5BCT) ceramics

It is observed that BCTZ10 (BZT-0.5BCT) ceramics exhibits higher piezoelectric coefficient (d_{33}=215 pC/N), which is lower than the reported result. It will be interesting to check whether the improvement of density and the increase in grain size could further enhance the piezoelectric property. The following steps are taken to improve the sintered density and grain size

i. By increasing the calcination temperature of synthesized powder
ii. By milling the synthesized powder after calcination(planetary mill for 30min) to break the agglomerates
iii. By increasing the sintering temperature and the soaking time (2-8 h)

Table 4.2.5: Sintered density, dielectric properties of BCTZ10 ceramics

Calcination temperature(°C)	Sintered density at 1300°C	Dielectric constant at 1kHz	tanδ at 1kHz
700	5.4±2%	2244	0.016
1000	5.41±2%	2053	0.017
1200	5.41±1%	2068	0.026

It is observed that the increase in calcination temperature has no significant effect on the sintered density of BZT-0.5BCT ceramics (summarized in Table 4.2.5) and the relative density is not improved beyond 93-94% (sintered at 1300°C/4h). No significant change in dielectric and piezoelectric properties is observed with variation in calcination temperature. Later, sintering temperature was increased to 1325^{o}C/4h, but that resulted sticking of sample with alumina base plate. XRD of the sintered ground pellet shows the growth of impurity phases ($BaTi_6O_{13}$, JCPDS no-70-1567) (Fig. 4.2.12). In the second attempt, planetary milling of the BZT-0.5BCT powder (after calcination) is carried out for 30 min to break the agglomerates in the calcined powder. It is observed that the sintered density of the pellets increased to 95% relative density and dielectric loss of the sample also increased, and sample could not be poled. Figure 4.2.13 shows the X-ray diffraction pattern of the ground pellet (sintered at 1300°C). It can be observed that impurity phases ($CaTiO_3$, JCPDS No 82-0229 and Ba_2ZrO_4, JCPDS No-77-0944) are present in sintered ceramics and that may be the reason for failure during poling. In the last attempt soaking time is varied for 2-8h, and it is observed that no significant improvement in the density and grain size of the ceramics.

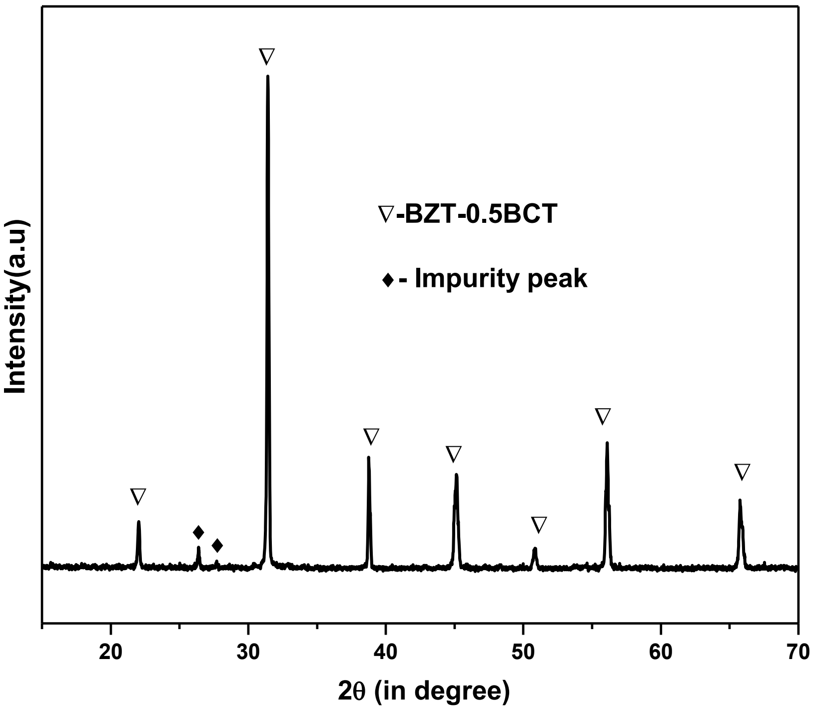

Figure 4.2.12. X-ray diffraction pattern of BZT-0.5BCT sintered at1325°C/4h

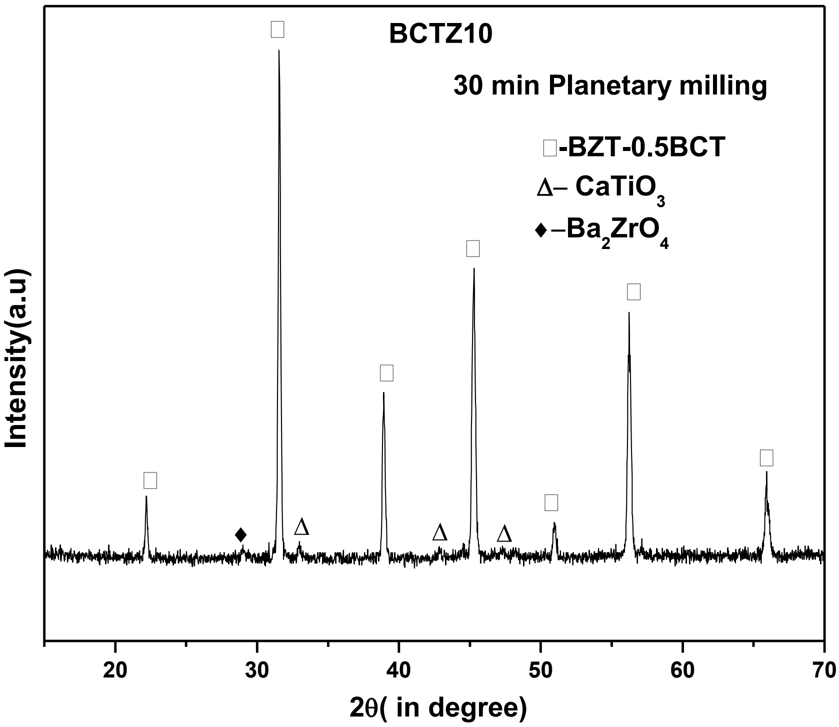

Figure 4.2.13. X-ray diffraction pattern of BZT-0.5BCT sintered at 1300°C/ 4h (Planetary milling, 30min)

4.2.3 Conclusions

The citrate-nitrate autocombustion method is found to be an advantageous alternative to the conventional method to produce $(Ba_{0.85}Ca_{0.15})(Ti_{1-x}Zr_x)O_3$ powder. Single-phase, and sub-micron $(Ba_{0.85}Ca_{0.15})(Ti_{1-x}Zr_x)O_3$ powders can be prepared at 700°C, which is much lower compared to the conventional method. These powders can be sintered at 1275°C-1300°C with a sintered density around 93-94% of theoretical density. From the temperature dependent dielectric behavior, the phase transition temperature (Tm) of BCTZ enhanced compared to BZT, peak height decreases and broadness increases significantly with incorporation of Ca. Enhanced piezoelectric and dielectric properties [d_{33} =215 pC/N, ε~2244 and tanδ = 1.6%] are obtained for $(Ba_{0.85}Ca_{0.15})(Zr_{0.1}Ti_{0.9})O_3$ composition, which is higher than that of other Pb-free piezoelectric systems. This composition can be represented by a pseudobinary solid solution where $Ba(Zr_{0.2}Ti_{0.8})O_3$- $(Ba_{0.7}Ca_{0.3})TiO_3$ (BZT-BCT) are two end members, and BCTZ10 is a 50-50 solid solution of BZT-BCT. The enhancement of dielectric and piezoelectric property can be explained by the existence of MPB in this composition. However, the piezoelectric and dielectric properties of combustion synthesized sample are lower than the earlier reported result of similar composition. Enhancement of sintering density and grain size was also studied to improve the piezoelectric property further. Further studies are required how to improve the sinterability and piezoelectric property of the BZT-0.5BCT.

Chapter-4.3

Effect of different preparation methods on densification, microstructure, dielectric and piezoelectric properties of $(Ba_{0.85}Ca_{0.15})(Zr_{0.1}Ti_{0.9})O_3$ [BZT- 0.5BCT]

4.3.1Introduction

In the previous section, we have observed that $(Ba_{0.85}Ca_{0.15})(Zr_{0.1}Ti_{0.9})O_3$[BZT-0.5BCT]ceramics exhibits excellent dielectric property and piezoelectric coefficient (d_{33}=215 pC/N). However, the value is lower than the reported result of similar composition. To improve the properties further, enhancement of sintering density and modifications of grain size may become fruitful. It has been understood from the literature review (Chapter 2), the properties of BZT-0.5BCT ceramics strongly depends upon the processing conditions. The dielectric and piezoelectric property intensely influenced by the density and grain size of the ceramics. Most of the research articles are focused on composition optimization ignoring the effect of processing conditions . It is well known that microstructure and their properties may differ greatly in ceramics with the same composition fabricated with different processes, even if the same technique but different processing parameters. Most of the literatures available on the preparation of BZT-0.5BCT ceramics are solid state mixing by ball mill [48, 83,138, 139, 221**]**. Planetary milling is a useful technique which comprises simultaneous mixing and grinding of the raw materials for multicomponent compound preparation [140,183, 233]. It will be interesting to study how the microstructure and electrical properties of BZT-0.5BCTceramics depend on different preparation method with an aim to improve the dielectric and piezoelectric properties further.

In this chapter, BZT- 0.5BCT will be prepared by different (namely, planetary milling, ball milling) method and the phase formation, powder property, densification, microstructure, dielectric and piezoelectric properties will be compared with the powder prepared by solution combustion technique (discussed in chapter 4.2).

4.3.2 Results and Discussions

4.3.2.1 Phase evolution

Figure 4.3.1 shows the X-ray diffraction patterns of the BZT-0.5BCT powders prepared by the planetary milling and calcined at different temperatures. It is observed that the perovskite phase is formed along with the impurity phases of $Ba_3Ca_2Ti_2O_9$ (JCPDS No. 42-0535) and $BaCO_3$ (JCPDS No.44-1487) after calcination at 800°C. The appearance of $Ba_3Ca_2Ti_2O_9$ is may be due to a lesser amount of solid solubility of Ca^{2+} in $BaTiO_3$ at low temperature (800°C). As the temperature increased to 1100°C, the peaks corresponding to $Ba_3Ca_2Ti_2O_9$ and $BaCO_3$ completely removed, while a small amount of $BaZrO_3$ (JCPDS No. 74-1299) and $CaTiO_3$ (JCPDS No.09-0365) remained. The gradual removal of the $Ba_3Ca_2Ti_2O_9$ from the samples above 1100°C, due to the increased solid solubility of the Ca^{2+} in $BaTiO_3$ with increasing calcination temperature [130,234]. It is to be mentioned that the impurity phases are removed only after calcinations at 1200°C. It can be concluded that the pure perovskite phase is formed via formation of the different intermediate compounds like $Ba_3Ca_2Ti_2O_9$, $BaZrO_3$, and $CaTiO_3$. Wang et al. observed a trace of impurity phases in the powders of similar composition calcined at 1300°C [139].

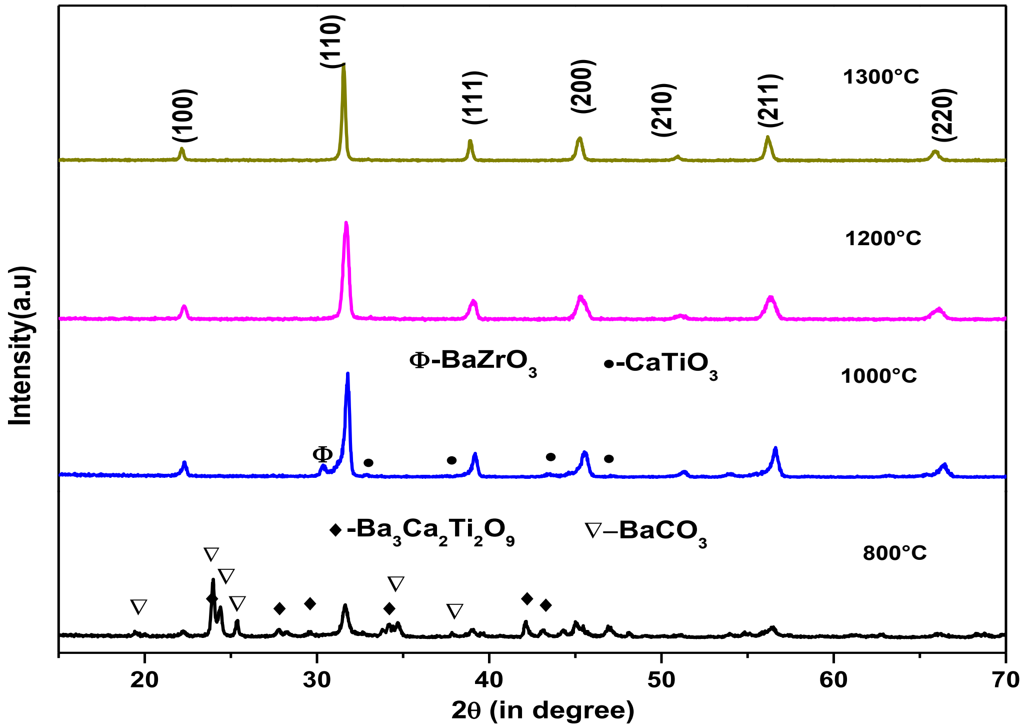

Figure 4.3.1X-ray diffraction patterns of BZT-0.5BCT powders prepared by planetary milling calcined at different temperatures

The BZT-0.5BCT powders also prepared by simple solid state mixing of the oxide ingredients by ball milling technique and calcined at different temperatures and analyzed by the X-ray diffraction (Fig. 4.3.2). However, in this case, a single phase perovskite phase is formed only after calcination at 1300°C, which is higher than the planetary milling method. The perovskite phase evolutions in both the cases are similar, but the phase formation temperature is different.

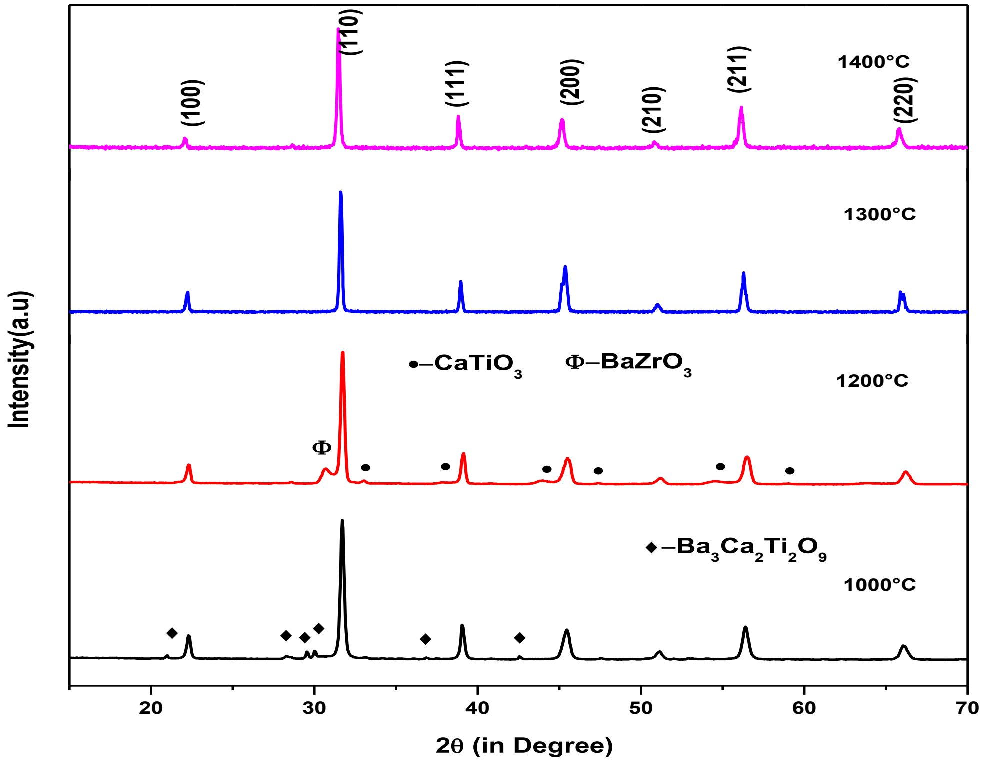

Figure 4.3.2 X-ray diffraction patterns of BZT-0.5BCTpowders prepared by ball milling with different calcination temperatures

In case of BZT-0.5BCT, prepared by solution autocombustion method (discussed in chapter 4.2), the phase pure powder obtained at 700°C which is significantly lower than the powder prepared by the planetary milling and ball milling technique where the phase purity obtained at 1200°C and 1300°C, respectively. These results suggest that Ca^{2+} and Zr^{4+} have been successfully incorporated into $BaTiO_3$ lattices to form a homogeneous solid solution. The average crystallite size is found to be 36 nm, 39nm and 46nm for powder prepared by planetary milling, solution combustion method and ball milling respectively, as calculated using the Scherrer formula[182] (mentioned in chapter 3, section 3.3.2.1). The result indicates that the crystallite size of the powder prepared by planetary milling method is lowest among these techniques.

The XRD patterns of BZT-0.5BCT are fitted with a combination of the tetragonal (space group P4mm) and the orthorhombic (space group Amm2) phase [132,188,222**]** The lattice parameters were refined using a least-square fitting method [186] and shown as in table 4.3.1.The X-ray analysis indicates the presence of orthorhombic and tetragonal phase in powder prepared by different methods. The coexistence of tetragonal and orthorhombic phases at room temperature was also reported by the other researchers [83,132].

Table 4.3.1 Lattice parameters of powders prepared by three different synthesis methods

Method	Space group	Lattice parameter (Å)
Planetary mill	P4mm	a=4.0091(28),c=4.0183(16)
	+	
	Amm2	a=4.0094(12),b=5.6706(4),c=5.6762(19)
Solution combustion method	P4mm	a=4.0087(5),c=4.0178(9)
	+	
	Amm2	a=3.9982(4),b=5.6558(2),c=5.6814(3)
Ball mill	P4mm	a=4.0057(2),c=4.0068(3)
	+	
	Amm2	a=4.0021(3),b=5.6651(3), c=5.6577(5)

It is well known that the precise identification of the three different phases (rhombohedral, orthorhombic, and tetragonal in $BaTiO_3$) by XRD is very difficult because of the proximity of the diffraction angle of these phases [206]. Therefore, the Raman spectroscopic investigations may put some light on the presence of different polymorphic phases at room temperature in BZT-0.5BCT samples. Figure 4.3.3 shows the Raman spectra in the region of 150–1000cm^{-1} of BZT-0.5BCT powders obtained by different synthesis methods at room temperature. Raman Spectra show almost identical behavior of BZT-0.5BCT powder obtained by the various methods. The main difference is observed for the solution combustion derived powder, where the bands shift more to higher frequencies compared to other two methods. Such phenomena of Raman spectrum shifting is attributed to the variation of localized chemical environments and strain [153]. The spectrum of combustion BZT-0.5BCTpowder was analyzed with five modes 196, 247, 296, 522, and 724cm^{-1}.The room temperature tetragonal phase is characterized by the band at 296 cm^{-1} and the asymmetric broader bands at 520 and 720 cm^{-1}. The vibration in the Raman patterns has a broadening effect, indicating that the structure disorder results from the lattice distortion. Broadening of all the peaks in the mixed system suggests the presence of higher disorder compared to pure $BaTiO_3$.Itcan be interpreted as the signature of coexistence mix ferroelectric phases. The peaks around 521 and 724 cm^{-1} correspond to phonon vibrations of the Ba-O bonds while the peaks in the range 180–300 correspond to the phonon vibrations of Ti–O bonds. The peak at 190 cm^{-1} is originated from orthorhombic symmetry as observed by the other researchers [225-227].

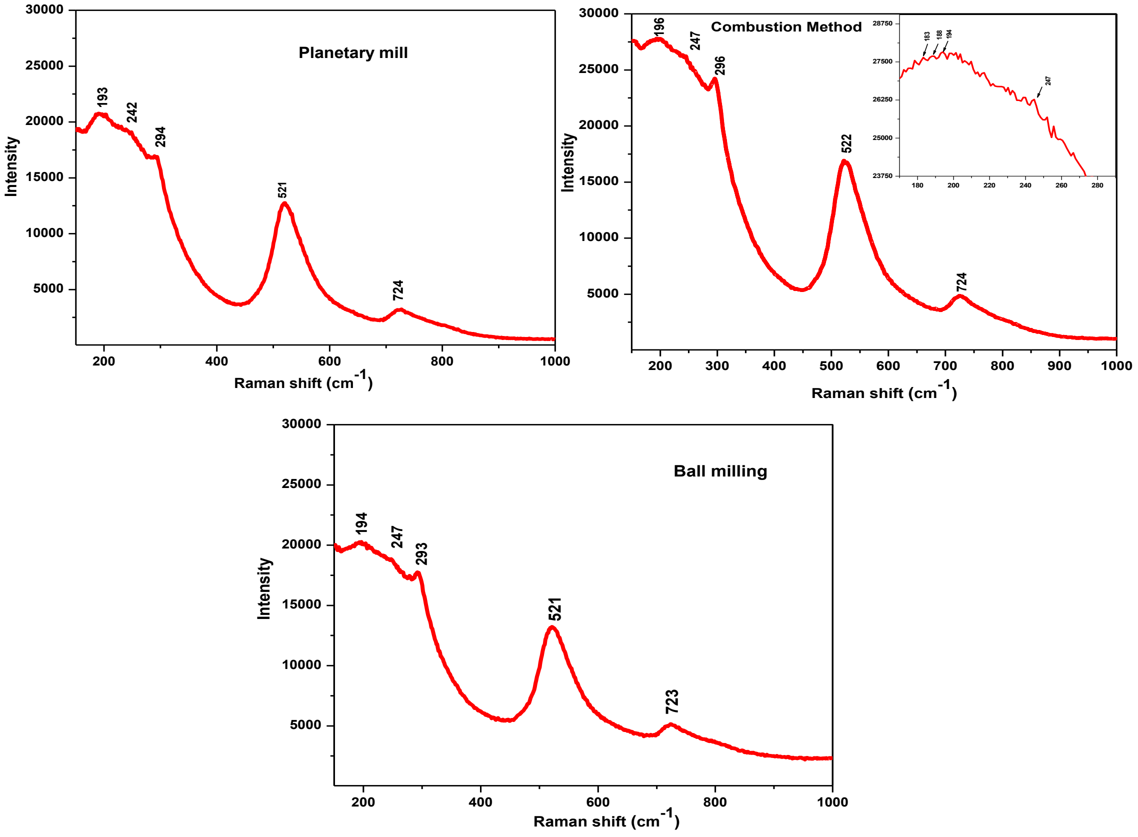

Figure 4.3.3 Raman spectra of BZT-0.5BCT powder prepared by different synthesis methods at room temperature

4.3.2.2 Powder morphology

Fig. 4.3.4 shows the microstructure of BZT-0.5BCT powders obtained by planetary milling, ball milling, and combustion method. It can be observed that the morphology of BZT-0.5BCT powder prepared through planetary mill and ball mill method are usually of a spherical particle of uniform size. The average particle size of BZT-0.5BCT powders is 0.15 -0.3µm for planetary milling and 0.6-0.9 µm for ball milling method. For combustion powder, the particles are agglomerated and agglomerate size is in the range of 0.25–0.40 µm with an irregular to spherical shape. It can be found that many fine particles with the size of 40 to 70 nm is present in the sample. The value of BET surface area of the BZT-0.5BCT powders are 1.88m^2/g, 2.58m^2/g and 0.4m^2/g for planetary milling, combustion and ball mill, respectively. It is found that combustion powders are thermodynamically unstable due to the large surface area compared to other two methods. The higher surface energy is leading to the powder agglomeration. It can be concluded that the powder prepared by planetary milling and combustion method are much finer compared to ball milling method.

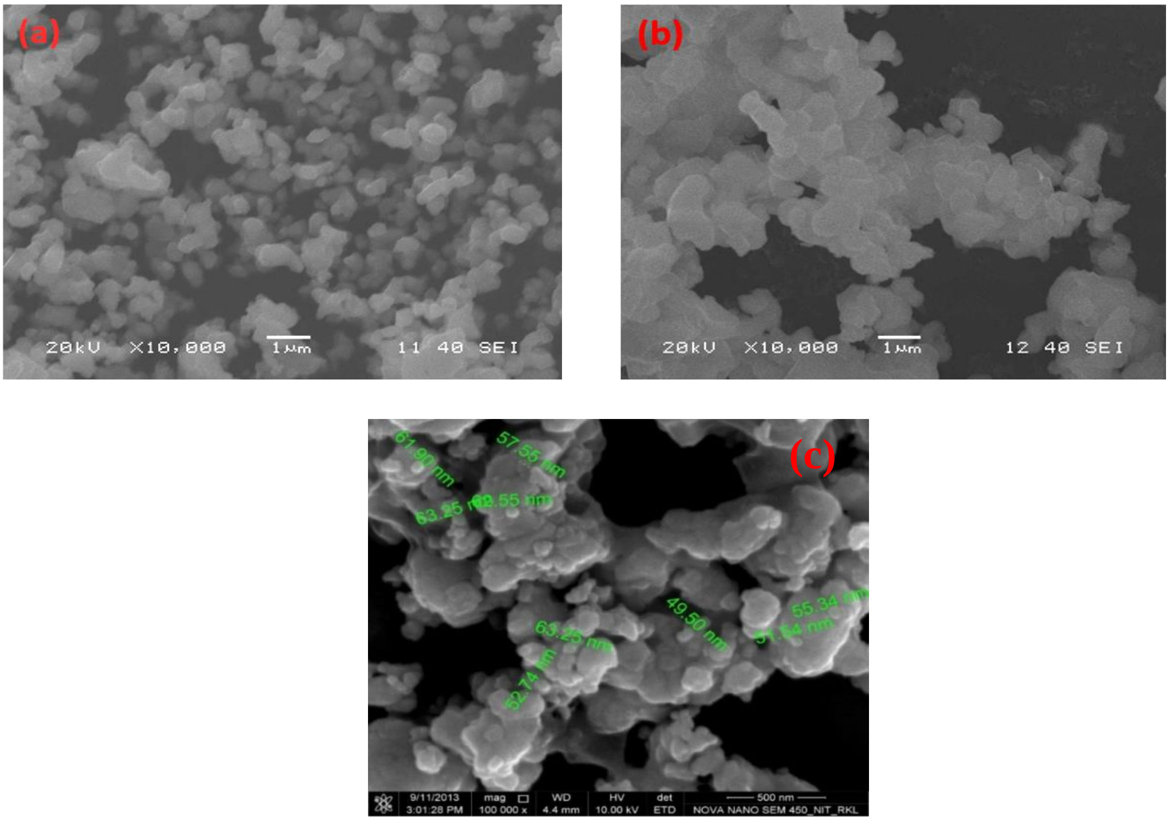

Figue4.3.4 Microstructure of BZT-0.5BCT powder prepared by (a) planetary milling (b) ball milling method (c) combustion method

4.3.2.3 Densification behavior

Figure 4.3.5 (a) and (b) shows the linear shrinkage and linear shrinkage rate as a function of temperature for BZT-0.5BCT prepared by the different method. The powders prepared by planetary milling starts to shrink (T_0) at 1120°C and reaches end of its densification (T_f) at around 1350°C with a linear shrinkage of 13.5%. In the case of the combustion synthesized powder, T_0, T_f and the linear shrinkage are 1138°C, 1298°C and 9.2%, respectively. In the case of the ball milled powder the linear shrinkage is approximately 4% and T_0, T_f are similar to that of the planetary milling powder. Linear shrinkage during heating is directly related with the densification of a material. The higher the shrinkage, the more will the density achieved. It can be seen that the BZT-0.5BCT powder prepared by planetary mill showed maximum shrinkage compared to other two methods. In contrast, the powder obtained by ball milling showed minimum shrinkage. It indicates that the powder prepared by combustion and planetary milling method consists of fine particles having relatively high surface area, which is the driving force for maximum shrinkage of the green pellet over a narrow temperature range. Two step shrinkage is observed in planetary mill and combustion powder, may be attributed to the presence of agglomerates which starts densification at different temperatures. After the densification of the agglomerates, the shrinkage rate increases sharply with temperatures which depend on the different preparation method. The shrinkage rate may be correlated with the densification rate. All the shrinkage and shrinkage rate related information are summarized in Table 4.3.2 for comparison. There are no reports available on the densification study of BZT-0.5BCT by dilatometry. It can be concluded that sintering process is much influenced by the preparation method and powder property.

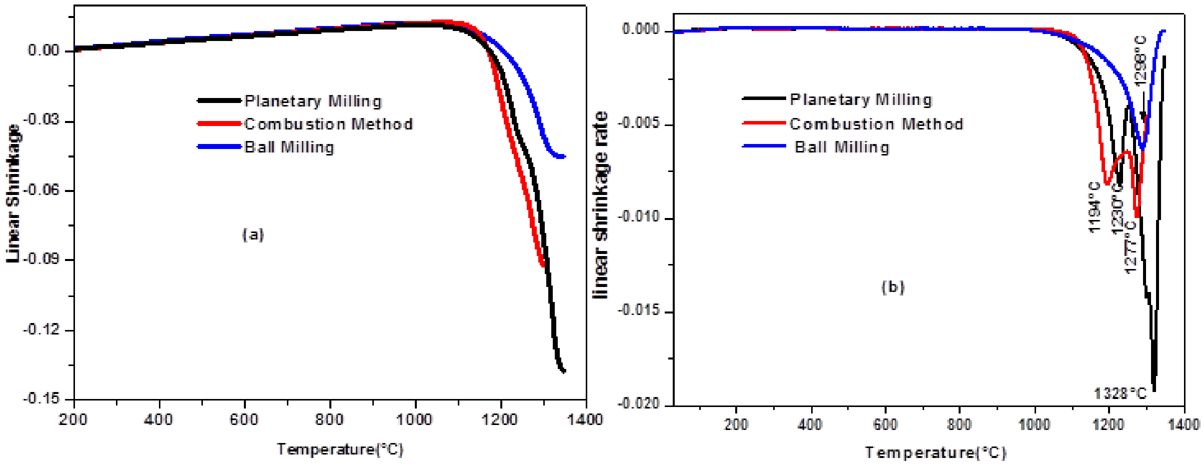

Figure 4.3.5 (a) Linear shrinkage and (b) linear shrinkage rate as a function of temperature for BZT-0.5BCT prepared by different synthesis methods.

Table 4.3.2: Result from dilatometer experiments: onset temperature (T_0), temperature of the maximum shrinkage rate (T_{Smax}), temperature at which densification stops (T_f) and width of the temperature interval, where shrinkage occurs ($\Delta Ts=T_f-T_0$)

BZT-0.5BCT	Planetary milling	Combustion	Ball milling
onset temperature T_0(°C)	1124	1138	1131
Ts max	1230,1328	1194,1277	1298
T_f	1346	1298	1340
$\Delta Ts=T_f-T_0$(°C)	222	160	209
Maximum shrinkage(%)	13.6	9.2	4.5

Fig 4.3.6 shows the variation of density with temperature of BZT-0.5BCT ceramic obtained by different preparation method. It reveals that, at the same sintering temperature (viz., 1300^{o}C), the density of the planetary mill samples is much higher than that of the other two methods. Density of all BZT-0.5BCT ceramics increases with increasing temperature. However, for the combustion samples, maximum density is observed at 1300°C, after that density decreases with increase in

temperature. The reason for the decrease in density is the generation of impurity phases (mentioned in chapter 4.2, section 4.2.2.7). From the figure, it is evident that the bulk density of the planetary milled samples is not varying much beyond 1350°C but may modify microstructure. For ball milled samples, the maximum density is observed at 1400°C. It is mentioned earlier that the particle size for ball milling method is larger than the other methods. This may be one of the possibilities which results in its low density because the smaller the particle size is, the easier to achieve high density.

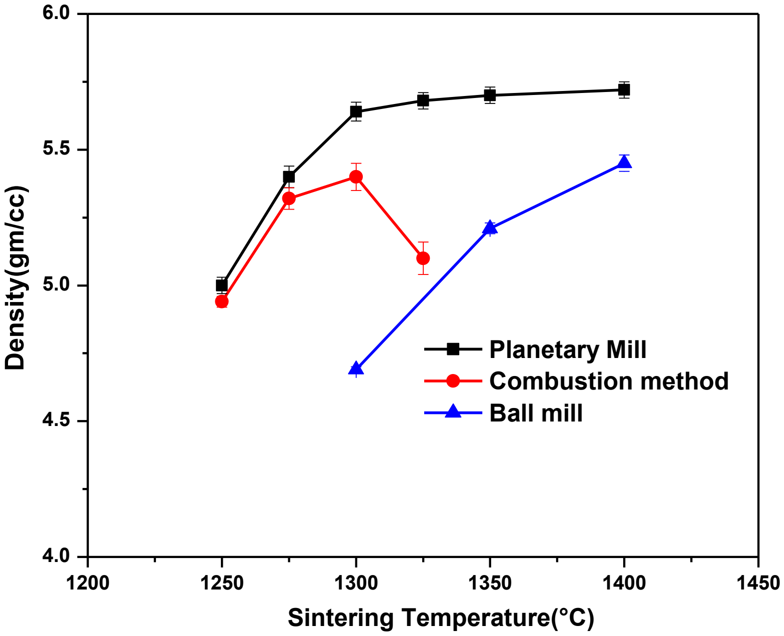

Figure 4.3.6 Variation of bulk density with sintering temperature of BZT-0.5BCT ceramic prepared by different synthesis methods.

4.3.2.4 Microstructure

The typical FESEM micrographs of BZT-0.5BCT ceramics prepared by different methods are shown in Fig 4.3.7. It is observed that the planetary milled sample has dense microstructure compared with the other two methods, and that is corroborating the density data. The average grain size of 1.2μm and 2.5 μm are obtained for the sample sintered at 1350°C and 1400°C, respectively. The grain size obtained, in this case, is much smaller than the reported result [221, 83]. However, the sample prepared by ball milling (average grain size 9.3 μm) and combustion method (average grain size 10.2 μm) have higher grain size compared to planetary milled sample. It is very important to mention that the grain size of sintered planetary milled sample is approximately four times compared to its initial particle size, whereas, it is twenty times in combustion synthesized sample and ten times in ball milled sample. Tan et al. obtained BZT-0.5BCT fine grain (0.4μm) ceramic by spark plasma sintering method at 1120°C. They also sintered BZT-0.5BCT by two-step sintering process where samples were initially kept at 1400°C and then sintered at1100°C/20h, and observed grain size of 10.8µm [142]. However, further studies are required to understand the different grain growth mechanisms in different preparation methods.

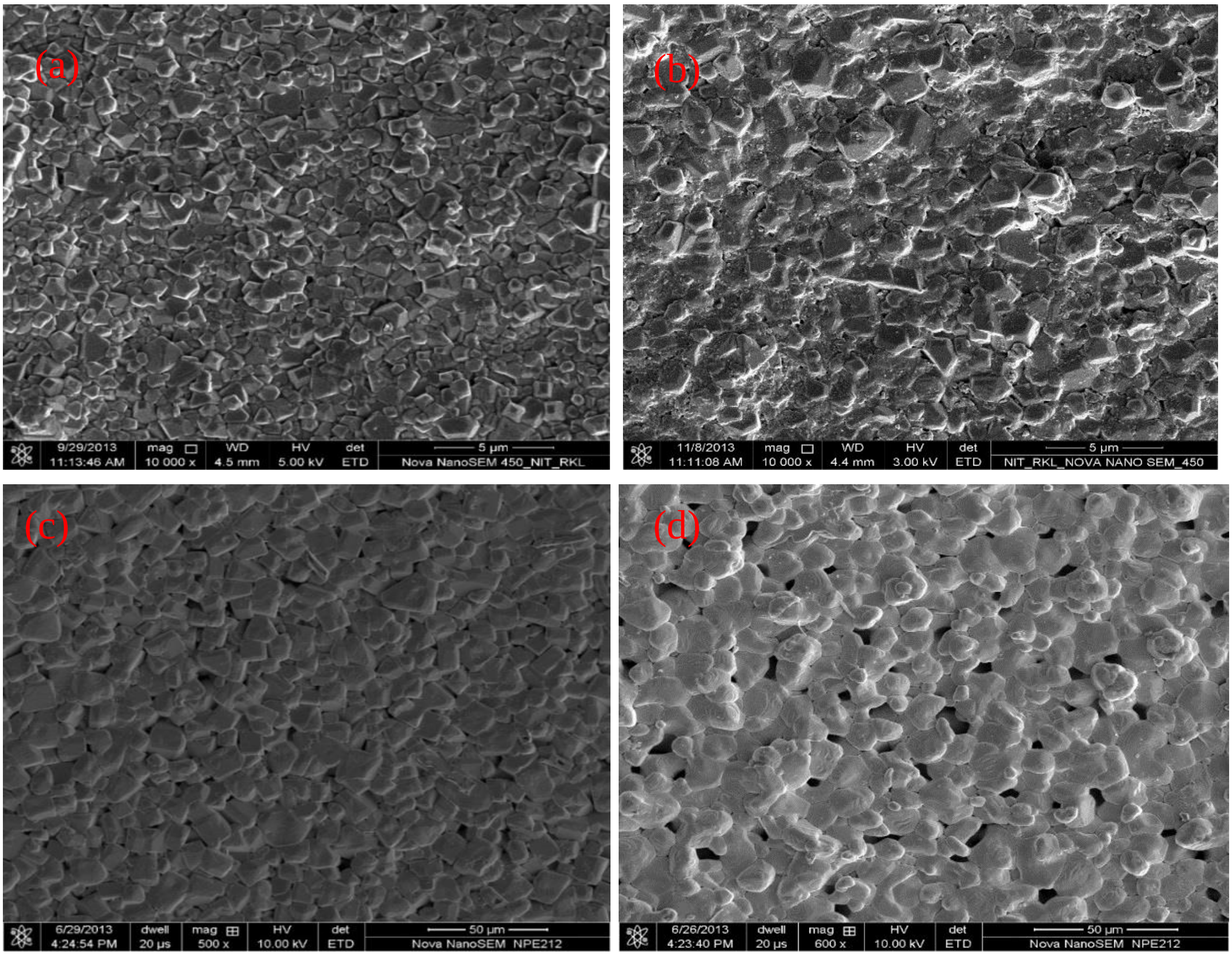

Figure 4.3.7 FESEM micrographs of BZT-0.5BCT ceramics prepared by different methods, planetary milling (a) 1350°C (b) 1400°C (c) combustion method (1300°C) (d) ball milling (1400°C).

4.3.2.5 Dielectric properties

Fig 4.3.8 shows the variation of the relative permittivity and dissipation factor with sintering temperature of BZT-0.5BCT ceramic. It reveals that the relative permittivity values of the sintered sample increases with the increase in sintering temperature. The planetary milling method sample has higher relative permittivity (3535) with low dissipation factor(1.4%) sintered at 1350°C, compared to other two methods and these values are better than those reported in literature [48,138]. The better dielectric property in the planetary milled sample may be attributed to the higher density of the sintered specimen. Dissipation factor of the BZT-0.5BCT ceramics have found to be less or equal to 2%, prepared via the three different methods and which is lower than most of the Pb-free piezoelectrics (viz. BNT, NKN) (~4%) [72,235]. From Fig. 4.3.8, it is noteworthy that the dissipation factor increases rapidly for combustion synthesized sample with increase in sintering temperature beyond 1300°C. It may be due to the formation of impurity phases (discussed in chapter 4.2, section 4.2.2.7). However, for the combustion method, the observed relative permittivity value (2244) is comparable to the sample prepared by conventional method[221] and wet chemical method [236] but it is much higher than that of other lead-free systems (viz. BNT, NKN) (ε <1000) [72,235]. This result indicates that the relative permittivity value strongly depends on the method of preparation and density of the sintered ceramic. The temperature dependence of the relative permittivity of BZT-0.5BCT ceramic prepared by the different method is shown in figure 4.3.9 (a). In the case of, planetary milled sample, two peaks are observed in the measured temperature range (25°C - 200°C). These two peaks correspond to the polymorphic phase transitions from orthorhombic phase to tetragonal phase at 35°C ($T_{O\text{–}T}$) and tetragonal phase to cubic phase at 85°C (T_C). These results are consistent with reported literature [139]. From Fig. 4.3.10 (b), it is noteworthy that the dissipation factor is around 2% for all our samples in the temperature range of 25°C - 200°C, which suggests good temperature stability.

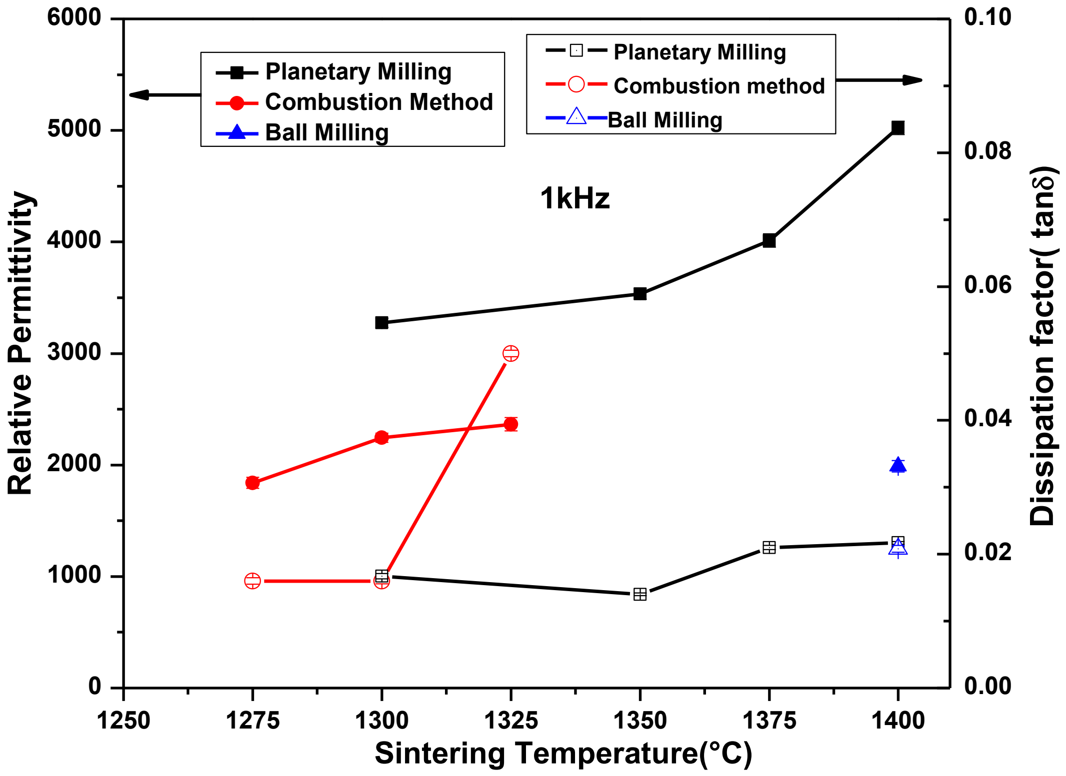

Figure 4.3.8 Relative permittivity and dissipation factor of BZT-0.5BCT ceramics at different sintering temperatures of BZT- 0.5BCT ceramic.

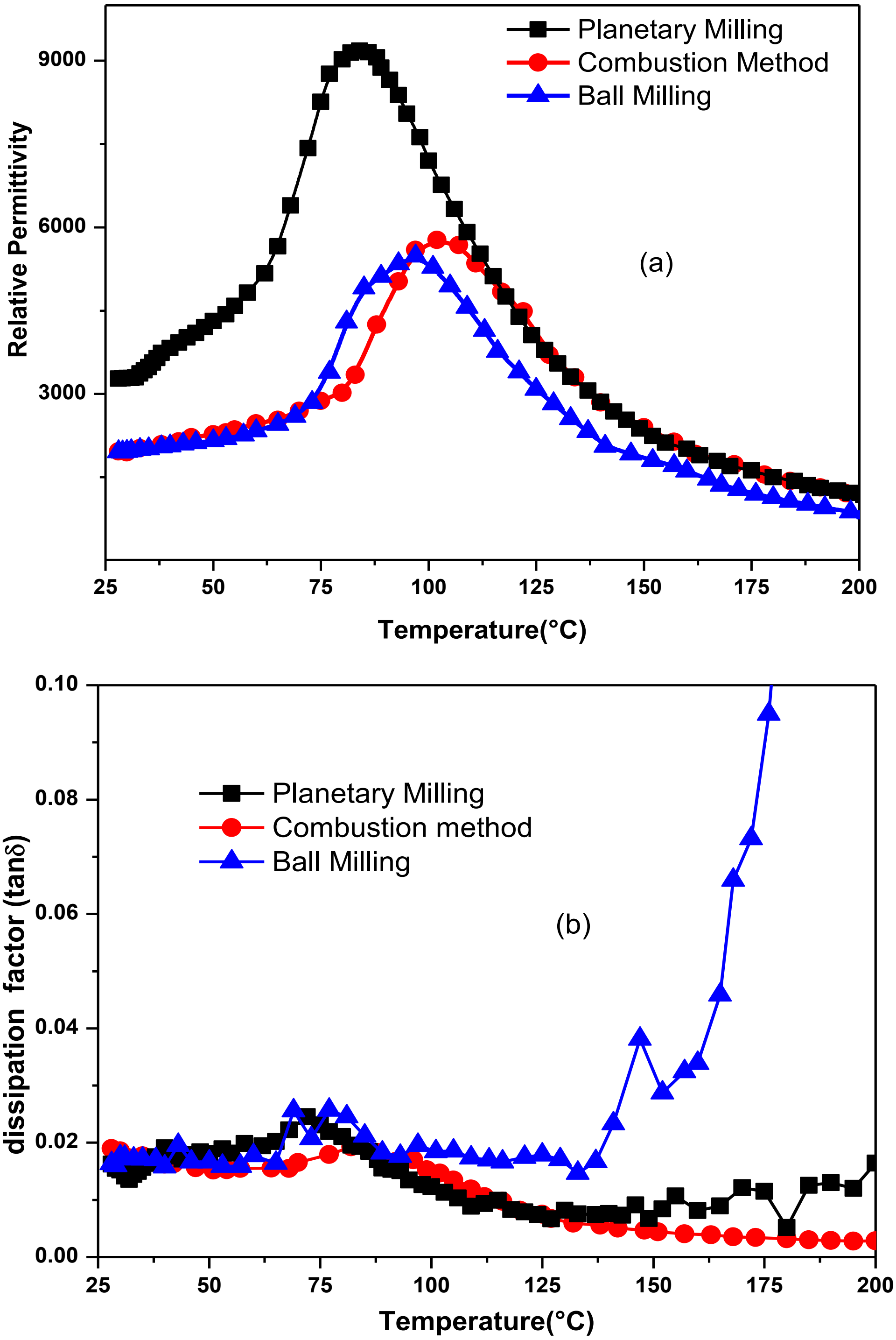

Figure 4.3.9 (a) Temperature dependent relative permittivity (ε) and (b) Dissipation factor of BZT-0.5BCT ceramic prepared by different synthesis methods.

The T_C of BZT-0.5BCT ceramics are 102°C, 96°C and 85°C for combustion method, ball milled and planetary milled sample, respectively. It is interesting to mention that the T_C value of BZT-0.5BCT is reported by different researchers lie in the range of 65 to 103°C [131,139,138, 236-238]. The possible reasons for the wide variation in T_C are the grain size, sintering temperature, processing condition and density of the sintered BZT-0.5BCT ceramics. Bai et al.[238] observed that the curie temperature increases to high temperature with increasing grain size. It may be due to the decrease in internal stress with the increase in grain size, which modifies both long-range electrostatic forces and short-range forces [238]. The other possible reasons for decrease or increase in the phase transition temperature are intergranular stress, ferroelectric domain sizes, and the compositional inhomogeneity [239]. In our case, the observation of lower T_C value in planetary milled sample is due to the smaller grain size (1.2µm) compared to combustion method (10.2µm) and ball milling (9.3µm) method. Krishna et al. demonstrated that the powder synthesis procedure affects the substitutional sites in multicomponent ceramics and this in turn, influence their physical behavior drastically [29]. In planetary milling method, the result of good dielectric properties may be attributed to the high dense ceramics. Moreover, all the BZT-0.5BCT ceramics exhibit a broad peak at around Curie temperature.

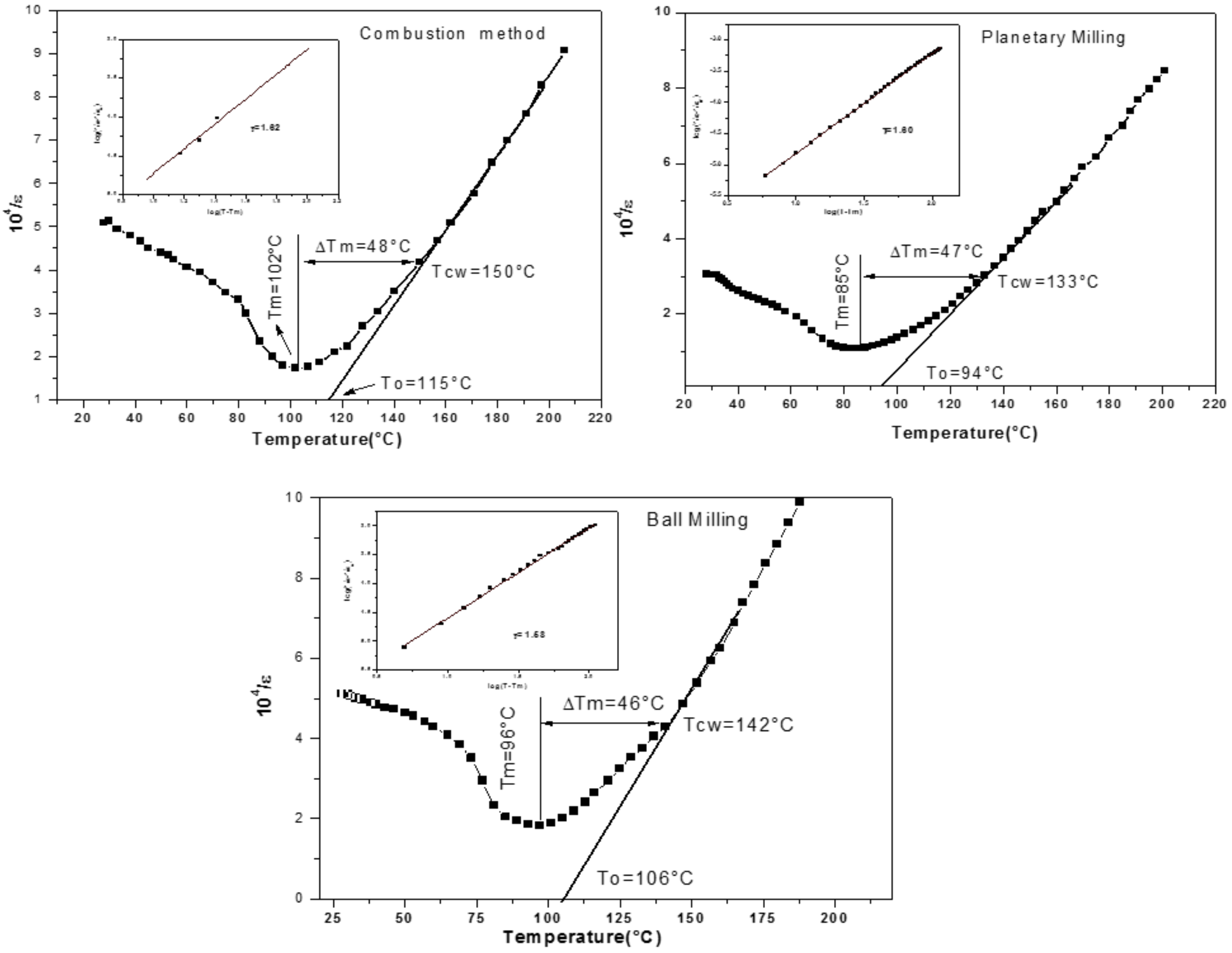

Figure 4.3.10. Curie-Weiss plot for inverse dielectric permittivity as a function of temperature for BZT-0.5BCT ceramics [insets showing the corresponding curves of log(1/ε- 1/ε_m) against log(T-T_m)].

The plot of log(1/ε−1/ ε_m) as a function of log (T−T_m) for BZT-0.5BCT ceramics is shown in Fig. 4.3.10. A linear relationship was obtained for all BZT-0.5BCT samples. The slope of the fitting curves is used to determine the γ value. The diffuseness constant γ are 1.58, 1.60 and 1.62 for ball mill, planetary mill, and combustion method, respectively. The detail results are shown in Table 4.3.3. This behavior of BZT-0.5BCT ceramics may be attributed to the cationic disorder and composition fluctuation induced by A and B site substitutions [240]. The results also indicate that the all BZT–0.5BCT ceramics have similar diffuse phase transition characteristics and not much dependent on the processing.

4.3.2.6 Ferroelectric and piezoelectric properties

Fig.4.3.11 shows the ferroelectric properties of BZT-0.5BCT with temperature. All ceramics are typically soft, with a very low coercive field E_c and a relatively high remnant polarization P_r. Hysteresis loops become slimmer with increasing temperature, accompanied by a fast drop of Pr values. The loop looks almost closed as the temperature is over 100°C, indicating that ferroelectric domains disappear. It is to be mentioned that in all the samples a finite polarization retained still above the Curie temperature which is also a signature of the diffuse phase transition.

The Piezoelectric coefficient (d_{33}) of BZT-0.5BCT ceramics are 350pC/N, 215pC/N and 200pC/N for planetary milling, combustion method and ball milling method, respectively. Piezoelectric properties obtained by the planetary milling method is quite similar to the reported literature [219,237], higher than that of reported by Li et.al. [83, 236] and lower than that of reported by Lue et.al. and Wang et al.[48, 139]. Hao et al.[142] reported a d_{33} value around 72pC/N for MPB composition with grain size of 0.4µm and higher d_{33} (470pC/N) obtained for grain size greater than 10µm. For the planetary milling method, the higher piezoelectric properties in low temperature sintered (1350°C) sample may be due to the achievement of the dense, uniform microstructure. Moreover, the enhanced piezoelectric properties should be attributed to the PPT occurring near room temperature [220,241**]** and the coexistence of multiple phases, which causes instability of the polarization state, so the polarization direction can be easily rotated, resulting in high piezoelectricity [242]. Lower value of d_{33} for BZT-0.5BCT ceramics obtained by combustion method and ball mill method may be due to lower density of ceramic hampering the efficient poling.

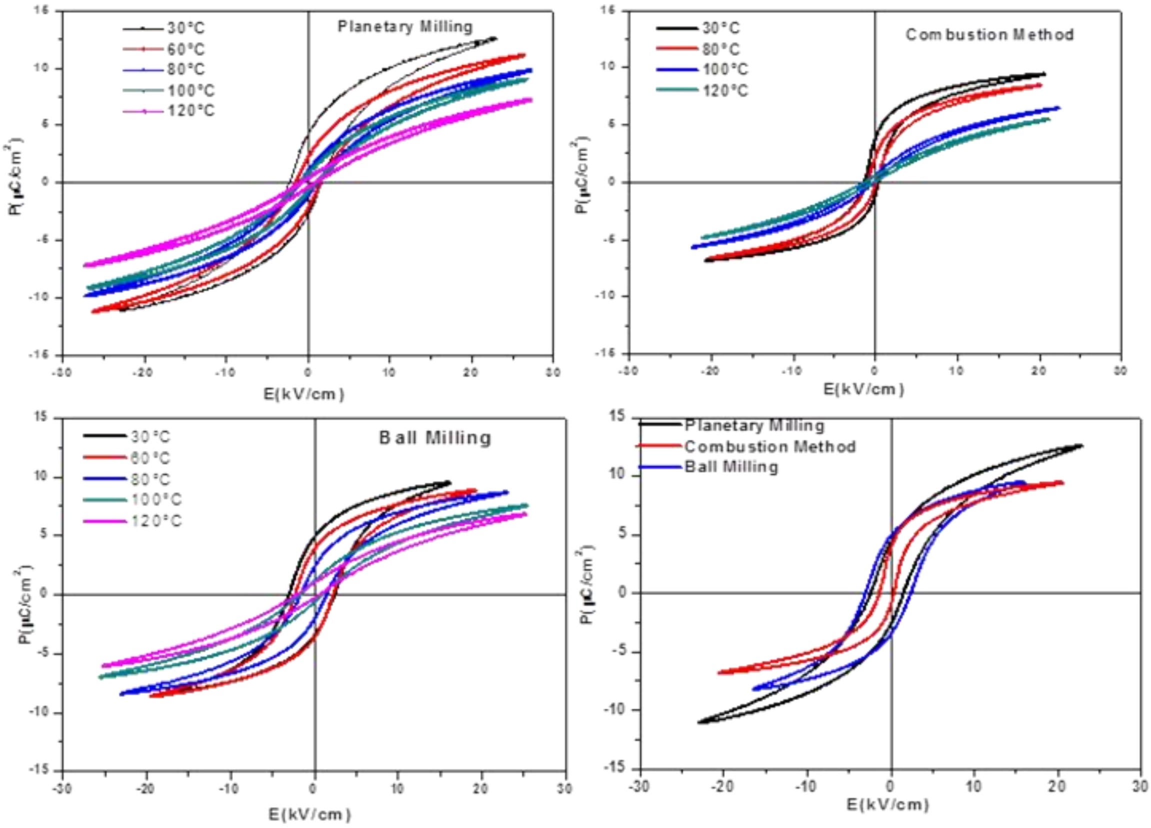

Figure 4.3.11 P-E hysteresis loop of BZT-0.5BCT ceramic with temperature (30°C-120°C) prepared by different synthesis methods

Table-4.3.3 Grain size, dielectric and piezoelectric properties of BZT-0.5BCT ceramics prepared by different technque.

BZT-0.5BCT	Planetary milling	Combustion	Ball milling
Average Grain Size	1.2μm(1350°C)	10.2μm(1300°C)	9.3μm(1400°C)
Relative permittivity (ε_r) at 1kHz	3535	2244	1989
Dissipation factor at 1kHz	0.014	0.016	0.0208
T_0 (^oC)	94	115	106
T_m (^oC)	86	102	96
T_{cw} (^oC)	133	150	142
$\Delta Tm=T_{cw}-T_m$	47	48	46
γ	1.60	1.62	1.58
d_{33} at 1.5kv/mm	350	215	200

4.3.3 Enhancement of grain size in planetary milling sample using microwave sintering

It is observed that planetary milled BZT-0.5BCT ceramics exhibits higher piezoelectric coefficient d_{33}=350pC/N with an average grain size of 1.2µm. However, lower value of d_{33} compared to Liu and Ren's report [48], may be due to the smaller grain size of these ceramics. Hao et al.[142] reported a d_{33} value around 470pC/N with grain size of 10.8µm and 72pC/N with grain size 0.4µm. In contrast, Coondoo et al. [221] reported a d_{33} value around 350pC/N with grain size of 25µm. In general, piezoelectric property depends not only on the density but also on grain sizes [238].To further enhance the grain size of the sintered ceramics, microwave sintering is used.

Microwave sintering (MS) is a useful technique for fabrication of dense ferroelectric ceramics at low temperature. This heating mechanism is advantageous over conventional sintering (CS) due to the following facts: enhanced diffusion processes, reduced energy consumption, very rapid heating rate, considerably reduced processing times, decreased sintering temperatures as well as improved mechanical, dielectric and magnetoelectric properties of the material [175,176,178].

In this section, planetary milled BZT-0.5BCT powders are sintered in microwave and the properties were compared with the conventional sintered sample.

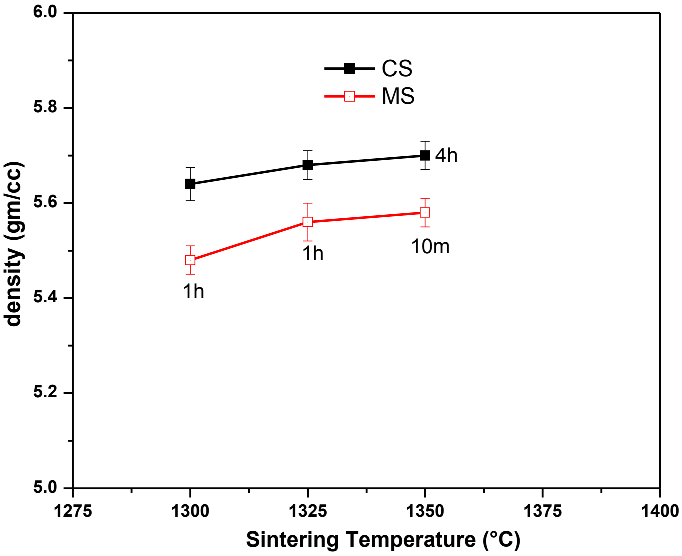

Figure 4.3.12 Bulk density of BZT-0.5BCT ceramics as a function of sintering temperature for CS and MS.

Figure 4.3.12 shows the density of BZT-0.5BCT ceramics as a function of sintering temperature for CS and MS. It reveals that, at the same sintering temperature, the density of the CS samples is marginally higher than that of the MS samples. As the sintering temperature increases, the density of BZT-0.5BCT ceramic tends to increase. Furthermore, the relative density of the MS samples reached 96.5% (5.58gm/cc) of theoretical density at 1350°C for 10 min. The density of the MS samples sintered only for 10 min is comparable to that of the samples conventionally sintered for 4h, at same sintering temperature. It indicates that the microwave sintering is helpful in getting comparable density in less time. For MS sample, as the sintering time increases from 10m to 30m at 1350°C, the samples stick to the alumina base plate. These results indicate that the sintering temperature and time are the important parameters for microwave sintering of BZT-0.5BCT ceramics.

Fig 4.3.13 shows the FESEM micrographs of CS and MS samples sintered at different temperatures. In both cases a dense microstructure observed. It is evident that the average grain size is ~8 μm for MS sample and 1.2μm for CS sample. It is noteworthy, microwave sintering successfully enhanced the grain size around seven times. The MS sample sintered at 1300°C/1h, contains small grain and the average grain size is around 0.8μm (microstructure is not shown here). From Table 4.3.4, it is clear that the dielectric property of MS sample is at par with CS. However, the d_{33} value is inferior in MS sample compared to CS. X-ray diffraction study of (Fig. 4.3.14) MS ground pellets revealed the presence of small amount of impurity phases ($Ba_4Ti_2O_{27}$ phases with JCPDS No. 44-0013) in the sample which probably reduces the piezoelectric property significantly but does not affect the dielectric property.

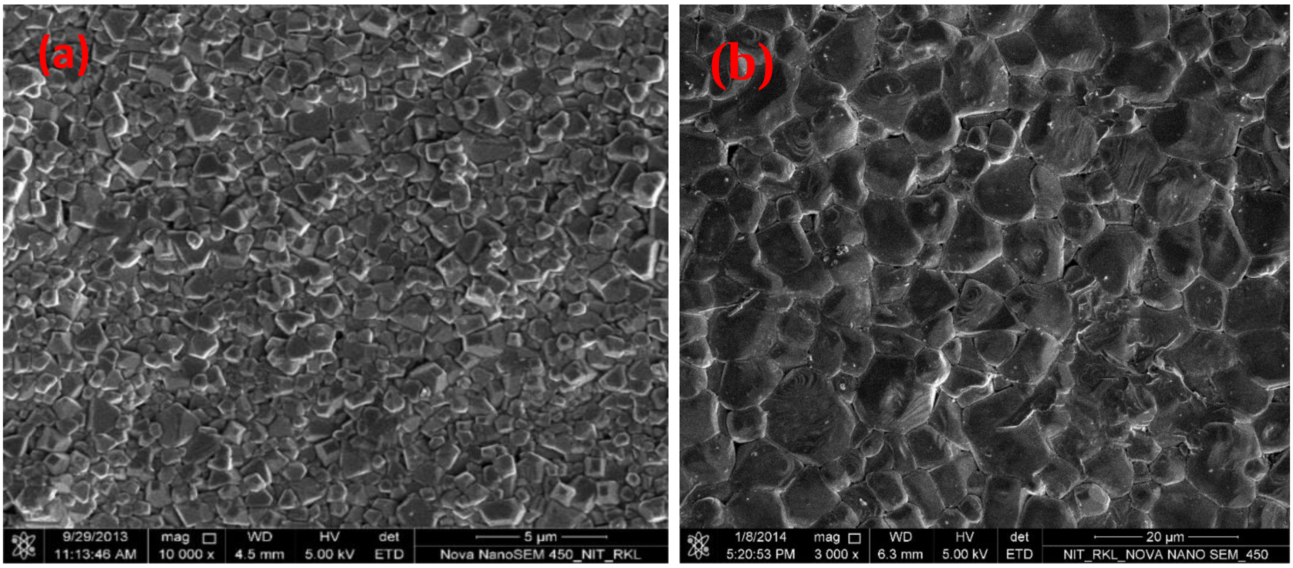

Figure 4.3.13 FESEM micrographs of (a) CS sample sintered at 1350°C/4h (b) MS samples sintered at 1350°C/10min.

Table 4.3.4 Comparison of different physical properties between CS and MS sample.

BZT-0.5BCT	Conventional Sintering	Microwave sintering
Sintering temperature (heating rate)	1350°C (3°C/min)	1350°C (20°C/min)
Soaking Time	4h	10min
Density	5.68gm/cc	5.58gm/cc
Grain size	1.2μm	8 μm
Total processing time	23h	2.5h
Dielectric Properties at room temperature	3535	3010
Dissipation factor at room temperature	0.014	0.016
d_{33} at 1.5kV/mm	350pC/N	150-200pC/N

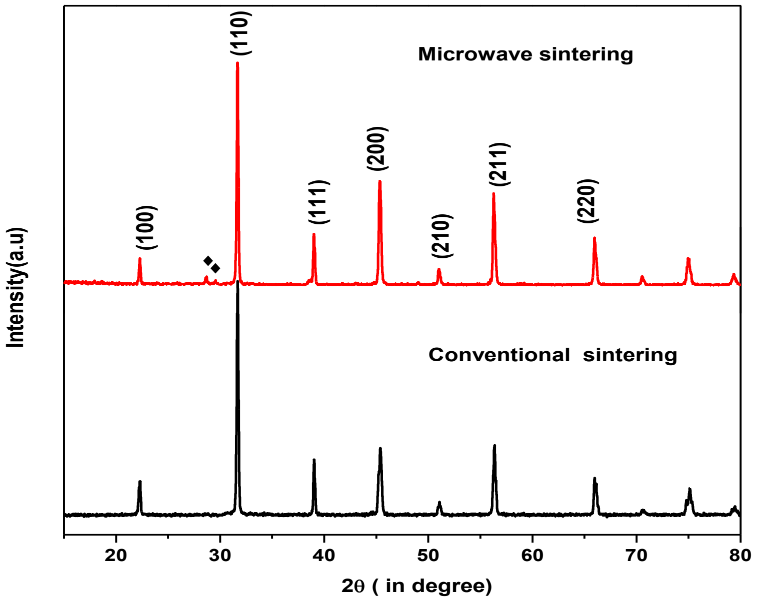

Figure 4.3.14. X-ray diffraction patterns of CS and MS sample sintered at 1350°C/4h and, 1350°C/10m, respectively

Table 4.3.5- summarizes the processing condition and electro-physical properties for our sample along with the reported data for BZT-0.5BCT ceramics for comparison. It is seen from Table 4.3.5 that the dielectric properties of our samples are better than the reported value and the piezoelectric constant is on par with the some of the published result.

Table 4.3.5.- Preparation route, calcination temperature, sintering temperature, density, grain size, dielectric permittivity and piezoelectric properties of BZT-0.5BCT Ceramics.

Synthesis Method	Calcination temperature	Sintering temperature	Density (%)	Grain size	ε at 1kHz	Tm (°C)	d_{33}(pC/N)	Ref
Solid State Synthesis	1200°C/4h	1450°C/4h		8-12µm	4800	65	328	[83]
	1300°C/3h	1450°C/2h			~3000	95	430(pulse poled)	[145]
	1150°C/6h	1500°C/6h	90-95	11µm	5800	60	350	[237]
	1200°C/6h	1450°C/2h		25 µm	2600	97	350	[221]
	1350°C/2h	1500°C/3h	~97		2892	103	410 (Tp=20°C, 4kV/mm), 360 (Tp=70°C)	[247]
	1350°C/2h	1400-1500 °C/3h	~96	10µm			360 (Tp=30°C), 423 (Tp= 90°C)	[246]
	1250°C/3h	1400°C/3h			3000	90	410	[245]
	1350°C/6h (double calcined)	1450-1500°C/3h	94	3µm	~3152		470	[244]
	1200°C/4 h	1120°C/5min (SPS), Two-step sintering: 1400°C/1100-1200°C/20h, Single step sintering: 1450-1500°C /4 h (CS).	96-4-97.2	0.4-32µm	~3000	87, 103	470 (10.8µm), 72(0.4µm)	[142]
Hydrothermal Method		1275°C/10 min Microwave			~2500	70	220	[236]
Solid State Synthesis via Planetary Milling	1200°C/4h	1350°C/4h	98.2	1.2µm	3535	86	350	Our work

4.3.4 Conclusions

The $(Ba_{0.85}Ca_{0.15})(Ti_{0.9}Zr_{0.10})O_3$(BZT-0.5BCT) ceramics has successfully prepared by three different methods namely, planetary milling, ball milling, and citrate-nitrate combustion method. The citrate-nitrate autocombustion method was found to be an advantageous alternative to the conventional method (ball mill & planetary mill) to produce single-phase and highly crystalline BZT-0.5BCTceramics at low-temperature. It has been found that calcination temperature to achieve phase purity and sinterability of the powder depends on the methods of preparation. The planetary milled powder can be sintered to more than 98% of theoretical density at 1350^{o}C. Lower sintering temperature compared to reported literature attributed to fine particle size. The average grain size of the sample prepared by ball milling, planetary milling and combustion method found to be 9.3 µm, 1.2 µm, and 10.2 µm, respectively. The relative permittivity values are found to be 3535, 1989 and 2244 for planetary milling, ball milling and solution combustion method, respectively. Low dielectric loss (tan δ less than 2%) is obtained for ceramic samples synthesized via all the methods. BZT-0.5BCT ceramic prepared by planetary milling shows high relative permittivity (3535) with low dielectric loss (0.014) with high piezoelectric coefficient (d_{33} = 350 pC/N) compared to other two methods. It is found that the T_C is dependent on the preparation methods and specifically on grain size. Microwave sintering is resulted in increase of the grain size seven times in case of planetary milled sample. However, Microwave sintering has no significant effect on dielectric property but degrades piezoelectric property due to growth of small amount impurity phases.

Chapter-4.4

Dielectric and piezoelectric properties of xBZT-(1-x) BCT ceramics at around MPB region

4.4.1 Introduction

In the previous section (chapter 4.2), we synthesized and characterized the $(Ba_{0.85}Ca_{0.15})(Zr_xTi_{1-x})O_3$[x= 0.05,0.1,0.15] solid solution and observed that particularly $(Ba_{0.85}Ca_{0.15})(Zr_{0.1}Ti_{0.9})O_3$ (BCTZ10) exhibits highest dielectric and piezoelectric property. It is explained by the formation of a pseudobinary solid solution where $Ba(Zr_{0.2}Ti_{0.8})O_3$-$(Ba_{0.7}Ca_{0.3})TiO_3$ (BZT-BCT) are two end members. BCTZ10 is a 50-50 solid solution of BZT-BCT, and the Morphotropic phase boundary (MPB) exists. The coexistence of two phase is also proved.

It is well-known that the crystal structure in the MPB compositions plays very important role in high piezoelectric response at MPB. It is reported that a small variation (~0.01) in composition in solid solution like PZT [248] and $BiFeO_3$-$PbTiO_3$ [249] can change the crystal structure and in effect significantly decrease the piezoelectric response. Very little work has been performed systematically to study the dielectric and piezoelectric properties of xBZT-(1-x)BCT at close compositional modifications around MPB. Li et al. [83, 246] and others [245, 247, 250**]** reported high dielectric and piezoelectric property away from MPB composition in contrast to Liu et al. who reported MPB at 50BZT-50BCT.

In view of this we decided to carry out detailed investigation of the phase formation, dielectric and piezoelectric response of xBZT-(1-x)BCT solid- solution on the compositions prepared at 1% interval for x= 0.47-0.53. In this case the xBZT- (1-x)BCT(0.47-0.53)is prepared by planetary milling method (discussed in chapter 3 and 4.3).

4.4.2. Results and Discussion

4.4.2.1 Phase evolution

Figure 4.4.1 shows the X-ray diffraction patterns of the xBZT-(1-x)BCT synthesized at 1200°C. The X-ray diffraction patterns revealed that all the obtained ceramics have a pure perovskite structure, and there is no evidence of the secondary phase formation. Formation of pure perovskite phase suggests that the Ca and Zr have completely diffused into the lattice site of $BaTiO_3$ to form a homogeneous solid solution. Moreover, it is clear that the position of the diffraction peaks shift towards the lower diffraction angles with an increase in BZT content from x= 0.47-0.49 and for the composition x=0.50, the diffraction peak marginally moved to higher angle and for higher values of x (0.51,0.52,0.53) it again turned to lower diffraction angle. Similar behavior is observed for Y_2O_3 modified BZT-BCT ceramics [158]. The shifting of the diffraction peaks to lower diffraction angles due to the distortion of crystal lattice, induced by the substitution of Ti^{4+}(0.605Å) by larger Zr^{4+}(0.72 Å) and increase the concentration of the Ba^{2+}(1.61Å) ion in place of the Ca^{2+}(0.134Å). XRD patterns are matched with the tetragonal and orthorhombic phases with JCPDS no. 89-1428 and 81-2100, respectively. All the BZT–BCT ceramics possess both orthorhombic and tetragonal phase [132, 222]. To determine the effect of small composition variations on the phase structure, the XRD patterns of all the compositions in the 2θ range of 44.5-46° and 65-67° are fine scanned and analyzed [Fig 4.4.1(b)]. It shows that all the compositions are fitted with the tetragonal (P4mm) and the orthorhombic (space group Amm2) phase [132,222].

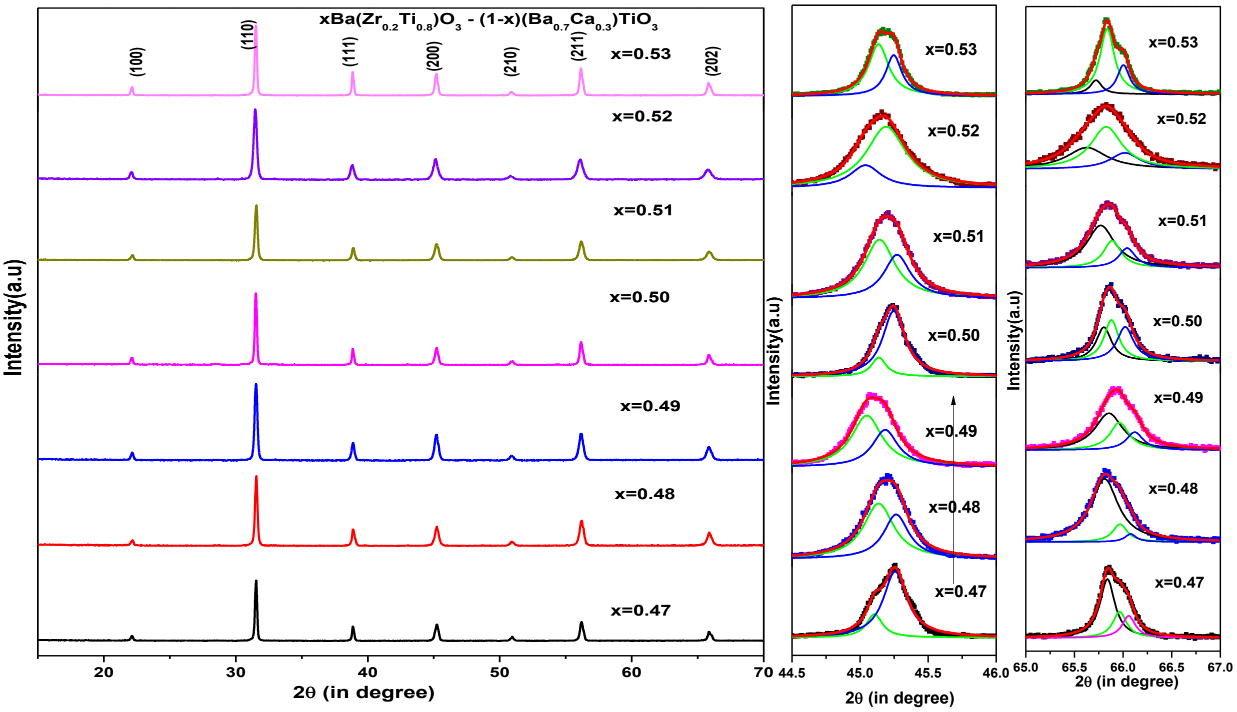

Figure 4.4.1(a) X-ray diffraction pattern of xBZT-BCT ceramics (b) The magnification Fig 4.4.1(a) in the range of 44.5°-46.0° and 65-67°.

The formation of triplet around (202) peak signifies the presence of the orthorhombic phase and doublet at (200) peak corresponds to tetragonal phase. In contrast to our report, many reports are available with a coexistence of tetragonal and rhombohedral phase near the morphotrophic phase boundary region of BZT-xBCT ceramics [132,83,143] and few have found that tetragonal and monoclinic phases coexist[240].Recently, Keeble et al. [132] reported the coexistence of orthorhombic and tetragonal phase near the MPB in the BZT-BCT composition.

Table 4.4.1: Lattice parameters and cell volume of xBZT-(1-x)BCT ceramics.

Composition	**Crystal structure**	**Lattice parameter(Å)**	**Cell volume(Å^3)**
x=0.47	*Tetragonal(P4mm)*	a=4.0081(4) , b=4.0150(11)	64.51
	+		
	Orthorhombhic(Amm2)	a=4.0083(6), b=5.6682(19) c=5.6738(19)	128.92
x=0.48		a=4.0089(21) b=4.0113(5)	64.46
		a=4.0076(6), b=5.6697(19), c=5.6713(16)	128.86
x=0.49		a=4.0109(21) b=4.0141(6)	64.58
		a=4.0098(3), b=5.6727(22), c=5.6747(16)	129.08
x=0.50		a=4.0091(28) c=4.0183(16)	64.58
		a=4.0094(12), b=5.6706(4), c=5.6762(19)	129.05
x=0.51		a=4.0098(28), b=4.0183(11)	64.49
		a=4.0091(3),b=5.6711(11),c=5.6720(10)	128.96
x=0.52		a=4.0099(12), c=4.0169(5)	64.59
		a=4.0087(6) b=5.6713(19) c=5.6738(19)	128.99
x=0.53		a=4.0099(6),b=4.0181(39)	64.61
		a=4.0088(6), b=5.6723(5),c=5.6773(3)	129.09

The identification of the phases by XRD in this solid solution is not very precise because of the proximity of the diffraction angle of these polymorphic phases [246]. Therefore, Raman spectroscopy may throw some light in order to detect the presence of some T and O or R modifications at room temperature in these BZT-BCT samples. The lattice parameters are summarized in Table 4.4.1.

Fig 4.4.2(a) to (g) shows the Raman spectra of BZT-BCT ceramics at room temperature. All the compositions of BZT-BCT ceramics show identical behavior. The main difference is that the peak positions of Raman modes, shift towards either the lower or higher frequency region.

Such phenomena of Raman spectrum shifting is attributed to the variation of associated tensile/compressive nature of the stresses [251,252].The spectrum of x=0.50 was analyzed with five modes 193, 242, 294, 521, and 724cm^{-1}.The room temperature tetragonal phase is characterized by the band at 294cm^{-1} and the asymmetric broader bands at 521 and 724cm^{-1}are well matched with tetragonal $BaTiO_3$as shown in fig 4.4.2 (a).It is to be mentioned that the intensity of the peak around 294cm^{-1} is decreased specifically for x= 0.50 (BZT-0.5BCT) and indicating an unusual structural change around this composition. The vibrations in the Raman patterns has a broadening effect, suggesting that the structure disorder results from the lattice distortion. Broadening of all the peaks in the mixed system suggests the presence of higher disorder compared to pure $BaTiO_3$. This can be interpreted as the signature of coexistence of mixed ferroelectric phases. Raman spectrum of the two phases such as the tetragonal and the orthorhombic relates to the feature in the range of 180cm^{-1} to 190 cm^{-1}. The peak at 190 cm^{-1} is originated from the orthorhombic symmetry as observed by the other researchers [225-227]. The shifting of peaks in xBZT-BCT to higher frequency compared to $BaTiO_3$ ceramic, especially at 518 and 720cm^{-1}is expected due to the difference in ionic radius between Ba^{2+} and Ca^{2+} as well as Ti^{4+} and Zr^{4+} which results in the distortion of the lattice and energy band widening [244].

All the xBZT-(1-x)BCT ceramics sintered at 1350°C for 4h having density more than ~97% of theoretical density. The ceramics possess dense microstructure and uniform grain size of 1-2µm.

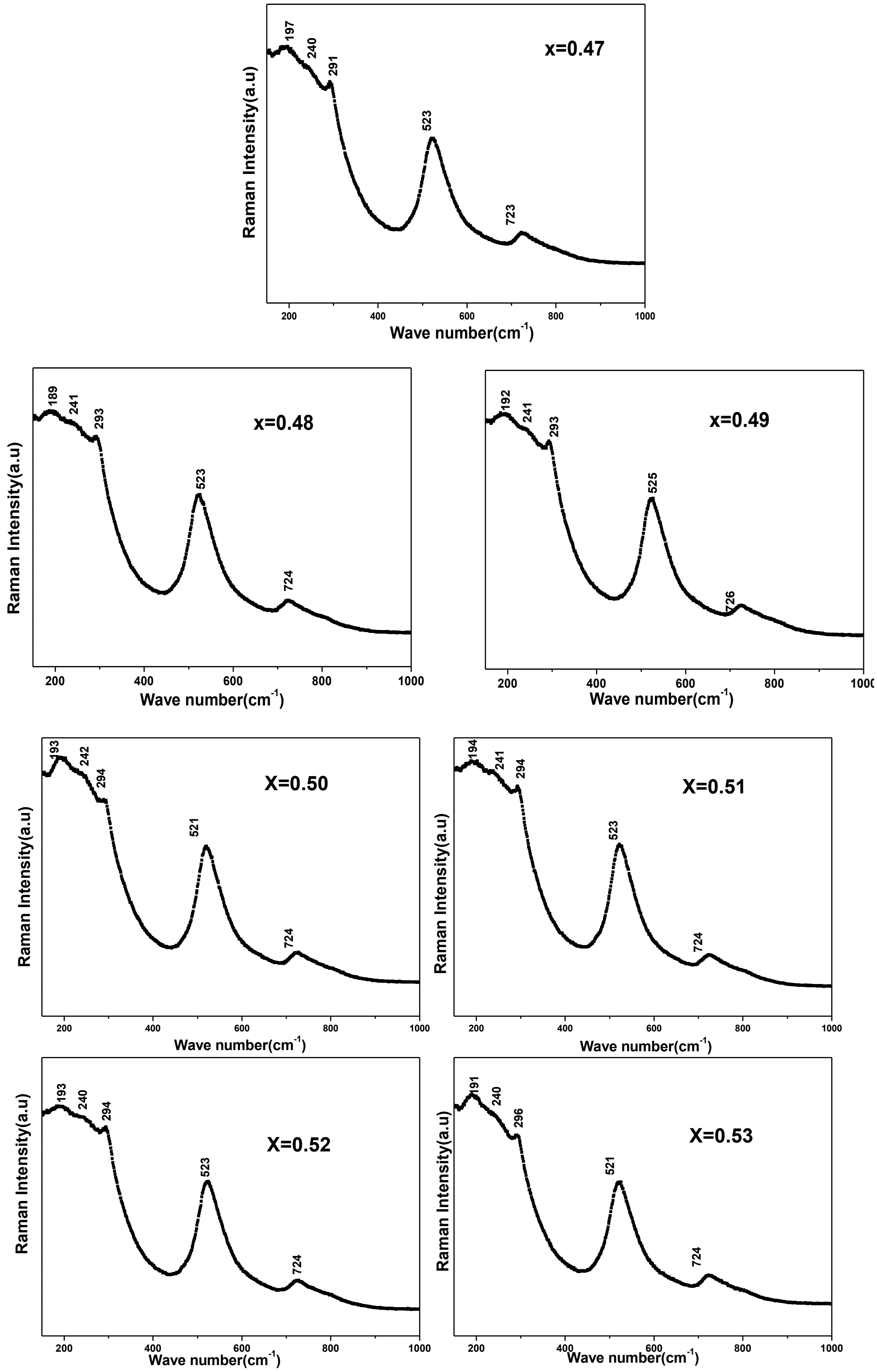

Figure 4.4.2.Raman spectra of xBZT-(1-x) BCT ceramics (a) x=0.47, (b) x=0.48, (c) x=0.49, (f) x=0.50, (e) x=0.51, (f) x=0.52, (g) x=0.53 at room temperature.

4.4.2.2 Dielectric properties

Fig 4.4.3 shows the room temperature relative permittivity and dissipation factor of xBZT-(1-x)BCT ceramics measured at 1kHz. It can be observed that maximum relative permittivity (3535) found in 0.5BZT-BCT composition which is relatively large as compared with reported literature [48].All the xBZT-BCT ceramics have high dielectric constant above 2900 and loss factor less than 2%. It also support an unusual phenomena around 50-50 compositions.

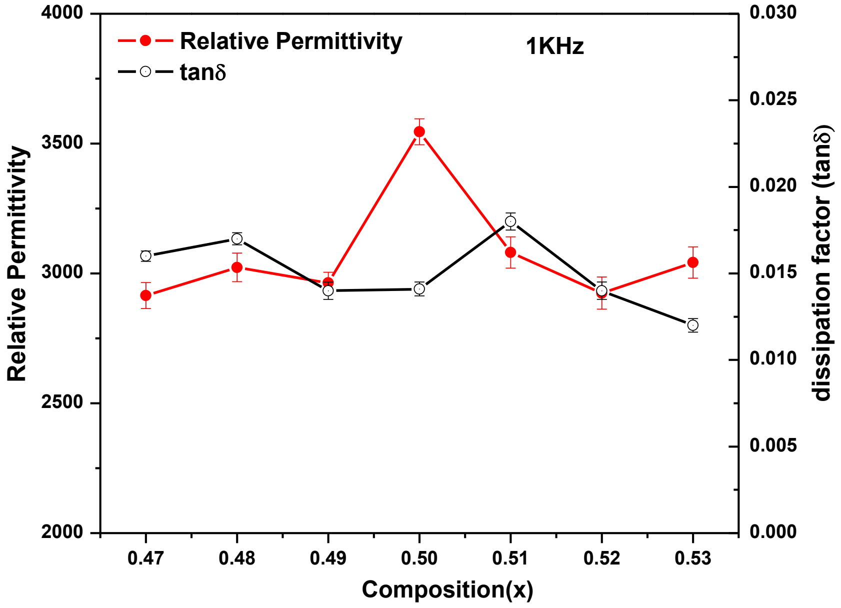

Fig.4.4.3 Room temperature relative permittivity and dissipation factor of xBZT-(1-x)BCT ceramic.

To study the phase transition behavior around the MPB composition, the temperature-dependent relative permittivity (ε_r-T) and dissipation factor (tanδ-T) at different frequency range (1kHz to 100kHz) were investigated [Fig 4.4.4(a)-(g)]. Inset of Fig.4.4.4 (a)-(g) shows the part of tanδ-T curves, respectively. It can be observed from ε_r-T, for all composition (x=0.47-0.53) two regions are prominent, one broad ε_{max} peak around 85^{o}C and a hump around 50^{o}C. However, for x = 0.47 and 0.48, the hump around 50^{o}C is not very clear. The ε_{max} peak denotes the ferroelectric to paraelectric transition (T_{T-C}) and the hump may be the summation of many peaks, denoting T_{R-O} and T_{O-T} or other transition. It is clear that the phase transition of tetragonal–cubic (T_{T-C}) is at around 85°C for x=0.5, which is in good agreement with literature [139,142]. It is to be noted that the temperature corresponding to ε_{max}, T_m decreases monotonously for x value from 0.47 to 0.53. The peak around 50^{o}C could be marked to T_{O-T}. In the case of $BaTiO_3$-based ceramics, the tanδ-T shows more sensitive character than ε_r-T [143, 253, 254]. It can be observed from the tanδ-T plot

(Inset), for all compositions (x=0.47-0.53) one peak around 71°C and two or more peaks available from room temperature to 60°C range. The peak around 71°C corresponds to ferroelectric to paraelectric transition though it is 10-15°C lower compared to ε_{max} peak depending on composition. Similar difference is reported by other researchers also [143]. For x = 0.47, one peak at 34°C and two small peak are observed at 51 and 59°C. For x = 0.48, the first peak shifts below 27°C and other two peaks at 48°C and 57°C. For x = 0.49 and x = 0.50, the first peak remains below 27°C and other two peaks at 41°C and 57°C. For x = 0.51, the first peak remains below 27°C and other peaks at 46°C and 56°C. For x = 0.52 and 0.53 peak near room temperature are not visible, probably shifts far below room temperature and other two peaks at 46°C and 56°C. The peak around 56°C (tanδ-T) could be correlated with the peak at 50°C of ε_r-T corresponds to T_{O-T}. The other peaks in tanδ-T plot, below 50°C could be due to T_{R-O} and some other unknown ferroelectric phase transition.

As described above, the BZT-BCT ceramics underwent complicated phase evolution driven by temperature and composition. These results indicate that the presence of an intermediate phase or multiple ferroelectric phases (difficult to be detected by XRD patterns) strongly depends on the temperature and ceramic composition. This unknown ferroelectric phase existing between R and T phases at very narrow region has also been mentioned in a recent article reported by Damjanovic et al. and Tian et al. supporting our findings [143,146].

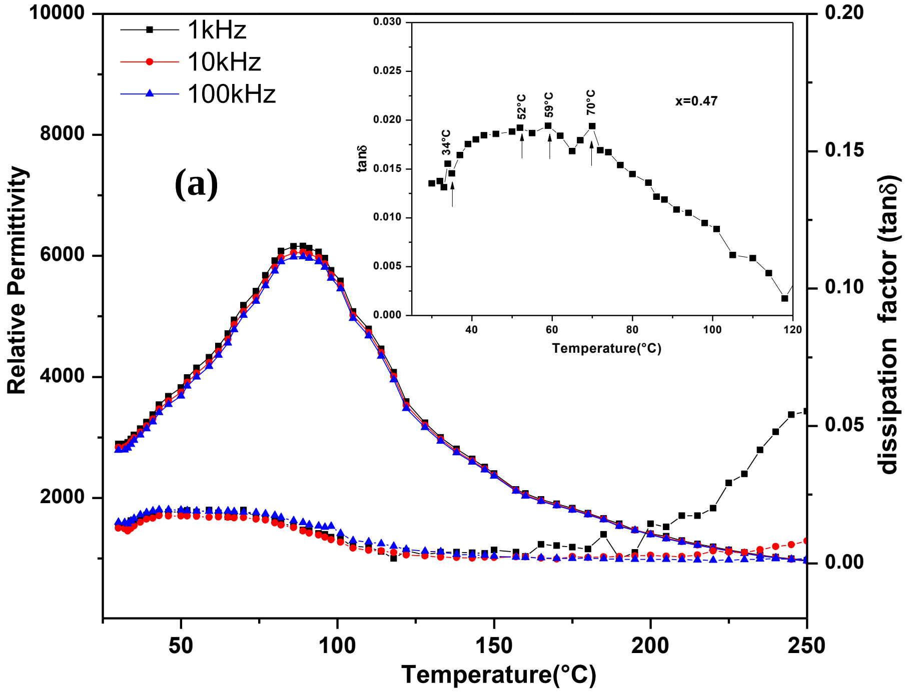

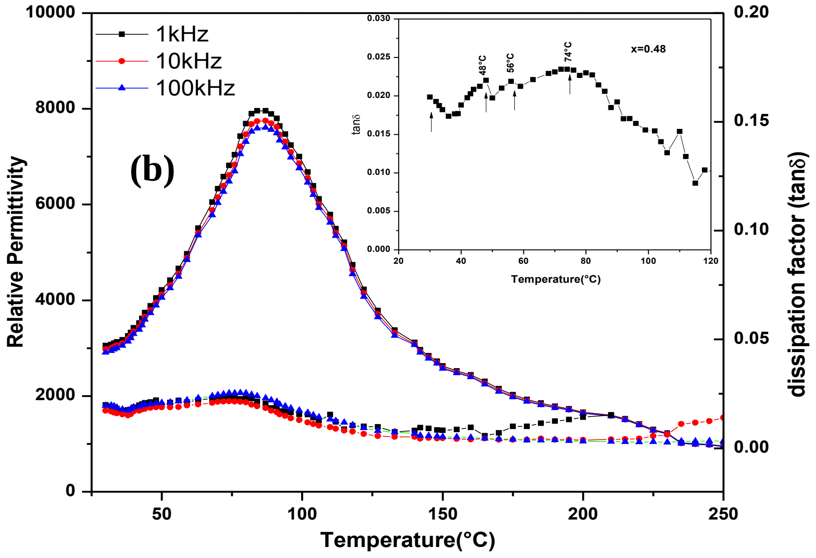
(b)
1kHz
10kHz
100kHz
Relative Permittivity
0
2000
4000
6000
8000
10000
dissipation factor (tanδ)
0.00
0.05
0.10
0.15
0.20
Temperature(°C)
50
100
150
200
250
x=0.48
tanδ
0.000
0.005
0.010
0.015
0.020
0.025
0.030
48°C
56°C
74°C
Temperature(°C)
20
40
60
80
100
120

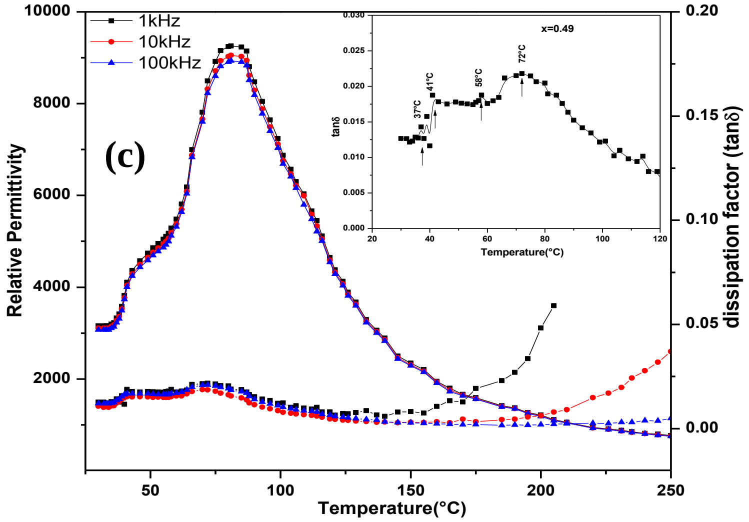
(c)
1kHz
10kHz
100kHz
Relative Permittivity
2000
4000
6000
8000
10000
dissipation factor (tanδ)
0.00
0.05
0.10
0.15
0.20
Temperature(°C)
50
100
150
200
250
x=0.49
tanδ
0.000
0.005
0.010
0.015
0.020
0.025
0.030
37°C
41°C
58°C
72°C
Temperature(°C)
20
40
60
80
100
120

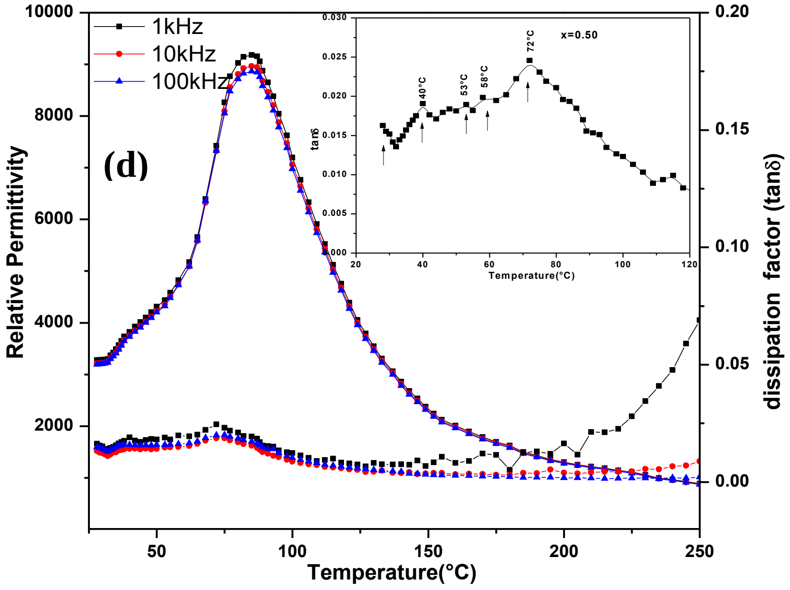
(d)
1kHz
10kHz
100kHz
Relative Permittivity
2000
4000
6000
8000
10000
dissipation factor (tanδ)
0.00
0.05
0.10
0.15
0.20
Temperature(°C)
50
100
150
200
250
x=0.50
tanδ
0.000
0.005
0.010
0.015
0.020
0.025
0.030
40°C
53°C
58°C
72°C
Temperature(°C)
20
40
60
80
100
120

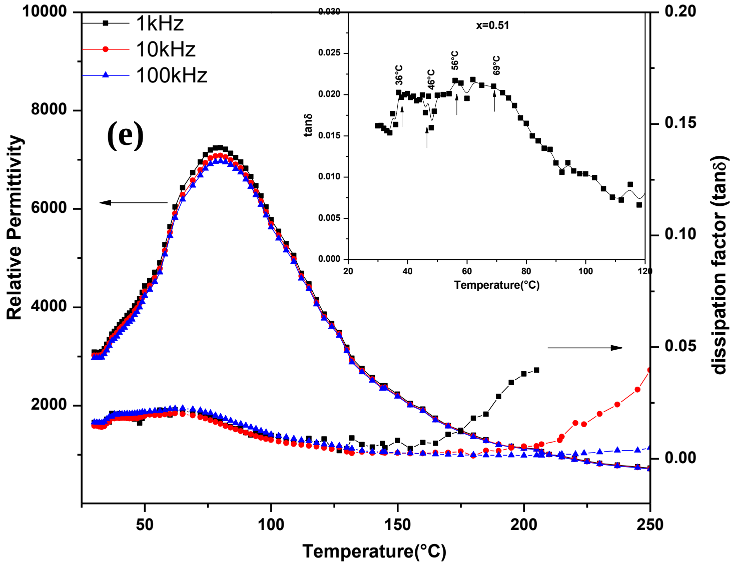
(e)
1kHz
10kHz
100kHz
Relative Permittivity
dissipation factor (tanδ)
Temperature(°C)
10000
8000
6000
4000
2000
0.20
0.15
0.10
0.05
0.00
50
100
150
200
250
x=0.51
tanδ
36°C
46°C
56°C
69°C
0.030
0.025
0.020
0.015
0.010
0.005
0.000
20
40
60
80
100
120
Temperature(°C)

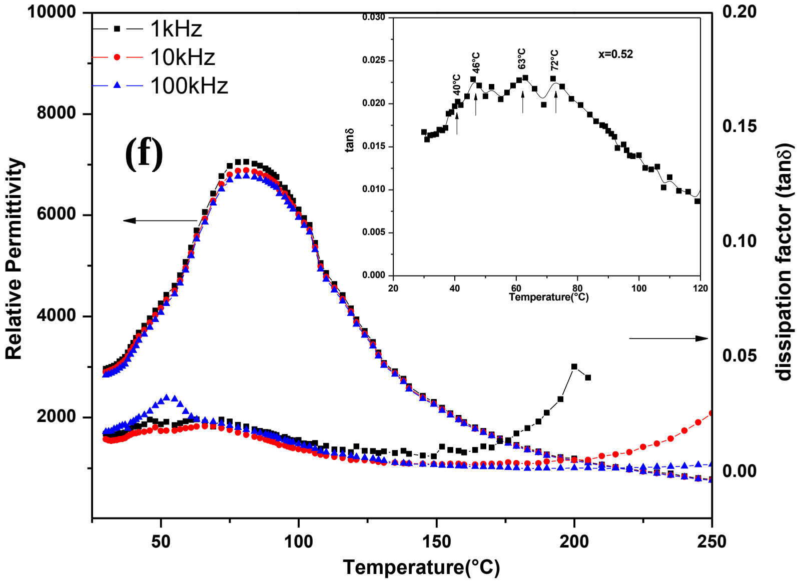
(f)
1kHz
10kHz
100kHz
Relative Permittivity
dissipation factor (tanδ)
Temperature(°C)
10000
8000
6000
4000
2000
0.20
0.15
0.10
0.05
0.00
50
100
150
200
250
x=0.52
tanδ
40°C
46°C
63°C
72°C
0.030
0.025
0.020
0.015
0.010
0.005
0.000
20
40
60
80
100
120
Temperature(°C)

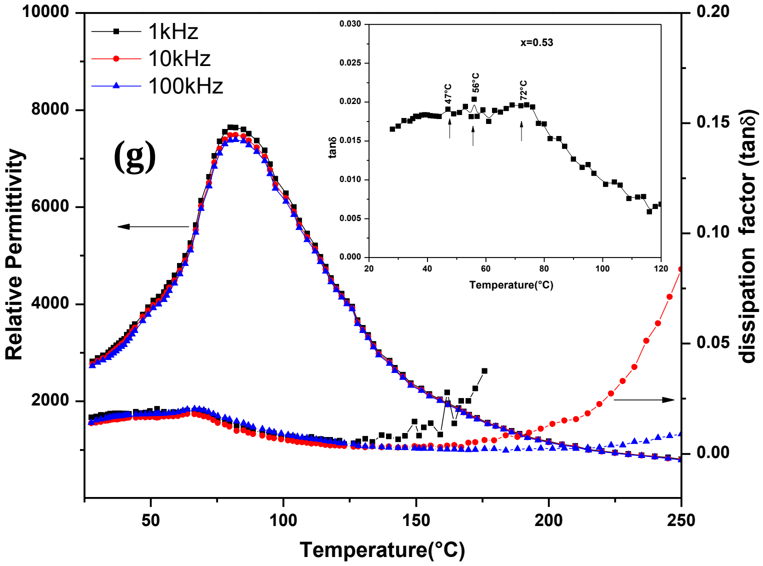
(g)
1kHz
10kHz
100kHz
Relative Permittivity
dissipation factor (tanδ)
Temperature(°C)
10000
8000
6000
4000
2000
0.20
0.15
0.10
0.05
0.00
50
100
150
200
250
x=0.53
tanδ
47°C
56°C
72°C
0.030
0.025
0.020
0.015
0.010
0.005
0.000
20
40
60
80
100
120
Temperature(°C)

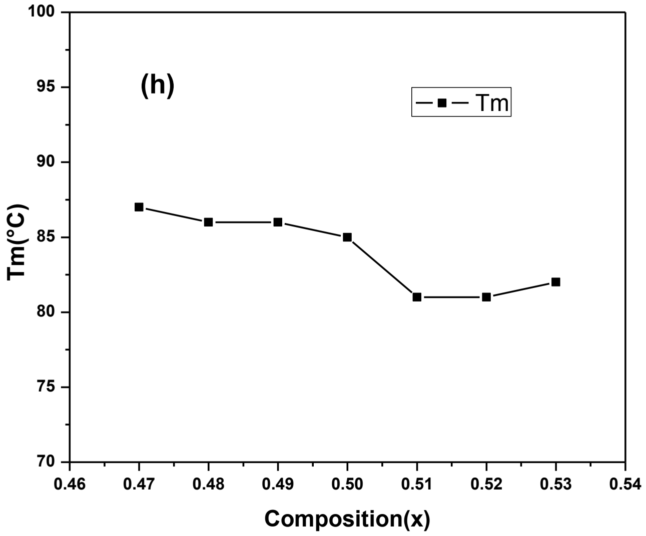

Figure 4.4.4 Temperature dependent relative permittivity (ε) and dissipation factor of xBZT- BCT ceramics at different frequency (a) x= 0.47, (b) x=0.48, (c) x= 0.49, (d) x=0.50, (e) x=0.51, (f) x=0.52 and (g) x=0.53.The inset of (a-g) shows the part of tanδ-T curves (h) T_m of xBZT-BCT ceramics.

4.4.2.3 Ferroelectric and Piezoelectric properties

Fig.4.4.5 shows the P–E hysteresis loops of xBZT-BCT ceramics. It can be observed that all ceramics are typically soft, with a very low coercive field E_c and a relatively high remnant polarization P_r. These results are in good agreement with reported result[138].The remnant polarization decreases marginally when composition other than x=0.5.

Fig.4.4.6 shows the piezoelectric coefficient (d_{33}) of xBZT-(1-x) BCT ceramics. The piezoelectric coefficient increases with the increase in BZT content and after peaking at 0.5 BZT content decreases sharply. It can be observed that high piezoelectric property (d_{33}~350pC/N) was obtained for the composition x=0.50.These values are quite consistent with the earlier results [218], and greater than that reported by Li et al. [83]. The large piezoelectric response is believed to be due to the presence of mixed multiple ferroelectric phases which driving easier polarization rotation near the Morphotropic phase boundary line [255].

The different physical properties of x BZT-(1-x) BCT are summarized in Table 4.4.2.

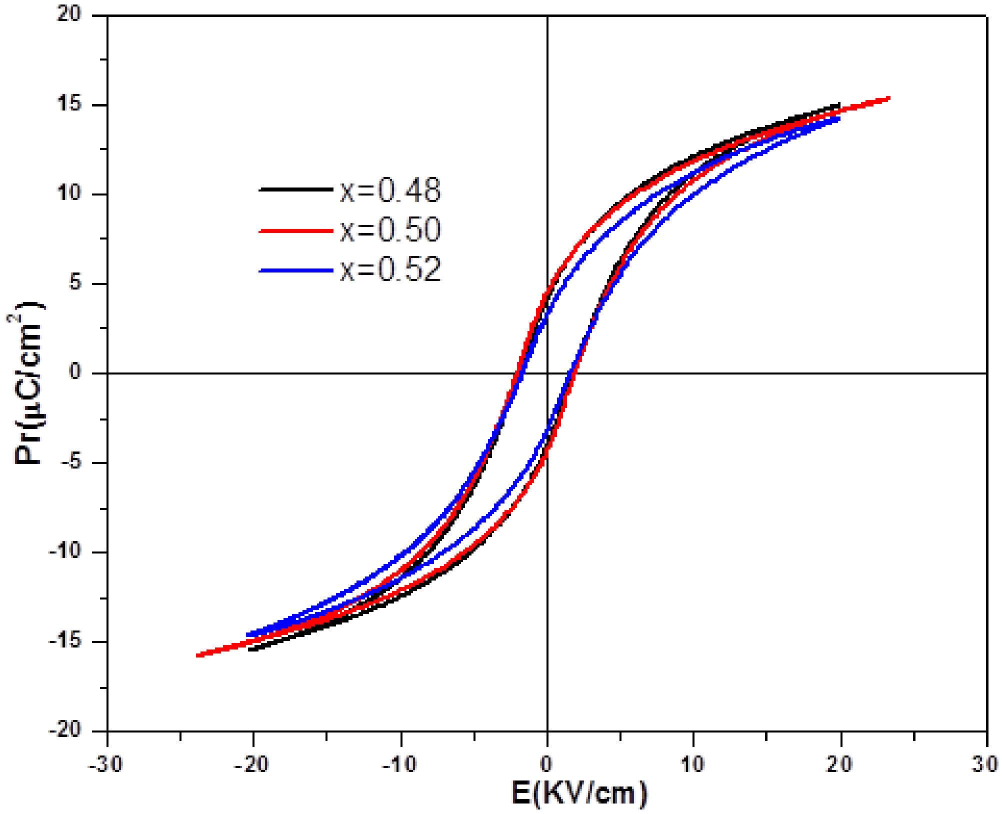

Figure 4.4.5.P–E hysteresis loops of xBZT-BCT ceramic at room temperature

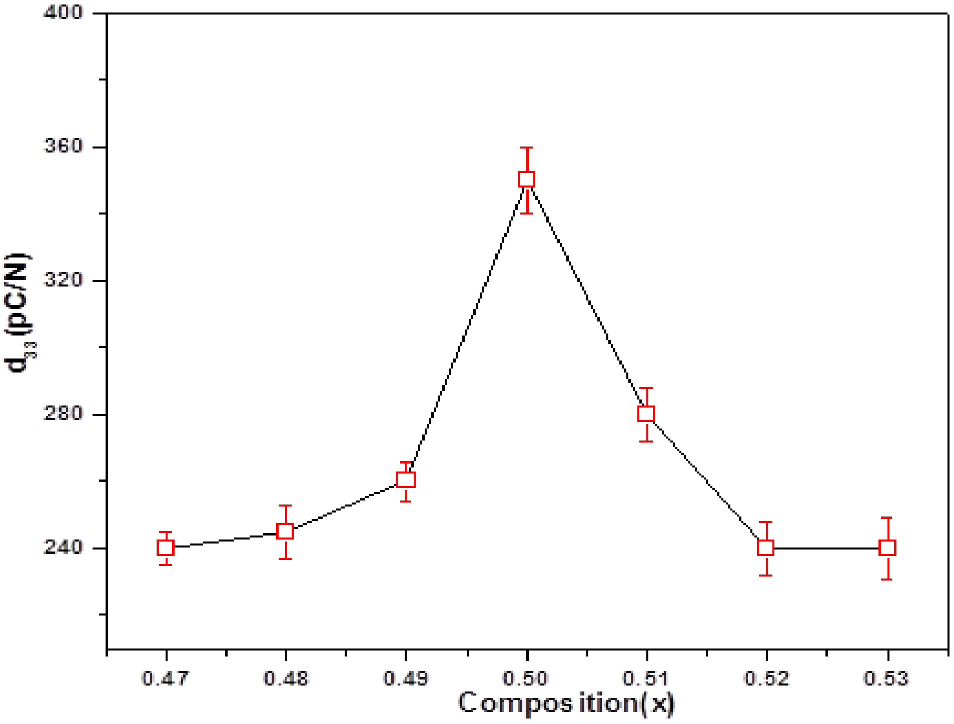

Figure 4.4.6 Piezoelectric coefficient (d_{33}) of xBZT-BCT ceramics

Table 4.4.2 Summary of the different physical properties of xBZT-(1-x) BCT ceramics.

Composition	ε at RT	tanδ at RT	T_m(°C)	$\varepsilon_m$at Tm	d_{33}(pC/N)
x=0.47	2915	0.016	87	6305	240
x=0.48	3023	0.017	86	8246	245
x=0.49	2964	0.014	86	9556	268
x=0.50	3545	0.014	85	9483	350
x=0.51	3081	0.018	81	7449	280
x=0.52	2924	0.014	81	7306	240
x=0.53	3042	0.012	82	7862	240

4.4.3 Conclusions

In summary, xBZT-(1-x)BCT ceramics with x varying from 0.47 to 0.53 are prepared by the planetary milling technique. It is found that the ceramics underwent a complicated phase evolution, driven by Ca and Zr contents. The results showed that the MPB of BZT-0.5BCT ceramics is closely related to the occurrence of multiple phases in narrow regions around orthorhombic and tetragonal phases, could be controlled by the content of Ca and Zr in the composition, as well as the temperature. Therefore, the MPB exhibits strong temperature dependence. It is to be mentioned that the XRD analysis and the Raman spectroscopy unable to explain precisely about the intermediate phases. Temperature dependence of dissipation factor indicated that the multiple phases might be unstable and served as structural bridge in MPB regions and played an important role in the large d_{33}(= 350 pC/N) and ε_r(=3535) near the MPB at room temperature.

Chapter-4.5

Low temperature sintering of BZT-0.5BCT ceramics using $LiBiO_2$ as a sintering aid

4.5.1 Introduction

The sintering of BZT-0.5BCT powder by conventional firing requires a relatively high temperature (1400^{o}C-1500^{o}C). In previous section preparation of highly sinterable BZT-0.5BCT powder was discussed and powder could be sintered to 98% of the theoretical density at 1350^{o}C. The lowering of sintering temperature will benefit the devices most, multilayer ceramic capacitor (MLCC) and multilayer layer actuator where co-firing of the metal electrode and ceramic is required. There are very few reports available on low temperature sintering of BZT-0.5BCT using dopants, but sintering temperature could not be lowered below 1300^{o}C [155-159]. It is difficult to co-fire BZT-0.5BCT and conductor inter-electrodes due to high sintering temperature. Few reports are available on the low temperature sintering of $BaTiO_3$ using lithium or bismuth as dopant. Chen et al. [256] investigated the effect of Bi on BZT-BCT ceramics reported the sintered temperature at 1450°C. Binhayeeniyi et al. [104] reported that 1.5% Li_2O in BZT(x=0.05) reduced the sintering temperature to 900°C and reported dielectric constant around 1250. Wu et al. [257] reported that the addition of small amounts of bismuth oxide in $BaTiO_3$ reduced the sintering temperature from 1300^{o}C to 1130^{o}C and reported dielectric constant of 2470 for 0.8mole% Bi_2O_3. Zadeh et al. [258] found that addition of the 2 wt.% LiF.$SrCO_3$ in $BaTiO_3$ could be achieved 98% of theoretical density sintered at 900°C, showed dielectric constant of 3160.Yang et al.[259] studied the effect of LiF into $BaTiO_3$ ceramic. They observed that the sintering temperature depends upon the lithium content in $BaTiO_3$ ceramics. The dielectric constant 2857 achieved at 4 mol% LiF addition into $BaTiO_3$ sintered at 1100°C.

There are no literatures available on low temperature sintering of BZT-0.5BCT ceramics. It is well known that $LiBiO_2$ or mixture of Li_2CO_3 and Bi_2O_3 is very effective for the densification of lead based ceramics (e.g. PZT, PMN-PT, PMN–PZT, PNN–PZT, PZT–SKN) by lowering the sintering temperature without degrading the dielectric properties [180,260]. Zhang et al. studied the low temperature sintering behavior of PZT–SKN piezoelectric ceramics with $LiBiO_2$ additives. He reported that the sintering temperature could be decreased by 300-350°C by addition of 6 wt. % $LiBiO_2$ or 1 wt%$LiBiO_2$ + 1 wt% CuO, due to the generation of liquid phase[261]. Mazumder et al. [180] reported low temperature densification of PZT using $LiBiO_2$ as the sintering aid. They have reported that 95% of the theoretical density could be achieved at 715^{o}C by adding 3 wt.% $LiBiO_2$. The sintered density was improved to 97% , of the theoretical density at 750^{o}C with 2 wt.%

of $LiBiO_2$addition. The dielectric and piezoelectric properties were better compared to the high temperature conventionally sintered PZT without LBO addition. To the best of our knowledge there are no report available on low temperature sintering of BZT-05BCT with $LiBiO_2$ additive.

The present work is focused on to study the densification behavior of BZT-0.5BCT in presence of Li_2CO_3 and Bi_2O_3 as a sintering aid which forms $LiBiO_2$ in-situ. Phase formation and dielectric properties of sintered specimen have been studied.

4.5.2 Results and discussion

4.5.2.1 Densification behavior

Fig. 4.5.1(a) and (b) shows the linear shrinkage [(dL/L_0)] and the corresponding shrinkage rate [$d(dL/L_0)/dt$] behavior of the pure BZT-0.5BCT and different concentration of LBO added sample. The pure BZT-0.5BCT ceramic starts to shrink at 1120°C and reaches end of its densification at around 1350°C with a linear shrinkage of 13.5%. Two-step shrinkage in BZT-0.5BCT may be attributed to the presence of agglomerates which starts densification at different temperatures [182]. It is observed that onset temperature for shrinkage decreases significantly for higher amount (3, 5, and 7 wt%) of LBO addition. However, lower concentration (1 wt%) of LBO addition was not effective sufficient as shrinkage starts at about 1011°C. The onset temperature for the 3, 5, and 7LBO sample was 698°C, 674, and 653^oC, respectively. It is also observed that densification completes around 1200^oC for LBO added samples and 13% shrinkage achieved at 1100^oC, is equivalent to the shrinkage that takes place for pure BZT-0.5BCT at 1350^oC. In case of higher concentration of LBO (5, 7%) addition two regions of shrinkage can be observed. Incidentally, LBO in BZT-0.5BCT forms a low melting liquid phase (melting point of LBO is 650^oC) that helps in the liquid phase sintering. In the liquid phase sintering, enhancement of densification results from enhanced rearrangement of the particles and matter transport through liquid phase [182]. In case of higher concentration of LBO (5, 7%) addition, the first shrinkage rate peak may be attributed to the rearrangement of the particles and the second shrinkage rate peak to the matter transport through liquid phase. Incidentally, for the lower amount of LBO addition, first peak is not prominent that may be due to the amount of liquid phase generated during melting is not sufficient for particle rearrangement. The results of dilatometer experiment are summarized in Table 4.5.1.

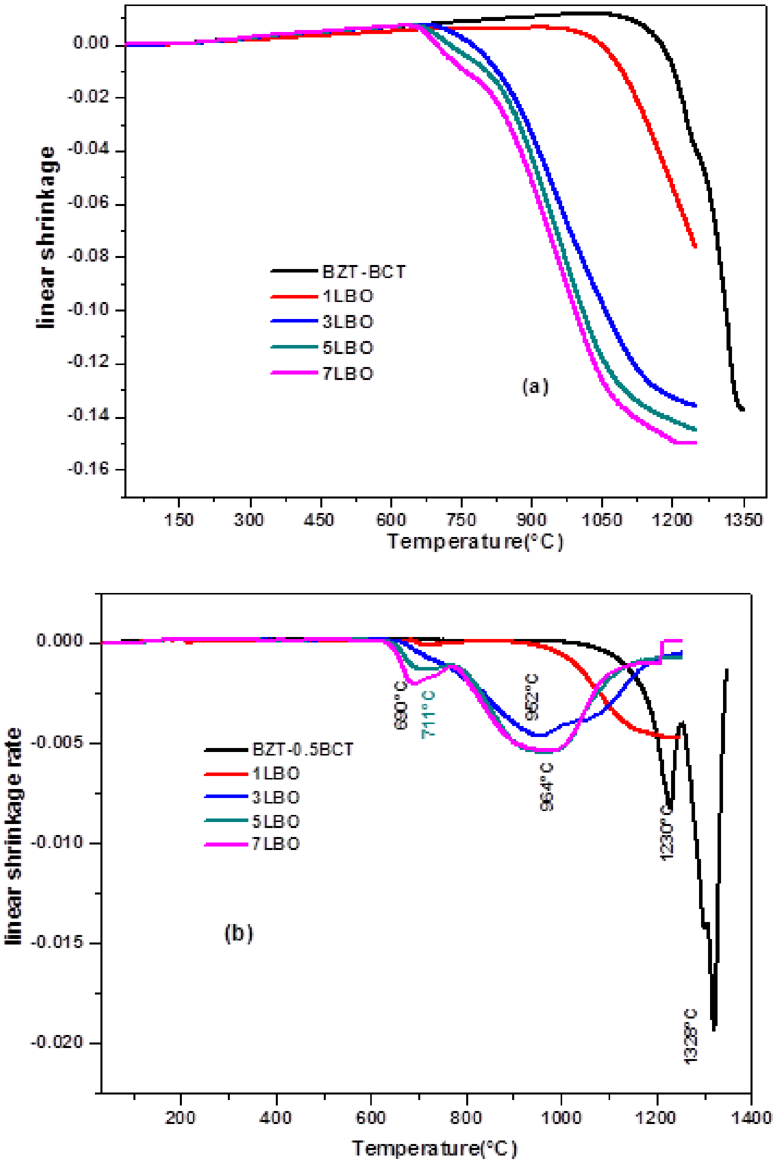

Fig.4.5.1(a)Linear shrinkage (b) Linear shrinkage rate as a function of temperature of LBO modified BZT-0.5BCT ceramics.

Fig. 4.5.2 depicts the effect of LBO addition on the sintered density of the pellets at two sintering temperatures, viz., 1100°C and 1200°C. From the figure, it is evident that the bulk density of the pellets [as a % of true density of BZT-0.5BCT (5.78 g/cm^3)] increased with an increasing amount of LBO addition up to 5wt% followed by a decrease with further addition of LBO. However, without LBO addition, the bulk density of BZT-0.5BCT after sintering at 1200^{o}C was only 72%.Incidentally, LBO in BZT-0.5BCT forms a low melting liquid phase (melting point of LBO is 650^{o}C) that helps in the liquid phase sintering. Above the optimum amount of LBO addition (~5wt%), the densification decreases because an excess liquid phase formed from a higher amount of LBO addition lowers the densification due to grain and pore growth [182, 262]. It may be mentioned here that, BZT-BCT samples without LBO addition can be sintered to 98% of the theoretical density (Fig.4.5.2a) only after firing at 1350°C and above.

Table 4.5.1: Results of dilatometer experiment: onset Temperature (T_0), Temperature of the maximum of the shrinkage rate ($T_s$max), Temperature at which densification stops (T_f) and width of temperature interval where shrinkage occurs ($\Delta Ts=T_f-T_0$)

Sample types	BZT-0.5BCT	1LBO	3LBO	5LBO	7LBO
Onset temperature T_0(°C)	1124	1011	698	674	653
Ts max	1230,1328	1150	952	711, 964	690, 964
T_f	1346		1220	1220	1208
T_f-T_0(°C)	222		522	546	555

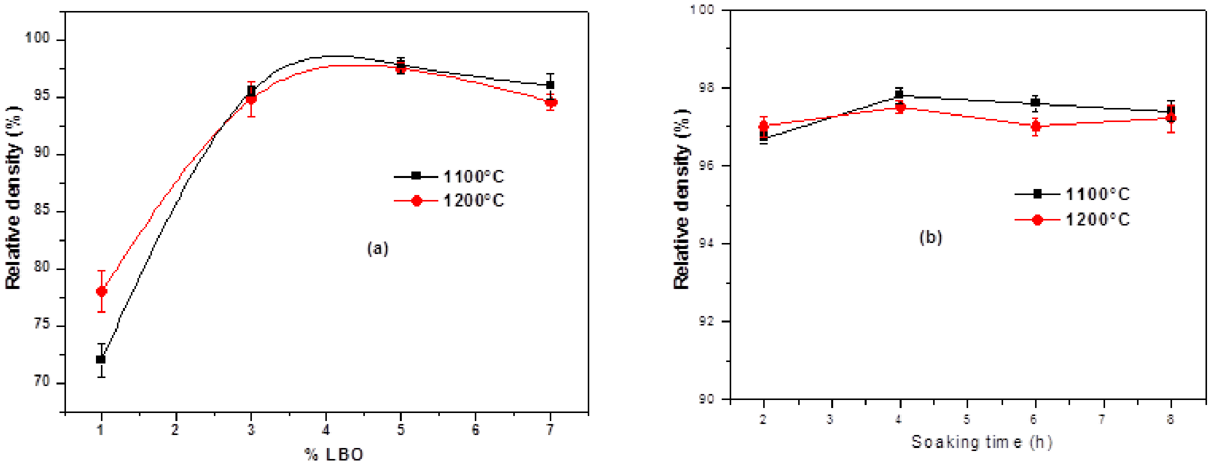

Figure 4.5.2 Relative density as function of (a) sintering temperature at 1100-1200°C for the LBO modified BZT-0.5BCT ceramics (b) soaking time from 2h to 8h at 1100-1200°C of 5LBO ceramic.

4.5.2.2 Phase evolution

Figure 4.5.3 shows the X-ray diffraction patterns of the BZT-0.5BCT and LBO modified BZT-0.5BCT ceramic sintered at 1100°C. The X-ray diffraction patterns revealed that all the obtained ceramics have a pure perovskite structure. These results suggest that Li^+ and Bi^{3+} have been incorporated into BZT-0.5BCT lattices and forms a homogeneous solid solution. Moreover, X-ray diffraction peak positions shift towards the lower diffraction angles with an increase in LBO content. This result suggests that the crystallographic structure changes from orthorhombic-tetragonal to pseudo-cubic with increasing LBO content [263,264]. The corresponding temperature dependence of dielectric constant also supports this result (Fig 4.5.6). It proves that LBO not only helps in the liquid phase sintering also modifies the structure by doping.

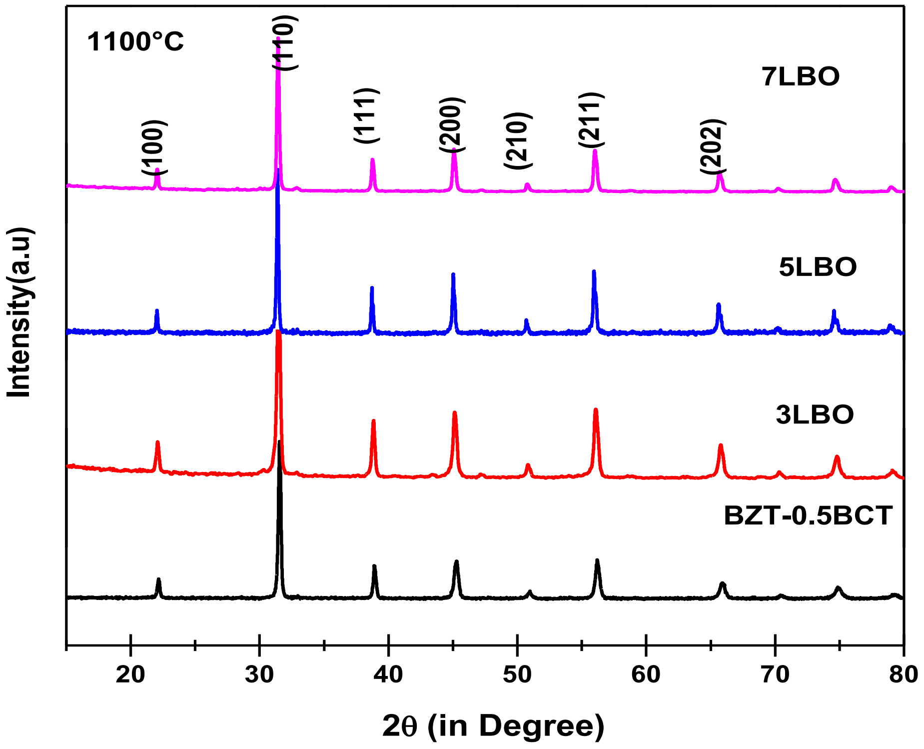

Fig.4.5.3 X -ray diffraction patterns of the LBO modified BZT-0.5BCT ceramics sintered at different temperature

4.5.2.3 Microstructure

Figure 4.5.4 shows the SEM micrographs of the fracture surfaces of the LBO modified BZT-0.5BCT ceramics sintered at 1100°C. Highly dense microstructure with the marginal increase in grain size is observed for increasing LBO addition. It is to mention that with the increase in LBO addition the fracture mode is changing to more intergranular in nature.

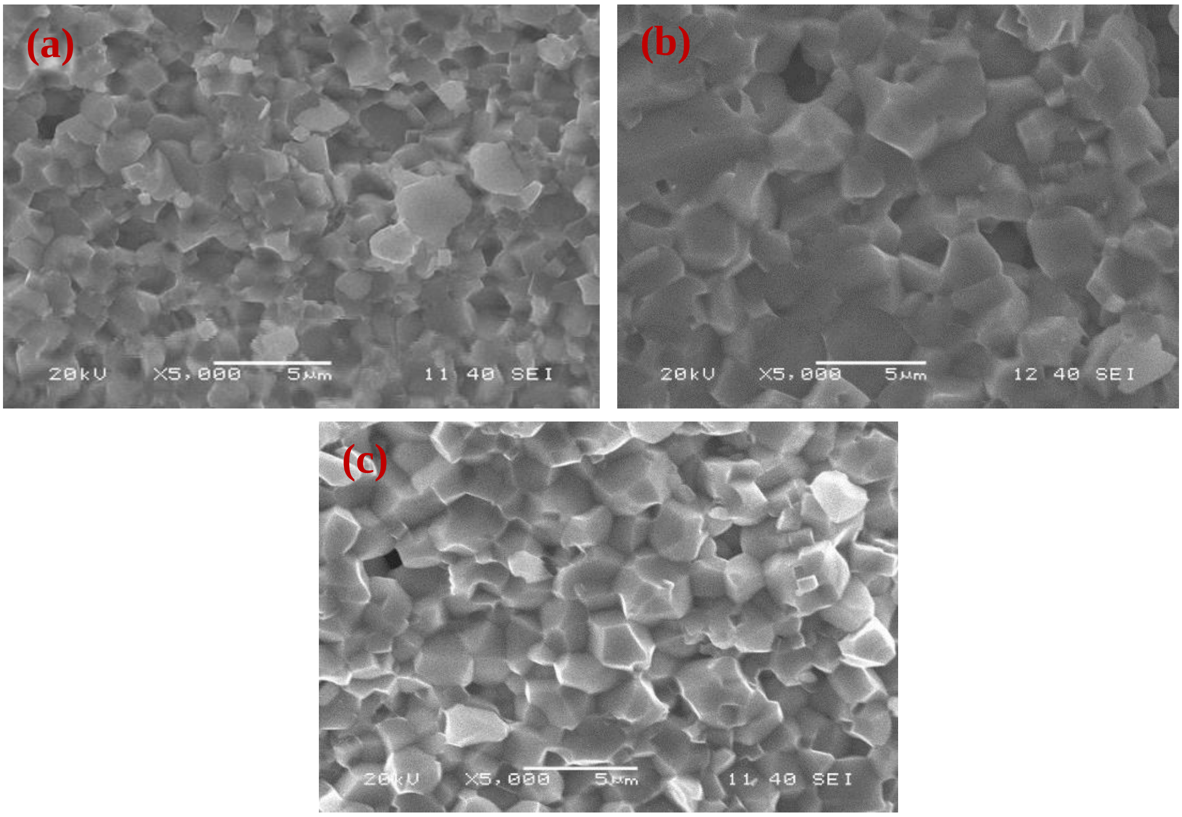

Figure 4.5.4 SEM micrograph of fracture surface of the LBO modified BZT-0.5BCT ceramics (a) 3LBO (b) 5LBO (c) 7LBO

4.5.2.4 Dielectric properties

Figure 4.5.5 (a) and (b) show the relative permittivity and dissipation factor versus frequency curves for LBO modified BZT-0.5BCT samples sintered under varying conditions. The relative permittivity (ε_r) increases with the increase in LBO addition (from 3 to 5 wt%) and then decreases with the further addition. Higher permittivity in 5LBO sample may be attributed to the higher density of the ceramics compared to other LBO added samples, since; in general, porosity lowers the permittivity. The decrease in permittivity for larger LBO addition may be understood by considering the formation of nonferroelectric low-ε LBO rich grain boundaries. Wang et al. showed by XPS analysis that some LBO remains at the grain boundaries of the sintered PZT ceramics [265]. Besides, some amount of lithium and bismuth doping in BZT-0.5BCT due to LBO addition is possible, as Bi^{3+} can also replace Ba^{2+}(donor doping)[258]. Also owing to its small ionic radius, Li^{+} can stay in the interstices [263].

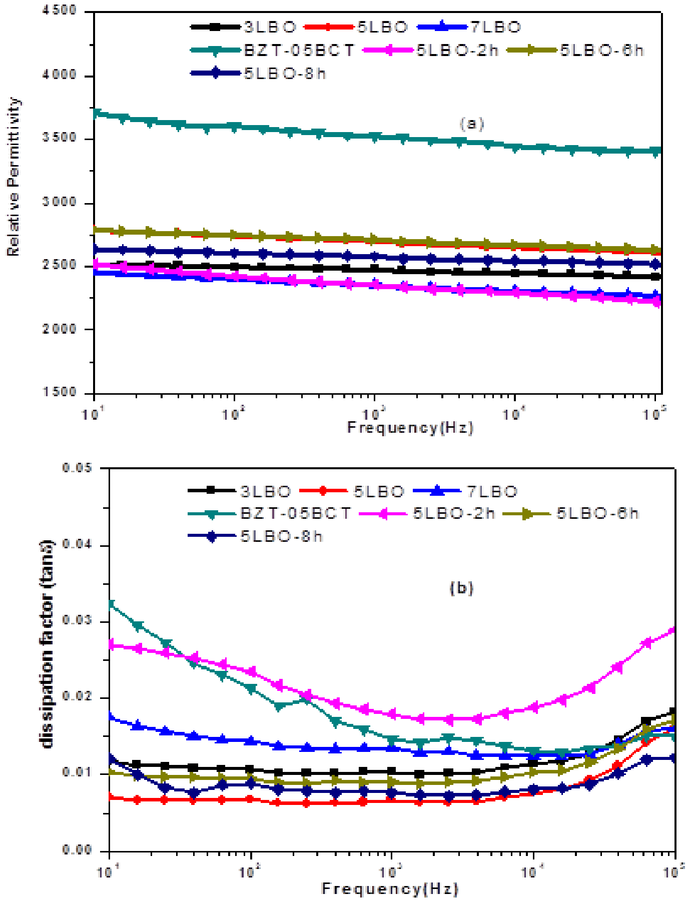

Figure 4.5.5(a) Relative permittivity and (b) dissipation factor versus frequency for LBO modified BZT-0.5BCT samples sintered under varying conditions

In the present case, some LBO incorporation into the BZT-BCT structure is confirmed by the X-ray diffraction peak position shifting and the loss of the tetragonality (Fig.4.5.3). Also the shifting of T_c with LBO addition (Fig. 4.5.6) justifies our former assertion. Chen et al.[256] reported similar lowering of T_c with doping of Bi in BZT-BCT and Yang et al. [259] also reported lowering of T_c with LiF doping in $BaTiO_3$. Fig 4.5.5(b) shows that LBO addition up to 5 wt% lowers the dissipation factor. However, with further LBO addition the dissipation factor increases marginally. Tao et al. reported p-type conduction in BZT-0.5BCT [266]. LBO addition promotes Bi^{3+} doping in A-site and that promotes n-type activity and counteracts p-type conductivity of BZT-BCT and results the decreases in dissipation factor. Again the increase in LBO content may promote a more n-type conductivity and the dissipation factor increases. However, in the present case, further studies are required to understand the doping process in detail for different concentrations of LBO addition. The dielectric property of BZT-0.5BCT (0% LBO) and BZT-0.5BCT (1% LBO) sintered at 1100°C could not be compared in this case because of poor density (<80%) of the samples. The dielectric properties of the LBO modified samples are also compared with BZT-0.5BCT sintered at 1350°C/4h. The ε_r of the BZT-0.5BCT ceramic at the room temperature shows the maximum value (3535) sintered at 1350°C. Fig 4.5.5 (b) shows the relative permittivity and loss factor for 5LBO ceramic as function of soaking time from 2h to 8h. This result shows that the relative permittivity slightly increases with increasing the soaking time from 2h to 4h after that decreases and loss factor decreases with increasing soaking time and then marginally increases. Moreover, this result shows that the sintering temperature and the soaking time strongly affects the dielectric property of the ceramics. It is also exident from the figure that the temperature stability of permittivity of the LBO added sample is better than the pure BZT-0.5BCT sintered at 1350^{o}C.

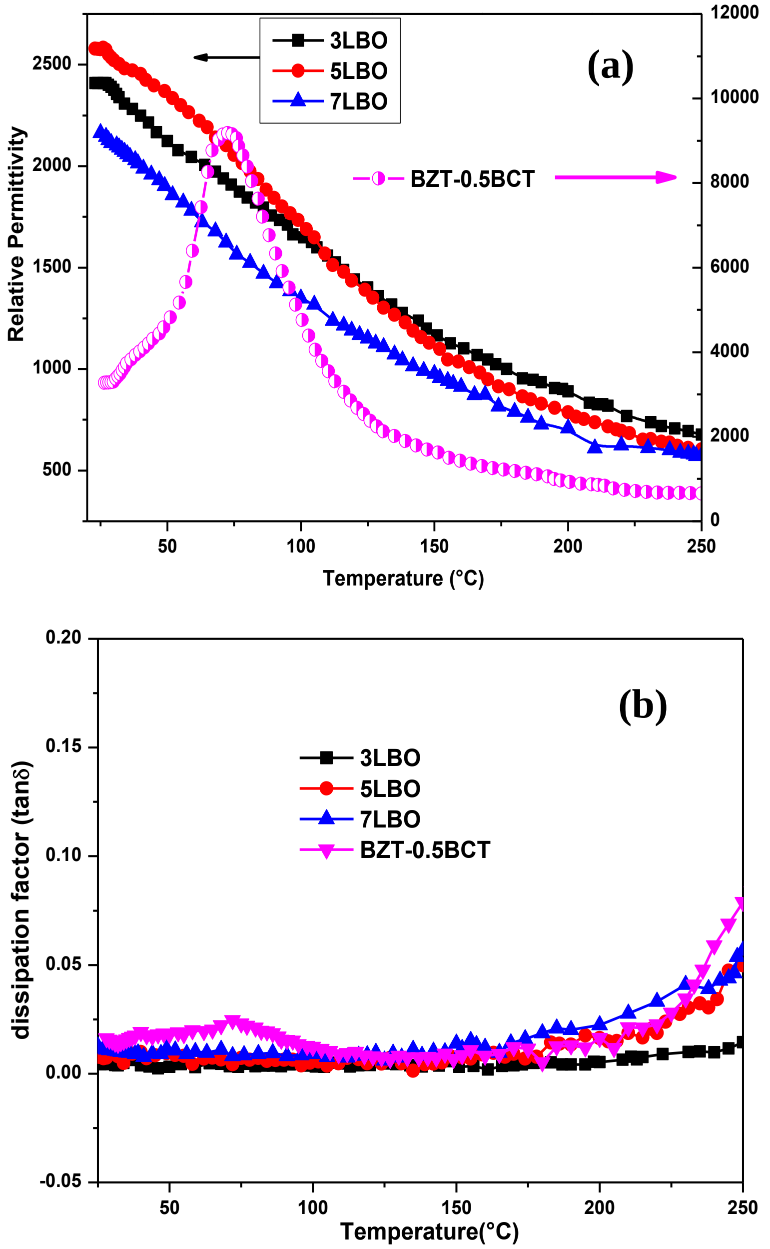

Figure 4.5.6 (a)) relative permittivity and (b) dissipation factor versus temperature dependence curves for LBO modified BZT-0.5BCT samples.

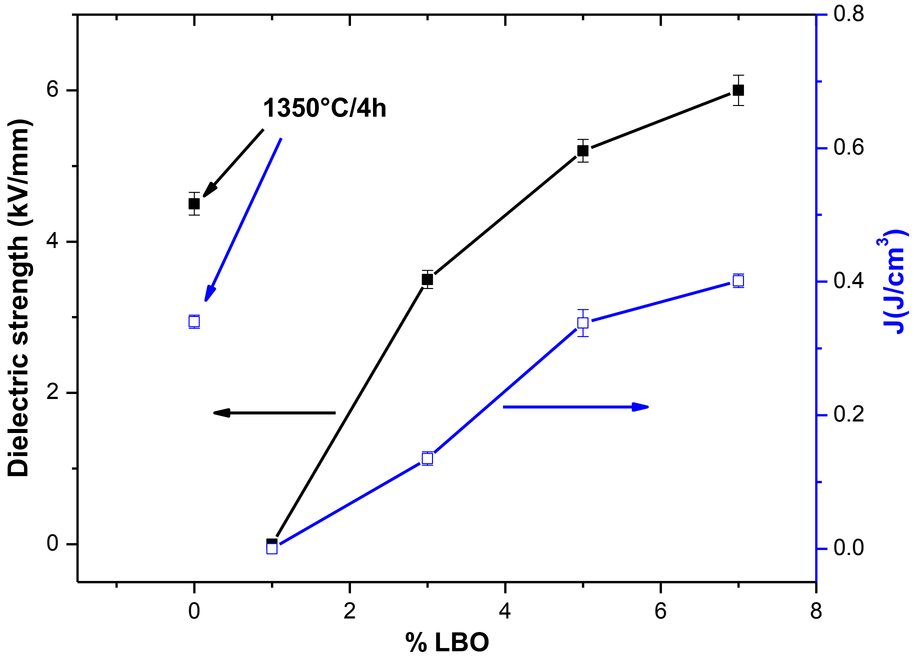

Figure 4.5.7 Dielectric breakdown strength and energy density of different concentration of LBO content in BZT-0.5BCT ceramics

Fig.4.5.7 shows the dielectric breakdown strength and energy density for different concentration of LBO content in BZT-0.5BCT ceramics at room temperature. The energy storage density were calculated using following formula J= $1/2(\varepsilon_0\varepsilon_r E_b^2)$[153].where E_b is the electric field in dielectric and ε_r is the relative permittivity. The energy storage density is related to relative permittivity and dielectric breakdown voltage, and it is necessary that electric breakdown voltage should be as high as possible. Generally, high dielectric constant materials such as ferroelectric oxides are limited by their relatively smaller breakdown strength [267].It can be observed that room temperature dielectric breakdown strength and energy storage density increases with increases in LBO content compared to pure BZT-0.5BCT ceramic which have the dielectric breakdown strength of 4.5kV/mm. Energy storage densities (J) for samples with x = 0, 0.01, 0.03, 0.05 and 0.07 are 0.34, 0, 0.135, 0.338,.401 respectively. It is to be noted that 5LBO sample sintered at 1100^{o}C has higher dielectric strength and comparable energy density with BZT-0.5BCT sintered at 1350^{o}C.
The different physical properties of LBO modified BZT-0.5BCT are summarized in Table 4.5.1.

Table 4.5.1 Summary of the different physical properties of LBO modified BZT-0.5BCT ceramics

Composition	**Sintering temperature(°C)**	**Density (gm/cc)**	**Dielectric Constant (1kHz)**	**Loss factor (1kHz)**	**Dielectric strength (kV/mm)**	**Energy density(J/cm^3)**
BZT-0.5BCT	1350	98	3535	0.016	4.5	0.34
3LBO	1100	95.5	2474	0.0067	3.5	0.135
5LBO	1100	97.8	2700	0.010	5.03	0.338
7LBO	1100	96	2355	0.013	7.0	0.401

4.5.4 Conclusions

BZT-0.5BCT is successfully sintered at 1100°C with the addition of a mixture of Li_2CO_3 and Bi_2O_3 as a sintering aid which form $LiBiO_2$ in-situ. 98% of theoretical density was achieved for 5 wt. % of LBO addition. It is interesting to note that relative permittivity values are not deteriorated much with this addition. The LBO addition shifts the relative permittivity peak maxima towards room temperature which is due to the Li+ and Bi^{3+} ion incorporation into the perovskite structure. The temperature stability of permittivity of the LBO added sample is better than the pure BZT-0.5BCT sintered at 1350°C. It is to be noted that 5LBO sample sintered at 1100°C has higher dielectric strength and comparable energy density with BZT-0.5BCT sintered at 1350°C.The sintering aid (LBO) in BZT-0.5BCT ceramics is suitable for Y5V based MLCC multilayer ceramic capacitor application.

Chapter-4.6

Dielectric and Piezoelectric Properties of (1-x) [$(Bi_{0.5}Na_{0.5})$ TiO_3]-x[$Ba(Zr_{0.2}Ti_{0.8})O_3$-$(Ba_{0.7}Ca_{0.3})TiO_3$] Ceramics

4.6.1 Introduction

In the earlier section, BZT-0.5BCT has been prepared by different methods and found planetary milling is better to get good dielectric and piezoelectric property. BZT-0.5BCT is a very promising leadfree piezoelectric, prospective to replace the lead based piezoelectrics. However, it has low Curie temperature (93°C), which may limit its practical application. Formation of solid solution with other high T_C leadfree ferroelectric may solve this problem. Also, BZT-0.5BCT could be used to improve the dielectric and piezoelectric property of other lead free piezoelectrics by forming the solid solution.

Bismuth sodium titanate, $(Bi_{0.5}\ Na_{0.5})TiO_3$ (BNT), discovered by Smolenskii et al. in 1960, considered to be a promising candidate for lead free piezoelectric materials [74]. It is reported in the literature that BNT shows strong room temperature ferroelectricity with a relative large remnant polarization (P_r = 38 μC/cm^2) and relative high Curie temperature (320°C) in single crystal. However, its high coercive field (E_c=73 kV/cm) and relatively large conductivity in ceramic form make pure BNT hard to be poled and its piezoelectric properties are not encouraging [74, 75]. Various attempts have been made to improve the piezoelectric properties of BNT-based lead-free piezoelectric ceramics by making solid solution with other perovskite based piezoelectric/ ferroelectric compound like $BaTiO_3$, $(Bi_{0.5}K_{0.5})TiO_3$, $NaNbO_3$, $BiFeO_3$ and $Ba(Cu_{0.5}W_{0.5})O_3$ to form solid solution which are easier for poling [74,75,268]. Liu and Ren [48] have reported that Pb-free BZT-0.5BCT solid solution exhibits high piezoelectric coefficient (d_{33}~300-600pC/N) near the tricritical point at room temperature which is superior to PZT based system. But, it has low Curie temperature (93°C), which may limit its practical application. Lee et al.[269] investigated crystal structure and ferroelectric properties of (1-x) BNT- x [$Ba(Zr_{0.05}Ti_{0.95})O_3$ (BZT)] ceramics. They have reported that the composition 0.94BNT-0.06BZT exhibits the maximum relative dielectric permittivity (ε_r~1283), loss (tanδ~0.043) and piezoelectric constant (d_{33}~136pC/N) at room temperature. Qiao et al.[270] reported the (1-x) $Bi_{0.51}(Na_{0.82}K_{0.18})_{0.50}TiO_3$- x (BZT-0.5BCT) ceramics, with x=0.02 exhibits good piezoelectric properties, d_{33}~205pC/N, at sintering temperature of 1180°C. Gou et al. [271] prepared the composition of (1 − x) BNT–x (BZT-0.5BCZ) ceramic by solid state mixing method, where x = 0.06 composition exhibit the highest piezoelectric constant d_{33} ~ 158 pC/N and k_p ~ 31.2%. It required calcination (850°C) and sintering (1150°C) at high temperature.

In this Chapter, first (1-x) [BZT-0.5BCT]- x [BNT] (x=0.01 and 0.05) has been prepared to check the phase compatibility and densification. In later stage lead-free [(1-x) BNT]- x[BZT-0.5BCT] (where x=0, 0.03,0.05,0.07) ceramics has also been prepared by planetary milling. The effect of BZT-0.5BCT content on the phase formation, microstructure, dielectric, ferroelectric and piezoelectric properties of BNT have been studied systematically.

4.6.2. Results and Discussions

4.6.2.1 Phase formation and sintering of (1-x) [BZT-0.5BCT]- x [BNT] Ceramic

The Lead free 0.95(BZT-0.5BCT)-0.05NBT ceramics was prepared by planetary milling. The pellets were sintered at different temperatures (1100°C, 1200°C and 1250°C for 4h) in the air.

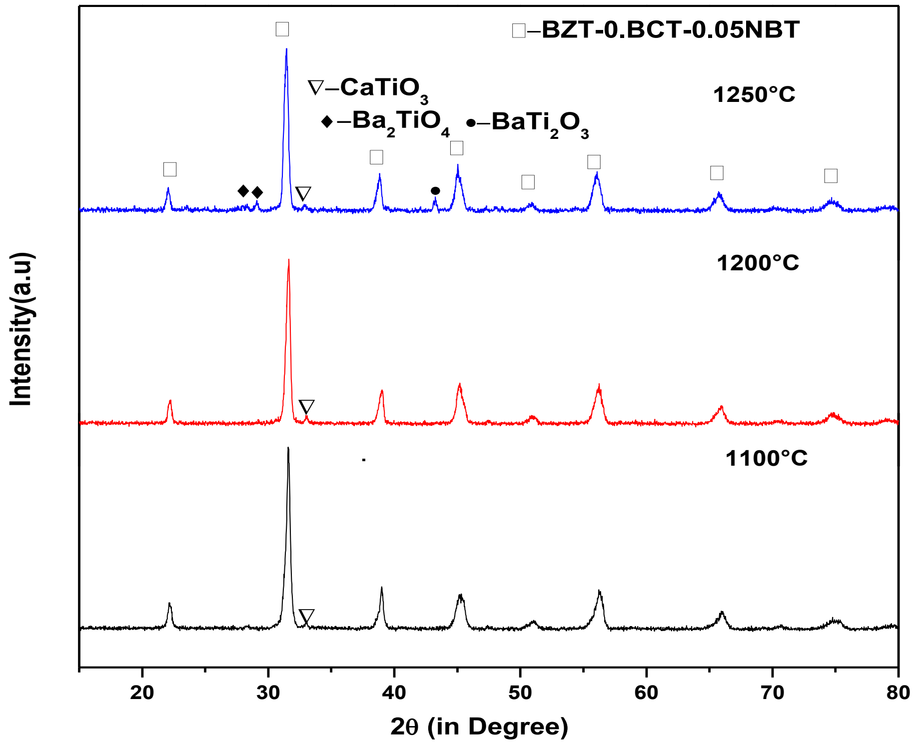

Fig 4.6.1 X-ray diffraction patterns of the 0.95(BZT-0.5BCT)-0.05NBT ceramic sintered at different temperatures.

The X-ray diffraction patterns of the 0.95(BZT-0.5BCT)-0.05NBT ceramics sintered at different temperatures are shown in figure 4.6.1. It is observed that the perovskite phase is formed along with the impurity phases of $CaTiO_3$ (JCPDS no. 09-0365) after sintering at 1100°C. As the sintering temperature increased to 1250°C, the impurity peaks of Ba_2TiO_4 (JCPDS no. 38-1481), $BaTi_2O_5$

(JCPDS no. 08-0368) and $CaTiO_3$ phase is found to be present. These results suggest that NBT may have solubility in BZT-0.5BCT, however, incorporation NBT, expelled the Ba^{2+}, Ca^{2+} from A-site generating the impurity phases. The NBT modified BZT-0.5BCT ceramics could not be sintered more than 82% of relative density (4.72gm/cc) after sintering at different temperatures (1100-1250°C for 4h). The lower density could be attributed to the higher sintering temperature of BZT-BCT (> 1250°C). The electrical properties could not be measured due to the poor density of sintered sample. These results suggest that the solid solution of (BZT-0.5BCT)- NBT is not very promising.

4.6.2.2 Synthesis and Characterization of [(1-x) BNT]- x[BZT-0.5BCT] Ceramic

4.6.2.2.1 Phase evolution

Fig.4.6.2 (a) shows the XRD patterns of (1-x) BNT- x(BZT-0.5BCT) (x=0, 0.03, 0.05, 0.07) powder calcined at 700°C. It can be observed that all compositions have pure perovskite structure. Absence of any secondary phases or impurity phase was detected in all these ceramics, suggesting that the Ba/Ca and Zr/Ti diffuses into the BNT lattice side, and forms a homogeneous solid solution. The expanded XRD patterns of these ceramics with different BZT-0.5BCT contents are shown in Fig.4.6.1(b). It can be observed that peak positions are shifted towards the lower diffraction angle with an increasing BZT-0.5BCT content, it indicates that an increase in unit cell volume. This may be due to the higher ionic radius of Ba^{2+} (~1.61Å) as compared to Na^{+}(~1.39 Å) and Bi^{3+}(~1.39 Å). Zr^{4+}(~0.72Å) also have higher ionic radius compared to Ti^{4+}(~0.605Å)[264]. The lattice parameters and unit cell volume of the BNT increase with the increase in BZT-0.5BCT content. It is known that BNT has rhombohedral crystal structure (space group: R3c). It is clear from the fig 1(b) that the $(204)_R$ peak of pure BNT undergoes an asymmetric broadening and finally splits into two peak $(002)_T$ and $(200)_T$ with increase in BZT-0.5BCT content. So, the addition of BZT-0.5BCT is converting the rhombohedral phase to tetragonal phase. The asymmetric broadening starts from 3 mol% BZT-0.5BCT addition.

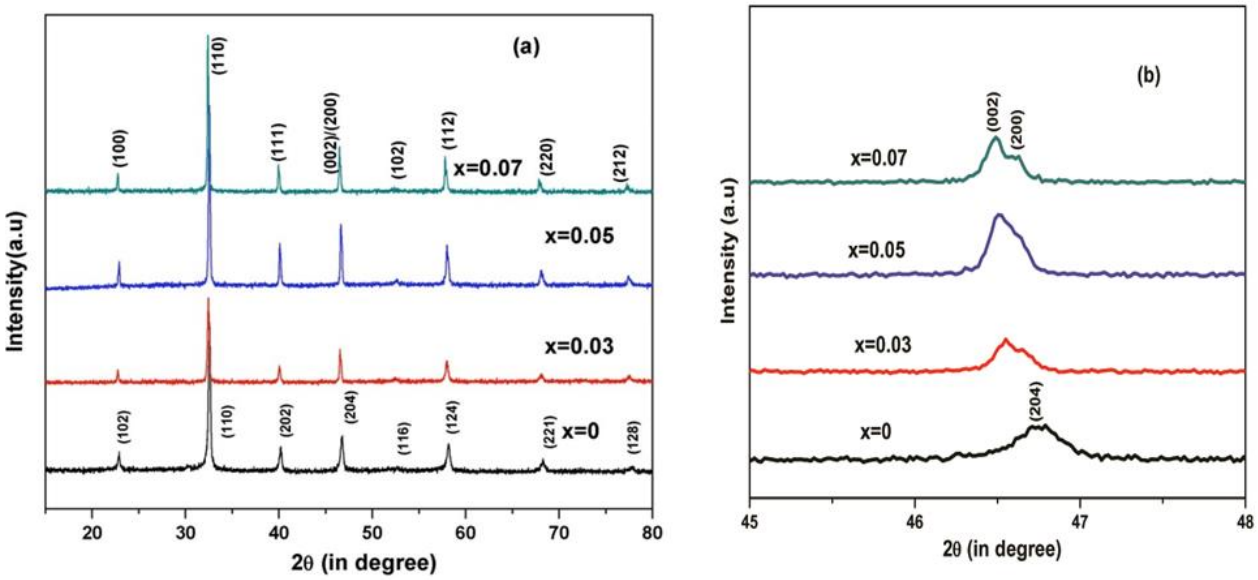

Figure 4.6.2 (a) X-ray diffraction patterns (b) expended X-ray diffraction patterns of the (1-x) BNT- x (BZT-0.5BCT) (x = 0–0.07) ceramics calcined at 700°C for 4h.

4.6.2.2.2 Particle size analysis and density

Fig.4.6.3 shows the particle size distribution of the (1-x) BNT- x(BZT-0.5BCT) (x = 0–0.07) powder.It can be observed that the agglomerate size of x=0.0 and x=0.03 in the range of 260-700 nm. But x=0.05 and 0.07 shows a narrow particle size distribution in the range of 200-530nm.

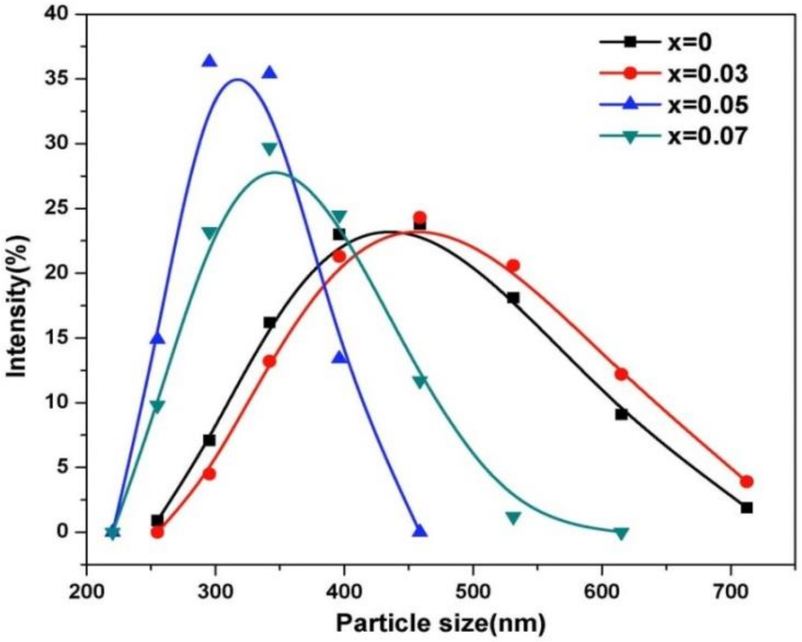

Figure 4.6.3 Particle size distribution of the (1-x) BNT- x (BZT-0.5BCT) (x = 0–0.07) powder calcined at 700°C/ 4h.

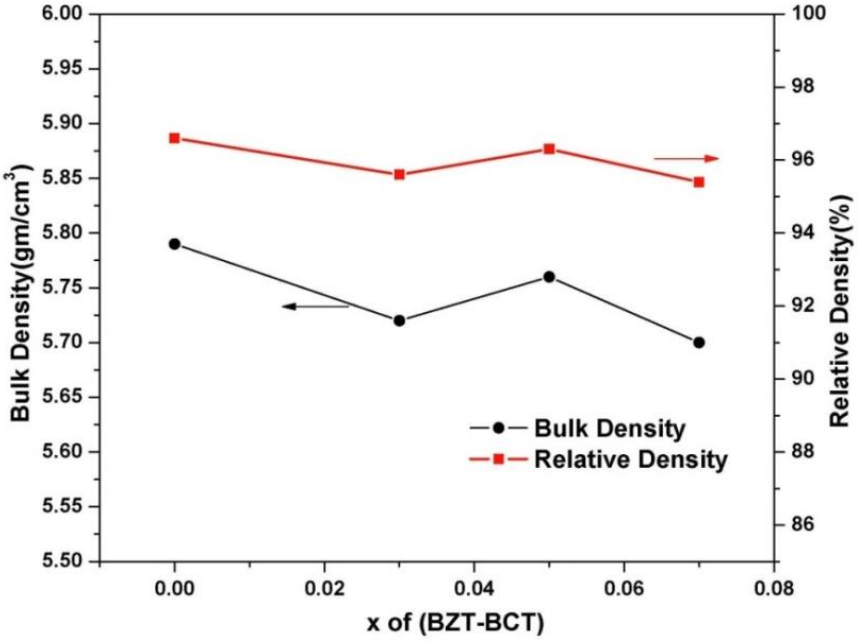

Figure 4.6.4 Bulk density and Relative density of the (1-x) BNT- x (BZT-0.5BCT) (x = 0–0.07) ceramics as a function of BZT-0.5BCT sintered at 1100°C. The error bars are within the size of the symbol.

Fig. 4.6.4 shows the bulk density and relative density of the (1-x) BNT- x (BZT-0.5BCT) (x = 0–0.07) ceramics as a function BZT-0.5BCT content, sintered at 1100°C. It can be observed that bulk density and relative density were slightly decreased with increasing BZT-0.5BCT content. It may be because with the increase in Ba and Zr content in the structure, the sample requires higher sintering temperature. However, sintering temperature was restricted to only 1100°C to avoid Bi and Na loss [272].It is to be mentioned that still all the samples were 95% of theoretical density. The reasonable density achievement at lower temperature may be attributed to very fine particle size of synthesized powder. The report on powder density is absent in other literature [271]. The bulk density value of the ceramic was in the range of 5.70-5.8gm/cm^3.

4.6.2.2.3 Microstructural properties

Fig. 4.6.5 (a)–(d) shows the SEM micrograph of the (1-x) BNT- x(BZT-0.5BCT) (x = 0–0.07) ceramics specimens sintered at 1100°C for 4h.The average grain size in the range of 1-3.5µm for pure BNT ceramic and decreases up to 0.5-2.5 µm for x=0.07. It can be observed that the average grain size decreases slightly with increasing BZT-0.5BCT content. It indicates that BZT-0.5BCT has an effect of suppressing the grain growth during the sintering. The shape of the grains was changed to cuboidal with increasing the BZT- BCT content.

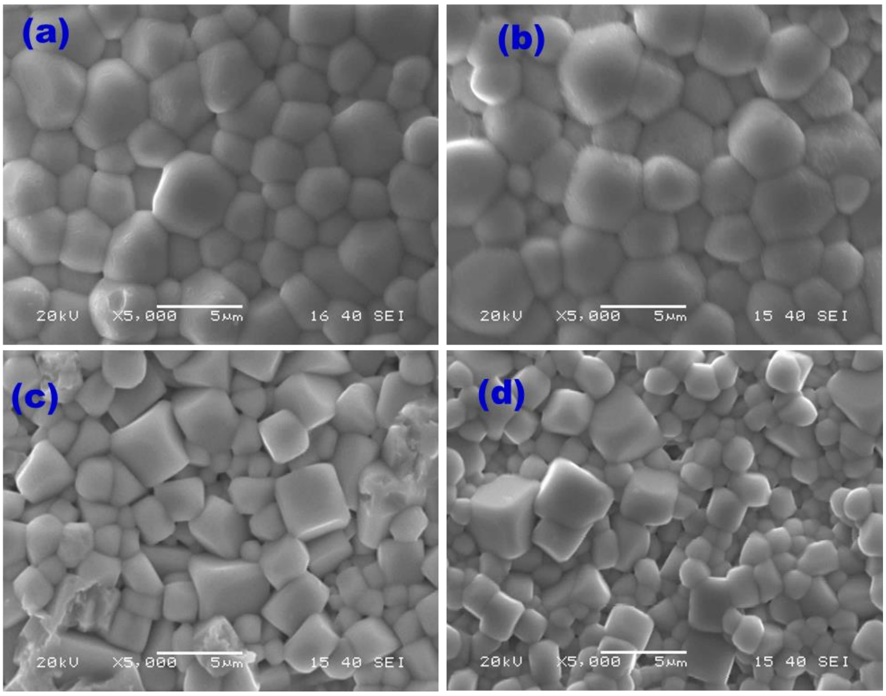

Figure 4.6.5 SEM micrograph of the (1-x) BNT- x (BZT-0.5BCT) (x = 0–0.7) ceramics sintered at 1100°C (a) x = 0 (b) x = 0.03 (c) x = 0.05 (d) x = 0.07

4.6.2.2.4 Dielectric properties

Fig 4.6.6 shows the room temperature relative permittivity and loss tangent of (1-x) BNT-x(BZT-0.5BCT) ceramics as a function of BZT-0.5BCT contents measured at 1kHz.The addition of BZT-0.5BCT significantly enhances the relative permittivity of BNT without major change in loss tangent. The improved dielectric properties can be attributed to the presence of rhombohedral and tetragonal phase in modified composition, explained earlier.

Fig. 4.6.7 (a) & (b) shows the temperature dependent relative permittivity and loss tangent of the specimens as a function of BZT-0.5BCT contents measured at 1kHz between RT to 450°C.The depolarization temperature (T_d) can be determined from the peak of tanδ vs temperature plot and relative permittivity maximum (T_m) can be determined from ε_r vs temperature plot[267].Fig4.6 7(c) shows the T_d & T_m of these ceramics. All these ceramics have two phase transition located at T_m and T_d where T_d is the depolarization temperature corresponding to the phase transition from ferroelectric state to antiferroelectric state and T_m is the maximum temperature at which the relative permittivity gets a maximum value corresponding to a phase transition from an antiferroelectric state to a paraelectric state [270].

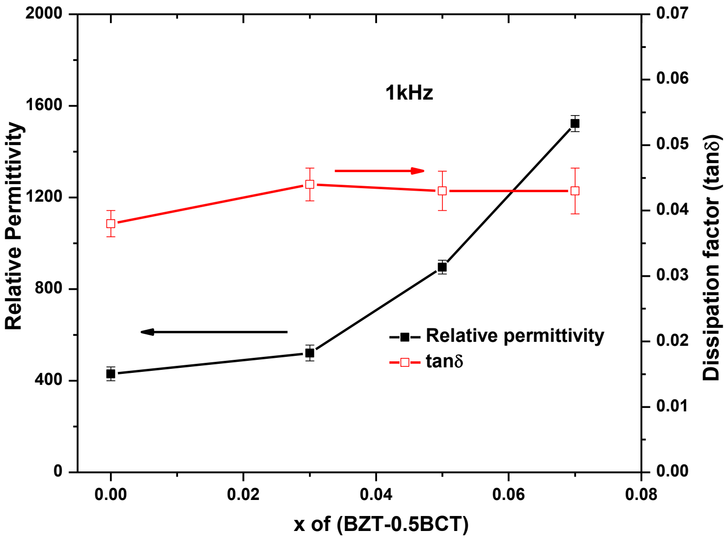

Fig. 4.6.6 Relative Permittivity and loss tangent of (1-x) BNT- x(BZT-0.5BCT) (x = 0–0.07) ceramics as a function of BZT-0.5BCT contents measured at 1 kHz.

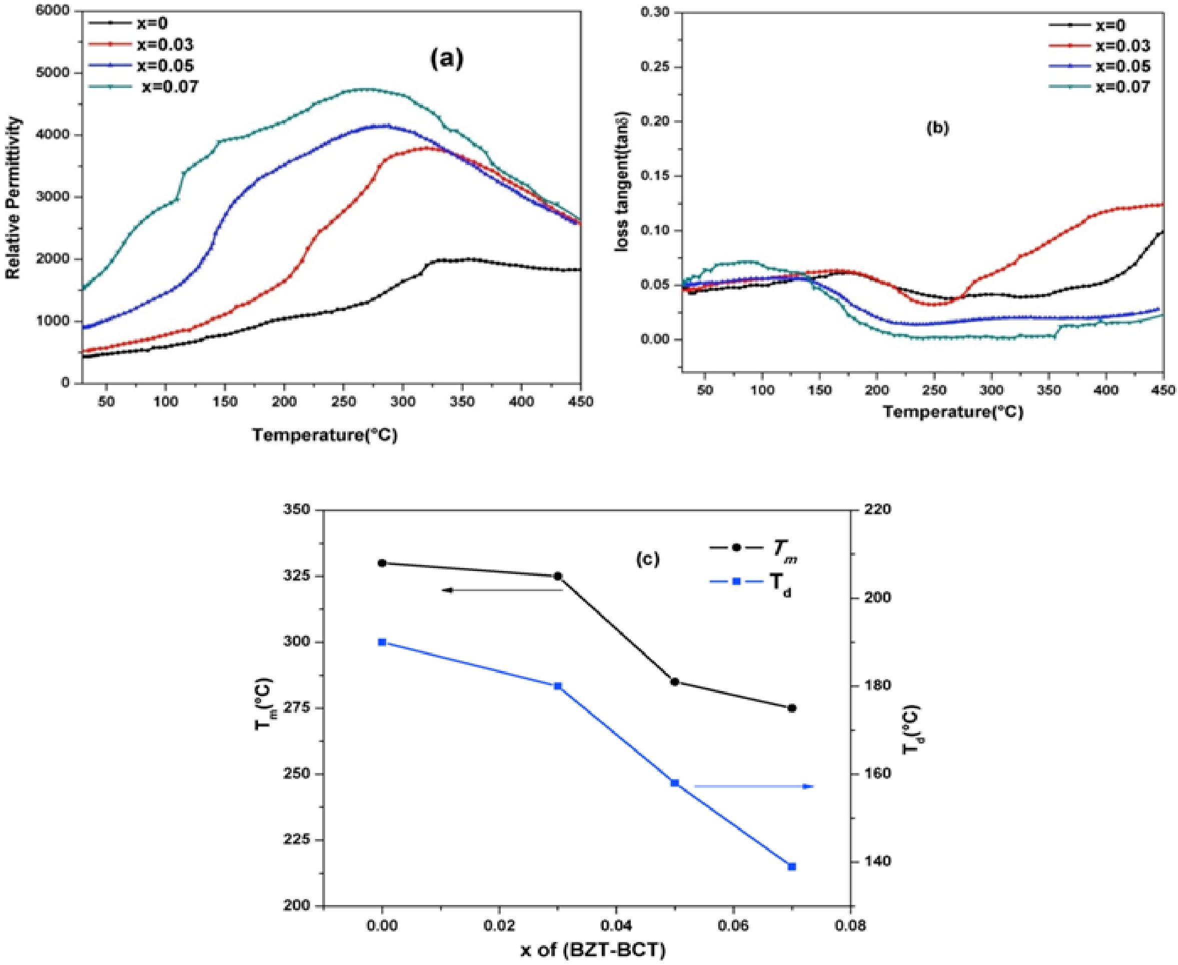

Figure.4.6. 7 (a) & (b) Temperature dependence of relative permittivity and loss tangent (c) T_d & T_m of (1-x) BNT- x(BZT-0.5BCT) (x = 0–0.07) ceramics as a function of BZT-0.5BCT contents.

It is observed that the temperature dependence relative permittivity becomes flatter with increasing BZT-0.5BCT content. That could be attributed to the disordering of the A-site and B site cations and compositional fluctuation [273]. It can be observed that T_d & T_m values decrease with increasing BZT-0.5BCT contents. The fall of T_d value is much higher compared to T_m value with BZT-0.5BCT addition.

4.6.2.2.5 Ferroelectric and Piezoelectric properties

Fig. 4.6.8 shows the piezoelectric coefficient (d_{33}) and T_d of specimen as the function of BZT-0.5BCT contents. The piezoelectric coefficient, $d_{33,}$ value gradually increases and reaches a maximum (d_{33}~142pC/N) at x=0.05 and then decreases with increasing BZT-0.5BCT content. The piezoelectric coefficient can be correlated to the T_d , which is the indication of stability of ferroelectric domain. It is mentioned in literature [274,275] that the lower depolarization temperature makes the domain less stable and it helps in reorientation of 90° domains, which improves the piezoelectric properties. However, reduction in T_d below 150°C, creates higher non-polar phase and promotes loss in piezoelectric properties [276] Further studies are required to get information of on nonpolar phase. The d_{33} value achieved for x=0.05 composition (which is sintered at 1100°C) is higher than those reported earlier where samples are sintered at high temperature [274].

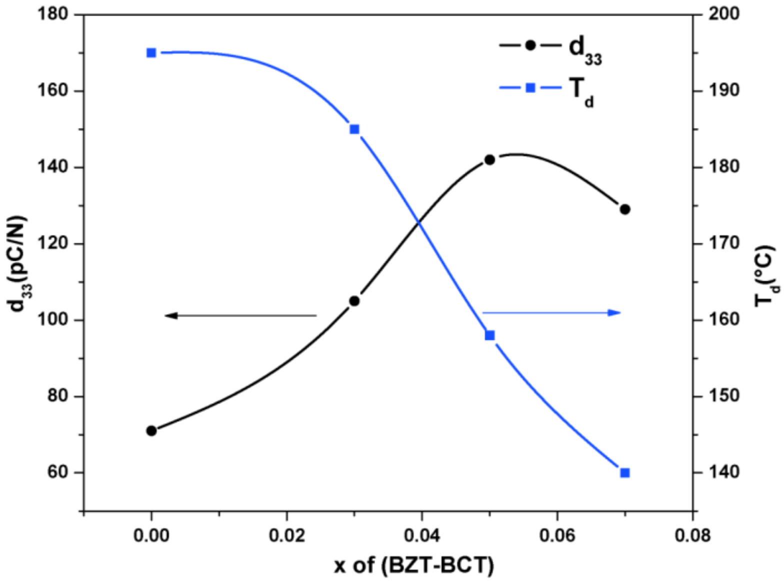

Figure 4.6.8 Piezoelectric properties and T_d of (1-x) BNT- x (BZT-0.5BCT) (x = 0–0.07) ceramics as a function of BZT-0.5BCT contents. The error bars are within the size of the symbol.

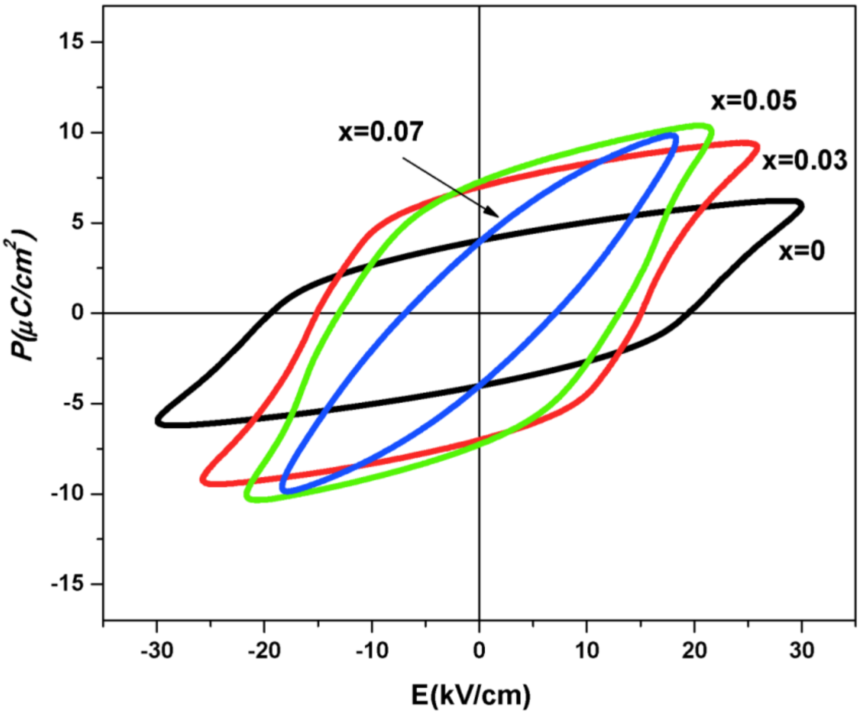

Figure 4.6.9 P-E hysteresis loop of (1-x) BNT- x (BZT-0.5BCT) (x = 0–0.07) ceramics as a function of BZT-0.5BCT contents.

Fig 4.6.8 shows the P-E hysteresis loop of (1-x) BNT- x (BZT-0.5BCT) ceramics as a function of BZT-0.5BCT contents measured at 50Hz. It can be seen that pure BNT ceramics has large coercive field (E_c ~ 19.54kV/cm). The coercive field (E_c) decreases with increasing BZT-0.5BCT content while the remnant polarization (P_r) value increases upto the x=0.05 and then decreases with increasing BZT-0.5BCT content. Increase remnant polarization can be attributed to the coexistence of rhombohedral and tetragonal phase.

The different physical properties of (1-x) BNT- x (BZT-0.5BCT) are summarized in Table 4.6.1.

Table 4.6.1 Summary of the various physical properties of (1-x) BNT- x (BZT-0.5BCT) ceramics

Composition	**Crystallite size (nm)**	**a_H(Å)**	**c_H(Å)**	**Cell volume $(Å)^3$**	**Density (gm/cc) at 1100°C**	**R. density (%)**	**ε_r at 1kHz**	**tanδ at 1kHz**	**d_{33} at poling field (3kV/mm)**
x=0	52	5.5144 (87)	13.4575 (4)	354.4	5.79	96.6	430	0.038	71
x=0.03	46	5.5186 (17)	13.4884 (4)	355.76	5.72	95.6	521	0.044	105
x=0.05	42	5.5208 (21)	13.5723 (59)	358.25	5.76	96.3	896	0.043	142
x=0.07	39	5.5223 (7)	13.5355 (16)	357.48	5.70	95.4	1523	0.043	129

4.6.3 Conclusions

The attempt to increase the T_C of BZT-BCT by incorporating NBT in BZT-BCT has been failed due to incompatibility between the two phases. However, the incorporation of BZT-0.5BCT in NBT is successful. The lead-free(1-x) $[(Bi_{0.5}\ Na_{0.5})TiO_3]$- $x[Ba(Zr_{0.2}Ti_{0.8})O_3$-$(Ba_{0.7}Ca_{0.3})TiO_3]$(where x=0, 0.03, 0.05, 0.07) has been prepared by planetary milling . The crystal structure of BNT changes with BZT-0.5BCT incorporation. A rhombohedral to tetragonal transformation occurs above 5 mol% of BZT-0.5BCT addition. The BZT-0.5BCT addition significantly enhances relative permittivity with decrease in T_d and T_m values. The improved dielectric properties can be attributed to the coexistence of rhombohedral and tetragonal phases in modified composition. BZT-0.5BCT addition makes the temperature dependence of relative permittivity broader and that could be attributed to the disordering of the A-site and B- site cations and compositional fluctuation. The piezoelectric coefficient is dependent upon the depolarization temperature T_d, which is an indication of stability of ferroelectric domain. The reduction in T_d below 150°C promotes loss in piezoelectric properties. The highest piezoelectric properties (d_{33} = 142pC/N) is observed at x=0.05 at sintering temperature of 1100°C.

Chapter 5

Conclusions and Scope for Future Work

Conclusions and scope of future work

5.1 Conclusions

The objectives of the present work were to prepare Zr and Ca modified $BaTiO_3$ at low temperature by exploring different powder preparation technique and to optimize Zr and Ca content in $BaTiO_3$ to get high dielectric and piezoelectric property. Another objective was low temperature sintering (<1200°C) of Zr and Ca modified $BaTiO_3$ with additives and to study its dielectric property. It was also explored whether the MPB composition could be used to form a solid solution with BNT with an aim to improve the dielectric, piezoelectric properties and Curie temperature of parent or BNT.

Some of the significant findings are summarized as follows:

i) $Ba(Zr_xTi_{1-x})O_3$ [BZT] (x=0.1, 0.15 and 0.2) ceramics have been prepared by a solution based auto-combustion method avoiding alkoxide precursors. The phase purity can be achieved at low temperature by synchronizing two fundamental processing parameters such as pH of the solution and Metal: Citric acid: EDTA ratio. The best results are obtained for Metal: Citric acid: EDTA= 1:1.5:0.1 and pH~9. It has been found that phase pure powder can be prepared at 800°C which is 500°C less than that normally required for powders prepared by solid state reaction. Such a low-temperature phase formation may be attributed to the effective complex formation with the metal ions, almost one-step decomposition of the metal complex and the auto-ignition at a low temperature. The powder can be sintered to more than 98% of the theoretical density at 1350°C. Low-temperature sintering is due to the fine particle size (~ 50 nm). The room temperature relative permittivity of all the composition is higher than the literature and dissipation factor is less than 2.5% that can be attributed to achieving high density and fine microstructure. Substitution of Ti by Zr has shown a diffuse phase transition. An increase in the Zr concentration decreased the Curie temperature and broadened the permittivity peaks. The piezoelectric properties depend upon the poling field, and optimum poling field for all ceramics are 1.5kV/mm at room temperature. The highest piezoelectric coefficient (d_{33} = 142 pC/N) is obtained for $Ba(Zr_{0.1}Ti_{0.9})O_3$ (BZT10) ceramics at electric field of 1.5kV. The results indicate that BZT10 ceramics is promising candidates for the lead-free piezoelectric applications.

ii) The citrate-nitrate autocombustion method is found to be an advantageous alternative to the conventional method to produce $(Ba_{0.85}Ca_{0.15})(Ti_{1-x}Zr_x)O_3$ powder. $(Ba_{0.85}Ca_{0.15})(Ti_{1-x}Zr_x)O_3$ (x=0.05, 0.1 and 0.15) powders can be prepared at 700°C which is 500°C less than that normally required for powders prepared by solid state reaction. These powders can be sintered to 93-94% of theoretical density at 1275°C-1300°C. From the temperature dependent dielectric behavior, the phase transition temperature (Tm) of BCTZ enhanced compared to BZT, peak height decreases and broadness increases significantly with incorporation of Ca. Enhanced piezoelectric and dielectric properties of d_{33} =215 pC/N, ε~2244 and tanδ = 1.6% are obtained for $(Ba_{0.85}Ca_{0.15})(Zr_{0.1}Ti_{0.9})O_3$ composition, which is lower than earlier reported result, but it is higher than that of other Pb-free systems (NBT, KNN). This composition can be represented by a pseudobinary solid solution where $Ba(Zr_{0.2}Ti_{0.8})O_3$- $(Ba_{0.7}Ca_{0.3})TiO_3$ (BZT-BCT) are two end members, and BCTZ10 is a 50-50 solid solution of BZT-BCT. The enhancement of dielectric and piezoelectric property can be explained by the existence of morphotropic phase boundary (MPB) in this composition.

iii) The $(Ba_{0.85}Ca_{0.15})(Ti_{0.9}Zr_{0.10})O_3$(BZT-0.5BCT) ceramics has also been prepared by solid state synthesis route via planetary milling and ball milling. The powder properties, densification and electrical properties are also compared with the solution combustion method. It has been found that the temperature to achieve phase purity and sinterability of the powder depends on the methods of preparation. The citrate-nitrate autocombustion method was found to be beneficial over the solid state synthesis route (ball mill & planetary mill) to produce single-phase and highly crystalline BZT-0.5BCTceramics at low-temperature. The particle size of BZT-0.5BCT powders is in the range of 0.15 -0.3µm for planetary milling and 0.6-0.9 µm for mixing by ball milling. For combustion powder, the particles are agglomerated and agglomerate size is in the range of 0.25–0.40 µm with an irregular to spherical in shape. It can be found that many fine particles with the size of 40 to 70 nm is present in the sample. The planetary milled powder can be sintered to more than 98% of theoretical density at 1350°C. Lower sintering temperature compared to reported literature attributed to fine particle size. On the contrary, the highest density achieved in combustion and ball milling powder is only 94%. The average grain size of the sample prepared by ball milling, planetary milling and combustion method found to be 9.3 µm, 1.2 µm and 10.2 µm, respectively. The grain size of sintered planetary milled sample is approximately four times compared to its initial particle size, whereas, it is twenty times in combustion synthesized sample and ten times in ball milled sample. The relative permittivity values are found to be 3535, 1989 and 2244 for planetary milling, ball milling and solution combustion method, respectively. Low dielectric loss (tan δ less than 2%) is obtained for ceramic samples synthesized via all the methods. BZT-0.5BCT ceramic prepared by planetary milling shows high relative permittivity (3535) with low dielectric loss (0.014) with the high piezoelectric coefficient (d_{33} = 350 pC/N) compared to other two method. It is found that the T_C dependent on the preparation methods and specifically on grain size. Microwave sintering is proved to be useful to increase the grain size seven times in case of planetary milled sample. However, Microwave sintering has no significant effect on the dielectric property but degrades piezoelectric property due to the growth of small amount impurity phases.

iv) The detailed investigation of the phase evolution, dielectric and piezoelectric response of xBZT-(1-x)BCT solid- solution has been carried out at 1% interval for x in the range of 0.47 to 0.53. In this case, the xBZT-(1-x)BCT (0.47-0.53) has been prepared by solid state synthesis via planetary milling. It is found that the ceramics underwent a complicated phase evolution, driven by Ca and Zr contents. The dielectric and piezoelectric response indicates that the MPB exist at 0.5BZT-0.5BCT composition. The MPB of BZT-0.5BCT ceramics is closely related to the occurrence of multiple phases in narrow regions around orthorhombic and tetragonal phases, could be controlled by the content of Ca and Zr in the composition, as well as the temperature. The MPB exhibits strong temperature dependence. The temperature dependence of the dissipation factor indicated that the multiple phases might be unstable and served as structural bridge in MPB regions and played an important role in the large d_{33}(= 350 pC/N) and ε_r(=3535) near the MPB at room temperature.

v) BZT-0.5BCT is successfully sintered at 1100°C with the addition of a mixture of Li_2CO_3 and Bi_2O_3 as a sintering aid which form $LiBiO_2$ in-situ. 98% of theoretical density was achieved for 5 wt. % of LBO addition. The LBO addition shifts the relative permittivity peak maxima to room temperature which is due to the Li^+ and Bi^{3+} ion incorporation into the perovskite structure. It is interesting to note that relative permittivity values are not deteriorated much with this addition. But piezoelectric property disappears due to T_C shifting below room temperature. The temperature stability of permittivity of the LBO added sample is better than the pure BZT-BCT sintered at 1350°C. It is to be noted that 5LBO sample sintered at 1100°C has higher dielectric strength and comparable energy density with BZT-BCT sintered at 1350°C.The (LBO) added BZT-0.5BCT ceramics is suitable for Y5V based MLCC multilayer ceramic capacitor application.

vi) The attempt to increase the T_C of BZT-BCT by incorporating NBT in BZT-BCT has been failed due to incompatibility between the two phases and poor sinterability of the resulted solid solution. However, the incorporation of BZT-0.5BCT in NBT is successful. Phase pure (1-x)

NBT- x[BZT-0.5BCT](where x=0, 0.03, 0.05, 0.07) solid solution has been prepared at 700°C. The crystal structure of NBT changes with BZT-0.5BCT incorporation. A rhombohedral to tetragonal transformation occurs above 5 mol% of BZT-0.5BCT addition. The BZT-0.5BCT addition significantly enhances relative permittivity with decrease in T_d and T_m values. The improved dielectric properties can be attributed to the coexistence of rhombohedral and tetragonal phases in modified composition. BZT-0.5BCT addition makes the temperature dependence of relative permittivity broader, and that could be attributed to the disordering of the A-site and B-site cations and compositional fluctuation. The piezoelectric coefficient is dependent upon the depolarization temperature T_d, which is an indication of stability of ferroelectric domain. The reduction in T_d below 150°C promotes loss in piezoelectric properties. The highest piezoelectric properties (d_{33} = 142pC/N) is observed at x=0.05 at sintering temperature of 1100°C. The doubling of piezoelectric constant in solid solution compared to pure NBT may be attributed to coexistence of two phases and reduction of the coercive field that resulted in efficient poling of the samples.

In summary, the BZT-0.5BCT ceramics developed here can be used in devices like sensors, low-power motor type transducers, receivers and low power generators, fuzes and ink jet printers, where extremely high dielectric constant and high "d" constant required. Also, the present study provided first comprehensive results to show how preparation techniques affect the microstructure, dielectric and piezoelectric property of BZT-0.5BCT.

5.2 Scope of Future work

Apart from the brief conclusion of the current research work there are several scopes for further improvement of dielectric and piezoelectric property of BZT-0.5BCT. However, the study has not answered some of the following points, which can be taken up as the future study:

i) Further studies are needed to improve the sinterability and piezoelectric property of the BZT-0.5BCT prepared by solution based auto-combustion method.

ii) Further studies are required why the grain growth in combustion synthesized sample is twenty times compared to its initial particle size, whereas grain growth is approximately four times in planetary milled sample and ten times in ball milled sample. Detailed sintering kinetics study in this sample could fetch some light.

iii) In Chapter 4.4 it is shown multiple phases present along MPB region but typical XRD analysis and Raman spectroscopy could not provide direct evidence. Synchrotron XRD measurement, Raman spectroscopy and dielectric measurement with temperature (low temperature and high temperature) are required to get exact feature along MPB composition region.

iv) In our thesis, the bulk piezoelectric effect was studied for different composition and explained. However, it will be interesting to explore the aspects of local piezo-response (grain and grain boundary level) and electric domain size of the xBZT-(1-x)BCT sample with close compositional modifications around morphotropic phase boundary (MPB). Piezoforce microscopy may be used to study the polar phenomena and associated piezoelectric effects in grain and grain boundary level in xBZT-(1-x)BCT ceramics around morphotropic phase boundary (MPB).

v) Though $LiBiO_2$ proved to be an effective additive for getting useful dielectric property but degrades piezoelectric property. Other oxide additives (viz. MnO_2, CuO, $PbGeO_3$) can be explored for low-temperature sintering of BZT-BCT without losing piezoelectric property.

vi) The low Curie temperature of BZT-BCT is hindering its application above room temperature. The formation of the solid solution with other high T_C ferroelectrics or suitable dopants may be useful to increase the T_C of resulted composite without hampering the piezoelectric property.

APPENDIX

A-1 Impedance and Modulus spectroscopy of various $BaZr_xTi_{1-x}O_3$ (x=0.1, 0.15, 0.2) ceramics:

In the present work, we report on the impedance analysis of BZT ceramics prepared from solution combustion synthesized powder. To understand the conduction mechanism in the zirconium substituted $BaTiO_3$ system, the complex impedance, and electric modulus formalisms have been reported.

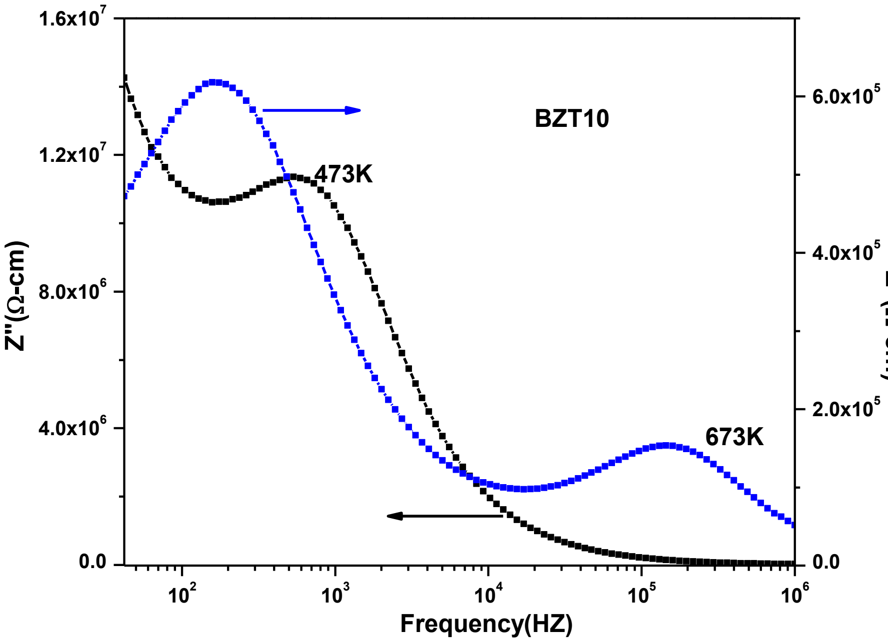

Figure A-1. Z″ vs frequency plots for BZT10 samples.

Z″ (f) spectra for BZT10 are displayed in Fig A-1. The peak associated with the bulk response starts to appear at 200°C. The peak height decreases and shifts to higher frequency with increasing temperature. Higher temperature IS measurements reveal the presence of a grain-boundary component in these ceramics. This means both the grain and grain-boundary regions have different impedance responses with a high resistance.

The impedance complex plane (Z′-Z″) plots for BZT samples at 673K show two semicircles that can be attributed to the bulk response at high frequency region and grain boundary response at low frequency region (Fig.A-2 (a)). The semicircle can be fitted with parallel RC circuits and the capacitance is estimated to be 0.22nF/cm at 673K for grains, which are very close to the values obtained by fixed-frequency measurements at the same temperatures. The dc resistivity of the ceramics was found out from the intersection point of the semicircle with the Z axis. The dc resistivity increases with increasing Zr content, although no significant change in resistivity is observed. The dc resistivity of BZT10 decreases with increasing temperature, which is characteristic of a thermally activated process. Similar behavior is observed for BZT15, BZT20 also. (Z′-Z″) plots for all three compositions at 673K are compared in Fig. A-2 (a- c).

The sample resistance was found to decrease with rise in temperature which suggests a typical semiconducting behavior of BZT ceramic. The grain, grain boundary capacitance and resistance values of BZT10 are $C_g = 2.06 \times 10^{-10}$ F/cm and $R_g = 4.8\times10^3$ Ω-cm; $C_{gb} = 4.5\times10^{-8}$ F/cm and $R_{gb} = 2.23\times10^4$ Ω-cm at 673K. The corresponding values of these elements for BZT15 are $C_g = 2.18\times10^{-10}$ F/cm and $R_g = 1.03\times10^4$ Ω-cm; $C_{gb} = 1.42\times10^{-8}$ F/cm and $R_{gb} = 7.09\times10^4$ Ω-cm at 673K. The R_g and R_{gb} for BZT20 are 4.01×10^4 Ω-cm and 6.18×10^5 Ω-cm, respectively at 673K. The capacitance of the grain and grain boundary could not be calculated separately from impedance plot for BZT20 because $f_{\max}$ was beyond the measured frequency range.

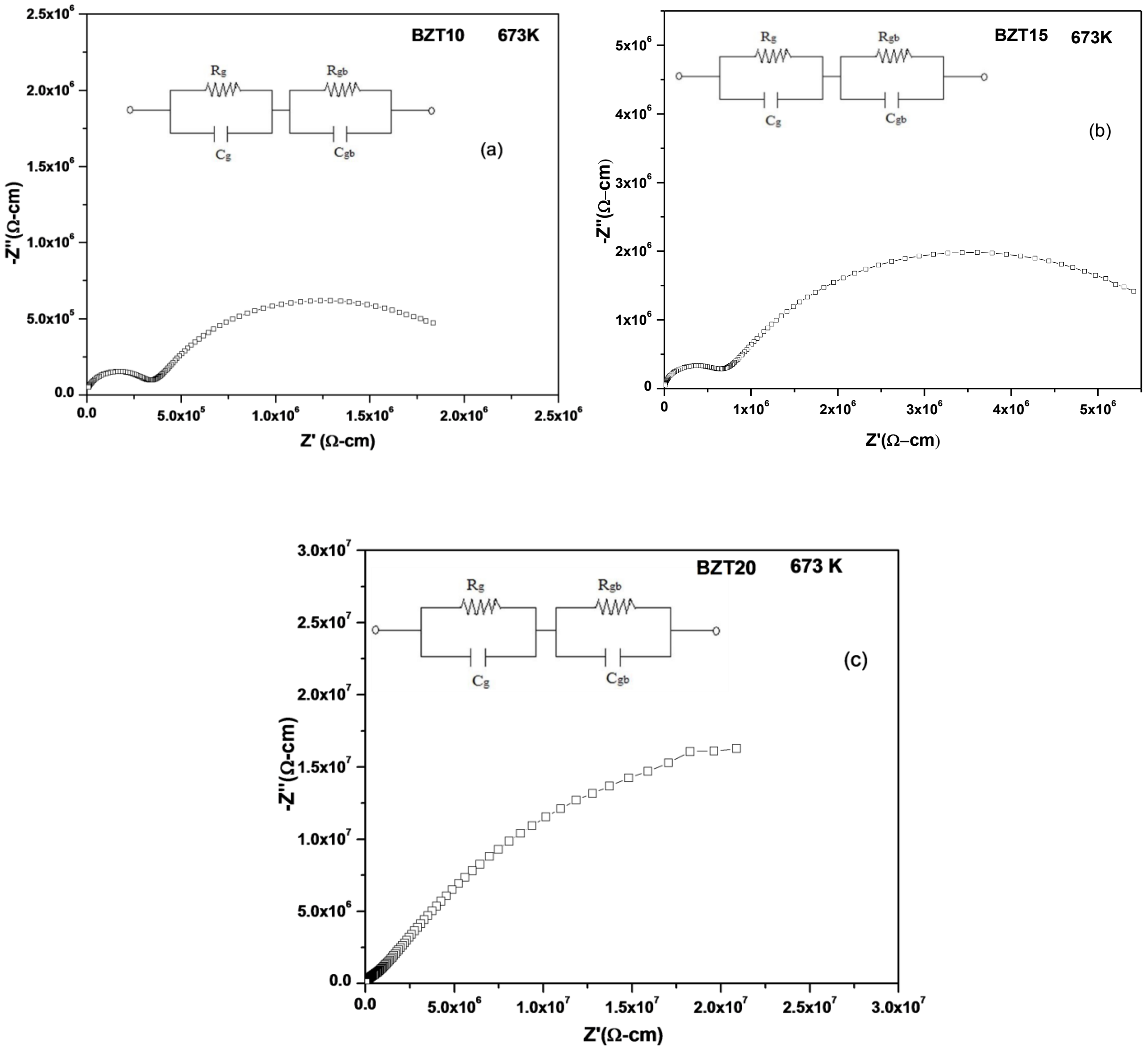

Figure A-2 Complex impedance plots (Z″ vs Z′) for BZT ceramics samples at measurement temperature (673 K).

In addition, the fitting results showed a higher value of R_{gb} (grain boundary resistance) as compared to R_g (grain resistance) due to a lower concentration of oxygen vacancies and trapped electrons in grain boundaries. This can be explained as; the creation of oxygen vacancies and other charge carriers (e.g. electrons and holes) are related to process parameters at various stages like calcination and sintering during the synthesis of the material at high temperatures. These defects significantly influence the conduction and dielectric relaxation behavior. While sintering at high temperature, oxygen loss increases leading to the formation of oxygen vacancies, accompanied by partial reduction in Ti^{4+} to Ti^{3+} ions by the following reactions

$$2O_O^x \leftrightarrow 2V_O^{\cdot\cdot} + O_2(g) + 4e^-$$

$$Ti^{4+} + e' \leftrightarrow Ti^{3+}.$$

However, when the temperature is slowly cooled to room temperature in air, are oxidation process occurs as $2V_O^{\cdot\cdot} + O_2(g) + 4e^- \leftrightarrow 2O_O^x$. The occurrence of this re-oxidation process at the grain boundaries leads to the formation an insulating grain boundary and highly conductive oxygen deficient grains [277,278]. The Increase in resistivity with Zr addition can be explained by the presence of less $Ti^{4+}$for reduction during sintering.

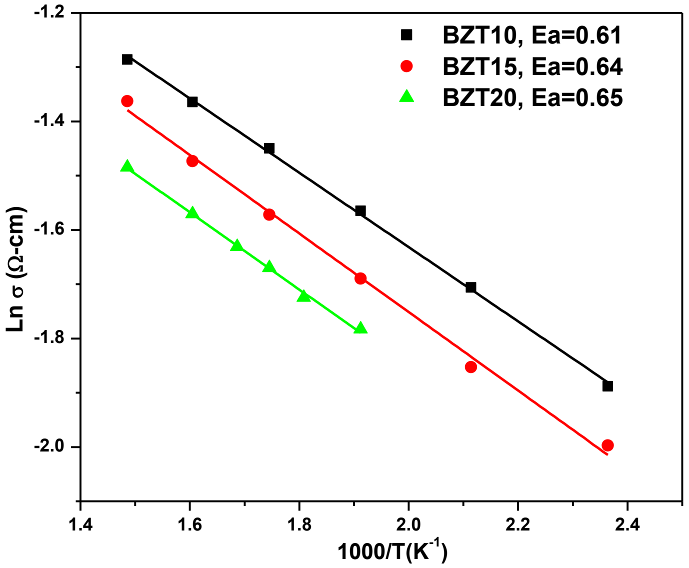

Figure A- 3 The Arrhenius plots of activation energy for BZT samples.

The activation energy (E_a) of BZT samples can be calculated from the temperature dependence of the bulk conductivity in an Arrhenius plot. Fig.A- 3 shows the data to fit the Arrhenius law.

The magnitude of E_a in BZT10, BZT15 and BZT20 are 0.61, 0.64 and 0.65 eV, respectively. The magnitude of E_a is close to the reported values from the similar analysis on $BaTiO_3$-based materials where activation energy of 0.69 eV obtained [277]. It may be due to the polaronic conduction of 3d electron on Ti^{3+} with low mobility must be predominant at low temperature [179]. Mahajan et al. reported the E_a values of 0.85 eV for microwave sintered $BaZr_{0.1}Ti_{0.9}O_3$ ceramics. [179]. The activation energy for grain boundary has also been calculated. The values lying in the range of 1-1.1eV for different BZT sample.

A-2 Modulus Spectroscopy

M″(f) spectra at various temperatures are shown in Fig.A-4 for BZT10, BZT15, BZT20. We observed that only one peak was present for BZT10 and BZT15 which corresponds to grain contribution of the material. It seems that there is only one relaxation in the sample. The reason for this may be because low capacitance was observed for grain, and thus it dominates. The frequency region below the peak maximum, M''_{max} determines the range in which charge carriers are mobile on long distances. At frequency above the peak maximum, the carriers are confined to potential wells which are mobile over short distance [279].

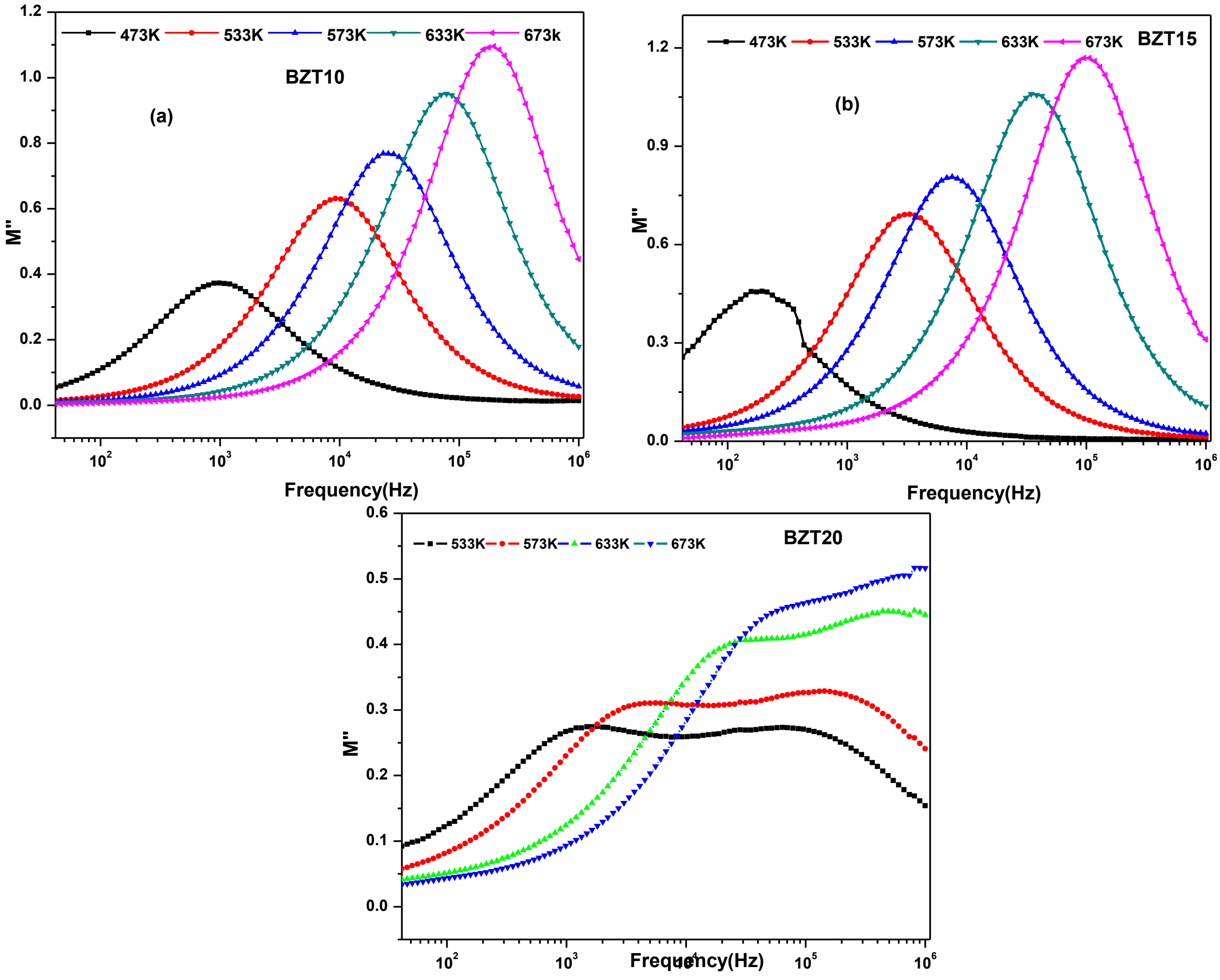

Figure A-4. Frequency dependence of imaginary part of Modulus M″ at different temperature of various BZT samples

It can be seen that peak maxima increase with increasing temperature and shifts to higher frequency side which can be attributed to the change in their relaxation time with temperature. Z″, M″ spectra of BZT20 are more complex, they exhibit quite different responses (Fig. A-5), and, in addition, are different from those observed for BZT10, BZT15. For BZT20, the M″ spectrum at 573K shows two close peak may be of bulk-type components (Fig. A-4), as high resistance, high capacitance grain-boundary response may not be appearing in M″ plot. Morrison et al.[277] also reported similar type bulk response in the $BaTiO_3$-based system. It may be due to that core, and outer region of the grain have different relaxation due to composition fluctuation or variations in oxygen content across the individual grain [277].

The peaks $P_{\tan\delta}$, $P_{Z''}$, and $P_{M''}$ are of relaxation processes within the bulk (grain) material. It can be determined whether the bulk response is due to long-range conductivity or localized relaxation by plotting these curves simultaneously (Fig. A-5). Generally localized relaxations result in separate Z″ and M″ peaks, whereas long-range conductivity results in overlapping Z″ and M″ peaks [280,179].

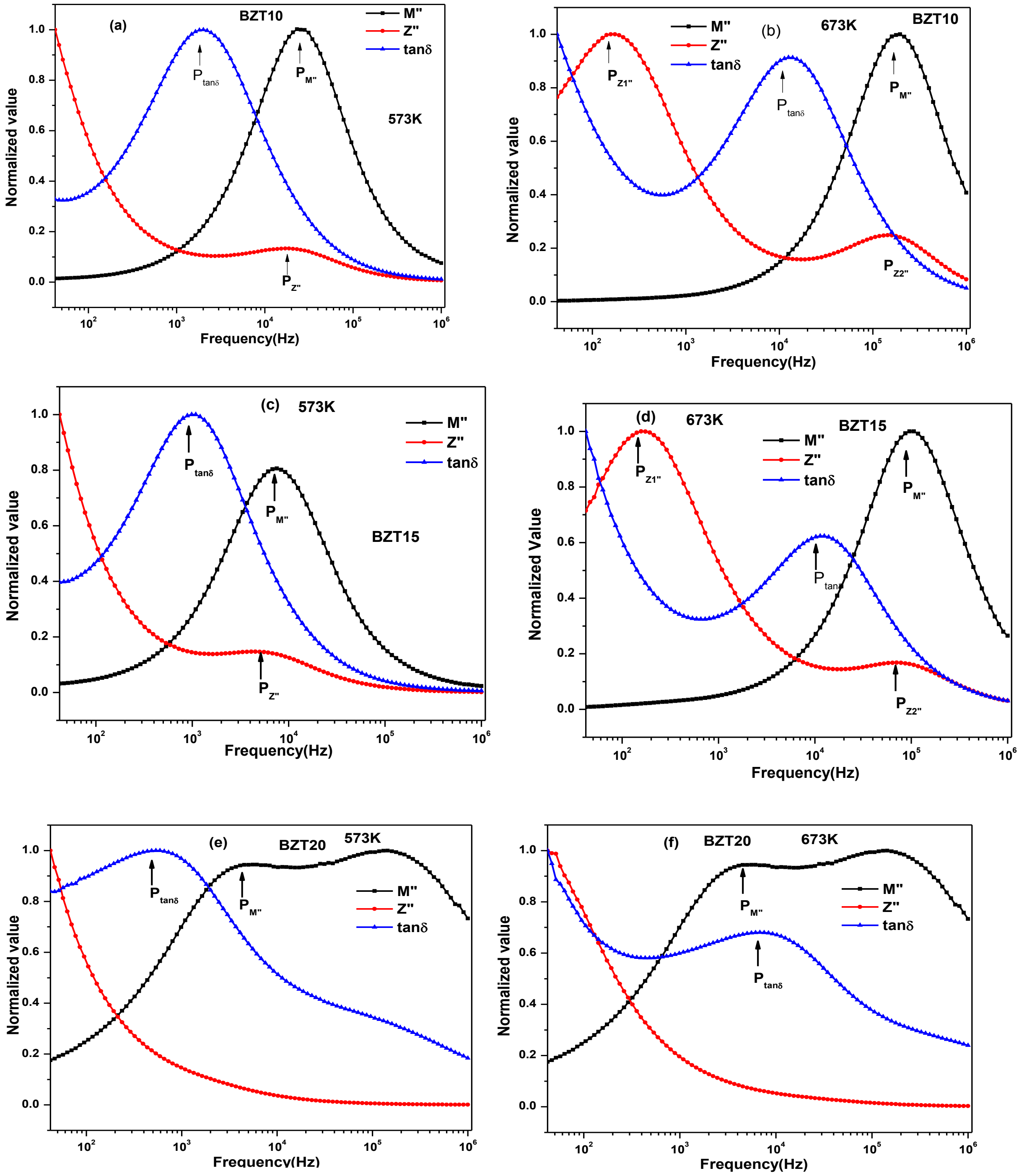

Fig A-5 Normalized peak height of Z″, M″, and tanδ with frequency for BZT samples

Figure A-5 shows the variation of normalized parameters tanδ/tanδ$_{max}$, M″/M″$_{max}$, and Z″/Z″$_{max}$ as a function of log frequency measured at 573 and 673 K for BZT10, BZT15, and BZT20. The peak of $P_{Z_2''}$, and $P_{M''}$ overlaps at 673 K for BZT10 samples, which show the oxygen ions or vacancies or hopping conduction mechanism (long range) contribute to the dc conductivity at higher temperatures [281]. In addition, this mismatch of two distinct curves at the lower temperature (< 673K) for BZT10 also suggests the polarization process due to localized conduction of multiple carriers. It confirms the presence of multiple relaxation processes in BZT10 at low temperature and in BZT15 and BZT20 up to high temperature. Additionally, the sequence of the three peaks in Fig. A-5 reveals that their relaxation times fulfill the following order: $\tau_{\tan\delta} > \tau_Z > \tau_M$ for BZT10 and BZT15 proposed previously.

A-3 Impedance and Modulus spectroscopy of BZT-BCT ceramics:

In the present report, we also studied impedance and modulus spectroscopy of BZT-BCT ceramics prepared by solution combustion synthesis (BZT-BCT–C) and solid state synthesis via planetary milling mixing (BZT-BCT-P) to understand the grain, grain-boundary characteristics.

The impedance complex plane (Z′-Z″) plots for BZT-BCT samples at 573K show two semicircles that can be attributed to the bulk response at high frequency region and grain boundary response at low frequency region. (Fig.A-6). The semicircle can be fitted with parallel RC circuits.

Let (R_g, R_{gb}) and (C_g, C_{gb}) are the resistances and capacitances of grains (or bulk) and grain boundaries, respectively. The corresponding values of these elements for BZT-BCT-C are Cg =2.59×10^{-10} F/cm and $R_g = 4.9\times10^5$ Ω-cm; $C_{gb} = 1.34\times10^{-8}$ F/cm and $R_{gb} = 1.26\times10^6$ Ω-cm at 573K. The corresponding values of these elements for BZT-BCT-P are $C_g = 4.06\times10^{-10}$ F/cm and $R_g = 1.5\times10^6$ Ω-cm; $C_{gb} = 2.69\times10^{-8}$ F/cm and $R_{gb} = 2.3\times10^6$ Ω-cm at 573K. The C_g value is very close to the values obtained by fixed-frequency measurements at the same temperatures and a characteristic one for bulk dielectrics and the C_{gb} value reveals the sample is well sintered, with narrow intergranular regions. [282].

The dc resistivity of the ceramics was found out from the intersection point of the semicircle with the Z axis. The dc resistivity increases with the incorporation of Ca in BZT10, although no significant change in resistivity is observed. The dc resistivity of BZT-BCT decreases with increasing temperature, which is characteristic of a thermally activated process.

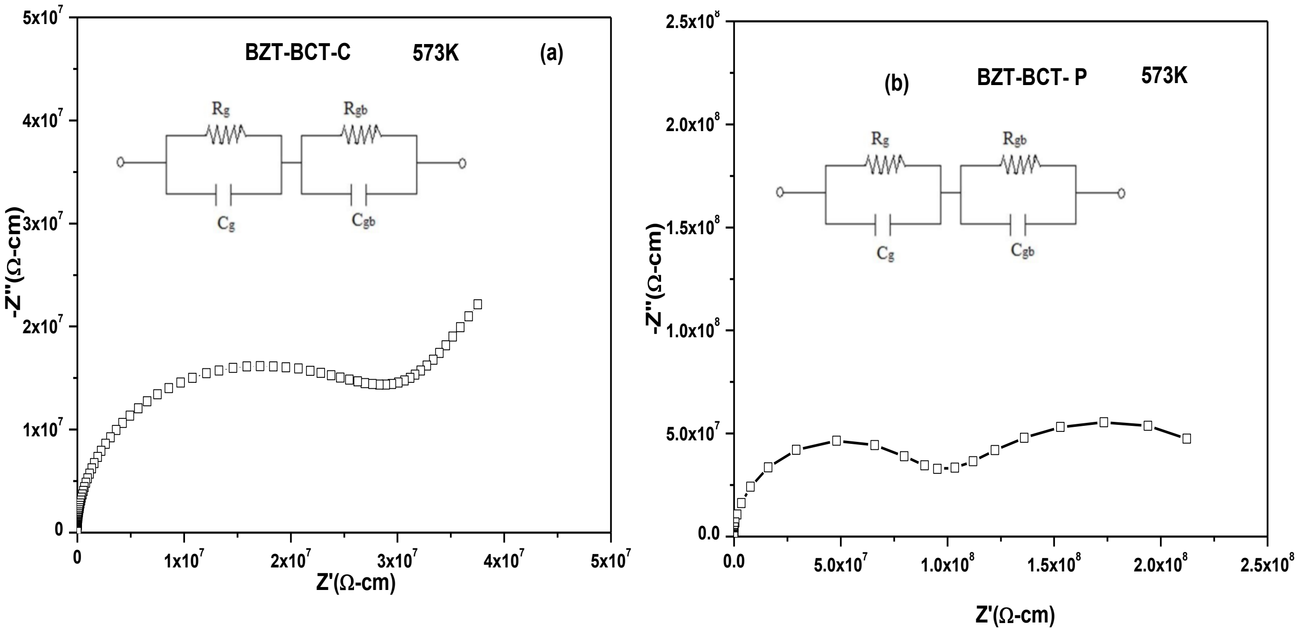

Fig A-6 Complex impedance plots (Z″ vs Z′) for BZT-BCT-C and BZT-BCT-P samples at 573K.

In addition, the fitting results showed that in both cases, a higher value of R_{gb} (grain boundary resistance) as compared to R_g (grain resistance) due to a lower concentration of oxygen vacancies and trapped electrons in grain boundaries. This can be explained as; the creation of oxygen vacancies and other charge carriers (e.g. electrons and holes) are related to process parameters at various stages like calcination and sintering during the synthesis of the material at high temperatures. These defects greatly influence the conduction and dielectric relaxation behavior. During sintering at high temperature, oxygen loss increases leading to the formation of oxygen vacancies, accompanied by partial reduction in Ti^{4+} to Ti^{3+} ions by the following reactions using Kroger-Vink notation

$$2O_O^x \leftrightarrow 2V_O^{\cdot\cdot} + O_2(g) + 4e^-$$

$$Ti^{4+} + e' \leftrightarrow Ti^{3+}.$$

However, when temperature is slowly cooled to room temperature in air, are oxidation process occurs as $2V_O^{\cdot\cdot} + O_2(g) + 4e^- \leftrightarrow 2O_O^x$. The occurrence of this re-oxidation process at the grain boundaries leads to the formation an insulating grain boundary and conductive oxygen deficient grains[277,278]. Combustion synthesized samples have higher R_{gb} and R_g compared to BZT-BCT -P. High temperature calcination and high energy milling may impart more defect in the BZT-BCT –P particle which may reduce the resistance.

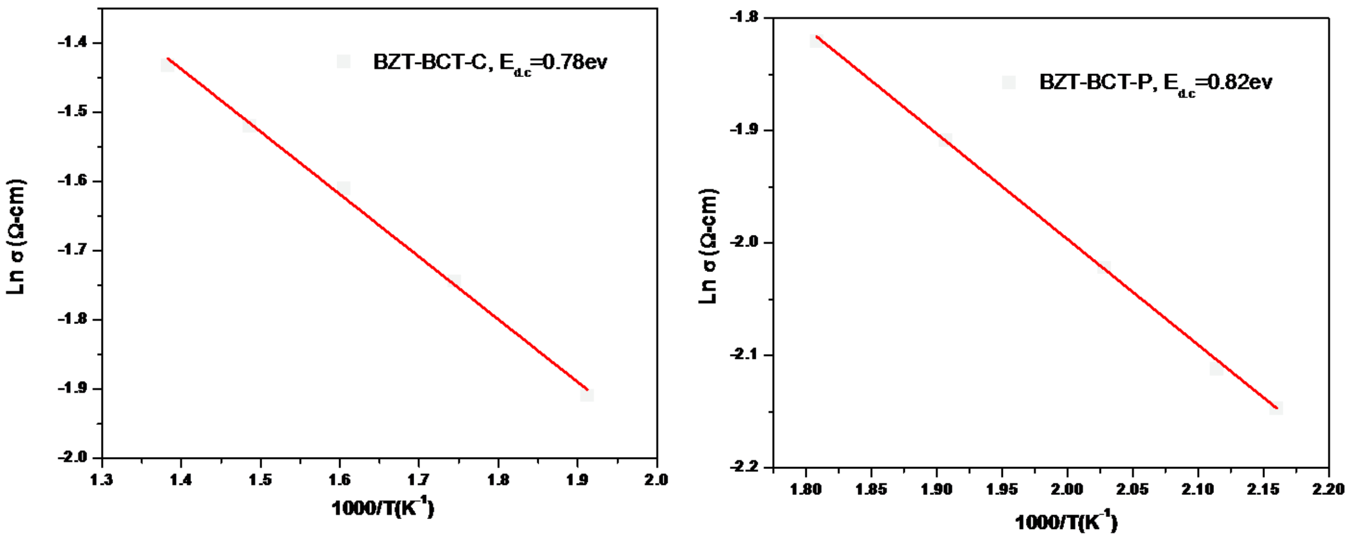

Fig A-7 The Arrhenius plots of activation energy for different BZT-BCT samples

The activation energy (E_a) of BZT-BCT samples can be calculated from the temperature dependence of the bulk conductivity in an Arrhenius plot. Figure A-7 shows the data to fit the Arrhenius law. The magnitude of E_a for grain in BZT-BCT –P and BZT-BCT -C are 0.82 and 0.78, respectively. The Ea values of our samples is comparable to that reported by kaushal et al.[278]. The activation energy for grain boundary has also been calculated. The activation energy for grain boundary has also been calculated. The values are lying in the range of 1-1.01eV for this two BZT-BCT sample.

A-4 Modulus Spectroscopy

M″(f) spectra at various temperatures are shown in Fig.A-8 for BZT-BCT –P and BZT-BCT -C. We observed that only one peak was present that corresponds to grain contribution of the material. It seems that there is only one relaxation in the sample. The reason for this may be because low capacitance was observed for grain and thus it dominates. The frequency region below the peak maximum M''_{max} determines the range in which charge carriers are mobile on long distances. At frequency above the peak maximum, the carriers are confined to potential wells which are mobile over short distance [279]. It can be seen that peak maxima increases with increasing temperature and shifts to higher frequency side which can be attributed to the change in their relaxation time with temperature.

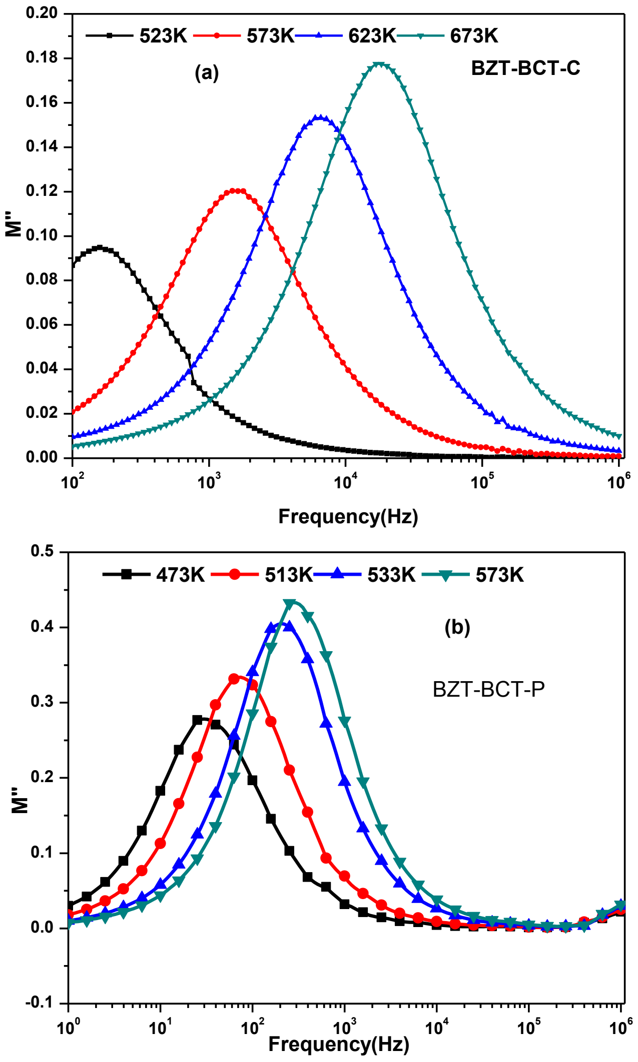

Fig A-8. Frequency dependence of imaginary part of Modulus M″ at different temperature for BZT-BCT-C and BZT-BCT-P samples.

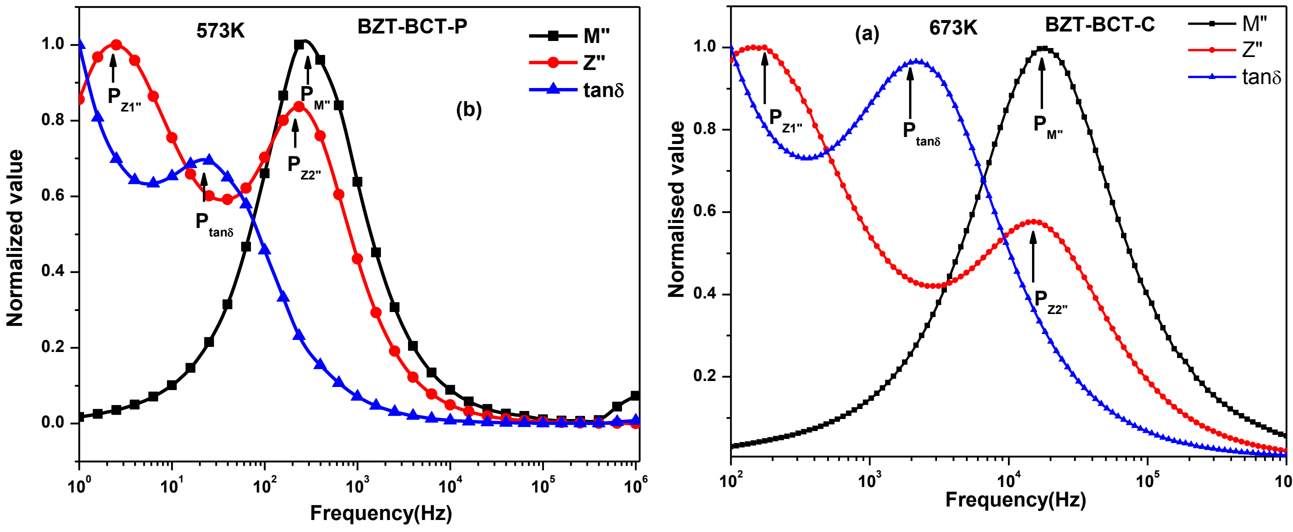

Fig A-9 Normalized peak height of Z″, M″, and tanδ with frequency for BZT-BCT-C and BZT-BCT-P samples.

The peaks $P_{\tan\delta}$, Pz_2'', and $P_{M''}$ are of relaxation processes within the bulk (grain) material. It can be determined whether the bulk response is due to long-range conductivity or to localized relaxation by plotting these curves simultaneously (Fig.A-9). Figure A-9 shows the variation of normalized parameters $\tan\delta/\tan\delta_{max}$, M''/M''_{max}, and Z''/Z''_{max} as a function of log frequency measured at 573 K for BZT-BCT –P and BZT-BCT –C at 673K. The peak of Pz_2'', and $P_{M''}$ overlaps at 573 K for both the samples, which show the oxygen ions or vacancies or hopping conduction mechanism (long range) contribute to the dc conductivity at higher temperatures [281]. Additionally, the sequence of the three peaks in Fig.A-9 reveals that their relaxation times fulfill the following order: $\tau_{\tan\delta} > \tau_Z > \tau_M$ for BZT-BCT –P and BZT-BCT -C proposed previously [283].

The summary of the impedance and modulus spectroscopy of BZT and BZT-BCT ceramics mentioned below:

Impedance spectroscopy shows both grain and grain boundary contributions to impedance. It also shows that grain has lower resistance and capacitance compared to the grain boundary region which manifests the defect creation during processing and reduction and re-oxidation during sintering. Spectroscopy analysis reveals a non-Debye relaxation phenomenon being its relaxation frequency moving with the increase of temperature. Bulk conductivity (σ) was found to increase with increasing temperature which follows the Arrhenius relationship. There are no significant changes observed in activation energy (E_a) for grain conduction with Zr^{4+} incorporation in $BaTiO_3$. The activation energy (E_a) for grain boundary conduction is higher compared to grain conduction. The grain boundary resistance is the dominating character of the overall electrical conduction behavior. The electrical relaxation process occurring in the material has been found to be temperature dependent. For BZT and BZT-BCT, long range conduction process is at higher temperature (>573 K) whereas a short range conduction process is active at the lower temperature (<573 K). The polarization process due to localized conduction of multiple carriers is active low temperature. Whereas the oxygen ions or vacancies or hopping conduction mechanism (long range) contribute to the dc conductivity at higher temperatures.

References

[1] G. H. Haertling, J. Am. Ceram. Soc., **82**,797–818, (1999).

[2] B. Jaffe, W. R. Cook Jr. and H. Jaffe, Piezoelectric Ceramics, Academic Press, New York (1971).

[3] W. Cao, L. E. Cross, Phys. Rev. B., **44**, 5, (1991).

[4] J. Fousek, V. Janovec, J. Appl. Phys., **40**, 135–142, (1969).

[5] S. Stemmer, S. K. Streiffer, F Ernst, and M. R¨uhle, Philos. Mag. A, **71**, 713, (1995).

[6] D. Damjanovic, Rep. Prog. Phys., **61**, 1267–324, (1998).

[7] L. Jin, F. Li, S.Zhang, J. Am. Ceram. Soc., **97**, 1–27, (2014).

[8] L. E. Cross, “Ferroelectric Ceramics: Tailoring Properties for Specific Applications”; pp. 1–85 in Ferroelectric Ceramics, Edited by N. Setter and E. L. Colla. Birkhauser Verlag, Basel, (1993).

[9] S.W. Cheong, M. Mostovoy, Nat. Mater., **6**, 13-20, (2007).

[10] R. E. Cohen, Nature, **358**, 136, (1992).

[11] A. P. Levanyuk, D. G. Sannikov, Sov. Phys. Usp., **17**, 199, (1974).

[12] B. B. Van Aken, M. T. T. Palstra, A. Filippetti, N. A. Spaldin, Nat. Mater., **3**, 164, (2004).

[13] G. A. Smolenskii, V. A. Isupov, Zh. Tekh. Fyz., **24**, 1375, (1954).

[14] G. A. Smolenskii, J. Phys. Soc. Jpn., **28**, 26, (1970).

[15] V. A. Isupov, I. P. Pronin, V. I. Sizykh, Ferroelectrics., **90**, 147, (1989).

[16] C. G. F. Stenger, A. J. Burgraaf, J. Phys. Chem. Solids., **41**, 17, (1980).

[17] A. E. Glazounov, A. K. Tagantsev, Phys. Rev. Lett., **85**, 2192, (2000).

[18] G. A. Samara, Phys. Rev. Lett., **77**, 314, (1996).

[19] C. Ang, Z. Yu, L. E. Cross, Phys. Rev. B., **62**, 228, (2000).

[20] E. Husson, A. Morell, Trans Tech, Switzerland, p., 217, (1992).

[21] V. Westphol, W. Kleeman, M. D. Glinchuk, Phys. Rev. Lett., **68**, 847, (1992).

[22] A. K. Tagantsev, A. E. Glazounov, Phys. Rev. B., **57**, 18, (1998).

[23] D. Viehland, S. J. Jang, L. E. Cross, J. Appl Phys., **68**, 2916, (1990).

[24] A. Levstik, Z. Kutnjak, C. Filipic, R. Pirc, Phys. Rev. B., **57**, 11204, (1998).

[25] D. Saha, A. Sen, Phil. Mag. Lett., **71**, 367, (1995).

[26] U. T. Höchli, K. Knorr, A. Loidl, Adv. Phys., **39**, 405, (1990).

[27] C. Ang, Z. Yu, P. M. Vilarinho, J. L. Baptista, Phys. Rev. B., **57**, 7403, (1998).

[28] T. Maiti, R. Guo, A. S. Bhalla, J. Am. Ceram. Soc., **91**, 1769–80, (2008).

[29] V. V. Shvartsman, D. C. Lupascu, J. Am. Ceram. Soc., **95**, 1–26, (2012).

[30] P. Hansen, D. Hennings, H. Schreinemacher, J. Electroceram., **2**, 85– 94, (1998).

[31] R. E. Newnham, Properties of materials Anisotropy, Symmetry, Structure, Oxford University Press Inc. New York (2005).

[32] D. Damjanovic, M. Demartin, J. Phys. Condens. Mat., **9**, 4943, (1997).

[33] G. Arlt, H. Dederichs, R. Herbiet, Ferroelectrics., **74**, 37, (1987).

[34] G. Shirane, K. Suzuki, A. Takeda, J. Phys. Soc. Jpn., **7**, 12, (1952).

[35] A.J. Moulson, J.M. Herbert, Electroceramics—Materials, Properties, Applications Chapman & Hall, London, (1990).

[36] N. J. Donnelly, T. R. Shrout, C. A. Randall, J. Am. Ceram. Soc., **90**, 490–495, (2007).

[37] S. E. Park, T. R. Shrout, J. Appl. Phys., 82, 1804–11, (1997).

[38] Y. M. Chiang, G.W. Farrey, A. N. Soukhojak, Appl. Phys. Lett., **73**, 3683–5, (1998).

[39] J. Rodel, W. Jo, K.T.P. Seifert, E.M. Anton, T. Granzow, D. Damjanovic, J. Am. Ceram. Soc., **92**, 1153–77, (2009).

[40] EU-Directive 2002/96/EC, Off. J. Eur. Union., **46**, 24–38, (2003).

[41] EU-Directive 2002/95/EC, Off. J. Eur. Union., **46**, 19–23, (2003).

[42] J. Li, K. Wang, F. Zhu, L. Cheng, F. Yao, J. Am. Ceram. Soc., **96**, 3677–3696, (2013)

[43] T. Lusiola, F. Bortolani, Q. Zhang, R. Dorey, J. Mater. Sci., **47**, 1938-1942, (2012).

[44] E.A. Patterson, P.D. Cann, Appl. Phys. Lett., **101**, 042905, (2012).

[45] V. Pal, R.K. Dwivedi, O.P. Thakur, Mater. Res. Bull., **51**, 189–196, (2014).

[46] S. Singh, P. Singh, O. Parkash, D. Kumar, J. Alloys Compd., **493**, 522–528, (2010).

[47] D.D. Gulwade, S. M. Bobade, A.R. Kulkarni, P. Gopalan, J. Appl. Phys., **97**, 074106, (2005).

[48] W. Liu, X. Ren, Phys. Rev. Lett., **103**, 257602, (2009).

[49] B. M. Wul, I. M. Goldman, Dokl. Akad. Nauk SSSR., **46**, 154–57, (1945).

[50] D. Hennings, H. Schell, G. Simon, J. Am. Ceram. Soc., **65**, 539–544, (1982).

[51] V.M Goldschmidt, Klasse., **2**, 8, (1926).

[52] E.A Wood, Acta crystallogr., **4**, 353-361, (1951).

[53] H. H. Wieder, Phys. Rev., **99**, 1161-1165, (1955).

[54] H. F. Kay, P. Vousden, Phil. Mag., **40**, 1019-1040, (1949).

[55] E. Aksel, J. L. Jones, Sensors., **10**, 1935-1954, (2010).

[56] B. T. Matthias, J. P. Remeika, Phys. Rev., **82**, 727, (1951).

[57] G. Shirane, H. Danner A. Pavlovic, R. Pepinsky, Phys. Rev., **93**, 672, (1954).

[58] K. Nakamura, Y. Kawamura, IEEE Trans. Ultrason., Ferroelect. Freq. Contr., **47**, 750, (2000).

[59] K. Nakamura, M. Oshiki, Appl. Phys. Lett., **71**, 3203, (1997),

[60] M. Davis, N. Klein, D. Damjanovic, N. Setter, A. Gross, V. Wesemann, S. Vernay, D. Rytz, Appl. Phys. Lett., **90**, 2904, (2007).

[61] L. Egerton, D. M. Dillon, J. Am. Ceram. Soc., **42**, 438–42, (1959).

[62] R. E. Jaeger, L. Egerton, J. Am. Ceram. Soc., **45**, 209–13, (1962).

[63] G. H. Haertling, J. Am. Ceram. Soc., **50**, 329–30, (1967).

[64] B. P. Zhang, J. F. Li, K. Wang, H. L. Zhang, J. Am. Ceram. Soc., **89**, 1605, (2006).

[65] P. Guo, K. Kakimoto, H. Ohsato, Appl. Phys. Lett., **85**, 4121-3, (2004).

[66] Y. Wang, D. Damjanovic, N. Klein, E. Hollenstein, N. Setter, J. Am. Ceram. Soc., **90** 3485–9, (2007).

[67] J. G. Wu, Y. Y. Wang, D. Q. Xiao, J. U. Zhu, P. Yu, L. Wu, and W. J. Wu, Jpn, J. Appl. Phys., **46** , 7375–7, (2007).

[68] B. Q. Ming, J. F. Wang, P. Qi, and G. Z. Zang, J. Appl. Phys., **101**, 054103, (2007).

[69] H. Y. Park, C. W. Ahn, H. C. Song, J. H. Lee, S. Nahm, K. Uchino, H. G. Lee, H. J. Lee, Appl. Phys. Lett., **89**, 062906, (2006).

[70] Y.Saito, H.Takao, T. Tani, T. Nonoyama, K. Takatori, T. Homma, T. Nagaya M. Nakamura, Nature, **432**, 84, (2004).

[71] E. K. Akdogan, K. Kerman, A. A. M. Safari, Appl. Phys. Lett., **92**, 112908, (2008).

[72] T. R. Shrout, S. J. Zhang, J. Electroceram., **19**, 111, (2007).

[73] S. O. Leontsev, R. E. Eitel, Sci. Technol. Adv. Mater., **11**, 044302, (2010).

[74] G. A. Smolenskii, V. A. Isupov, A. I. Agranovskaya, N. N. Krainik, Sov. Phys.- Solid State., **2**, 2651, (1961).

[75] T. Takenaka, K. Maruyama, K. Sakata, Jpn. J. Appl. Phys., **30**, 2236, (1991).

[76] V.A. Shuvaeva, D. Zekria, A.M. Glazer, Jiang Q, S.M. Weber, P. Bhattacharya, P.A. Thomas, Phys. Rev. B., **71**,174114, (2005).

[77] S. E. Cummins, L. E. Cross, J. Appl. Phys., **39**, 2268, (1968).

[78] H. S. Shulman, M. Testorf, D. Damjanovic, N.Setter, J. Am. Ceram. Soc., **79**, 3124, (1996).

[79] Y. Noguchi, M. Miyayama, Appl. Phys. Lett., **78**, 1903, (2001).

[80] C.A. Araujo, J. D. Cuchlaro, L. D. McMillan, M. C. Scott, J. F. Scott, Nature, **374**, 627, (1995).

[81] X. X. Wang, X. G. Tang, H. L. W. Chan, Appl. Phys. Lett., **85**, 91, (2004).

[82] P. Zheng, J. L. Zhang, S. F. Shao, Y. Q. Tan , C. L. Wang, Appl. Phys. Lett., **94**, 032902, (2009).

[83] W. Li, Z. Xun, R. Chu, P. Fu, G. Zang, Physica B, **405**, 4513, (2010).

[84] Y. P. Guo, K. Kakimoto, H. Ohsato, Appl. Phys. Lett., **85**, 4121–3, (2004).

[85] J. G. Wu, Y. Y. Wang, D. Q. Xiao, J. G. Zhu, and Z. H. Pu, Appl. Phys. Lett., **91**,132914, (2007).

[86] S. J. Zhang, T.R. Shrout, H. Nagata, Y. Hiruma, T. Takenaka, IEEE Trans. Ultrason., Ferroelect. Freq. Contr., (in press).

[87] C. M. Wang, J. F. Wang, S. J. Zhang, T. R. Shrout, Phys. Status Solidi., **3**, 49, (2009).

[88] X. P. Jiang, Q. Yang, C. Chen, N. Tu, Z. D. Yu and Y. M. Li, J. Inorg. Mater., **25**, 1169, (2010).

[89] L. Zhao, J. X. Xu, N. Yin, H. C. Wang, C. J. Zhang, J. F. Wang, Phys. Status Solidi A, **2**, 111, (2008).

[90] Z. Yu, C. Ang, R. Guo, A.S. Bhalla, J. Appl. Phys., **92**, 1489, (2002).

[91] Z. Yu, R. Guo, A.S. Bhalla, J. Appl. Phys., **88**,410–415, (2000).

[92] T.N. Verbitskaya, G.S. Zhdanov, Y.N. Venevtsev, S.P. Solov'ev, Sov. Phys. – Crystallogr., (Engl Transl) **3**, 182–92, (1958).

[93] X.G. Tang, K.H. Chew, H.L.W. Chan, Acta Mater., **52**, 5177–5183, (2004).

[94] N. Nanakorn, P. Jalupoom, N. Vaneesorn, Ceram. Int., **34**, 779–782, (2008).

[95] P.W. Rehrig, S. Park, S. T. McKinstry, G.L. Messing, B. Jones, T. R. Shrout, J. Appl. Phys., **86**, 1657, (1999).

[96] P. S. Dobal, A. Dixit, and R. S. Katiya, Z. Yu, R. Guo, A. S. Bhalla, J. Appl. Phys., **89**, 8085, (2001).

[97] L. Dong, D.S. Stone, R.S. Lakes, J. Appl. Phys., **111**, 084107, (2012).

[98] C.E. Ciomaga, M. Viviani, M.T. Buscaglia, V. Buscaglia, L. Mitoseriu, A. Stancu, J. Eur. Ceram. Soc., **27**, 4061–4064, (2007).

[99] J. Bera, S. K. Rout, Mater. Lett., **59**, 135-138, (2005).

[100] F. Moura, A.Z Sim˝oes, B.D. Stojanovic, M.A. Zaghete, E. Longo, J.A. Varela, J. Alloys Compd., **462**,129–34, (2008).

[101] M.L.V. Mahesh, V.V. Bhanuprasad, and A.R. Jamese, J. Electron. Mater., **12**, 42, (2013).

[102] X. G. Tang, J. Wang, X.X. Wang, H.L.W. Chan, Solid State Comm., **131**, 163–168, (2004).

[103] X .G. Tang, Q.X. Liu, J. Wang, H.L.W. Chan, App. Phys., A, **96**, 945–952, (2009).

[104] N. Binhyeeniyi, P. Sukvisut, C. Thanachayanont, S. Muensit, Mat. Lett., **64**, 305-308, (2010).

[105] C. Thanachayanont,V. Yordsri , S. Kijamnajsuk, N. Binhayeeniyi , N. Muensit, Mat. Lett., **82**, 205–207, (2012).

[106] X. Chen, W. Cai, C. Fu, H. Chen, Q. Zhang, J. Sol Gel Sci. Techno., **57**, 149-156, (2011).

[107] N. Chakrabarti and H. S. Maiti, J. Mater. Chem., **6**, 1169 – 1173, (1996).

[108] J. Phongthorn, B. Theerachai, Curr. App. Phys., 11, S60-S65, (2011).

[109] P. Julphunthong, S. Chootina, T. Bongka, Ceram. Int., **39**, S415–S419, (2013).

[110] M. I. B. Bernardi, E. Antonelli, A. B. Lourenco, C. A. C. Feitosa, L. J. Q. Maia, A.C. Hernandes, J. Therm. Anal. Calorim., **87**, 725–30, (2007).

[111] M. Deluca, C. A. Vasilescu, A. C. Ianculescu, D. C. Berger. C. E. Ciomaga, L.P. Curecheriu, L. Stoleriu, A. Gajovic, L. Mitoseriu, C. Galassi, J. Eur. Ceram. Soc., **32**, 3551–3566, (2012).

[112] R. Vivekanandan, S. Philip, T.R.N. Kutty, Mat. Res. Bull., **22**, 99-108, (1986).

[113] B.W. Lee, S.B. Cho, J. Eur. Ceram. Soc., **25**, 2009–2012, (2005).

[114] S. B. Reddy, K. P. Rao, M.S. R. Rao, Scripta Mater., **57**, 591–594, (2007).

[115] J.Q. Qi, Y. Wang, W.P. Chen, L.T. Li and H. L.W. Chan, J. Nano. Res., **8**,959–963, (2006).

[116] Z.Q. Zhuang, M.P. Harmer, D.M. Smyth, R.E Newnham, Mater. Res. Bull., **22**, 1329, (1987).

[117] P.S.R. Krishna, D. Pandey, V.S. Tiwari, R. Chakravarthy, App. Phys. Lett., **62**, 231, (1992).

[118] V.S. Tiwari, N. Singh, D. Pandey, J. Am. Cream. Soc., **77**, 1813, (1994).

[119] R.C. Devries, R. Roy, J. Am. Ceram. Soc., **38**, 142, (1955).

[120] C. Kuper, R. Pankrath, H. Hesse, Appl. Phys., A, **65**, 301, (1997).

[121] D.A. Berlincourt, F. Kulesar, J. Acoust. Soc. Am., **24**, 709, (1952).

[122] M.C. McQuarrie, F.W. Behnke, J. Am. Ceram. Soc., **37**, 539, (1954).

[123] T. Mitsul, W.B. Westphal, Phys. Rev., **124**, 1354, (1961).

[124] K. Wakino, K. Minai, Y. Sakabe, High-Dielectric Constant Ceramics for Base Metal Monolithic Capacitors. Murata Manufacturing Co., Ltd., Japan.

[125] V.S. Tiwari, D. Pandey, P. Groves, J Phys., D, **22**, 837, (1989).

[126] L. Zhang, O. P. Thakur, A. F. Gillian, M. K. Andrew, G. Mould, D. C. Sinclair, A R. West, Appl. Phys. Lett., **90**, 142914, (2007).

[127] D.F.K. Hennings, H. Schreinemacher, J. Eur. Ceram. Soc., **15**, 795–800, (1995).

[128] H. Kishi, Y. Mizuno, H. Chazono, Jpn. J. Appl. Phys., **42**,1–15, (2003).

[129] T.A. Jain, K.Z. Fung, J. Chan, J. Alloys Compd., **468**, 370–374, (2009).

[130] D. Hennings, H. Schreinemacher, Mat. Res. Bull., **12**, 1221-1226, (1977)

[131] J. Wu, D. Xiao, W. Wu, J. Zhu, J. Wang, J. Alloys Compd., **509**, L359– L361, (2011).

[132] D.S. Keeble, F. Benabdallah, P. A. Thomas, M. Maglione, J. Kreisel, Appl. Phys. Lett., **102**, 092903, (2013).

[133] D. Xue, Y. Zhou, H. Bao, C. Zhou, J. Gao, X. Ren, J. Appl. Phys., **109**, 054110, (2011).

[134] W. Li, Z. Xu, R. Chu, P. Fu, G. Zang, J. Am. Ceram. Soc., **93**, 2942–2944, (2010).

[135] W. Li, Z. Xu, R. Chu, P. Fu, G. Zang, Mater. Sci. Eng. B., **176**, 65–67, (2011).

[136] W. Li, Z. Xu, R. Chu, P. Fu, G. Zang, Mater. Lett., **64**, 2325–2327, (2010).

[137] S. Zhang, H. Zhang, B. Zhang, S. Yang, J. Alloys Compd., **506**, 131–135, (2010).

[138] F. Benabdallah, A. Simon, H. Khemakhem, C. Elissalde, M. Maglione, J. Appl. Phys., **109**, 124116, (2011).

[139] P Wang, Y. Li, Y. Lu, J. Eur. Ceram. Soc., **31**, 2005–2012, (2011).

[140] S. Su , R. Zuo, S. Lu, Z. Xu, X. Wang, L. Li, Curr. App. Phys., **11**, S120-S123, (2011).

[141] J. Gao, D. Xue, Y. Wang, D. Wang, L. Zhang, H. Wu, S. Guo, H. Bao, C. Zhou, W. Liu, S. Hou, G. Xiao, X. Ren, Appl. Phys. Lett., **99**, 092901, (2011).

[142] J. Hao, W. Bai, W. Li, J. Zhai, J.Am. Ceram. Soc., **95**, 1998-2006, (2013).

[143] Y. Tian, L. Wei, X. Chao, Z. Liu, Z. Yang, J. Am. Ceram. Soc., **96**, 496–502, (2013).

[144] Y. Tian, L. Wei, X. Chao, Z. Liu, Z. Yang, J. Appl. Phys., **113**, 184107, (2013).

[145] S. Yao, W. Ren, H. Ji, X. Wu, P. Shi, D. Xue, X. Ren, Z.G. Ye, J. Phys. D: Appl. Phys., **45**, 195301, (2012).

[146] D. Damjanovic, A. Biancoli, L. Batooli, A. Vahabzadeh, and J. Trodahl, Appl. Phys. Lett., **100**, 192907, (2012).

[147] H. Bao, C. Zhou, D. Xue, J. Gao, X. Ren, J. Phys. D: Appl. Phys., **43**, 465401, (2010).

[148] V. Vinothini, P. Singh, Ceram. Int., **32**, 99, (2006).

[149] Z. Tan, W. Fu, X. Deng, R. Yang, X. Guan, C. Lu, Y. Zhang, L. Han, Adv. Mater. Res., **148-149**, 1480-1485, (2011).

[150] R. Yang, X. Fu. W. Deng, Z. Tan, Y. Zhang, L. Han, C. Lu, X. Guan, Adv. Mater. Res., **148-149**, 1062-66, (2011).

[151] M. Wang, R. Zuo, S. Qi, L. Liu, J. Mater. Sci: Mater Electron., 23, 753, (2012).

[152] J. P. Praveen, K. Kumar, A.R. James, T. Karthik, S. Asthana, D. Das, Curr. Appl. Phys., **14**, 396-402, (2014).

[153] V. S. Puli, A. Kumar, D. B. Chrisey, M. Tomozawa, J. F. Scott, R. S.Katiyar, J. Phys. D: Appl. Phys., **44**, 395403, (2011).

[154] A. R. Montero, L. Pardo, R. L. Juárez, A.M. González , M.P. Cruz, M.E. Castrejón, J. Alloys Compd., **584**, 28–33, (2014).

[155] J. Wu, D. Xiao, W. Wu, Q. Chen, J. Zhu, Z. Yang, J. Wang, Scripta Mater., **65**, 771–774, (2011).

[156] Y. Cui, X. Liu, M. Jiang, Y. Hu, Q. Su, H. Wang J. Mater. Sci. Mater. Electron., 23,1342–1345, (2012).

[157] Y. Cui, X. Liu, M. Jiang, Y. Hu , Q. Su, H. Wang, Ceram. Int., 38, 4761–4764, (2012).

[158] Y. Cui, X. Liu, M. Jiang, Y. Hu , Q. Su, H. Wang, J. Mater. Sci. Mater. Electron., 24, 654–657, (2013).

[159] C. Hana, J. Wu, C. Pub, S. Qiao, B. Wu, J, Zhu, D. Xiao, Ceram. Int., 38, 6359–6363, (2012).

[160] Q Lin, M. Jiang, D. Lin, Q. Zheng, X. Wu, X. Fan, J. Mater. Sci. Mater. Electron., **24**, 734-739, (2013).

[161] W. D. Kingery, H.K. Bowen, D.R. Ulihmann, Introduction to Ceramics, Cambridge, Massachusetts, June (1975).

[162] H. Aoto, US Patent, $BaTiO_3$-$PbTiO_3$ series single crystal and method of manufacturing the same piezoelectric type actuator and liquid discharge head using such piezoelectric type actuator., US 6783588 B2, Aug 31, 2004.

[163] S. Ezhilvalavan, T. Tseng, Mater. Chem. Phys., **65**, 227–248, (2000).

[164] J. Wang, T. Zhang, R. Pan, J. Jiang, Z. Ma, C. Xiang, Mater. Chem. Phys., 121 28–31, (2010).

[165] J. Jeon, J. Eur. Ceram. Soc., **24**, 1045–104, (2004).

[166] H. Kawano, K. Mori, Y. Nakayama J. Appl. Phys., **73**, 5141, (1993),

[167] T. Hungr, M. Alguero, A. B. Hungr, A. Castro, Chem. Mater., **17**, 6205-6212, (2005).

[168] C. Fu, F. Pan, H. Chen, et al., J. Mater. Sci.: Mater. Electron. **18**, 453–456, (2007).

[169] M. Kuwabara, K. Morimo, T. Matsunaga, J. Am. Ceram. Soc., **79**, 997-1001, (1996).

[170] H.Y. Tian, Y. Wang, J. Miao, H.L.W. Chan, C.L. Choy, J. Alloys Compd., **431**, 197–202, (2007).

[171] W. Chen, B. Liu, Q.F. Liu, S.T. Chen, J. Chin. Ceram. Soc., **28**, 1999, (2000).

[172] V.V. Shvartsman, W. Kleemann, J. Dec, Z.K. Xu, S.G. Lu., J. Appl. Phys., **99**, 124111, (2006).

[173] S.G. Lu, Z.K. Xu, H. Chen, Appl. Phys. Lett., **22**, 85–88, (2004).

[174] X. Wei, X. Yao, Mater. Sci. Eng. B., **137**, 184–8, (2007).

[175] P. Yadoji, R. Peelamedu, D. Agrawal, R. Roy, Mater. Sci. Eng. B., **98**, 269–278, (2003).

[176] D. K. Agrawal, Curr. Opin. Solid St. M., **3**,480, (1998).

[177] O.P. Thakur, C. Prakash, D.K. Agrawal, J. Ceram. Proc. Res., **3**, 75-79, (2002).

[178] D. Agrawal, J. Mat. Edu., 19, 49–58, (1999).

[179] S. Mahajan, O. P. Thakur, D.K. Bhattacharya, J. Am. Ceram. Soc., **92**, 416–423, (2009).

[180] R. Mazumder, A. Sen, J. Eur. Ceram. Soc., **28**, 2731–37, (2008).

[181] K. C. Patil, M. S. Hegde, T. Rattan, S. T. Aruna, Chemistry of Nanocrystalline Oxide Materials Combustion Synthesis, Properties and Applications. World Scientific publishing; Singpore (2008).

[182] M.N. Rahaman, Ceramic Processing and Sintering, (CRC Press, Taylor & Francis Group) (2007).

[183] H. Mio, J. Kano, F. Saito, Chem. Eng. Sci., **59**, 5909-5916, (2004).

[184] B. D. Cullity, Elements of X-Ray diffraction Second edition ed., (1978).

[185] H. M. Rietveld, J. Appl. Cryst., **2**, 65, (1969).

[186] http://www.ing.unitn.it/~maud/] [Maud software 2.23 version]

[187] R.A. Young, Rietveld Method, International Union of Crystallography, Oxford University Press, (1996).

[188] L. E. Smart, E. A. Moore, Solid State Chemistry, (Taylor & Francis, London, (2005).

[189] M.W. Barsoum, Fundamentals of Ceramics, McGraw–Hill, Boston, (1997).

[190] A. J. Mouson, J. M. Herbert. Electroceramics- Materials properties, applications. Chapman and Hall, London, (1990).

[191] E. Barsoukov, J. R. Macdonald, Impedance Spectroscopy: Theory, Experiment, and Applications, John Wiley & Sons. Second edition (2005).

[192] J. Zang, M. Li, D. C. Sinclair, W. Jo, J. Rodel, J. Am. Ceram. Soc., **97** [5] 1523–1529 (2014)

[193] R. Gerhardt, J. Phys. Chem. Solids, **55** [12] 1491–506 (1994).

[194] A. Dixit, S.B. Majumder, R.S. Katiyar, A.S. Bhalla, J. Mater. Sci., **41**, 87, (2006).

[195] D. Ricinschi, C.E. Ciomaga, L. Mitoseriu, V. Buscaglia, M. Okuyama, J. Eur. Ceram. Soc., **30**, 237–241, (2010).

[196] S. Luo, Z. Tang, W. Yao, Z. Zhang, Micro. Engg., **66**, 147–152, (2003).

[197] S. Liu, X. Tan, K. Li, R. Hughes, Ceram. Int., **28**, 327–335, (2002).

[198] Y. Li, J. Zhao, B. Wang, Mater. Res. Bull. **39**, 365–374, (2004).

[199] A. Saberi, F. G. Fard, H. Sarpoolaky, M. W. Porada, G. Thorsten, R. Simon, J. Alloys Compd., **462**, 142–146, (2008).

[200] M. T. Buscaglia, V. Buscaglia, R. Alessio, Chem. Mater., **19**, 711, (2007).

[201] W. Cai, C. Fu, J. Gao, H. Chen, J. Alloys Compd., **480**, 870–873, (2009).

[202] H. Chen, C. Yang ,C. Fu , J. Shi, J. Zhang , W. Leng, J. Mater. Sci. Mater. Electron., **19**, 379–382, (2008).

[203] S. J. Kuang, X.G. Tang, L.Y. Li, Y.P. Jiang , Q.X. Liu, Scripta Mater., **61**, 68–71, (2009).

[204] Swanson, Fuyat., Natl. Bur. Stand. (U.S.), Circ. 539, **3**, 45, (1954).

[205] H. Huang, H. Chiu, N. Wu, M. Wang, Metallurgical and Materials Transactions A 39A (2008).

[206] A. Dixit, S.B. Majumder, P.S. Dobal, R.S. Katiyar, A.S. Bhalla, Thin Solid Films, **447–448**, 284–288, (2004).

[207] R. Farhi, M. E. Marssi, A. Simon, J. Ravez, Eur. Phys. J. B., **9**, 599-604, (1999).

[208] C.J. Xiao, Z.H. Chi, W.W. Zhang, F.Y. Li, S.M. Feng, C.Q. Jin, X.H. Wang, X.Y. Deng, L.T. Li, J. Phys. Chem. Solids., **68**, 311–314, (2007).

[209] W. Zhang, L. Chen, C. Jin, X. Deng, X. Wang, L. Li, J. Electroceram., **21**, 859–862, (2008).

[210] http://imagej.nih.gov/ij/index.html

[211] G. Arlt, D. Hennings, G. de With, J. Appl. Phys., **58**, 1619, (1985).

[212] S. Ke, H. Fan, H. Huang, H.L. W. Chan, S.Yu, J. Appl. Phys., **104**, 034108, (2008).

[213] J. W. Xiong, B. Zeng, W. Q. Cao, J. Electroceram., **21**,124–127, (2008).

[214] J. Fu, R. Zuo, Y. Liu, J.Alloys Compd., **493**, 197–201, (2010).

[215] W. Li, Z. Xu, R. Chu, P. Fu, G. Zan, Braz. J. Phys., **40**, 3, (2010).

[216] E. Hollenstein, M. Davis, D. Damjanovic, N. Setter, Appl. Phys. Lett., **87**, 182905, (2005).

[217] L.L. Zhang, X.S. Wang, H. Liu, X. Yao, J. Am. Ceram. Soc., **93**, 1049, (2010).

[218] X. Wang, C.N. Xu, H. Yamada, K. Nishikubo, X.G. Zheng, Adv. Mater., **17**, 1254, (2005).

[219] S.W. Zhang, H.L. Zhang, B.P. Zhang, G.L. Zhao, J. Euro. Ceram. Soc., **29**, 3235, (2009).

[220] J.L. Zhang, X.J. Zong, L. Wu, Y. Gao, P. Zheng, S.F. Shao, Appl. Phys. Lett., **95,** 022909, (2009).

[221] I. Coondoo, N. Panwar, H. Amor, M. Alguero, A.L. Kholkin, J. Appl. Phys., **113**, 214107, (2013).

[222] A.B. Haugen, J.S. Forrester, D. Damjanovic, B. Li, K. J. Bowman, J. L. Jones, J. Appl. Phys., **113**, 014103, (2013).

[223] A. Chaves, R. S. Katiyar, S.P.S. Proto, Phys. Rev. B., **10**,3523–33, (1974).

[224] J. Pokorný, U. M. Pasha, L. Ben, O. P. Thakur, D. C. Sinclair, I. M. Reaney, J. Appl. Phys., **109**, 114110, (2011).

[225] J. Ghosh, S. Mazumder, Phase transitions., **85**, 694, (2012).

[226] U. D. Venkateswaran, V. M. Naik, R. Naik, Phys. Rev. B., **58**, 14256, (1998).

[227] C. J. Xiao, C. Q. Jin, X. H. Wang, Mater. Chem. Phys., **111**, 209, (2008).

[228] G.S. Rohrer, Annu. Rev. Mater. Res., **35**, 99–126, (2005).

[229] W. Jo, D.-Y. Kim, N.-M. Hwang, J. Am. Ceram. Soc., **89**, 2369–2380, (2006).

[230] S.-J.L. Kang, M.-G. Lee, S.-M. An, J. Am. Ceram. Soc., **92**, 1464–1471, (2009).

[231] N. Sawangwan, J. Barrel, K. Mackenzie, T. Tunkasiri, Appl. Phys. A., **90**, 723, (2008).

[232] J. Wu, D. Xiao, B. Wu, W. Wu, J. Zhu, Z. Yang, J. Wang, Mater. Res. Bull., **47**, 1281-1284, (2012).

[233] M. Matsubara, T. Yamaguchi, W. Sakamoto, K. Kikuta, T. Yogo, S. Hirano, J. Am. Ceram. Soc., **88**, 1190–1196, (2005).

[234] S. Zhang, H. Zhang, B. Zhang, G. Zhao, J. E. Ceram. Soc., **29**, 3235–3242, (2009).

[235] T. Takenaka, H. Nagata, J. Eur. Ceram., Soc., **25**, 2693, (2005).

[236] Z. Sun, Y. Pu, Z. Dong, Y. Hu, X. Liu , P. Wang , M. Ge, Mater. Lett., **118**, 1–4, (2014).

[237] S. Ye, J. Fuh, L. Lu, J. Alloys Compd., **541**, 396–402, (2012).

[238] W. Bai, B. Shen, F. Fu, J. Zhai, Mat. Lett., **83**, 20–22, (2012).

[239] P. Victor, R. Ranjith, S.B. Krupanidhi J. Appl. Phys., **94**, 7702, (2003).

[240] Z. Yang, Y. Chang, B. Liu, L. Wei, J. Mater. Sci. Eng. A., **432**, 292–298, (2006).

[241] S. Zhang, R. Xia, T.R. Shrout, G. Zang, J. Wang, J. Appl. Phys., **100**, 104108, (2006).

[242] D. Damjanovic, J.Am. Ceram. Soc., **88**, 2663–76, (2005).

[243] A. Yang, C.A. Wang, R. Guo, Y. Huang, C.W. Nan., Ceram. Int., **36**, 549–54, (2010).

[244] V. R. E, A. Mahajan, M.P.F. Graca, S.K. Mendiratta, M.A. Valente, Mater. Res. Bull., **48** 4395–440, (2013).

[245] W. Wang, W.L. Li, D. Xu, W.P. Cao, Y.F. Hou, W.D. Fei, Ceram. Int., **40,** 3933–3937, (2014).

[246] B. Li, M. C. Ehmke, J. E. Blendell, K. J. Bowman, J. Eur. Ceram. Soc., **33**, 3037–3044, (2013).

[247] J. Wu, D. Xiao, W. Wu, Q. Chen, J. Zhu, Z. Yang, J. Wang, J. Eur. Ceram. Soc., **32**, 891–898, (2012).

[248] B. Noheda, D.E. Cox, G. Shirane, J.A. Gonzalo, L.E. Cross, S.E. Park, Appl. Phys. Lett., **74**, 2059, (1999).

[249] S. Bhattacharjee, S. Tripathi, D. Pandey, Appl. Phys. Lett., **91**, 042903, (2007).

[250] B Li, J. E. Blendell, K. J. Bowman, J. Am. Ceram. Soc., 1–3, (2011).

[251] G. A. Rossetti, L. E. Cross, K. Kushida, Appl. Phys. Lett. **59**, 2524, (1991),

[252] P. S. Dobal, S. Bhaskar, S. B. Majumder, and R. S. Katiyar, J. Appl. Phys., **86**, 828 (1999).

[253] S. Nowick ,B. S. Berry, Anelastic, Relaxation in Crystalline Solids, Ch. 3, Academic Press, New Yorks, (1972).

[254] B. L. Cheng, B. Su, J. E. Holmes, T. W. Button, M. Gabbay, G. Fantozzi, J. Electroceram., **9**,17–23, (2002).

[255] H. Fu,R. E. Cohen, Nature (London) 403, 281, (2000).

[256] T. Chen, T. Zhang, J. Zhou, J. Zhang, Y. Liu, G. Wang Mater. Res. Bull., **47**, 1104–1106, (2012).

[257] S. Wu, X. Wei, X. Wang, H. Yang and S.Gao, J. Mater. Sci. Technol., **26**, 472-476, (2010).

[258] H. N. Zadeh, C. Glitzky, W.Oesterle, T. Rabe, J. Eur. Ceram. Soc., **31**, 589–96, (2011).

[259] W.G. Yang, B. Zhang, N. Ma, L. Zhao, J. Eur. Ceram. Soc., **32**, 899–904, (2012).

[260] T. Hayashi, T. Inoue, Y. Nagashima, J. Tomizawa, Y. Akiyama, Ferroelectrics, **258**, 53–60, (2001).

[261] W. Zhang, R. E. Eitel, J. Am. Ceram. Soc., **94**, 3386-3390, (2011).

[262] R. M. German, Sintering Theory & Practice. John Wiley & Sons, New York, (1996).

[263] L. T. Benziada, H.S. Hilal, R. Mühll, Solid State Sci., **8**, 922, (2006).

[264] N. Ma, B. P. Zhang, W.G. Yang, J. Electroceram., **28**, 275–280, (2012).

[265] X. X. Wang, K. Murakami, O. Sugiyama, S. Kaneko, J. Eur. Ceram. Soc., **21**, 1367–1370, (2001).

[266] J. Tao, Z. Yi, Y. Liu, M. Zhang, J. Zha, J. Am. Ceram. Soc., **96**, 1847–1851, (2013).

[267] G. R. Love, American Ceramic Society Spring Meeting (Pittsburgh), (1987).

[268] C. Chen, X. Jiang, Y. Li, F. Wang, Q. Zhang, J. Appl. Phys., **108**, 124106, (2010).

[269] W. Lee, Y. Lee, M. Tseng, C. Huang, Y Wu, J. Am. Ceram. Soc., **92**, 1069–1073, (2009).

[270] S. Qiao, J. Wu, B. Wu, B. Zhang, D. Xiao, J. Zhu, Ceram. Int., **38**, 4845–4851, (2012).

[271] Q. Gou, J. Wu, A. Li, B. Wu, D. Xiao, J. Zhu, J. Alloys. Comp., **521**, 4– 7, (2012).

[272] E.M. Anton, W. Jo, D. Damjanovic, J. Rodel, J. Appl. Phys., **110**, 094108, (2011).

[273] W. Ge, H. Cao, C. DeVreugd, J. Li, D. Viehland, J. Am. Ceram. Soc., **94**, 3084–3087, (2011).

[274] D. Damjanovic, N. Kelin, J. Li, Ferroelec, Mater. Let., **3,** 5-13, (2010).

[275] D.M. Lin, K.W. Kwok, H.L.W. Chan, Sol. State Ion., **178**, 1930–1937, (2008).

[276] B. Chu, D. Chen, G. Li, Q Yin, J. Eur. Ceram. Soc., **22,** 2115–2121, (2002).

[277] F.D. Morrison, D.C. Sinclair, A. R. West, J.Am.Ceram. Soc., **84**,531–538, (2001).

[278] A. Kaushal, S.M.Olhero, B. Singh, D. P. Fagg, I. Bdikin, J.M.F. Ferreira Ceram. Int., **40**, 10593–10600, (2014).

[279] A. R. West, D. C. Sinclair and N. Hirose J. Electroceramics 1:1, 65-71, (1997).

[280] A. S. Nowick, D. Y. Wang, D. S. Park, J. Griffith, ‘‘Oxygen Ion conductor’’ in Fast Ion Transport in Solids, Electrodes and Electrolytes Edited by P. Vashishta, J. N. Mundy, and G. K. Shenoy, Amsterdam, North Holland Publishing, 673–7, (1979).

[281] M. Jacs, M. Takahashi, Y. Noguchi, M. Miyayama, Solid State Ionics, **172**, 325–40, (2004).

[282] J. T. S. Irvine, D. C. Sinclair, and A. R. West, Adv. Mater., **2** [3], 132–8, (1990).

[283] W. Q. Cao, R. Gerhardt, Solid State Ionics, 42,213–21, (1990).

Publications resulting from the Ph. D. Work

1. Ganesh K. Sahoo and Ranabrata Mazumder, Dielectric and Piezoelectric Properties of Lead Free (1-x) $[(Bi_{0.5}Na_{0.5})TiO_3]$- $x[Ba(Zr_{0.2}Ti_{0.8})O_3$-$(Ba_{0.7}Ca_{0.3})TiO_3]$ Ceramics, Ferroelectrics 458:13–24, (2014).
2. Ganesh K. Sahoo and Ranabrata Mazumder, Low temperature synthesis of $Ba(Zr_{0.2}Ti_{0.8})O_3$-$0.5(Ba_{0.7}Ca_{0.3})TiO_3$ nanopowder by solution based autocombustion method, Journal of Materials Science: Materials in Electronics 25: 3515–3519, (2014).
3. Ganesh K. Sahoo and Ranabrata Mazumder, Dielectric and piezoelectric properties of lead free $(Ba_{0.85}Ca_{0.15})(Ti_{1-x}Zr_x)TiO_3$ ceramics prepared by solution based autocombustion method, Journal of the European Ceramic Society (Under Review)
4. Ganesh K. Sahoo, Ranabrata Mazumder and Swadesh K. Pratihar, Enhancement of dielectric and piezoelectric properties of BZT-BCT lead free ceramics at the morphotropic phase boundary (Under Review).
5. Ganesh K. Sahoo and Ranabrata Mazumder , Dielectric properties of Low temperature sintered $0.5Ba(Zr_{0.2}Ti_{0.8})O_3$–$0.5(Ba_{0.7}Ca_{0.3})TiO_3$ with $LiBiO_2$ as a sintering aid. (Under Review)
6. Ganesh K. Sahoo, Swadesh Kumar Pratihar and Ranabrata Mazumder, Dielectric and piezoelectric properties of lead free $Ba(Zr_xTi_{1-x})O_3$ ceramics prepared by solution based autocombustion method (Under Review)
7. Ganesh K. Sahoo, and Ranabrata Mazumder, Effect of different preparation methods on microstructure, dielectric and piezoelectric properties of BZT- 0.5BCT ceramics (Under Review)

Conference Publication

1. Dielectric and piezoelectric properties of lead free $Ba(Zr_xTi_{1-x})O_3$ ceramics prepared by solution based autocombustion method, National Conference on sensors and actuators : science to technology, CGCRI, Kolkota, March11-12, 2011.
2. Dielectric and piezoelectric properties of lead free $(Ba_{0.85}Ca_{0.15})(Ti_{1-x}Zr_x)TiO_3$ ceramics prepared by solution based autocombustion method, Ganesh Kumar Sahoo and Ranabrata Mazumder, International Conference on Electroceramics (**ICE-2011**) **Sydney, Australia** December 12 – 16 (2011).
3. Dielectric and piezoelectric properties of lead free $xBa(Zr_{0.2}Ti_{0.8})O_3$ – (1-x) $(Ba_{0.7}Ca_{0.3})TiO_3$ ceramics, Ganesh Kumar Sahoo and Ranabrata Mazumder, International Conference On "Energy Efficient Materials, Manufacturing Methods & Machineries for Ceramic Industries" (**IC2E4MCI-11**), Shilpgram, Agra, December 19-22 (2011)**(Best Poster Award)**.
4. Dielectric and Piezoelectric Properties of Lead Free (1-x) $[(Bi_{0.5}Na_{0.5})TiO_3]$-$x[Ba(Zr_{0.2}Ti_{0.8})O_3$-$(Ba_{0.7}Ca_{0.3})TiO_3]$ Ceramics, Ganesh K. Sahoo and Ranabrata Mazumder, The 8th Asian meeting on Ferroelectrics(**AMF-8**) **Pattaya, Thailand**, December 9-14, (2012).
5. Effect of Different Synthesis Method on Dielectric and Piezoelectric Properties of High Performance lead-free BZT-BCT Ceramic ,Ganesh Kumar Sahoo, Swadesh Kumar Pratihar and Ranabrata Mazumder, 17th National Conference on Ferroelectrics and Dielectrics (**XVII NSFD-2012**) Bhubaneswar, December 17-19 (2012).
6. Dielectric properties of Low temperature sintered $0.5Ba(Zr_{0.2}Ti_{0.8})O_3$–$0.5(Ba_{0.7}Ca_{0.3})TiO_3$ with $LiBiO_2$ as a sintering aid, Ganesh Kumar Sahoo , Alok Patro, Ranabrata Mazumder, National conference on Condensed Matter Physics (**CMDAYS-2013**) Rourkela, August 29- 31, (2013)

Curriculum Vitae

Ganesh Kumar Sahoo

Department of Ceramic Engineering,

National Institute of Technology

Rourkela-769008, Odisha, India

Mobile: +91-9040481019

Email: gksahoo84@gmail.com

Date of Birth: 15.06.1984

Education: M.Sc. (Physics), M.Tech (Ceramic Engg.)

Research Interest: Ferroelectric Ceramic, Electro-Ceramic. Nano material synthesis

Technical Exposure: Publications: 8, Conference: 12

Publications:

1. Ganesh K. Sahoo and Ranabrata Mazumder Grain Size Effect on the Dielectric Properties of Molten Salt Synthesized $BaTiO_3$" Ferroelectrics 402: 193-199 ,(2010).
2. Ganesh K. Sahoo and Ranabrata Mazumder, Dielectric and Piezoelectric Properties of Lead Free (1-x) $[(Bi_{0.5}Na_{0.5})TiO_3]$- $x[Ba(Zr_{0.2}Ti_{0.8})O_3$-$(Ba_{0.7}Ca_{0.3})TiO_3]$ Ceramics, Ferroelectrics 458:13–24, (2014).
3. Ganesh K. Sahoo and Ranabrata Mazumder, Low temperature synthesis of $Ba(Zr_{0.2}Ti_{0.8})O_3$-$0.5(Ba_{0.7}Ca_{0.3})TiO_3$ nanopowder by solution based autocombustion method, Journal of Materials Science: Materials in Electronics 25: 3515–3519, (2014).
4. Ganesh K. Sahoo and Ranabrata Mazumder, Dielectric and piezoelectric properties of lead free $(Ba_{0.85}Ca_{0.15})(Ti_{1-x}Zr_x)TiO_3$ ceramics prepared by solution based autocombustion method, Journal of the European Ceramic Society (Under Review)
5. Ganesh K. Sahoo, Ranabrata Mazumder and Swadesh K. Pratihar, Enhancement of dielectric and piezoelectric properties of BZT-BCT lead free ceramics at the morphotropic phase boundary (Under Review).
6. Ganesh K. Sahoo and Ranabrata Mazumder, Dielectric properties of Low temperature sintered $0.5Ba(Zr_{0.2}Ti_{0.8})O_3$–$0.5(Ba_{0.7}Ca_{0.3})TiO_3$ with $LiBiO_2$ as a sintering aid. (Under Review)
7. Ganesh K. Sahoo, Swadesh Kumar Pratihar, and Ranabrata Mazumder, Dielectric and piezoelectric properties of lead free $Ba(Zr_xTi_{1-x})O_3$ ceramics prepared by solution based autocombustion method (Under Review)
8. Ganesh K. Sahoo, and Ranabrata Mazumder, Effect of different preparation methods on microstructure, dielectric and piezoelectric properties of BZT- 0.5BCT ceramics (Under Review).